University of Science and Technology of China

A dissertation for doctor's degree

Polyethylene-Based Hybrid Nanocomposite Separators for Energy Storage Devices

Author: Dafaalla Mahjoub Dafaalla Babiker

Specialty: Materials Science and Engineering

Supervisor： Prof. Liangbin Li

Finished time: May, 2023

中国科学技术大学学位论文原创性声明

本人声明所呈交的学位论文,是本人在导师指导下进行研究工作所取得的成果。除已特别加以标注和致谢的地方外，论文中不包含任何他人已经发表或撰写过的研究成果。与我一同工作的同志对本研究所做的贡献均已在论文中作了明确的说明。

作者签名：_____　　签字日期：_____

中国科学技术大学学位论文授权使用声明

作为申请学位的条件之一，学位论文著作权拥有者授权中国科学技术大学拥有学位论文的部分使用权，即：学校有权按有关规定向国家有关部门或机构送交论文的复印件和电子版，允许论文被查阅和借阅，可以将学位论文编入《中国学位论文全文数据库》等有关数据库进行检索，可以采用影印、缩印或扫描等复制手段保存、汇编学位论文。本人提交的电子文档的内容和纸质论文的内容相一致。

保密的学位论文在解密后也遵守此规定。

□公开　　□保密（____年）

作者签名：_____　　导师签名：_____

签字日期：_____　　签字日期：_____

DEDICATION

This thesis is dedicated to:

*My beloved grandfather (**Dafaalla Babiker)** and my uncle (**Abdallah Dafaalla)**, they meant and continue to mean so much to me. Although they are no longer part of this life. Yet, their memories continue to regulate my life. May your souls rest in peace.*

Father

Mother

Brothers

Sisters

Lineages

Friends

Teachers

ACKNOWLEDGMENTS

I would like to express my sincere gratitude to my advisor **Prof. Liangbin Li** for allowing me to join his research group and for his advice, encouragement, and support throughout my Ph.D. program. I sincerely appreciate his help and advices. My experience of working alongside him had a profound impact on me as a person as well as a researcher.

I am grateful to all my lab fellows and colleagues at Prof. Li's lab (**Soft Matter Group**) for their help and for making this lab a perfect workplace. I am especially grateful to my colleagues in our sub-group (***Functional Polymer Films***) for their cooperation. I also would like to thank **Dr. Xin Chen**, **Dr. Caixia Wan**, and **Dr. Lingpu Meng** for aiding me whenever I needed help.

I am extremely grateful to my **Family** for their unconditional love and encouragement. Without their support, I wouldn't have made it so far. I am grateful to them for always standing by me and giving me the freedom and support to chase my ambitions.

Finally, my appreciation and deep gratitude go to everyone who has helped me emotionally, morally, mentally, and financially since the beginning of my study and throughout my entire life.

Last but not least, I would like to express my sincere gratitude to the University of Science and Technology of China (**USTC**) and the National Synchrotron Radiation Laboratory (**NSRL**) for allowing me to be a member of such inspiring organizations. My sincere appreciation to the Chinese Academy of Sciences (**CAS**) and the World Academy of Sciences (**TWAS**) for sponsoring my Ph.D. studies.

I wish the acknowledgement page was large enough to contain the names of everyone who has significantly impacted my life.

ABSTRACT

The rapid growth of the world economy, the day-to-day development of science and technology, and the continuing progress of living standards in modern society have indeed caused an increase in the need for energy. The widespread usage of fossil fuels to meet global energy needs generates thousands of tons of carbon dioxide (CO_2) and other pollutants yearly, accelerating global warming and causing significant climate change. Renewable energy sources such as wind, solar, and geothermal energy are viable alternatives to fossil fuels to reduce serious environmental risks. To integrate and distribute energy supply, these renewable energies require effective, advanced, and highly efficient electrochemical energy storage devices. The demand for energy storage devices, for example, lithium/sodium-ion batteries (LIBs/NIBs) for hybrid electric vehicles (HEVs) and autonomous electrical appliances, has increased rapidly over the past decade due to their high power density, long cycle life, extraordinary coulombic efficiencies, minimal memory effects, and environmental friendliness. The typical components of LIBs and NIBs batteries are electrodes (cathode and anode), electrolytes, and a microporous separator.

Microporous membrane separators (MMS) are at the heart of rechargeable LIBs and NIBs because they prevent short circuits and serve as a channel for ion transport during charge-discharge operations. Despite being an inactive section of the battery, the membrane separator's structure and properties have a significant impact on the battery's safety, electrochemical performance, and reusability. Regardless of the abundance of commercially available separators, their thermal stability and service life severely limit the battery's efficiency and reliability. Although no ideal separator can still provide optimal electrochemical performance, and safety under all operating conditions, most efforts to find alternatives to polyethylene (PE) separators have failed because

they are still preferable to other separators when all criteria are evaluated. Polyethylene-based membrane separators are favourable for LIBs and NIBs batteries but suffer from inherent hydrophobic behaviour that permits poor electrolyte absorption, and low thermal stability causes an inevitable dimensional shrinkage at high temperatures. Continuous efforts have been made to modify PE separators to increase safety and improve electrochemical performance. In this thesis, we overview the state-of-the-art fundamental requirements and properties of ideal separators for LIBs and NIBs. Correspondingly, in-depth descriptions of the fabrication and development of hybrid composite separators based on porous polyethylene (PE) membranes for rechargeable lithium-ion (Li-ion) and sodium-ion (Na-ion) batteries are provided. In an effort to develop battery separators with enhanced electrochemical performances and thermal stability. In this dissertation, we focus our research on constructing PE-based membranes to design innovative high-performance hybrid separators with good thermal stability, as well as superior electrochemical performance compared to conventional PE membranes.

Initially, a commercialized hybrid nanocomposite membrane between very high molecular weight polyethylene (VHMWPE) and silicon dioxide (SiO_2) is prepared via a sequential biaxial stretching process and used as separators LIBs. The existence of silica SiO_2 nanoparticles into the VHMWPE matrix results in significant increase of porosity, air permeability improves, thermal stability, wettability, electrolyte uptake, ion conductivity, and electrochemical performance with silica SiO_2 content. The obtained LIBs cells with the hybrid nanocomposite separator achieved excellent cycle capacity with a great coulombic efficiency of 99.93% over 100 cycles and C-rate capability 146.2 mAh g^{-1} at a current rate of 1C.

Afterwards, combining the industrialized biaxial stretching technique with the electron beam irradiation (E.B) crosslinking method, the advanced nanocomposite separator with great

commercialization potential is developed using very high molecular weight polyethylene (VHMWPE) and inorganic silicon dioxide (SiO_2) nanofillers. The E.B irradiation crosslinking improves the thermal properties, electrolyte wettability, ionic conductivity, and electrochemical performances of the VHMWPE-SiO_2 nanocomposite separator. The modified nanocomposite separator has an extraordinary electrolyte uptake (575 %) and excellent ionic conductivity (1.60 mS cm^{-1}). And the E.B cross-linked nanocomposite VHMWPE/SiO_2 separator can withstand higher current densities (e.g. 116.7 mAh g^{-1} at high C-rate 8C) than the non-cross-linked version.

Finally, a novel PE-based membrane modified with a hybrid organic-inorganic coating layer for lithium-/sodium-metal (LMBs/NMBs) batteries is fabricated. The advanced separator is developed by incorporating heat-resistant boehmite (BH) and multipolar self-polymerizing dopamine (DA) into biaxially oriented poly(ethylene) via a facile and in-situ solvent methodology with the help of corona discharge activation and pre-treatment. The advanced separator can promote rapid electrolyte absorption, accelerate Li^+/Na^+ transference without sacrificing the macrostructure and physiochemical properties of the matrix, and endow excellent dimensional stability (~ 0%) at temperatures higher than 140 °C. LMB cells（Li || $LiFePO_4$）employing the hybrid separator endow outstanding life span stability and excellent capacity retention of approximately ~88 % after 500 cycles at a C-rate of (1C). And the hybrid separator can also operate stably under the sodium metal battery system. This work presents an efficient and scalable strategy for constructing safe, long-life next-generation batteries.

Keywords: Energy storage devices, Battery safety, Polyethylene separators, Composite separators, Inorganic nanoparticles.

ABBREVIATIONS AND SYMBOLS

Symbol	Abbreviations
HEVs	Hybrid electric vehicles
ESS	Energy storage systems
LIBs	Lithium-ion batteries
NIBs	Sodium-ion batteries
LMBs	Lithium-metal batteries
NMBs	Sodium-metal batteries
MMS	Microporous membrane separators
PMS	Porous membrane separators
PP	Polypropylene
PE	Polyethylene
VHMWPE	Very high molecular weight polyethylene
E.B	Electron beam
DA	Dopamine
PDA	Polydopamine
AlOOH	Aluminum oxide hydroxide known as boehmite (BH)
TIPS	Thermally induced phase separation
NIPS	Non-solvent induced phase separation

VIPS	Vapour-induced phase separation
PSμM	Phase separation micromolding
ALD	Atomic layer deposition
R2R	Roll to roll
CVD	Chemical vapour deposition
oCVD	Oxidative chemical vapour deposition
*i*CVD	Initiated chemical vapour deposition
LbL	Layer-by-layer
PVD	Physical vapour deposition
CDT	Corona discharge treatment
Cu	Copper
Al	Aluminum
Li^+	Lithium ions
Na^+	Sodium ions
MO	Metal oxide
INPs	Inorganic nanoparticles
NMP	N-Methyl-2-pyrrolidone
SiO_2	Silicon dioxide
Al_2O_3	Aluminum oxide
TiO_2	Titanium dioxide
ZrO_2	Zirconium dioxide
NiO	Nickel oxide
CeO_2	Cerium oxide
MgO	Magnesium dioxide

pHVDS	Polyhexavinyldisiloxane
$Mg(OH)_2$	Magnesium hydroxide
$Ca_3(PO_4)_2$	Calcium phosphate
HMDSO	Hexamethyldisiloxane
AlF_3	Aluminium fluoride
VTMS	Vinyltrimethoxysilane
AF	Phenolic resin
Tris–HCl	Tris–hydrochloride buffer
PLA	Polylactic acid
PU	Polyurethane
PMMA	Polymethyl methacrylate
PVDF	Polyvinylidene fluoride
PVDF-HFP	Poly(vinylidene fluoride-co-hexafluoropropylene)
PTFE	Polytetrafluoroethylene
PEI	Polyethyleneimine
PI	Polyimide
POSS	Polyhedral oligomeric silsesquioxane
PEO	Poly(ethylene oxide)
PEG	Poly(ethylene glycol)
PAN	Polyacrylonitrile
PVC	Poly(vinyl chloride)
PVB	Polyvinyl butyral
PET	Poly(ethylene terephthalate)
PVA	Poly(vinyl alcohol)

PEDOT	Poly(3,4-ethylenedioxythiophene)
PEEK	Polyether ether ketone
PEI	Polyethyleneimine
PBI	Polybenzimidazole
BPO	Benzoyl peroxide
TMPM	3-(trimethyloxysilyl)propyl methacrylate
TEOS	Tetraorthosilicate
MS	Molecular sieve
SMF	Sulfonated melamine formaldehyde
T_m	Melting temperature
T_g	Glass transition temperature
MD	Machine direction
TD	Transverse direction
CO_2	Carbon dioxide
N_2	Nitrogen
W_d	The dry separator weight
W_w	The wet separator weight
A	The area of the separators
ρL	The density of the liquid
V_m	The separator volume
τ	Tortuosity
R_o	Resistivity of the dry separator
R_s	Resistivity of the wet separator
LSV	Linear sweep voltammetry

EU	Electrolyte uptake
JIS	Japanese Industry Standard
G	Gurley value
η_{air}	Air viscosity
V	Volume
L	Separator thickness
d	Separator thickness
ΔP	Pressure difference
SS	Stainless steel
R_b	Bulk resistance
σ	Ionic conductivity
R_0	The impedance before polarization
R_S	The impedance after polarization
ΔV	Voltage difference
I_0	Initial values
I_S	Final values
CE	Coulombic Efficiency
SSBs	Solid-state batteries
SSEs	Solid-state electrolytes
PEs	Polymer electrolytes
SPEs	Solid polymer electrolytes
GPEs	Gel polymer electrolytes
SCEs	Solid ceramic electrolytes
CPEs	Composite polymer electrolytes

HSEs	Hybrid solid-state electrolytes
EC	Ethylene carbonate
DEC	Diethyl carbonate
PC	Propylene carbonate
DMC	Dimethyl carbonate
EMC	Ethyl methyl carbonate
FEC	Fluoroethylene carbonate
DFEC	Difluoroethylene carbonate
$LiPF_6$	Lithium hexafluorophosphate
$NaPF_6$	Sodium hexafluorophosphate
LiFSI	Lithium bis(fluorosulfonyl)imide
$LiCoO_2$	Lithium cobalt oxide
$LiFePO_4$	Lithium iron phosphate
Li_2MnO_4	Lithium manganate
Na_2MnSiO_4	Sodium manganese orthosilicate
CNT	Carbon nanotubes
LiMnO	Lithium Manganese Oxide
$Li_4Ti_5O_{12}$	Lithium titanium oxides
$Li[NiCoMn]_{1/3}O_2$	Lithium nickel manganese cobalt oxide
NCA	Lithium nickel-cobalt-aluminum oxide
NCM523	Nickel-manganese-cobalt
NVP	N-Vinylpyrrolidone
$NaClO_4$	Sodium perchlorate
SEM	Scanning electron microscopy

EDS	Energy dispersive spectrometer
WAXS	Wide-angle X-ray scattering
X_c	Crystallinity
L_{hkl}	Crystal size
FWHM	Full width at half maximum
ATR-FTIR	Attenuated Total Reflection, Fourier Transform Infrared
XPS	X-ray photoelectron spectroscopy
TGA	Thermo-gravimetric analysis
DCS	Differential scanning calorimetry
ΔH	The heat of fusion
LECA	Liquid electrolyte contact angle
EU	Electrolyte uptake
LSV	Linear sweep voltammetry
EIS	Electrochemical impedance spectroscopy

TABLE OF CONTENTS

LIST OF FIGURES

LIST OF TABLES

CHAPTER 1. Introduction and Background

1.1. General background on porous polymeric membranes

Porous polymeric membranes (PPMs) have drawn scientists' attention since they can combine the features of porous structures with functional polymers [1; 2]. Due to their combination of specialized qualities such as permeability, manufacturing simplicity, fouling resistance, selectivity, chemical and thermal stability, and low cost, PPMs have been widely used in industrial processes [3]. They can be used extensively in various fields, for instance, filtration or/and separation materials, adsorption materials, gas storage and separation, battery separators, sensors, and electrode materials for energy storage (**Figure 1-1**) [1]. Manufacturing processes of polymeric membranes have been industrialized mostly depending on the characteristics of the base components and the anticipated uses. For their production, porous polymeric membranes can be made by several methods. Usual approaches include phase inversion, melt-spinning, and cold-stretching, electrospinning, track etching, and sintering, while novel technologies include phase separation micromolding, imprinting/soft molding, manual punching, and three-dimensional (3D) printing [3]. Moreover, a number of methods have been reported for fabricating porous membranes, for example, thermally induced phase separation (TIPS), vapor-induced phase separation (VIPS), non-solvent induced phase separation (NIPS), phase separation micromolding (PSμM), and biaxial stretching technology [4]. Among these techniques, the biaxial stretching process is considered to be one of the best commercial processes for producing microporous membranes and has achieved great success in the entire polymer industry [5]. The biaxial stretching process can be simultaneously, sequentially, or multi-stage stretching "for example, a combination of both simultaneous and sequential stretching" [6]. The biaxial stretching is the process of stretching a polymer in the machine direction (MD) and transverse direction (TD). During the stretching procedure, the polymer chains are oriented in two perpendicular directions, resulting in a polymer film with balanced properties in both MD and TD [7]. In addition, owing to the long-chain nature of semi-crystalline polymers, stretching is an effective process that can change/improve the crystalline properties of the polymer, thereby obtaining membranes with excellent mechanical and thermal properties with a high productivity rate [5].

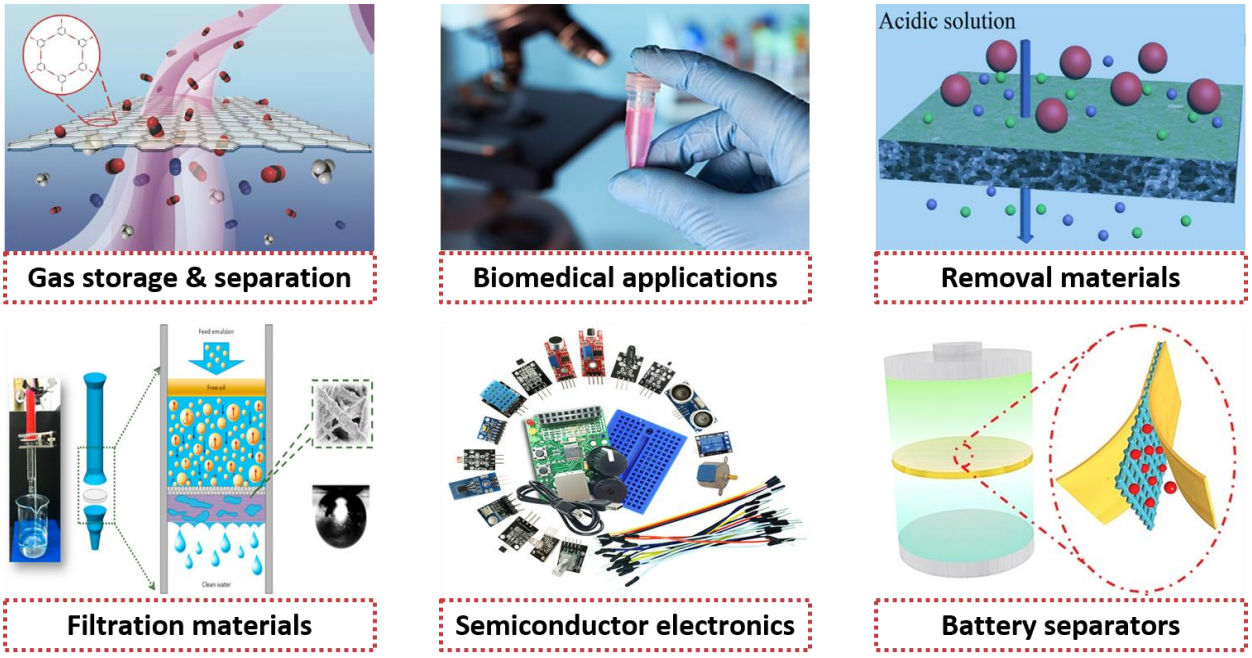

Figure 1-1: Porous polymeric membranes applications.

The polymeric composite membrane is a modified type of polymeric membranes with nano particles materials distributed in their matrices. Polymeric nanocomposite membranes have been widely applied in organic solvent nanofiltration, water treatment, gas separation, direct methanol fuel cells, sensor applications, fuel cells and battery separators. The development of composite separators by adding, coating, and incorporation of micro-and nano-sized ceramic fillers in polymer membranes like (PE) result in improved mechanical strength, wettability, thermal stability, and ionic conductivity of the PE separator by facilitating the rapid migration of lithium/sodium ions through membrane microstructure, which is considered one of the most actively researched procedures to improve the performance and safety of battery separators. Various representative inorganic ceramics nanoparticles (INPs) were used for developing composite separators, including silicon dioxide (SiO_2), aluminium oxide (Al_2O_3), aluminium oxide hydroxide known as boehmite (AlOOH), titanium dioxide (TiO_2), cerium oxide (CeO_2), magnesium dioxide (MgO), nickel oxide (NiO), and zirconium dioxide (ZnO_2). Inorganic ceramic particles can be coated or grafted onto the surface of PE separators or incorporated directly into the PE matrix to fabricate composite membranes. This considerably improves the physicochemical and electrochemical performance of these two types of composite membranes [8]. Numerous previous studies have verified the importance of inexpensive, simple-to-use inorganic micro/nanomaterials to construct composite

separators for battery applications, improving separators' thermal and mechanical properties and electrolyte uptake capacity [9]. The composite membranes made by coating inorganic ceramic nanoparticles onto the polymer substrate surface with the help of binders are called inorganic particle-coated composite membranes. The composite membranes formed by grafting organic-inorganic materials onto polymer substrates using irradiation treatments such as plasma and electron beam are called inorganic nanoparticle-grafted composite separators. Inorganic particle-filled composite membranes are constructed by directly mixing inorganic nanofillers into the polymer matrix. Commonly, inorganic ceramic nanoparticles are coated directly and construct an organic-inorganic network structure on the PE substrate surface through the doctor blade casting process, deep-coating, sol-gel coating, or grafting. The hydrophilic nature of ceramic nanoparticles can provide affinity towards electrolytes, which enhances electrolyte uptake and ionic conductivity. The inorganic nanoparticles' high melting temperature and the binder's adhesive nature can produce a thermally stable coating for the separator and offer superior heat resistance [10]. However, specific difficulties exist in inorganic particle-coated composite PE membranes: (1) With the incorporation of inorganic particle-coating layers on the PE separator, the thickness increases and the porosity inevitably decreases, leading to higher internal resistance and decreased energy/ power density. (2) The interaction strength between the inorganic particle-coating layer and the polymeric substrate is weaker because of the differences in their chemical and physical characteristics. (3) Given the difference in expansion coefficients between the inorganic particle coating and the polymer matrix, the ceramic particle coating layer on the separator frequently peels off during charge/discharge processes. Regardless, inorganic ceramic particle-filled composite separators can suitably tackle these difficulties. Physical and chemical stability are improved by directly incorporating inorganic particles into the polymer matrix. Further, it improves the separator's and electrolyte's affinity, reducing the internal resistance, which increases the ionic conductivity. Accordingly, the results suggest that the inorganic particle-filled composite membrane separators outperform the inorganic ceramic particle-coated composite membranes in terms of overall performance.

1.2. Battery separators

The demand for practical applications of batteries is expanding daily. Secondary batteries for energy storage and conversion have accelerated rapidly in recent years, particularly in the last decade (**Figure 1-2**).

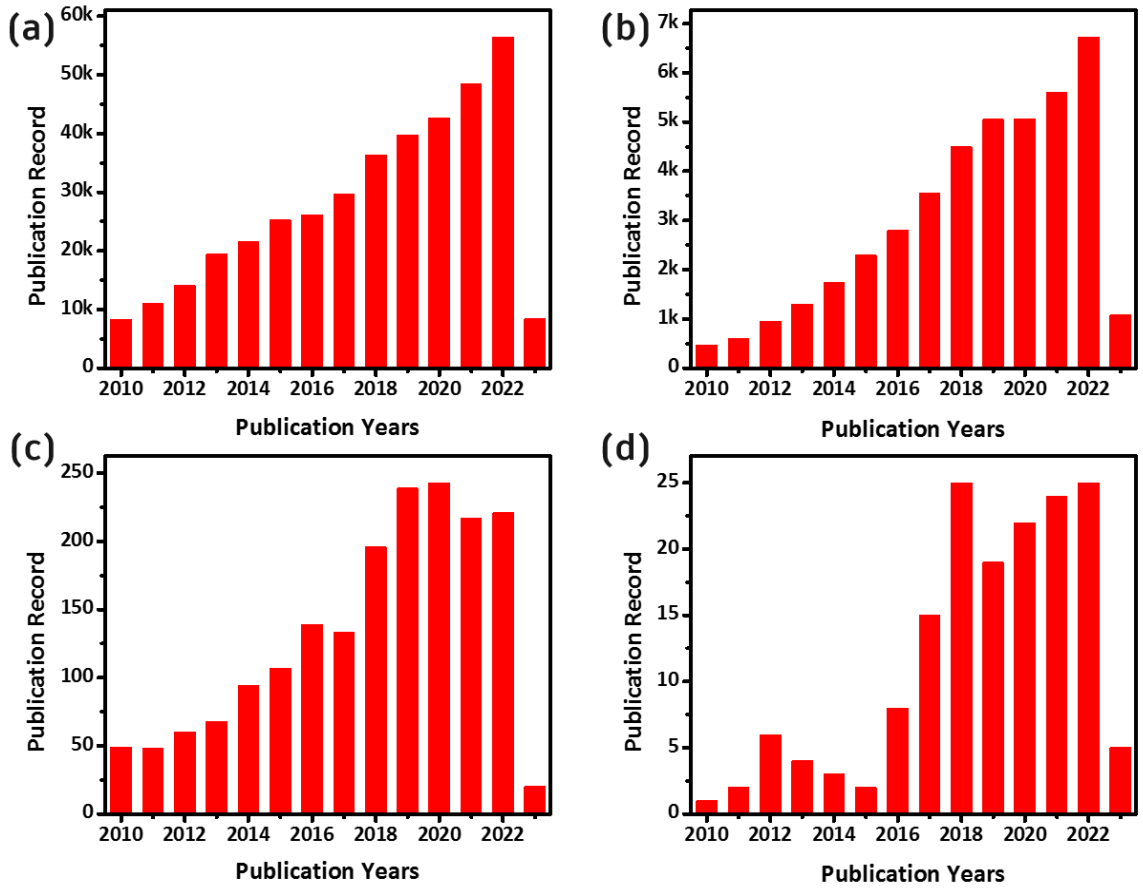

Figure 1-2: The number of publications dealing with lithium/sodium ion batteries and polyethylene separators used in each. The keywords used for the search in web of science (**a**) lithium batteries "Topic", (**b**) lithium batteries + polyethylene separator "Topic", (**c**) sodium batteries "Topic", and (**d**) sodium batteries + polyethylene separator "Topic". Refined by: Publication Years: 2010-2023. (Data collected from web of science on March, 2023).

Secondary lithium-ion batteries (LIBs) are regarded as the most favourable and dominate a vast majority of the market for large energy storage systems in a variety of applications (**Figure 1-3**), ranging from electronic devices and electric vehicles to our everyday uses (e.g., power tools, mobile phones, laptops, digital cameras, etc.) [11-15]. Recently, the commercial use of sodium-ion

batteries (NIBs) as an alternative to LIBs has aroused increasing attention due to their availability and low cost, relying on the earth-abundant and nontoxic sodium ions (Na^+) as charge carriers [16; 17]. Given this, their impact on the entire modern globe will remain more in-depth. It's challenging to make a fair assessment between current LIB technology, which has been in use since 1991, and NIB technology, which is nearly in the engineering industrialization stage. The elemental structure/compositions of sodium (Na^+) are similar to those of lithium (Li^+), so material testing processes are equivalent, and manufacturing procedures are comparable. Considerable efforts continue to be made to develop the technologies for both Li/Na-ion batteries to reach a greater level of safety and steadfastness, lower industrial and experimental costs, and accomplish a long service life with higher energy densities and fast energy charge rates [18]. Components of the cell, electrode manufacturing steps, and cell preparations were deeply investigated [19-21].

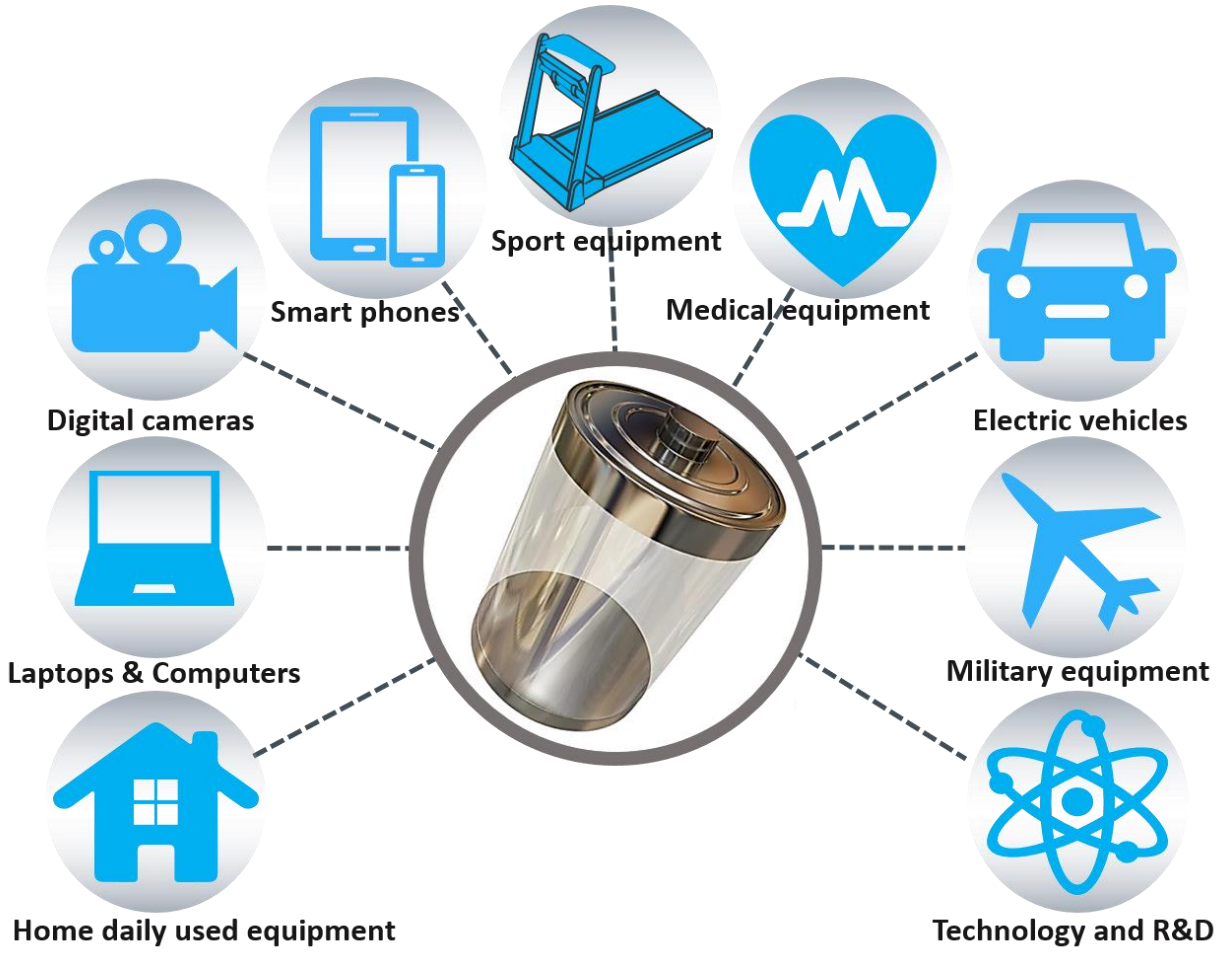

Figure 1-3: The modern applications of secondary batteries.

The typical architecture of rechargeable LIBs and NIBs involves the following components: a current collector, liquid electrolyte, porous membrane separator, and electrodes, which are the cathode (positive electrode), and an anode (negative electrode) (**Figure 1-4**) [22; 23].

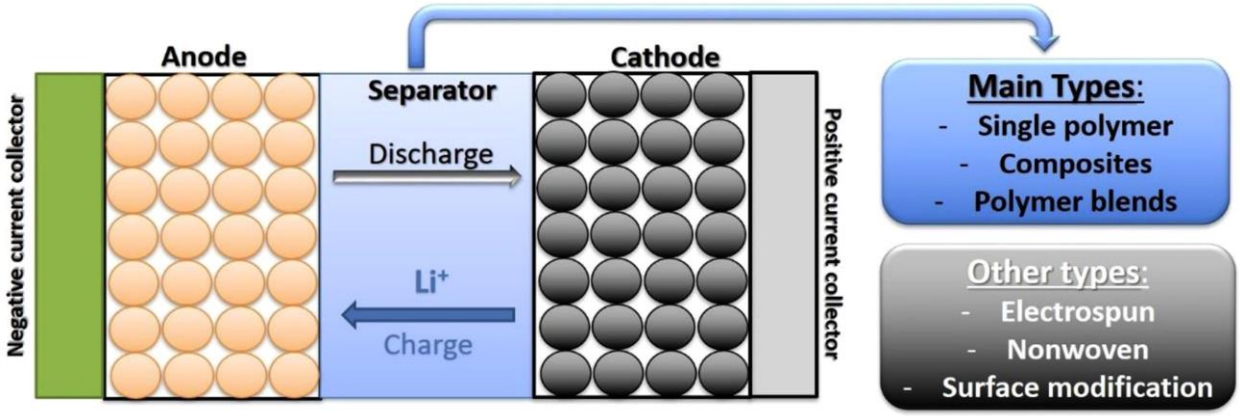

Figure 1-4: Schematic illustration of the major battery components and the various battery separator types [24].

Typically, the slurry-casting technique is used for preparing commercial electrodes (**Figure 1-5**). The conductive agent (e.g., carbon black), active powder materials (cathodes and anodes), a polymer binder (e.g., PVDF), and solvent, e.g., N-Methyl-2-pyrrolidone (NMP), are prepared and cast onto metal foils. Polyethylene (PE) membrane is regarded as the most commercialized polyolefin separator for LIBs and NIBs, which have the benefits of excellent chemical/mechanical properties, interconnected microporous networks, and good electrochemical performance and stability [25; 26]. However, they have poor thermal stability, which may cause safety issues at elevated temperatures. As their melting point is low, they suffer inevitable thermal shrinkage at high temperatures, causing an internal short circuit. Another major drawback of PE separators is their natural hydrophobic surface behavior, which results in poor wettability toward polar liquid electrolytes. Although commercial PE separators may not be well compatible with NIB electrolytes, the optimizations of PE separators extensively developed for LIBs over a long period represent a perfect scenario for developing ideal separators for NIBs. Moreover, there is still no single ideal separator for all batteries that provides optimal performance under all operational circumstances.

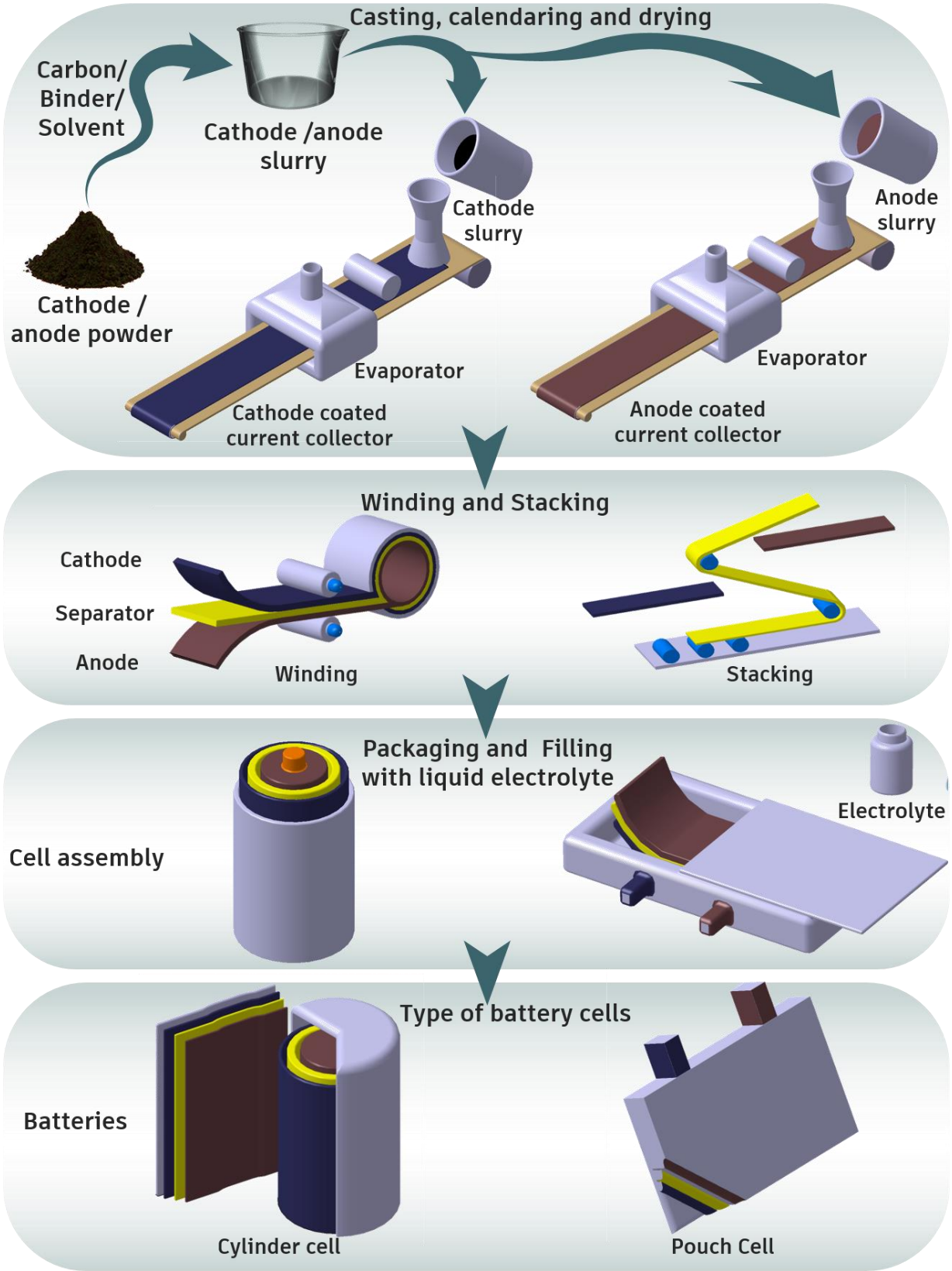
Casting, calendaring and drying
Carbon/
Binder/
Solvent
Cathode /anode
slurry
Cathode
slurry
Anode
slurry
Cathode /
anode powder
Evaporator
Evaporator
Cathode coated
current collector
Anode coated
current collector
Winding and Stacking
Cathode
Separator
Anode
Winding
Stacking
Packaging and Filling
with liquid electrolyte
Electrolyte
Cell assembly
Type of battery cells
Batteries
Cylinder cell
Pouch Cell

Figure 1-5: Simplified overview of large-scale cell manufacturing chain and components of commercial Li-ion/Na-ion batteries. For LIBs, the commonly used cathode current collector is aluminium (Al) foils, and the anode current collector is based on copper (Cu) foil. In comparison, NIBs enable Al current collectors to be used on both anode and cathode. The active cathode materials in LIBs are mainly based on transition metal oxides, e.g., lithium cobalt oxide ($LiCoO_2$) and lithium iron phosphate ($LiFePO_4$). In contrast, various cathode materials were investigated to be employed in NIBs, including polyanionic compounds and transition metal oxides, for instance, sodium manganese orthosilicate (Na_2MnSiO_4) [27]. Carbon-based active materials (e.g., graphene and carbon nanotubes (CNT)), and non-carbon composite-based active materials, e.g., lithium titanium oxides ($Li_4Ti_5O_{12}$), are extensively used LIBs anodes. In contrast, NIBs usually use hard carbon as anode active materials.

Accordingly, given the limitations of conventional PE separators, numerous methodologies have been applied over the last few decades to mitigate these limitations and construct safe and advanced separators for LIBs and NIBs with improved performance and stability [28]. Among these optimizations, composite separators based on PE and various inorganic nanoparticle materials were extensively developed. The most commonly used inorganic materials for optimizing the performance and safety of microporous PE separators are based on ceramic oxides with high melting temperatures and excellent affinities for electrolytes, such as SiO_2 [29-32], Al_2O_3 [33; 34], TiO_2 [35], and ZrO_2 [36; 37]. Composite PE separators offer considerable benefits and fewer drawbacks than conventional PE separators. Overall, composite PE separators afford improved thermal stabilities, excellent electrolyte wettability, and exceptional ionic conductivities, increasing battery performance and safety.

1.3. The motivation of the study and objectives

Polyethylene (PE) separators are the most widely used in rechargeable lithium/sodium-ion batteries (LIBs/NIBs) due to their advantages, including excellent mechanical properties, electrochemical stability, and low cost. Nonetheless, the surface of the PE separator is non-polar and has poor wettability to the organic electrolyte. Besides, it has a low melting point (130-138 °C) and tends to shrink at high temperatures, which is always a significant invisible threat to the battery. One straightforward strategy is introducing and add in multifunctional and thermostable inorganic

ceramic materials on the surface of PE separators. In recent years, numerous researchers have developed methodologies for constructing composite membranes to overcome the limitations of PE separators and improve the overall battery performance by grafting or coating with hybrid organic-inorganic materials and blending with other polymers. However, each modification process has advantages and shortcomings, such as increasing cost and compromising the battery separator's properties and electrochemical performance. Attracted by their excellent thermal stability and outstanding wettability in addition to good mechanical properties comparable to other materials, INPs proved to be promising materials to improve thermal stability, considerably improving the physicochemical properties and the electrochemical performance of polyolefin-based battery separators. INPs can promote the absorption of the liquid electrolyte to achieve a good electrolyte uptake during the charge-discharge process, which will enhance the battery's performance. Manufacturing composite membranes using the scalable biaxial stretching process is anticipated to provide better solutions for the battery separator field for various reasons, such as the fabrication process has already been commercialized and is widely used in the industry and can be scalable and customized. It can combine the fabrication of the PE microporous separator and SiO_2 NPs modification in one step. Mixing SiO_2 nanoparticles with VHMWPE polymer can also guarantee electrochemical stability, maintain mechanical properties, enhance thermal properties, and obtain higher battery performance. Furthermore, the combination of SiO_2 nanoparticles and VHMWPE polymer can provide an alternative way of using it to overcome challenges in high-performance composite separators for energy storage systems. Driven by the problems detailed above, with the aim of contributing to the search for solutions, the main goals and objectives of this work were:

- ★ To study and understand the role of biaxial stretching technology when blending organic (VHMWPE)-inorganic silica (SiO_2) nanoparticles materials.
- ★ To process and fabricate commercial VHMWPE-SiO_2 nano-composite separators via the scalable biaxial stretching for batteries.
- ★ To characterize and study the influence of different quantities of SiO_2 on VHMWPE microporous membranes as a comparative system to understand the behavior and structure of VHMWPE film before and after the combination of SiO_2.

- ★ Apply the high-energy electron beam (E.B) irradiation for crosslinking without post-treatments toward enhancing commercial separators and improving the thermal and mechanical properties.
- ★ To investigate the influence of E.B irradiation crosslinking on the microstructure, mechanical and thermal properties of nanocomposite VHMWPE-SiO_2 separators.
- ★ To modify VHMWPE separators with organic-inorganic nanocomposite layers Inspired by the unique advantages of dopamine and inorganic boehmite.
- ★ To deeply characterize and understand the surface morphology, pore size, chemical structure and composition, mechanical properties, and thermal behavior/shrinkage of nanocomposite membranes.
- ★ To examine the performance of the as-prepared and modified nanocomposite microporous membranes/separators in rechargeable lithium/ sodium ion batteries including electrolyte uptake, porosity, electrolyte wettability and uptake, ionic conductivity, charge-discharge performance and electrochemical stability and safety.

1.4. Research Methodology

The research will be conducted within four tasks:

- ➘ Literature survey, with the purpose of gathering and collecting scientific information related to microporous membranes, their fabrication technologies, modifications, and applications in batteries.
- ➘ Experimental plans including the selection of appropriate materials, picking scalable and commercialized process route to construct microporous membranes in order to obtain final nanocomposite membrane separators with as-expected properties.
- ➘ The characterization of the nanocomposite membranes including surface morphologies, chemical structure & compositions, thermal stability, mechanical properties, wettability, and dimensional stability (thermal shrinkage).
- ➘ Measure the performance of electrochemical parameters for the as-prepared nanocomposite membrane separators in rechargeable batteries including

electrolyte uptake, porosity, electrolyte wettability, ionic conductivity, electrochemical stability, rate capabilities, charge-discharge and cyclic performances.

1.5. Thesis organization

The thesis covers six chapters divided as following.

- **Chapter 1** generates an overall introduction and background of the work. Some background information on porous polymeric membranes, battery separators for energy storage, rechargeable batteries (e.g., LIBs and NIBs) and their typical architecture, the motivation of the study and objectives are also given.

- **Chapter 2** provides an overview and discusses the significance of microporous membrane separators in lithium/sodium-ion batteries (LIBs and NIBs). The basic requirements and properties of an ideal separator are briefly described with respect to LIBs and NIBs. It summarizes assorted classifications of porous separators based on their chemical/ mechanical stability, physiochemical properties and electrochemical performance in batteries: microporous membranes, non-woven membranes, modified microporous membranes, composite membranes, and electrolyte membranes. At the end, a summary of some composite membranes based on PE matrix using ceramic nanoparticles (NPs) materials for modification, their preparation processes, and electrochemical performance as separators for rechargeable batteries.

- **Chapter 3,** we describe successfully prepared hybrid very high molecular weight polyethylene (VHMWPE)/silicon dioxide (SiO_2) nanocomposite membranes via a sequential biaxial stretching process to produce microporous membranes used as separators in LIBs. The chapter systematically investigates the influence of SiO_2 on the structure and properties of VHMWPE membranes through various

characterizations techniques. It also reveals details on the achieved excellent performance of hybrid VHMWPE/SiO_2 nanocomposite membranes as revealed by their properties and their evaluated electrochemical performance when used as separators in LIBs.

- **Chapter 4** covers a deep study on the combining the industrialized biaxial stretching technique with the high-energy electron beam irradiation (E.B) crosslinking procedure to produce hybrid VHMWPE/SiO_2 separators modified by E.B irradiation for LIBs. The chapter intensely studies the impacts of the E.B irradiation cross-linking on the microstructure, mechanical and thermal properties, electrolyte absorption/wettability, and electrochemical performances of E.B cross-linked VHMWPE/SiO_2 separators.

- In **Chapter 5,** we describe successfully advanced hybrid inorganic-organic separator by incorporating heat-resistant boehmite (BH) and multipolar self-polymerizing dopamine (DA) onto biaxially stretched polyethylene (BSPE) membranes for lithium/sodium metal batteries (LMBs/NMBs). The chapter gives a detailed discussion of the fabrications, macrostructure and physiochemical properties the hybrid layer modified PE separators. In addition, it discloses details on the achieved excellent performance of the hybrid PE membrane separators as revealed by their evaluated electrochemical performance in LMBs and NMBs.

- Last but not least, **Chapter 6** concludes the whole work covered in this thesis and provides the outlook for further directions.

CHAPTER 2. Literature Review

2.1. Background on porous membrane separators

Membrane engineering has emerged as an indispensable part of modern society because it represents well-established technologies in a wide range of applications in our day-to-day lives, ranging from environmental remediation, and petrochemicals to energy storage and conversion. Porous membrane separators (PMS) based on polymers have conquered an enormous percentage of the membrane market with vast growth possibilities in energy storage systems (ESS) due to their cost-effectiveness, lightweight, manufacturing scalability, low environmental impact, adjustable pore size, energy efficiency, and ability to adjust their properties and performance in response to demands [38; 39]. Due to their unique advantages and superior performance, polymer-based membrane separators are considered the heart of any secondary battery (e.g., lithium/sodium ion batteries) [40]. The porous polymeric separator's core purpose is to avoid direct electrical touch while simultaneously playing a significant function in delivering ions between the positive (cathode) and negative (anode) electrodes [41]. For years, scientists have been searching for the most scalable, cost-effective, environmentally friendly, and reliable polymeric membranes for ESS survivability by achieving high performance, extending service life, and safeguarding batteries. Currently, porous membrane separators made of polyolefin materials, for instance, polyethylene (PE), polypropylene (PP), PE/PP and PP/PE/PP, are commonly adopted in commercial batteries because of their excellent mechanical properties, strong chemical stability, adequate porosity, and controllable thicknesses. Furthermore, polyolefin-based porous membranes offer several advantages, including successful commercialization through versatile manufacturing procedures. In industrial production, biaxially stretched polyethylene (BSPE) through the wet process and uniaxially stretched polypropylene (PP) through the dry process have become the main focus for the preparation of polyolefin-based microporous membranes for secondary batteries (**Figure 2-1**) [40]. The wet method is a procedure that includes mixing, heating, solidification (extrusion), stretching (biaxial stretching), solvent extraction, and heat treatment. In this process, polyolefins are first merged with hydrocarbon liquid (paraffin oil), anti-oxidant materials, and other additives at high temperatures (above their melting temperature T_m) to make a homogeneous solution using a twin-screw extruder. The homogeneous composite solution is then extruded onto a chill roll to

produce casting films (gel-like sheets). The gel-like films are biaxially stretched in both the machine direction (MD) and the transverse direction (TD), simultaneously or sequentially, followed by the extraction of the solvent and heat treatment stages [42]. Finally, microporous polyolefin membranes with interconnected pore architectures and good mechanical characteristics are achieved. For more information, DeMeuse, Mark T. reported a comprehensive overview of the wet process [43].

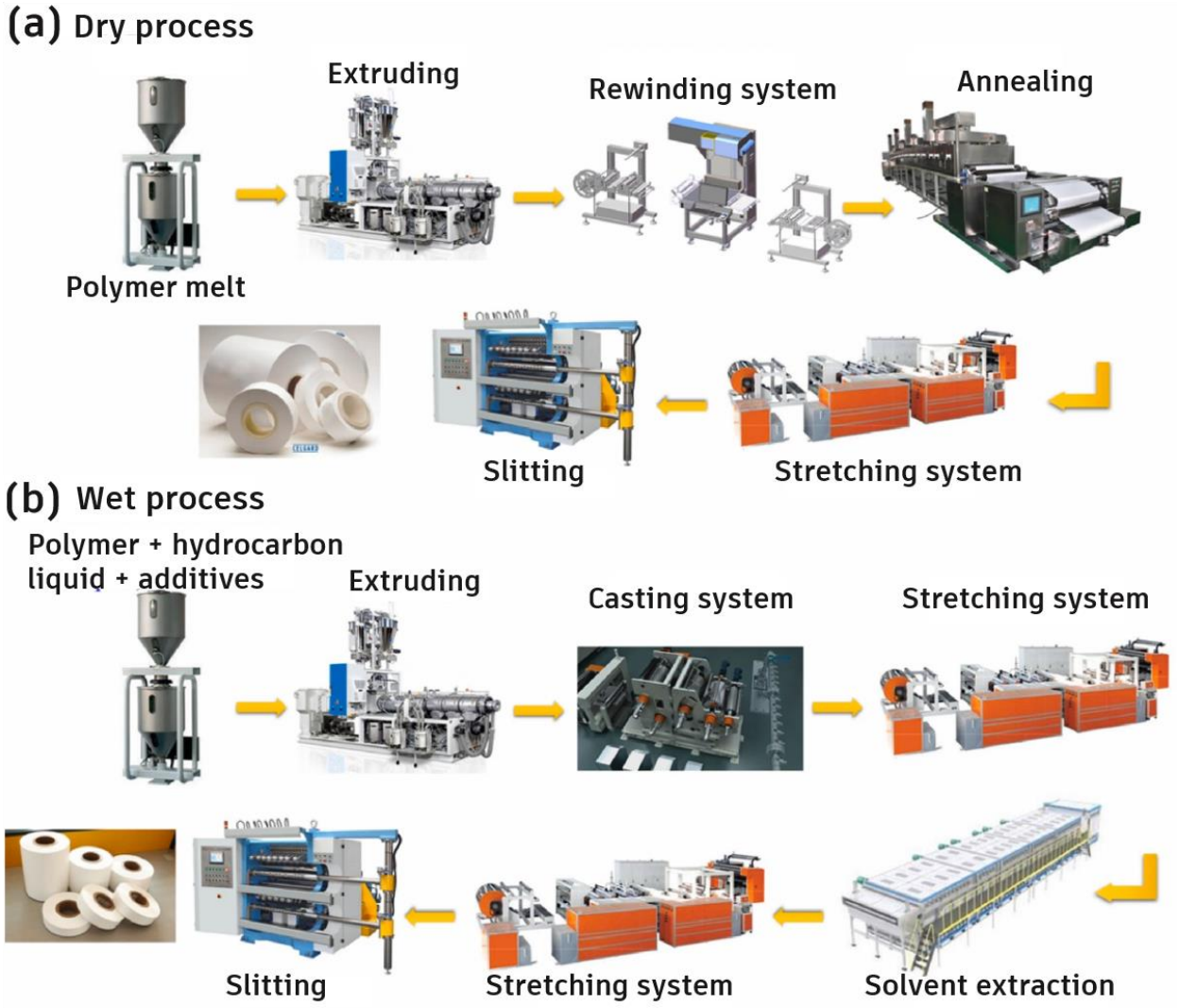

Figure 2-1: Industrial fabrication processes of the microporous membranes: (a) dry process, and (b) wet process [44].

In the dry process, there are four fundamental steps: (i) extrusion, (ii) annealing, (iii) stretching, and (iv) heat setting. In this process, polyolefins are melted at high temperatures, extruded and cast or blown into a film, and then annealed to produce non-porous polyolefin films

with high crystallinity and controllable crystallite size. The melt is then stretched at high temperatures in the machine direction (MD) to peel off the crystal interface [44]. A row of lamellar crystal structures is produced during this process, and the lamellar interface is then torn during uniaxial stretching, forming highly-oriented slit-like micropores. The dry process is suitable for polymers with higher crystallinity and has the advantages of simple operation, environmental protection, and increased productivity. However, the membrane prepared by this method shows no stretch in the transverse direction and easily gets torn apart during production. DeMeuse, Mark T et al. [45] reported a comprehensive and detailed overview of the dry process. Polyolefin microporous membranes' morphology and porous structure can be controlled by stretching parameters (e.g., temperatures, speed, draw ratio, etc.). Dry-processed membranes are better suited for high-power-density batteries due to their open and straight porous structure. Wet-processed membranes are better suited for long-cycle life batteries because their interconnected pores and tortuous microstructures help to avoid dendrite formation during charge-discharge operation [13].

2.2. The purpose of this review chapter

Scientists' significant concern is heading for the preparation and development of novel separators for high-performance batteries. Accordingly, to provide academics with as much data and content on battery separators as possible, scientists have reported numerous reviews on the field of LIBs separators and few for NIBs separators. Most of them focus on describing different categories of separators, their requirements, production, applications, and performance, but rare scientists comprehensively discuss a specific type of separator. This chapter provides an overview and discusses the significance of microporous membrane separators in lithium-/ sodium-ion batteries. The basic requirements and properties of an ideal separator are briefly described with respect to LIBs and NIBs. The chapter introduces and summarizes assorted classifications of porous separators based on their chemical/ mechanical stability, physiochemical properties and electrochemical performance in batteries: microporous membranes, non-woven membranes, modified microporous membranes, electrolyte membranes, and composite membranes. More importantly, this chapter surveys the historical background of the recent progress and highlights recent scientific achievements in preparing, designing, and developing composite separators based on polyethylene (PE) membranes and their applications in lithium/sodium ion batteries.

2.3. Basic requirements and features of battery separators

As a vital unit of Li-ion/Na-ion batteries, the porous membrane separator must possess several fundamental aspects and specific characteristics to ensure the consistent operation of the batteries. The ideal membrane separator for rechargeable LIBs and NIBs batteries requires numerous characteristics, including isolation, continuous pores, high affinity toward organic liquid electrolytes, and good mechanical strength during cell assembling. In addition, the separator must have a low resistance to the permeability of Li^+/ Na^+ ions during charge-discharge operations and excellent thermal resistance in high thermal conations. Also, under abnormal circumstances, the separator's micropores block to prevent penetration of lithium ions and shut off the current [46]. Although membrane separators are generally inactive parts of the battery, their network and characteristics are critical to battery safety, rate capability, energy density, and reusability [47]. Commonly, the separator continues to fail as a result of one of the following reasons: (i) high temperatures cause the separator to soften, shrink, or even burn; (ii) accidental interference and damage by extrusion and collision, resulting in direct contact between the positive (cathode) and negative (anode) electrodes; and (iii) metal dendrites generated by overcharging penetrate the separator, resulting in an internal short circuit [48]. Regarding those mentioned above, the ideal separator must have the following features: (1) It must have unique characteristics to avoid the formation and growth of dendrites. (2) Excellent chemical and electrochemical stability for organic liquid electrolytes and electrode materials. (3) It has a remarkable thermostability when used at higher temperatures. (4) Robust mechanical characteristics that withstand strain and stress throughout the cell-assembly process. (5) The porosity of the separator should be adequate to provide outstanding electrochemical performance. (6) Superb wettability to absorb liquid electrolytes toward achieving extraordinary ionic conductivity and outstanding electrolyte uptake. (7) Thickness and corrosion resistance are other significant characteristics required. Concerning these fundamentals, the distinctive structural characteristics of separators are presently attracting considerable interest since they represent an essential option for battery development. Thus, several factors must be considered when selecting a separator for battery applications. **Table 2.1** summarizes the general requirements and demands for separators used in rechargeable batteries (in the case of separators for LIBs) *[49; 50] [51]*. As illustrated in **Figure 2-2**, these factors are categorized as structural properties, physical/chemical properties, functional properties, and other necessary properties.

Table 2.1: General requirements for separators used in batteries (e.g., typical LIBs)

Parameter	Requirement
Thickness (μm)	20 − 25
Pore size (μm)	<1
Porosity (%)	40 − 60
Permeability (Gurley) (s μm^{-1})	<0.025
Shutdown temperature (°C)	~130
High temperature melt integrity (°C)	>150
Electrical resistance ($\Omega - cm^2$)	<2
Puncture strength (g μm^{-1})	>300/25.4
Mechanical strength (MPa)	98.06 (>1000 kg cm^{-1})
Ionic conductivity (S cm^{-1})	$10^{-3} - 10^{-1}$
Wettability and uptake	Become wet fast and absorb sufficient electrolyte
Transference number	The closer to 1, the better the battery performance
Thermal shrinkage (%)	<5% after heat annealing at 90 °C for 60 minutes
Dimensional stability	Must lay flat without any shrink and curl
Electrochemical/chemical stability	Long-term stability in batteries

2.3.1. Structural properties

2.3.1.1. Morphology and pore structure

The microstructural morphology of membrane separators for LIBs and NIBs plays an essential role in the batteries' performance, safety, and sustainability. The separator should have a uniform morphology and unique pore size distribution, affecting the current distribution within a cell. Microscopy techniques usually characterize the microstructure of the separator, e.g., scanning electron microscopy (SEM). The size and interconnection of separator pores can influence how

well the electrolyte is absorbed into the separator structure. The pore size should be large enough to transport lithium/sodium ions through the absorbed liquid electrolyte but small enough to prevent internal short circuits. Separators used in lithium/sodium batteries must have pore sizes that are smaller than the particle size of their electrodes' components (for example, active materials and conductive additives) [52]. The pore size of the separator should be distributed uniformly and must be less than 1μm [13]. This ensures uniform current distribution and ion flow stability through the separator while hindering lithium growth on the anode. High porosity will reduce the mechanical strength of the separator, bring possible hazards, and low porosity will be detrimental to electrolyte storage and increase battery resistance. Moreover, the wide pore size distribution of separators leads to inhomogeneous Li/Na-ion flux during charging-discharging operation, potentially inducing the growth of Li/Na dendrites puncturing the separator, thereby causing a terrible safety hazard [53]. The size and distribution of separator pores can be assessed and evaluated by capillary flow porometer [52].

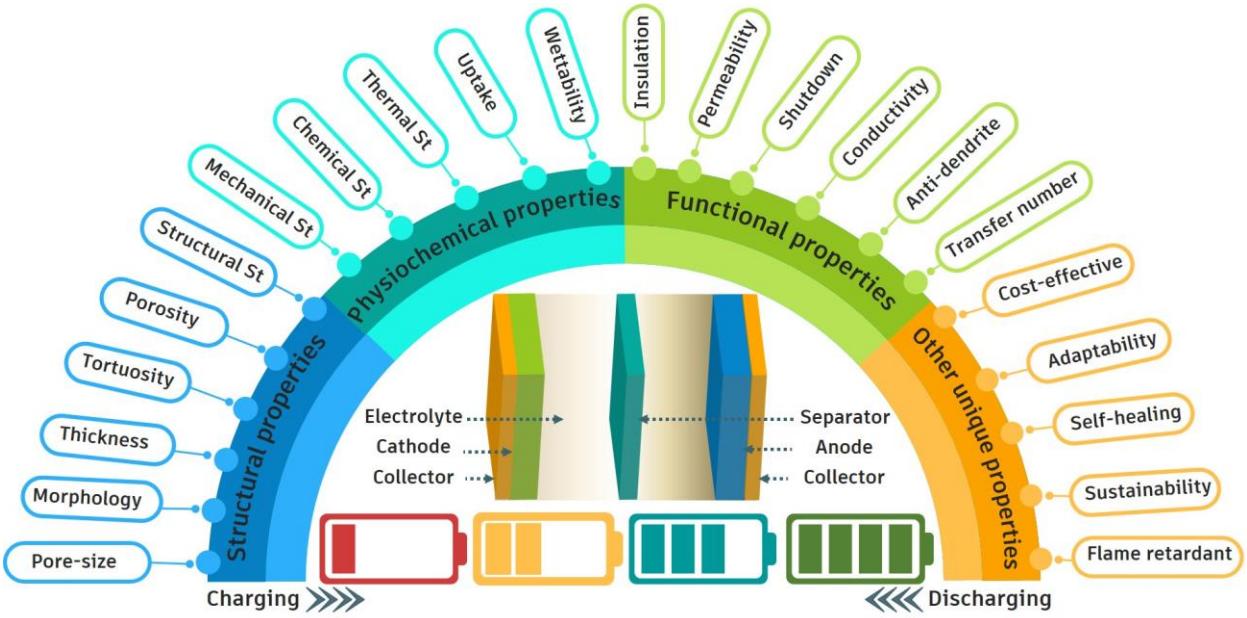

Figure 2-2: The basic requirements and characteristics of battery separators (St for stability).

2.3.1.2. Thickness

High-energy battery applications require a minimum thickness of separators. Nevertheless, this negatively affects the mechanical strength of separators and their safety. The thickness of the

separator should be uniform to sustain stability for as many charging-discharging cycles as possible and provide uniform Li^+/Na^+ transfer, thereby delaying the formation of dendrites. Typically, commercially available PE separators have a 25 μm thickness [54]. The thicker the membrane, the more stable it is against punctures, which means higher ion diffusion resistance. The thinner separator enhances the energy capacity and rate capability by increasing contact area and decreasing internal resistance [55]. Because the internal electrical resistance of battery separators can be reduced by decreasing their thickness, the thinner separator facilitates higher rate capacities and higher current densities across the membrane [52]. Moreover, thinner separators qualify for thinner electrodes, which means smaller batteries with comparable power and more cycles can be manufactured. In addition, the separator should be of uniform thickness to promote uniform current distribution for the duration of cell operation [56].

2.3.1.3. Porosity and tortuosity

The porosity of the separator is an essential factor in battery performance. In general, the porosity of separators should be greater than 40%, with pore dimensions typically less than 1 μm. Commercial membrane separators used in LIBs typically have porosity values in the 40-60% range, which is required for efficient and fast ion transmission. High porosity contributes to better electrolyte uptake and lowers internal resistance, improving battery performance [49]. Mechanical properties typically decrease as separator porosity increases. Accordingly, these two characteristics of the separator have opposite trends. Therefore, the trade-off between these two properties is important for battery separator performance. An extremely huge porosity may conceivably impede the separator's ability to shut down. In addition, uniform porosity and pore size distribution are needed within the entire area of the separator to get identical current distribution [52]. Therefore, optimizing the porosity of the separator is crucially important for the electrochemical performance and safety of the battery [48]. Porosity represents the ratio of pore volume to separator volume and can be calculated according to the following Eq. (2-1):

$$\textbf{Porosity}\ (\%) = (\boldsymbol{W_w} - \boldsymbol{W_d}) / (\boldsymbol{\rho_L} \times \boldsymbol{V_m}) \times \mathbf{100}\% \qquad \textbf{(2-1)}$$

where $\boldsymbol{W_d}$ represents the dry separator mass and $\boldsymbol{W_w}$ is the wet separator mass after being immersed in liquid, $\boldsymbol{\rho_L}$ represents the liquid density, and $\boldsymbol{V_m}$ is the volume of the separator.

The tortuosity (τ) refers to the membrane's average pore conductivity that offers an intermediate value to allow a low ion diffusion resistance but high enough to avoid dendrite growth. Increasing the tortuosity of the separator can hinder dendritic growth, but it can also increase ionic resistance. If the thickness and porosity of the separator remain constant, the tortuosity will be reflected in the permeability [56]. The tortuosity (τ) can be calculated using the following Eq. (2-2) [48]:

$$\boldsymbol{Tortuosity}\ (\boldsymbol{\tau}) = \mathbf{Sqrt}\left(\boldsymbol{\varepsilon} \times \frac{\boldsymbol{R_s}}{\boldsymbol{R_o}}\right) \qquad \textbf{(2-2)}$$

where R_o *and* R_s symbolize the resistivity of separator before and after immersion in electrolytes. The geometric transfer coefficient $\delta=\varepsilon/\tau$ indicates the effective ionic transfer capacity of the separator geometry.

2.3.1.4. Structural stability

In rechargeable batteries, the structural stability of the membrane separator is an essential property to guarantee that the morphology, dimensions, thickness, and porous of separators remain without damage by battery materials (e.g., active materials of electrodes and conductive additives). The separator in LIBs and NIBs must be structurally and chemically stable to the liquid electrolytes because the separator is not part of the oxidation-reduction (redox) reaction that produces an electrical current. The separator operates under strongly oxidizing and reducing conditions. Thus, they must have not only excellent structural stability but also great mechanical properties and be able to withstand high stress during cell assembly and operation. The structure should be kept after electrolyte soaking (swell, shrinkage, and wrinkle) [20].

2.3.2. Physical and chemical properties

2.3.2.1. Mechanical properties

The mechanical strength of the battery separator must be high enough to handle the cylindrical battery winding machine and survive the tension during cell assembly, making it the primary factor contributing to the safety of the battery cell. The mechanical strength of the membrane separator is crucial in battery preparation, cell assembly, and the prevention of Li

dendrite formation. Separator mechanical properties are characteristically represented by puncture and tensile strength in both the machine/transverse directions (MD/TD). The materials and manufacturing process determine the mechanical strength of the membrane separator. The separator's microstructure morphology, thickness, pore size, and porosity significantly impact mechanical strength. The membrane separator must be flexible and have a high tensile strength when stressed or compressed during manufacturing, storage, and applications to safeguard the battery and guarantee excellent insulation of opposite electrodes [57]. According to ASTM D882 and D638, the minimum tensile strength of separators with a thickness of 25 μm is 98.06 MPa [13]. When battery separators are wet with liquid electrolytes, their mechanical properties will change dramatically [58]. Commonly, mechanical abuse is caused by vehicle collisions and battery pack penetration, which can cause a battery to short-circuit and burn the cells. Thus, the excellent mechanical strength of the battery separator can ensure structural integrity in the probability of an accident crash.

2.3.2.2. Puncture strength

The battery separator must be physically strong and have sufficient puncture strength to withstand the basic battery fabrications (e.g., handling procedures and cell assembly) and operation processes (e.g., charge-discharge cycling). The puncture strength of the separator is the maximum force required for the needle to pass through the separator entirely. The high puncture strength increases the resistance of the separator to dendrite penetration during the battery operation under harsh circumstances [56]. It can be determined by the materials used in its manufacture along with the method of manufacture. The puncture strength of the separator can be improved by optimizing some polymer features (e.g., high polymer entanglements and orientation) [59]. Separators with a puncture strength (> 300 g for 25 μm thick) keep both electrodes electrically isolated during cell assembly and protect against dendritic penetration during operations [20].

2.3.2.3. Chemical and electrochemical stability

The electrochemical stability of the separator is a critical factor for its practical applications in LIBs and NIBs. The membrane separator must be chemically stable against the cell components, including electrodes (cathode and anode) and liquid electrolytes, especially in highly reducing and

oxidizing conditions when the battery is completely charged. The separator chemical stability can be estimated by measuring the wear resistance, expansion rate, and contraction after immersion in electrolytes for a while (e.g., immersion for 4 to 6 h at 50 °C) [56; 60]. In addition, the separator must be electrochemically stable and satisfied under the reducing and oxidizing conditions during the charging and discharging cycles. The electrochemical stability window describes how the oxidative decomposition of the electrolyte on the positive electrode can lead to battery safety hazards [61]. The wide electrochemical window is a necessary feature for advanced electrochemical performance. The electrochemical stability window of the membrane/separator can be determined via linear sweep voltammetry (LSV). To test oxidative decomposition, an electrolyte-soaked separator is placed between a stainless steel (SS) working electrode and an ion metal as a counter and reference electrode at a adjustable scanning rate and voltage range [62].

2.3.2.4. Thermal stability and dimensional shrinkage

The membrane separator's thermal and dimensional stability behavior is essential for avoiding thermal runaway and guaranteeing battery safety. Although the thermal stability of separators could not entirely prevent the battery from runaway, it is still a crucial requirement in protecting cells [63]. When the temperature rises to the separator's meltdown temperature, a thermal runaway occurs because of the breakage of the separator, leading to a short circuit between the two electrodes (cathode and anode) [61]. Likewise, winding, bending, and tilting the separator during battery assembly can cause contact between the cathodes and anodes, resulting in an internal short circuit. Membrane separators must remain stable (lower thermal shrinkage, excellent dimensional stability) during battery operation, even at high temperatures. The suggested requirement for thermal shrinkage in both directions (MD and TD) for separators is less than 5% after heating at 90 °C for 60 minutes. The following formula (Eq. 2-3) can be used to calculate the thermal shrinkage percentage of separators.

$$\textbf{Thermal shrinkage}\ (\%) = (\boldsymbol{L_0} - \boldsymbol{L_1})/\boldsymbol{L_0} * \mathbf{100}\% \qquad \textbf{(2-3)}$$

where $\boldsymbol{L_0}$ and $\boldsymbol{L_1}$ are the length of separators in MD or the width of separators in TD before and after annealing at different temperatures, respectively.

2.3.2.5. Electrolyte wettability and uptake

One of the most crucial parameters for the performance of LIBs and NIBs is indeed the wettability of the battery separator by electrolytes, which is generally affected by the surface structure and the chemical properties of the separators [64]. The separator should have good electrolyte wettability to realize effective ion transmission and minimize internal resistance. The poor electrolyte wettability of the separator results in a non-uniform transfer of ions across the separator, which results in non-uniform Li^+/Na^+ deposits on the electrodes, leading to a short circuit in batteries. Incomplete and non-uniform wetting causes an inhomogeneous distribution of current density, influencing cell performance and causing dendrite formation in the anode, posing a safety risk [65]. Therefore, improving the electrolyte wettability of the separator is key to promoting uniform Li^+/Na^+ deposition/dissolution in LIBs and NIBs. Contact angle measurements and electrolyte uptake can be used to investigate the wetting behaviour of separators. The contact angle test is used to evaluate the wetting speed of the separator with electrolytes, which depends on the separator type and microstructure [48]. The angle between the separator surface and the curvature of an electrolyte droplet will be small if the separator has a great affinity for liquid electrolytes. However, if the separator seems to have a low affinity for liquid electrolytes, it will have a large contact angle. The high electrolyte uptake (EU) can ensure rapid ion transmission, which results in superb ionic conductivity. EU can be determined by soaking separators in electrolytes for a particular time and calculated according to Eq. (2-4):

$$\boldsymbol{Electrolyte\ uptake\ (EU) = (W_a - W_b)/W_b * 100\%} \qquad \textbf{(2-4)}$$

where $\boldsymbol{W_b}$ is the dry separator weight and $\boldsymbol{W_a}$ is the wet separator weight (after immersed).

2.3.3. Functional properties

2.3.3.1. Air permeability

The air permeability of the separator is determined by numerous morphological aspects, including thickness, porosity, pore size, and pore size distribution. The Gurley number is a standard parameter used to define air permeability [44]. The Gurley value is commonly used to express the MacMullin number, which is proportional to air permeability. As defined by the

Japanese Industry Standard (JIS), the Gurley value is the time in seconds it takes for 100 cm^3 (100 ml) of air to pass through a separator area (2.54 cm^2) at a pressure difference of 12.40 cm of water (1.21 kPa) [47]. The Gurley value is often used to characterize separators because the test is accurate and easily performed. In addition, it can be done in a fast time frame. Also, deviations from specific values are a good indicator of problems; thus, Gurley values can be used in quality control situations. The Gurley value (G) can be calculated by Eq. (2-5) [48]:

$$\textbf{Gurley value } (\boldsymbol{G}) = (\boldsymbol{\eta_{air}} \times \boldsymbol{V} \times \boldsymbol{L}) / (\boldsymbol{\kappa} \times \boldsymbol{\Delta P} \times \boldsymbol{A}) \qquad \textbf{(2-5)}$$

where η_{air} is the air viscosity, V is the air volume, L is the separator thickness, κ is the permeability, ΔP is the pressure difference, and A is the area of the separator.

2.3.3.2. Electric insulation and resistivity

The separator must have a high electrical insulator to maintain electrical isolation between the cathode and anode and avoid short-circuiting between those electrodes. In general, polymeric separators are electrical insulators since they are organic compounds linked by covalent bonds with an evenly distributed electron density between the joining atoms. The existence of polar groups such as (-OH) in the polymer chains' periphery, the conjugation of double bonds in the conducting polymers, or the incorporation of metal nanoparticles accounts for the insulation properties [66]. In practice, commercial separators have an electrical resistivity of 10^{12} – 10^{14} [20].

2.3.3.3. Shutdown effect

The separator with a thermal-shutdown function is also crucial to prevent thermal runaway by shutting down the battery's electrochemical reaction. When the shutdown happens, the porous polymeric membrane becomes a nonporous isolating layer between the two electrodes. Thus, separators with a thermal shutdown function can successfully block ion transport and cut off the current at a specific elevated temperature. In the meantime, they should be able to preserve their dimensional and mechanical integrity to prevent direct contact between electrodes [14]. Generally, thermal-shutdown separators consist of at least two kinds of materials. On the one hand, one of the materials has an appropriate melting point, and it will melt to close the pore of a separator when the battery is heated abnormally. On the other hand, other materials must have a high melting point

to prevent the cathode and anode from short-circuiting [48]. The melting point of the materials should be lower than the battery's thermal-runaway temperature. The type, molecular weight, crystallinity, and process history of the separator define its ability to shut down the battery. For example, ultra-high molecular weight PE will have different shutdown features than high-density PE, showing various shutdown features compared to low-density PE. Additionally, PP/PE/PP trilayered structure separator is a popular approach employed to shut down lithium ions' conduction pathway and has already been commercialized. As the battery's internal temperature exceeds 130 °C, the PE layer gradually melts, shutting the pores inside the separator and preventing ion permeation, while the PP layer offers mechanical support to maintain overall dimensional stability and preventing internal short-circuiting. Typically, the separator shutdown is monitored by analyzing the separator's impedance as the temperature climbs linearly. In LIBs, a shutdown temperature of 130 °C is typically adequate to manage cell heating and inhibit thermal runaway [59].

2.3.3.4. Ionic conductivity

Ionic conductivity is indeed one of the most crucial features of battery separators. It indicates how quickly and significantly charged ions can pass through the separator. The conductivity of Li^+/Na^+ ions between the electrodes is associated with the absorbing capacity of electrolytes by separators. The measurement unit of the ionic conductivity (σ) is Siemens (S) per meter (m). Siemens (S) is the resistance/impedance unit. The ionic conductivity of an electrolyte-containing separator is typically in the range of 10^{-3} to 10^{-1} S/cm. There are numerous ways for calculating the ionic conductivity. The most representative and commonly used way to estimate the ionic conductivity is that the bulk resistance (R_b) must first be determined by electrochemical impedance spectroscopy (EIS) [56], which will then be used to calculate the ionic conductivity by the following formula Eq. (2-6):

$$\textbf{Ionic conductivity } (\boldsymbol{\sigma}) = \boldsymbol{d/RA} \qquad \textbf{(2-6)}$$

where σ is the ionic conductivity (S cm^{-1}), $\boldsymbol{R}$ is the bulk resistance/impedance, $\boldsymbol{d}$ is the separator thickness, and $\boldsymbol{A}$ is the separator surface area.

2.3.3.5. High Transference number

The transference number (also denoted as the transport number) is the fraction of the total charge in the battery carried by the primary ion type. The perfect strategy is to have only the main ion type (involved in the intercalation of electrodes) carry the charge. In the case of LIBs, this ion is Li^+, and for NIBs, this ion is Na^+. When ions in electrolytes transport charges from one electrode to another, not all charges are carried by the same type of ion. As a result, another important property to consider when estimating electrolytes is their transference number, as they provide an essential route for their ion's transport. The high migration and storage state of Li^+/Na^+ ions are excellent determinants for identifying whether the battery can function normally and efficiently. For instance, the transference number in LIBs (t_{Li^+}) is defined as the relative quantity of the transferred Li^+ compared to the counter anion, which is generally less than 1 [67]. t_{Li^+} influences the charge-discharge rate, energy density, and service life of batteries. If only half of the total charge is carried by ions, then the transference number is 0.5. The closer the t_{Li^+} is to 1, the faster the battery's charging rate will be. The transference number in LIBs (t_{Li^+}) can be calculated by Eq. (2-7).

$$\boldsymbol{t_{Li^+} = \frac{I_S(\Delta V - I_0 R_0)}{I_0(\Delta V - I_S R_S)}} \qquad \textbf{(2-7)}$$

($\boldsymbol{R_0}$ and $\boldsymbol{R_S}$) the impedance before and after polarization, ($\boldsymbol{I_0}$ and $\boldsymbol{I_S}$) the initial and final values of the variation of steady-state current, and ($\boldsymbol{\Delta V}$) the constant voltage value of 10 mV [68].

2.3.3.6. Anti-dendrite

Lithium/ sodium metals are among the most promising anodes for next-generation batteries because of their unique properties. Metallic lithium, for example, has a high specific energy density, a low anode potential, and a low weight density. However, utilizing lithium metal as an anode in batteries remains challenging since the lithium dendrite created during the Li^+ ion plating/stripping process can pose issues such as low coulombic efficiency, rapid capacity fading, electrolyte consumption, and safety risks. The formation of dendrites is a possible cause of potential dangers in batteries since they can penetrate the separator and come into direct contact with cathode materials, resulting in short circuits and potentially causing thermal runaway or explosion threats

[69] The formation of dendrites on the anode can lead to poor overall cell performance including lower Coulombic Efficiency (CE), a shorter lifetime and increased side reactions [70]. Several parameters can influence dendrite growth, such as temperature, current density, and electrolytes [71]. As a solution, considerable attempts have been made to prevent dendrite growth in lithium metal batteries, such as developing 3D structured lithium anodes, introducing solid electrolytes, electrolyte additives, and functionally modified separators. Among these attempts, the most effective is the use of functional separators, which can inhibit the formation of lithium dendrites via mechanical barriers or regulate Li^+ ion passage and deposition without considerably increasing the weight or/and volume of batteries [72]. This modified separator with high puncture strength tends to improve the separator resistance to the penetration of dendrite [20]. The strategies for suppressing Li dendrites by functional separators can be categorized into three catalogues: (i) preventing Li dendrite growth via mechanical barriers, (ii) redistributing Li^+ ion flux when passing through the separator, and (iii) inducing uniform deposition of Li^+ nucleation sites for ions on the anode.

2.3.4. Other unique properties

In addition to the basic properties that need to be taken into account when designing battery separators, there are some new requirements for battery separators to consider as well, including cost-effectiveness, safety, flame retardancy, self-healing properties, good adaptability to the volume changes of electrodes, high Li^+/Na^+ transference number, and sustainability. Along with the above dendrite growth resistance and dimensional stability at high temperatures, the separator must be flame retardant to avoid an explosion. Thermally conductive membranes promote heat dissipation and reduce the risk of explosion, which may help minimize temperature rise under operating conditions. The cost of separators can reach 20% of the total cost of high-power LIBs, making the design of new materials and technologies for separators a critical issue for industrial applications. High wettability, nanoporous construction, dimensional stability up to 180 °C, mechanical flexibility, and robustness separators can be achieved.

2.3.4.1. Flame retardant properties

The flame retardant property of thermally stable separators is a unique characteristic. Although it is not a mandatory requirement that the separators work at high temperatures, employing a non-flammable separator will improve the battery's safety. When the temperature of the battery rises above the thermal inception, it produces uncontrollable heat, which causes a chain reaction that results in smoke, fire, and even explosions, putting people's lives and property in jeopardy. Therefore, the rechargeable battery's uncontrollable temperature rise has significantly hindered the battery industry's development [48]. When batteries burn out, the separator can continue functioning correctly, preventing further degradation and possibly acting as a fire extinguisher. To be precise, a lighter is used to fire the separator. It is characterized as "flammable" if the separator is burnt all at once and continues to burn after the lighter is withdrawn. "Self-extinguishing" refers to a fire that stops after the lighter is removed. When there is no burning at all during the firing action, the separator is regarded as "flame retardant" (continued for at least 30s) [73]. Therefore, developing advanced commercial separators with excellent flame retardant properties is urgently needed for next-generation and safe energy storage devices. Three different approaches can be used for creating battery separators with flame-retardant features [74]: (1) the development of the non-flammable polymer by nature as a matrix with the introduction of inorganic nanoparticles to improve electrochemical performance or other properties. (2) through nanocomposite technology, flame retardant additives can be incorporated into the matrix by dispersing and mixing them into the polymer during the separator preparation. (3) the coating and attaching of flame retardant additives to the surface of polymeric separators (e.g., polyolefin separators) through adhesives to achieve flame retardancy. They are usually derived from laboratory-synthesized or industrially available products and include halogen-or phosphorus-containing elements. This process has been widely applied for the optimization of polyolefin separators. For example, Lei Song et al. prepared an advanced sandwiched separator with outstanding flame retardant and significantly enhanced electrochemical performance by simply coating ammonium polyphosphate and silica on a commercial polyolefin matrix [69]. Yi Cui et al. proposed a flame-retardant, electrochemically stable separator by covering the surface of the commercial PE separator with flame-retardant additives that are insoluble in the electrolyte [75].

2.3.4.2. Good adaptability and compatibility to electrolytes/electrode volume changes

Separators adaptable well to electrode volume variations can prevent contact failure between the separator and electrodes during lithium plating and stripping, resulting in a stable electrolyte/electrode interface throughout battery cycling [76]. Besides, a separator's good adaptability and chemical compatibility are adventurously anticipated to bear superior chemical stability and wettability for organic electrolytes. Initially, the separator must be compatible with other battery components such as electrodes and electrolytes while ensuring that it does not interact with them and maintaining its structural integrity. Boosting the separator's and electrodes' compatibility is an effective strategy to mitigate dendrite growth and volume expansion. The separator should also have a strong affinity for liquid electrolytes and a high porosity to store adequate electrolytes, which will help prevent electrolyte leaks eventually [48]. The self-healing materials have high viscoelasticity, allowing them to better adapt to electrodes' volume changes and improve their wettability. In the meantime, the self-bonding ability of the self-healing polymer can prevent contact failure caused by cracks during cycling [77]. Due to their different electrolyte solutions (organic solvents and conductive salts) and electrode materials, sometimes separators for LIBs cannot be directly employed for NIBs. Commercial porous PP and PE separators demonstrate poor wetting behavior for NIB electrolytes with high-viscosity solvents such as propylene carbonate, significantly increasing interfacial resistance and reducing ion transfer numbers. Therefore, considering the slight differences between LIBs and NIBs, mainly their electrolytes and electrodes, it is essential to give special consideration to engineering high-safety separators toward satisfying the rapid development of both LIBs and NIBs according to their characteristics.

2.3.4.3. Self-healing properties

Self-healing properties such as fiber-reinforced polymer composites, self-healing coatings, and self-healing ceramics are relatively new research directions in materials science and batteries. Batteries are made of components and interphases that operate in thermodynamically metastable conditions and are subject to various degradation processes [21]. Because of the chemical/mechanical degradation of separators and the formation of dendrites, damage and cracks easily occur during battery operation. Self-healing capabilities refer to the separators' ability to mend damage and cracks on their own, which enhances battery safety, quality, and reliability and

can extend the separators' service life and efficiency [76]. Preventive procedures such as coatings and additives can improve batteries' safety, quality, longevity, and reliability as they operate under various conditions that significantly impact the ageing process, such as temperature, current density, and mechanical stress [21]. Particularly, self-healing approaches to battery systems should be developed for different components of the cell and their functionalities should indeed be synchronized with the battery cell chemistry. Emerging technologies and the ongoing development of all-solid-state electrolytes such as solid polymer electrolytes (SPEs) in LIBs can enhance safety and have self-healing behavior. Considering that some damaged or broken SPEs can result in severe battery failure due to a short circuit, Xue et al. fabricated a flexible, self-healing and highly stretchable SPEs via quadruple hydrogen bonding [78]. The developed SPEs was able to heal cutting damage in 2 h at 30 ℃ with no external stimuli and provide good stretchability.

2.3.4.4. Sustainability and cost-effective

Long-term and sustainable battery manufacturing requires battery separators produced and developed using industrial techniques with cost-effective and environmentally friendly materials. The production cost is also an influential factor in the commercialization of the separator. In LIBs technology, the cost of separators accounts for about 20% of the overall cost, and it is concentrated on the preparation process of the separator. Therefore, developing low-cost, simple and intelligent separator manufacturing technology can accelerate the development of the battery industry [79]. As raw materials are comparatively cheaper, reducing the thickness of separators is a perfect way to reduce costs. Contrariwise, reducing the separator thickness can increase the power and energy density of the battery but inevitably decrease its mechanical properties, resulting in another safety concern [44]. Therefore, in practical applications, trade-offs between maintaining good structural properties, performance, cost, and safety of rechargeable batteries must be balanced since their properties are equivalent and related to each other. **Table 2.2** summarizes the costs of various common polymer separator raw materials provided by He et al [49].

Table 2.2: The cost of typical polymers used in separators

NO	Polymer	Cost ($ kg^{-1})	Company
1	Polyethylene (PE)	≈1.5	LG. Co. Ltd
2	Polypropylene (PP)	≈1.5	LOTTE Chemical Co. Ltd
3	Cellulose	≈5	Dupont Co. Ltd
4	Polylactic acid (PLA)	≈5	NatureWorks
5	Polyurethane (PU)	≈6.5	Bayer Co. Ltd
6	Polymethyl methacrylate (PMMA)	≈10	LG. Co. Ltd
7	Polyvinylidene fluoride (PVDF)	≈25	Solvay S.A
8	Poly(vinylidene fluoride-co-hexafluoropropylene) (PVDF-HFP)	≈30	Solvay S.A
9	Polytetrafluoroethylene (PTFE)	≈30	Dupont Co. Ltd
10	Polyethyleneimine (PEI)	≈25	Dupont Co. Ltd
11	Polyimide (PI)	≈85	Dupont Co. Ltd
12	Polyhedral Oligomeric Silsesquioxane (POSS)	≈155	Dupont Co. Ltd

2.4. Classification and development of battery separators

The past 30 years have witnessed a growing interest in rechargeable battery separators in terms of their raw materials and enormous progress in preparation techniques, resulting in different types of separators. Recently, the most common polymeric materials used for preparing porous membranes for rechargeable batteries, such as LIBs and NIBs, are based on cellulose and its derivatives, polyethylene (PE), polypropylene (PP), polyvinylidene fluoride (PVDF), polyesters, poly(tetrafluoroethylene) (PTFE), polyimide (PI), poly(ethylene oxide) (PEO), poly(ethylene terephthalate) (PET), polyamide (PA), polyethersulfone (PES), poly(vinyl chloride) (PVC), and polyacrylonitrile (PAN), polymethyl methacrylate (PMMA) or their blends (**Table 2.3**) [41; 80-82].

Table 2.3: The chemical structures of some typical polymers used for making separators

Polymer	Chemical structure	Polymer	Chemical structure
Polyethylene (PE)	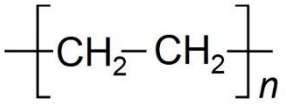	Polypropylene (PP)	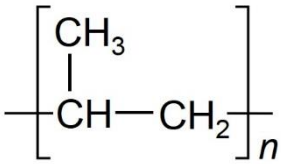
Poly(vinyl alcohol) (PVA)	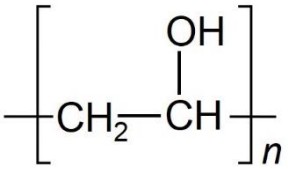	Polyvinyl Chloride (PVC)	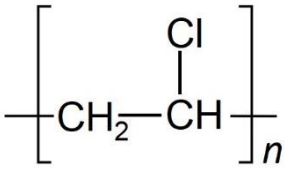
Polyvinylidene fluoride (PVDF)	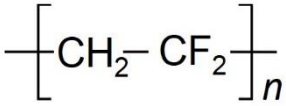	Polytetrafluoroethylene (PTFE)	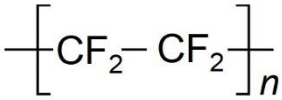
Polyacrylonitrile (PAN)	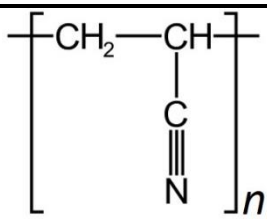	Poly(ethylene oxide) (PEO)	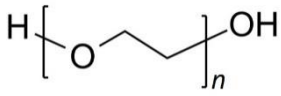
Polyimide (PI)	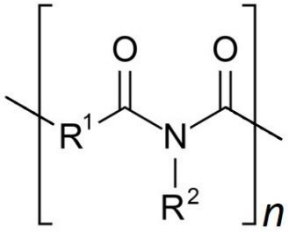	Polymethyl methacrylate (PMMA)	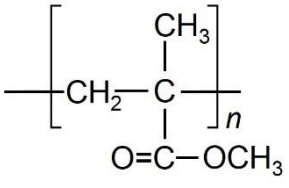

There are numerous categories of separators according to diverse structures and compositions, and each one significantly influences the battery's performance. Based on their design and construction, battery separators can be classified into five types, as shown in **Figure 2-3**: (1) microporous membranes, (2) nonwoven mats, (3) modified microporous and other porous membrane separators, (4) composite membranes, and (5) electrolyte membranes.

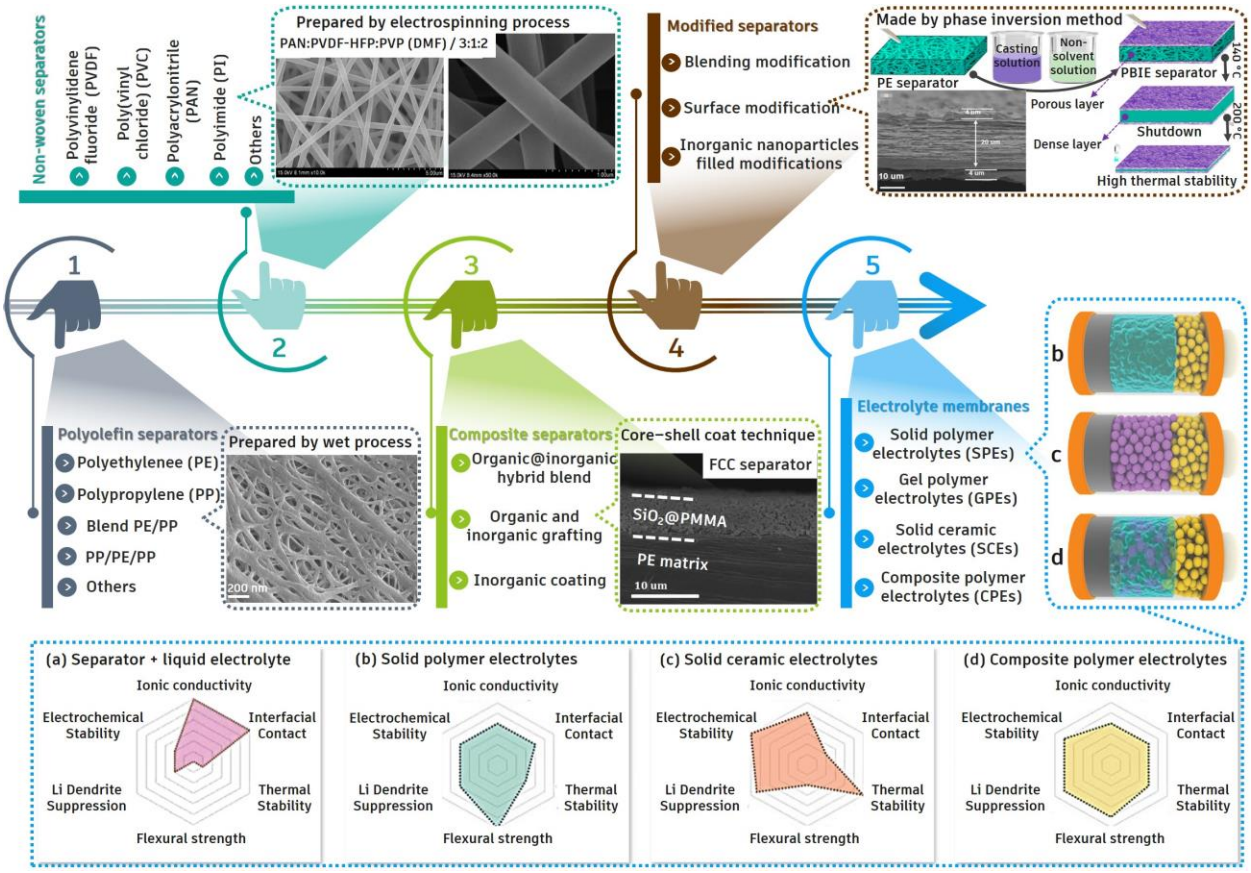

Figure 2-3: The development and classifications of battery separators. (**Part 1**) microporous polyolefin separators "SEM image of biaxially stretched PE microporous membrane made in our lab via the wet process as described in our previous report [83]". (**Part 2**) non-woven separators "SEM image of the PAN/PVDF-HFP nanofibers separator [84]. (**Part 3**) composite separators such as silica–PMMA modified PE separator "SEM cross-section of composite PE separator [30]. (**Part 4**) modified separators such as sandwich-like membrane with a shutdown function "The shutdown process and cross-section SEM images of the membrane (a) before and (b) after heat treatment at 140 °C for 0.5 h [85]. (**Part 5**) different types of electrolyte membranes and their ranking of properties compared to liquid electrolytes + separators [86].

The preparation methods have a crucial influence on the safety of separators. As summarized in **Figure 2-4**, various technologies have been utilized to construct porous polymeric membranes for batteries, including biaxial stretching process (wet/dry methods), solution casting, doctor blade coating, phase separation, electrospinning, deep coating, etc [24; 87].

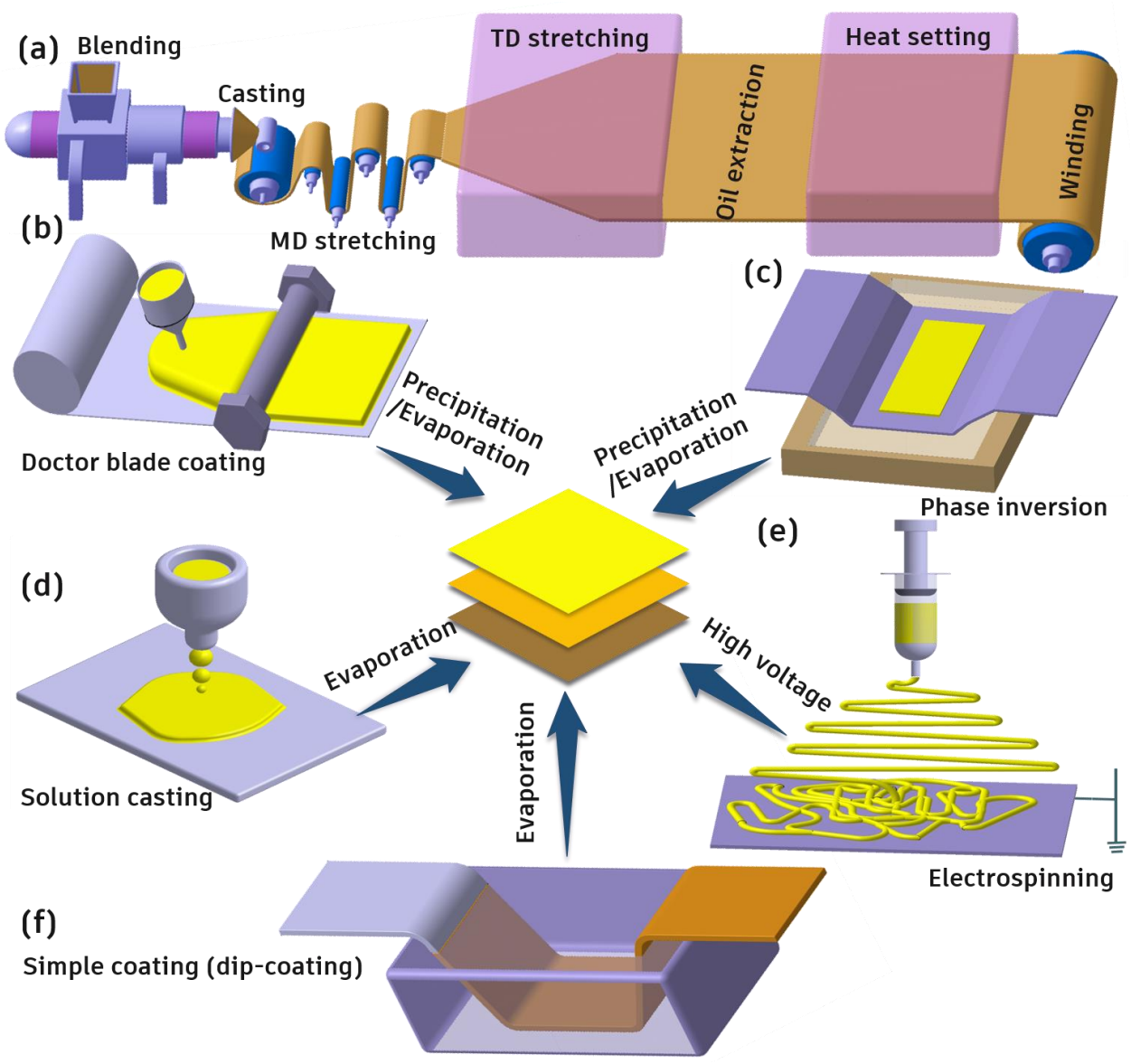

Figure 2-4: Industrial processes and modification techniques for different porous membrane separators. (**a**) Engineering biaxial stretching technique of PE separators. (**b–f**) Advanced fabrication and modification approaches include (**b**) blade casting, (**c**) phase inversion, (**d**) solution casting, (**e**) electrospinning, and (**f**) dip-coating process.

Among these numerous categories, researchers primarily focused on three kinds of porous separators: (i) polyolefin (PP or PE) composite separators modified by organic or inorganic materials; (ii) nonwoven mats prepared by electrospinning methods; and (iii) porous separators prepared by solution casting and phase inversion [48]. This section briefly summarizes the different types of membranes used for batteries and their manufacturing processes.

2.4.1. General classifications of battery separators

2.4.1.1. Microporous polyolefins membrane separators

Microporous polyolefin membranes (polyethylene (PE) and polypropylene (PP) and their blends) have occupied the commercial separator market for secondary rechargeable batteries using liquid electrolytes such as LIBs and NIBs, owing to their high mechanical strength, chemical and electrochemical stability, controllable factors such as pore size, and low production and materials costs. Unfortunately, commercial polyolefin-based membranes are rarely employed in NIBs due to the typically carbonate-based (such as propylene carbonate) electrolytes used in NIBs, which make it difficult for the separators to wholly wet and absorb adequate electrolytes [44]. Polyolefin-based microporous separators have drawbacks, such as poor thermal stability due to low melting points and flammability. Likewise, their hydrophobic nature induces poor wetting, resulting in a significant decrease in ionic conductivity and, eventually, low power densities, limiting their use in high-performance batteries. Polyolefin-based microporous membranes in high-performance batteries must be optimized with organic or inorganic materials through different preparation techniques to modify their required properties and overcome the above-mentioned shortcomings [88]. According to differing production procedures and structures, they can be classified as monolayer, multilayer, modified or composite microporous separators. The simplest microporous membrane separators used in batteries are monolayer polyolefin membranes, mainly PE or PP. Polyolefins have been broadly used to manufacture monolayer microporous separators because of their excellent mechanical strength and chemical stability [15]. Owing to the low melting point (nearly 130 °C for PE, and 165 °C for PP), monolayer separators manufactured only of PP or PE tend to experience thermal shrinkage at high temperatures. The PE-PP bilayer and PP-PE-PP tri-layer separators are the most common multilayer polyolefin separators [44]. Companies have

developed microporous multilayer membranes made of PP and PE (PE-PP bilayer and PP-PE-PP trilayer) as a favorable thermal shutdown mechanism in view of the fact that they combine the PE low-temperature shutdown capability with the PP high-temperature melt integrity (e.g., Celgard 2325) [41]. In the multilayer construction, the porosity of the PE layer collapses, and the PE layer melts after the temperature approaches its melting point, blocking the ionic conduction path, thus terminating the electrochemical reaction. Meanwhile, the PP layer can retain its dimensional structure and mechanical strength, preventing the electric short between the cathode and anode [13].

Table 2.4: Typical manufacturing process of microporous membranes for batteries

Process	Mechanism	Materials	Properties	Membranes	Producers
Wet process	Phase separation	Polymer + solvent	Isotropic film	PE	Asahi, Tonen
		Polymer + Solvent + Filler	Large pore size High porosity	PE	Asahi
Dry process	Drawing	Polymer	Simple process Anisotropic film	PP, PE, PP/PE/PP	Celgard, Ube

Table 2.5: Typical properties of some commercial microporous polyolefins membrane separators

Separator // properties	**Asahi Hipore**	**Tonen Setela**	**Celgard 2730**	**Celgard 2400**	**Celgard 2325**
Structure	Monolayer	Monolayer	Monolayer	Monolayer	Trilayer
Composition	PE	PE	PE	PP	PP-PE-PP
Porosity (%)	40	41	43	40	42
Thickness (um)	25	25	20	25	25
Gurley (s)	-	-	520	620	645
Melt temperature (°C)	138	137	135	165	135/165

Table 2.5 Summarized the typical properties of some commercial microporous polyolefins membrane separators. The typical pore structures of different types of polyolefin separators made by both dry and wet processes are presented in **Figure 2-5.** More detailed information on dry and wet processes and their representative features, properties, and performance as battery separators are intensely discussed in [13; 43-45; 50; 89].

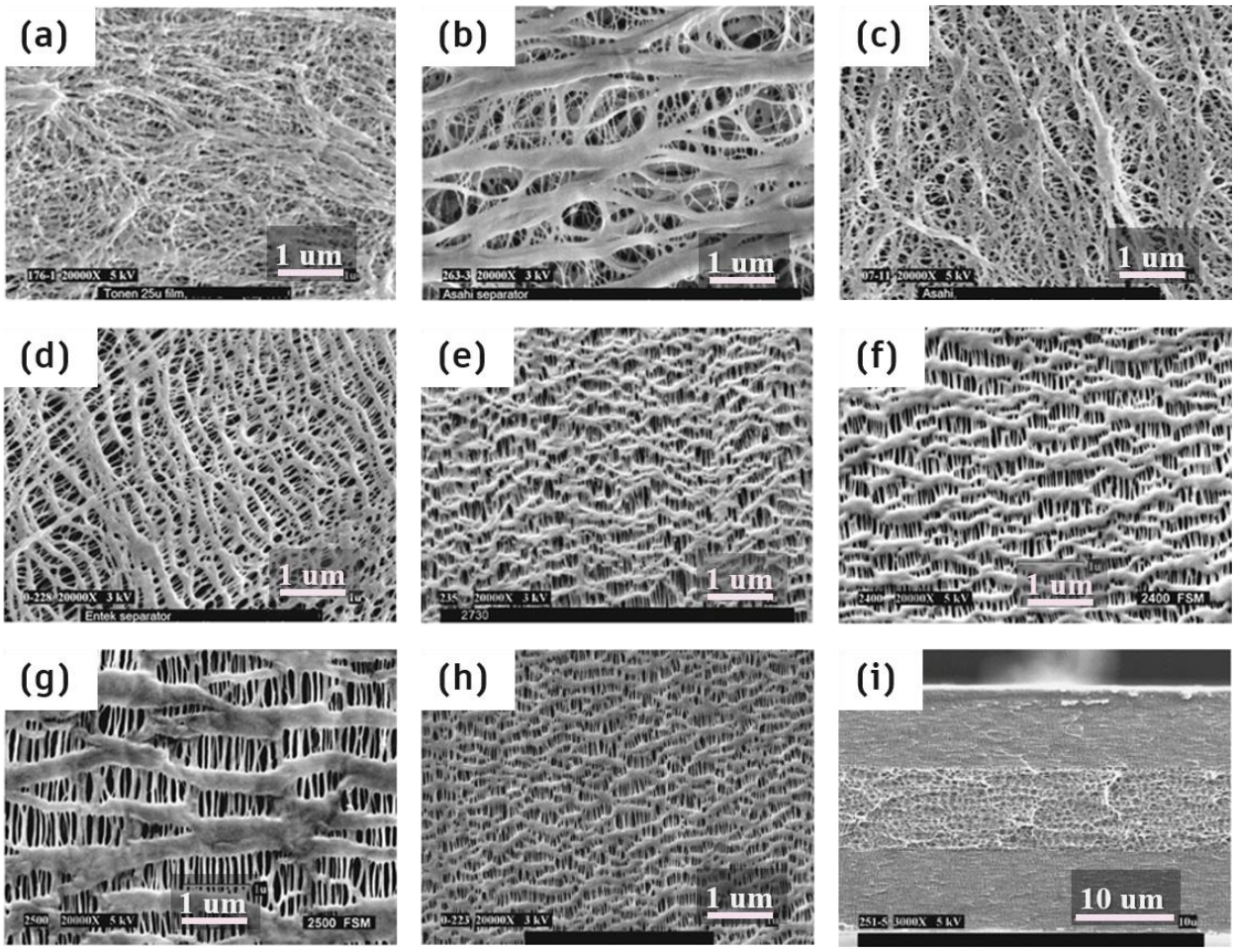

Figure 2-5: SEM micrographs of some commercial microporous polyolefins membrane separators used in batteries: (a–d) Commercial monolayer separators made by the wet process. (**a**) Setela (Tonen), (**b**) Hipore–1 (Asahi), (**c**) Hipore–2 (Asahi), and (**d**) Teklon (Entek). (**e–g**) Celgard separators made by the dry process. (**e**) 2730 (PE), (**f**) 2400 (PP), and (**g**) 2500 (PP), (**h** and **i**) The SEM surface and corresponding cross-section of Celgard 2325 trilayer microporous separator, respectively [41].

2.4.1.2. Non-woven separators

Microporous non-woven membranes made of ultra-fine fibers, which can be directionally or randomly arranged with fiber diameters ranging from several micrometers to tens of nanometers, can be constructed through an innovative and effective fabrication technique called electrospinning [90]. Based on their characteristics, polyimide (PI) [91], polyacrylonitrile (PAN) [92], polyethylene terephthalate (PET) [93], polytetrafluoroethylene (PTFE), polyvinylidene fluoride (PVDF) and its copolymer [84; 94] have been extensively produced and investigated as electrospun nanofibrous-based membrane separators. The non-woven composite separator via electrospinning is an effective strategy to coat the surface of polyolefin separators with inorganic and organic materials that have excellent properties and improved thermal stability [95]. Likewise, some heat-resistant or flame-retardant materials can be processed into non-woven separators (such as PTFE, PI, PEEK, and inorganic materials), prompting the separator to exhibit excellent heat-resistant and flame-retardant properties. Among many organic polymers, PVDF is popular and has attracted considerable attention for non-woven separators owing to its high affinity with nonaqueous electrolytes, good film-forming properties, outstanding thermal stability, good electrochemical spinning ability, and high electrochemical stability [96]. Compared to polyolefin separators, the non-woven separators produced through this technology typically have a porous structure with 30–90% porosity, a large specific surface area, a good affinity for liquid electrolytes, and high thermal stability [96; 97]. In the electrospinning approach, the slurry of polymer and additive is initially created by stirring and heating it at a particular temperature in a water bath. After that, a syringe is loaded with the blended polymeric solution, pumped through the needle, and manifests as droplets at the needle tip. The electrostatic force and surface tension compete when a high voltage is put between the needle and the collector, forming a Taylor cone. The hybrid solution from the syringe emits toward the collector in the direction of an electric field after electrostatic force surpasses the droplet's surface tension, as shown in **Figure 2-4e**. Owing to their distinct 1D structure and high porosity, which guarantees high electrolyte uptake and extraordinary ionic conductivity, electrospun nanofibrous membranes have emerged as an alternate choice for separators [11; 51]. Despite the desirable structure of electrospun non-woven separators, their fabrication process is slow, and their mechanical properties are still relatively weak, making large-scale commercialization challenging [51]. These separators, on the other hand, lack flexibility, especially

when they are thin. Consequently, one approach might be to employ them directly as coating layers on commercial separators [81]. As summarized in **Figure 2-6**, electrospun non-woven separators can be classified into; (1) monolayer separators, (2) multilayer separators, (3) modified separators, (4) composite separators, and (5) gel polymer electrolytes [98]. The monolayer separator is considered the most straightforward electrospun-based membrane, made from just one type of precursor material. The membrane structure in this method is created from randomly distributed fibers and solidified in the collector. This type of membrane has been widely used to create various electrospun separators for batteries (**Figure 2-6**) [99; 100].

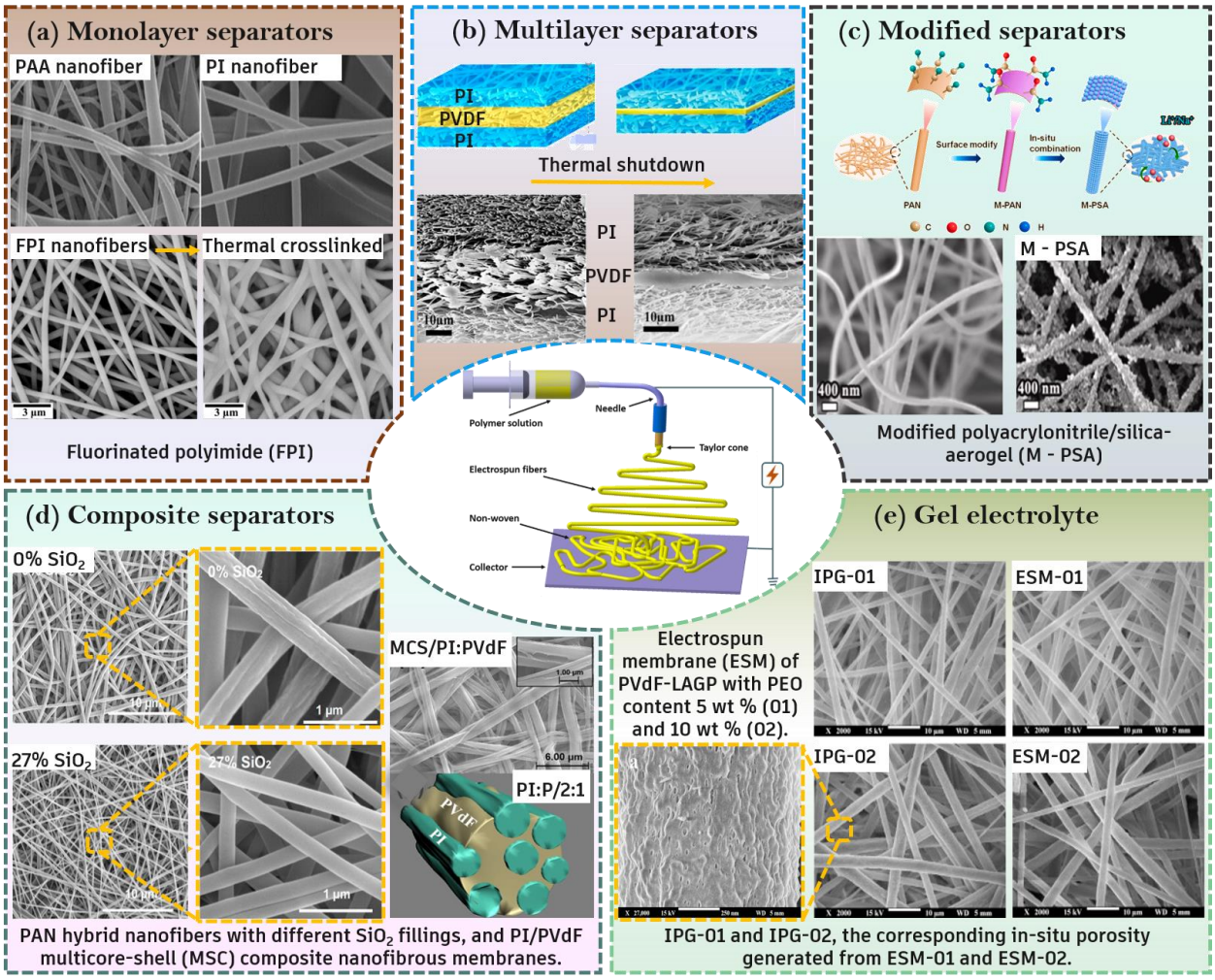

Figure 2-6: Electrospun non-woven membranes: (**a**) Monolayer separators. Reproduced from ref [99]. (**b**) Multilayer separators [101]. (**c**) Modified separators [102]. (**d**) Composite separator [103], and core-shell-shaped separator [104]. (**e**) Gel polymer electrolyte [105].

Electrospun multilayer separators can be made easily via sequential spinning, thanks to the unique operational characteristics of the electrospinning technique. Multilayer separators can provide the best mechanical strength, high thermal stability, and battery performance by combining the benefits of various precursor solutions and fiber layers [106-108]. In this type, PVDF and PE layers are typically constructed as a thermal shutdown layer to increase battery safety [98]. Also, sandwich-type PI/PVDF/PI separators with the thermal shutdown function fabricated by the electrospinning process (**Figure 2-6b**) [101]. In modified separators, the structure, surface morphology, and physical and chemical characteristics of raw electrospun separators are modified effectively to enhance their electrochemical performance. The most popular technique for modifying electrospun separators is dip coating, and the parameters of separators are affected by the incorporated coating materials "The separator is immersed for a while in coating solutions containing ceramic or organic nanoparticles". For instance, modified electrospun polyacrylonitrile/silica-aerogel as high-safety separators for lithium/sodium-ion batteries are reported (**Figure 2-6c**) [102]. Modifying electrospun separators through hydrolysis and heat treatments are alternative research directions to enhance their porosity, mechanical properties, and performance [84]. The electrospun composite separator is another beneficial approach to improving the characteristics and functionality of electrospun-based separators for batteries by combining different organic polymers and inorganic nanoparticle fillers to create an electrospinning solution, which is then used directly to fabricate composite nanofibers via electrospinning (**Figure 2-6d**) [103; 109].Additionally, a coaxial electrospinning apparatus (with a concentrically constructed needle) produced a core-shell-shaped composite membrane separator, which has lately drawn research attention due to its distinctive structure [104; 110]. With the introduction of inorganic particles, composite electrospun separators containing multiple polymer materials can gain better comprehensive properties, forming enhanced thermal stability and excellent electrolyte affinity compared to separators emanating from only a single polymer precursor [111]. Based on electrospinning, gel polymer electrolytes (GPE) can serve as both a separator and an electrolyte in a battery cell, avoiding the leakage issue associated with utilizing liquid electrolytes for batteries. Polymer membranes made via electrospinning are typically immersed in an electrolyte solution for quite a while to create GPE (**Figure 2-6e**) [105]. The extra liquid electrolyte on the membrane surface is flushed away after membrane gelatinization, and then the as-prepared GPE is ionically conductive. To create a swollen gel, the electrolyte solvent delivered to the membrane is first stored

in the cavities of the host polymer. Gelatinization is completed when the swollen fiber blocks the membrane mat's porous structure and prevents additional liquid solution absorption [98; 112].

2.4.1.3. Modified and other porous separators

Currently, commercial microporous polyolefin separators fabricated by wet and dry processes are limited by the physical characteristics of PE and PP, including low thermal stability and their hydrophobic nature, which decreases wetting performance, resulting in insufficient ionic conductivity. Polymeric-based membranes from different raw materials were prepared to substitute polyolefin membranes via various fabrication approaches (**Figure 2-4**) such as phase inversion [113-115], doctor blade/solution casting [25; 116-118], and electrospinning [26; 90; 119; 120]. Numerous methods, such as vacuum-assisted filtering [74], solvent evaporation [115], and deep-coating strategy, can also be used to fabricate and modify PMS for batteries. The most popular polymers for making PMS for LIB and NIB batteries are those based on cellulose [118; 121-123], PVDF and their copolymers [124; 125], PVA [126], PVB [127], PEO [128], PAN [129], PI [130], and PEEK [114] thanks to their high hydrophilicity, high dielectric constant, ease of film-forming ability, mechanical strength, and high melting temperature. Despite single polymer separators' benefits, because they are made of just one component and have manufacturing defects, single-component membranes cannot wholly meet the requirements for battery applications [10]. No single separator can be regarded as "ideal" for all chemistries and geometries of rechargeable batteries under all operating conditions [41]. Accordingly, most efforts to find alternatives to polyolefin separators have failed because PE and PP separators are still preferable to other separators when all criteria are contemplated and estimated [131]. Therefore, current research focuses on enhancing PE membranes' wettability, thermal stability, safety, and ion transfer capabilities, eventually leading to higher battery performance. Different approaches for modifying PE membranes using inorganic materials are summarized in **Table 2.6**.

2.4.1.4. Composite porous separators

Composite porous separators based on polymeric membranes can be sorted into two main parts: (i) blending composite separators in which nanoparticle fillers are dispersed in the polymer's casting solution and mixed with the polymers' matrices; and (ii) thin-film composite separators in

which nanoparticles are self-assembled on the surface through graft polymerization, blade-coating, plasma treatments, layer-by-layer self-assembly, electron beam, vacuum filtration, gamma irradiation, and dip coating into microporous membrane separators' surface [88]. The nanoparticle fillers of microporous polymeric membrane separators are based on oxides or nitrides with high melting points and decomposition temperatures (e.g., SiO_2, TiO_2, Al_2O_3, and ZrO_2) [8]. After composite materials are blended with the polymer base or incorporated by self-assembly, the safety of the resultant separator is enhanced, and the electrochemical performance of batteries is effectively improved subsequently due to the combinations of different materials through facile methods used in the composite processes [11]. Composite separators can be prepared by various methodologies, for example, wet/dry techniques, phase inversion, solution casting, electrospinning, and surface coating/grafting. Each preparation method significantly impacts the properties and performance of the as-prepared hybrid separator. The most commonly used techniques and materials for designing composite PE separators are summarized in (**Table 2.6**).

2.4.1.5. Electrolyte membrane separators

The development of all-solid-state batteries (SSBs) shall enable higher storage capacities and higher safety by replacing the liquid electrolyte in batteries with a solid ion conductor [21]. The main strategy to develop novel safer, lighter, and non-flammable electrolyte systems and to provide batteries with improved resistance against dendrite formation is the introduction of a mechanically resistant solid electrolyte sandwiched between both electrodes, the so-called solid polymer electrolyte. SSBs are a safer alternative to conventional batteries but are costly and challenging to custom design [132]. The replacement of conventional liquid electrolytes with solid electrolytes also opens the path toward flexible LIBs capable of withstanding large mechanical deformations with no leakage and short-circuit. The categorization of characteristics for different electrolyte membranes in comparison to liquid electrolytes can be seen in **Figure 2-3**. As classified, solid-state electrolytes (SSEs) can be divided into polymer electrolytes (PEs) which are divided into solid polymer electrolytes (SPEs) and gel polymer electrolytes (GPEs), solid ceramic electrolytes (SCEs), composite polymer electrolytes (CPEs). The drawing in **Figure 2-7** represent a description of conventional SSE manufacturing processes.

2.4.1.5.1. SPEs Solid polymer electrolytes (SPEs)

SPEs are ionically conducting materials and have the peculiarity of functioning as electrolytes and separators [133]. SPEs are made of organic polymer matrices such as cellulose derivatives, PEO, PMMA, PVDF, PVDF-HFP, or PAN dissolved with Li^+/Na^+ salts, ionic liquids, or other inorganic materials yielding a composite, , for instance, propylene carbonate (PC), ethylene carbonate (EC), dimethyl carbonate (DMC), diethyl carbonate (DEC), and ethyl methyl carbonate (EMC) [134; 135]. Their flexible mechanical enables a surplus of designs for batteries at the same time that alleviates drawbacks associated with the volume changes of electrodes as a consequence of recycling. Based on their structures, they have been categorized as homogeneous or heterogeneous SPEs [135]. Homogeneous SPEs are pure polymeric solid ion solutions, whilst non - homogenous SPEs can be any solid polymeric material composed of multiple phases/structures with varying ion transport capacities.

2.4.1.5.2. Gel polymer electrolytes (GPE)

GPEs are polymer matrices that have been plasticized or gelled, with the addition of a plasticizer resulting in a polymer matrix swelling in a liquid electrolyte. Plasticizers rise the conductivity of PEs as they promote the movements of molecular chain segments. Introducing a plasticizer can effectively improve the dielectric constant of the whole system. The increase in the dielectric constant of the system diminishes the electrostatic interaction between negative and positive ions, lowering the dissociation energy of lithium ions and facilitating ions' motion [135]. GPEs are obtained through trapping Li^+-containing solutions such as lithium hexafluorophosphate ($LiPF_6$) in a carbonate-based solvent within a polymeric gel-type membrane such as PVDF, PEO, PAN, and PMMA. They combine the advantages of liquid and solid polymeric electrolytes, namely the high ionic conductivity provided by the diffusion properties of liquids and the adequate mechanical stability arising from the cohesive properties of solids. Based on their preparation procedures, GPEs can be divided into two categories [136]: (1) physical GPEs, in which the liquid electrolyte is contained in a polymer matrix without bond formation between the matrices and the solvent; and (2) chemical GPEs, where a cross-linker causes a chemical bond to form between the functional group of the polymer and the cross-linker.

2.4.1.5.3. Solid ceramic electrolytes (SCEs)

Inorganic SCEs are commonly single Li^+ ion conductors with high ionic conductivity at room temperature. Regardless, their practical applications are limited because most of them are mechanically rigid and breakable, resulting in poor interfacial contact and complicated materials processing [137]. In contrast, Li^+ conductive polymer-based SSEs are usually flexible with outstanding processability. Thus, making thin structures and flexible polymer SSEs film is easy. The interfacial contact between the soft polymer and the electrode is also better than inorganic SCEs, leading to lower interfacial resistance [138].

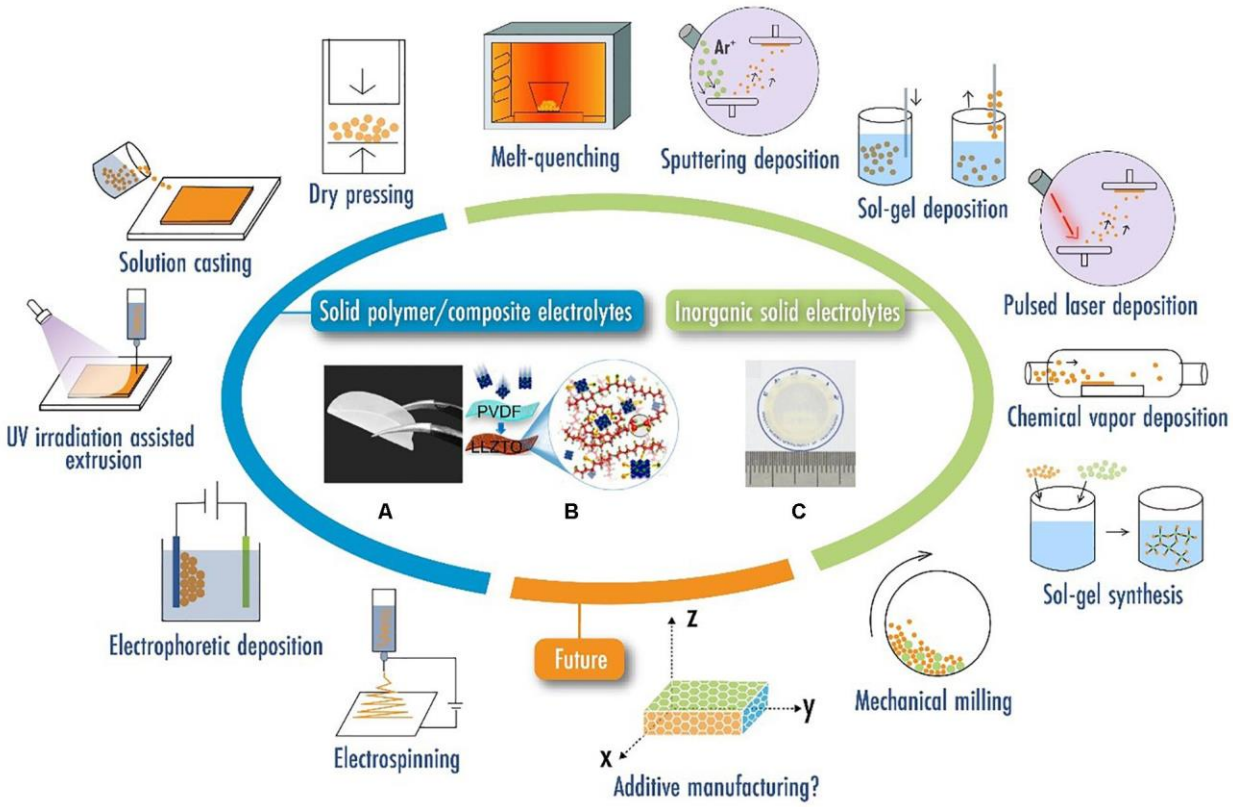

Figure 2-7: Schematics of traditional manufacturing strategies with (A) Optical image of a polyethylene oxide (PEO) based solid polymer electrolyte. (B) Schematic of a solid composite electrolyte combining $Li_{6.75}La_3Zr_{1.75}Ta_{0.25}O_{12}$ (LLZTO) and polyvinylidene fluoride (PVDF). (C) Optical image of a $Li_{0.34}La_{0.56}TiO_3$ (LLTO) ceramic electrolyte film [139].

2.4.1.5.4. Composite polymer electrolytes (CPEs)/hybrid solid-state electrolytes (HSEs)

CPEs/HSEs are composed of SPEs or GPEs reinforced with high-surface-area inorganic fillers nanoparticles to increase the ionic conductivity, enhance thermal stability, and mechanical strength of the hosting polymeric matrix [140; 141]. These particles are ceramic metal oxide and can be the size of micrometers or nanometers [20]. HSEs have the ability to bring together the advantages of inorganic and polymer electrolytes while overcoming the drawbacks of each component when used individually [140]. Inorganic SCEs electrolytes, for example, are often brittle, and challenges including such grain boundary resistance, both electrochemical and chemical stability with the electrodes, and increased prices. Moreover, the limited ionic conductivity of polymer electrolytes at room temperature restricts their practical application. When compared to inorganic and polymer electrolytes, hybrid composite electrolytes get the advantages of both materials excellent ionic conductivity, superior mechanical characteristics from the inorganic component, and low interfacial resistance from the polymer component. Electrolyte membrane separators for solid-state batteries will not be considered or discussed here, and for more detailed information, readers are encouraged to refer to the recent review works [86; 136-138; 142-144].

2.4.2. Polyethylene based composite battery separators

The development of composite separators by adding, coating, and incorporation of micro- and nano-sized ceramic fillers in polymer membranes like PE result in improved mechanical strength, wettability, thermal stability, and ionic conductivity of the PE separator by facilitating the rapid migration of lithium/sodium ions through membrane microstructure, which is considered one of the most actively researched procedures to improve the performance and safety of battery separators. Various representative oxide-based ceramics were used for developing composite separators, including silicon dioxide (SiO_2), aluminium oxide (Al_2O_3), aluminium oxide hydroxide known as boehmite (AlOOH), titanium dioxide (TiO_2), cerium oxide (CeO_2), magnesium dioxide (MgO), nickel oxide (NiO), and zirconium dioxide (ZnO_2). Inorganic ceramic particles can be coated or grafted onto the surface of PE separators or incorporated directly into the PE matrix to fabricate composite membranes. This considerably improves the physicochemical and electrochemical performance of these two types of composite membranes [8]. Numerous previous studies have verified the importance of inexpensive, simple-to-use inorganic micro/nanomaterials

to construct composite separators for battery applications, improving separators' thermal and mechanical properties and electrolyte uptake capacity [9]. The composite membranes made by coating inorganic ceramic nanoparticles onto the polymer substrate surface with the help of binders are called inorganic particle-coated composite membranes. The composite membranes formed by grafting organic-inorganic materials onto polymer substrates using irradiation treatments such as plasma and electron beam are called inorganic nanoparticle-grafted composite separators. Inorganic particle-filled composite membranes are constructed by directly mixing inorganic nanofillers into the polymer matrix. Commonly, inorganic ceramic nanoparticles are coated directly and construct an organic-inorganic network structure on the PE substrate surface through the doctor blade casting process, deep-coating, sol-gel coating, or grafting. The hydrophilic nature of ceramic nanoparticles can provide affinity towards electrolytes, which enhances electrolyte uptake and ionic conductivity. The inorganic nanoparticles' high melting temperature and the binder's adhesive nature can produce a thermally stable coating for the separator and offer superior heat resistance [10].

2.4.2.1. Inorganic nanoparticle-coated polyethylene separators

A straightforward approach is coating multifunctional and thermostable inorganic-organic materials on the surface of PE separators. Nowadays, methodologies for developing composite membranes are mainly by surface coatings of separators using composite ceramic solution or deposition of inorganic ceramic materials, coating composite gel polymers onto the separator or just a combination of both methods. Ceramic materials can prevent the cell from being harmed by high temperatures and maintain the stability of the cell's structure. At the same time, gel polymer can absorb enough electrolytes, improving ionic conductivity. As a kind of composite material, ceramic-coating materials are gaining more and more interest from researchers for their combination of the heat resistance from inorganic powder and the characteristics of the coated material. The ceramic composite separator consists of a matrix and ceramic layer. Furthermore, the inorganic ceramic particles (such as Al_2O_3, SiO_2, and so on) are mainly coated onto the PE separator surface with the help of binders (e.g., PVFD), and additives [145], as well as the coating percentage varies according to application scenarios [146]. These kinds of composite polyethylene separators have the following characteristics: (1) The high mechanical strength and chemical

stability are well maintained due to the use of polyolefin separators; (2) Introducing heat-resistant materials dramatically improves the poor thermal stability polyethylene separators; (3) The cost of this composite separator is also reasonably controlled due to the simple preparation process and cheap commercial polyolefin separators, which is beneficial for the large-scale application among energy storage devices [48]; and (4) Although the coated particle layer enhances the separator's wettability and electrolyte uptake, it may add additional resistance for Li/Na ions diffusion [147]. In addition to the various inorganic coating material categories, many other factors influence the characteristics of coated PE separators. **Table 2.6** summarizes some of these inorganic nanofillers, their corresponding preparation methods and their performance. Among different preparation methods, the deep-coating process has been employed to construct a uniform coating layer with diverse thicknesses on PE membranes for batteries. The general formula for developing the coated separator is as follows: Inorganic nanofillers disperse into organic solvents, and then a specific polymer binder is added into the homogeneous solution and kept stirring for a particular period at room temperature or specific temperature. The PE separator is dipped into a resultant composite solution to build a coated separator. Afterwards, it dries under a vacuum at a specific temperature.

2.4.2.1.1. Silicon dioxide

Silicon dioxide (SiO_2) is the most valuable and fruitful material for membrane separators due to its environmental friendliness, low cost, ease of production, high chemical/thermal stability, and polarity [142]. Silica (SiO_2) particles have been widely used in medicine, energy, photonics, and the environment. SiO_2 morphology can be controlled through various synthetic methods, such as surface modification and the formation of nano-powders and nanowire. Currently, SiO_2 nanoparticles have been conducted to modify the surface of polymeric (e.g., polyolefin) separators to improve thermal stability and electrolyte affinity. Moreover, SiO_2 nanoparticles have also been utilized as nanofillers to improve the separators' mechanical strength and thermal stability [53]. Silica-based nanofillers are most frequently investigated and employed for composite separators for batteries because they are very affordable, the production of a SiO_2-based modified layer on the separator is relatively simple, and the procedure is consistent with standard battery production [142]. The high polarity and high thermal stability of SiO_2 make it a suitable material to support the matrix of polymer separators for batteries [29]. **Figure 2-8 (a-b)** summarized numerous studies have also been using SiO_2 silica to modify PE separators via different coating methods.

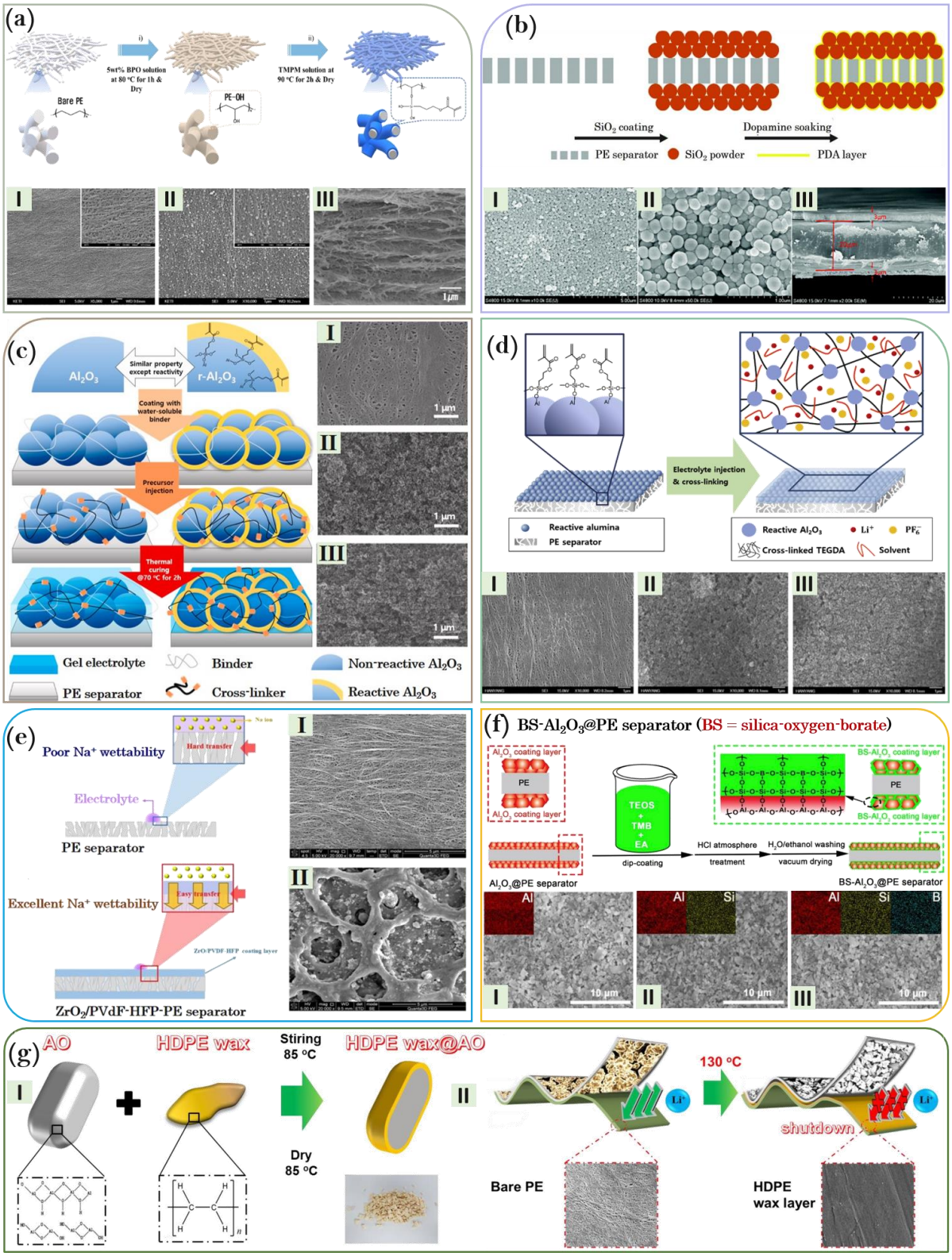

Figure 2-8: Inorganic ceramic-coated onto composite PE separators: (**a**) Schematic of the preparation of incorporating TEOS into PE separators; SEM micrographs of (**I**) bare PE separator;

(**II**) TEOS-coated PE separators; and (**III**) Cross-sectional SEM photograph of the TEOS-PE separator [29]. (**b**) Schematic illustration of the preparation of SiO_2 -modified PE separator through dip-coating process; SEM images of the surface (**I** and **II**) and cross-section (**III**) of PE–SiO_2@PDA separators [148]. (**c**) Schematic illustration for the preparation of Al_2O_3-coated PE separators; SEM photographs of surface of (**I**) pristine PE; (**II**) None-reactive Al_2O_3-coated; and (**III**) Reactive Al_2O_3-coated separators [149]. (**d**) Schematic for the coating of the PE separator with reactive alumina Al_2O_3 particles via a doctor blade coating process; surface SEM pictures of the of (**I**) pristine PE; (**II**) non-reactive alumina-coated PE; and (**III**) reactive alumina-coated PE separators [150]. (**e**) Schematic diagrams of Na^+ transfer pathways in the bare PE separator and the composite Z-PE separator "coated the PVdF-12 wt%HFP co-polymer and ceramic ZrO_2 particles onto the PE separator through deep-coating process"; FE-SEM image of the (**I**) bare PE separator; and (**II**) Composite Z-PE separator [37]. (**f**) Schematic illustrations for the preparation of BS-Al_2O_3@PE separator; Surface SEM snapshots and corresponding EDS elemental maps (Insets) of (**I**) Al_2O_3@PE; (**II**) S–Al_2O_3@PE; and (**III**) BS-Al_2O_3@PE separators [151]. (**g**) Schematic illustration showing the (**I**) preparation process of HDPE wax@AO particles; (**II**) the shutdown mechanism of separators with HDPE wax@AO coating layer [152].

2.4.2.1.2. Aluminum oxide

Aluminum oxide (Al_2O_3) is one of the favorable inorganic reinforcements, often known as fillers, in the context of polymer matrix composites. An alumina-based coating provides appropriate dispersion and suitable interfacial bonding; thus, adding small amounts of nanosized alumina particles to the polymeric matrix can dramatically enhance mechanical parameters[153]. Due to its high thermal stability and affinity for electrolytes, alumina is also regarded as a favorable ceramic coating material to enhance the thermal characteristics, electrolyte wettability, and ionic conductivity of polymeric membrane separators for batteries [154]. **Figure 2-8 (c-d)** shows some earlier reports focused on utilizing aluminium-based nanoparticles for modifying PE separators through different fabrication methods for batteries.

2.4.2.1.3. Zirconium dioxide

Zirconium dioxide (ZrO_2) ceramic nanoparticles are white crystalline oxides of zirconium. It is known to be environmentally friendly and is widely incorporated with polymer-based matrices

to serve as composite membrane separators in batteries [155-158]. Among various categories of ceramic nanoparticles, ZrO_2 is well known to possess superior chemical and thermal stability compared with other ceramic nanoparticles such as Al_2O_3, SiO_2, and TiO_2. When added to polymer electrolyte membranes for batteries, it boosts ionic conductivity and Li^+ transference number while also enhancing high interfacial stability between metal electrodes and electrolytes. **Figure 2-8**e displays an example report applying ZrO_2 for modifying PE separators via deep coating process.

2.4.2.1.4. Titanium dioxide

Titanium dioxide (TiO_2) nanoparticles are another commonly used reinforcement filler in polymer composites. Due to their outstanding structural and cycling stability, high discharge voltage, environmental friendliness, high safety, and low cost, titanium-based materials have been widely used as active materials for a variety of applications, including sensors, solar cells, energy storage and conversion devices, particularly rechargeable batteries [159; 160]. Nano-sized TiO_2 particles have been intensively deliberated for the modification of battery separators because of their high hydrophilicity, excellent chemical stability, and superior thermal stability [161]. The TiO_2 nanoparticles with a highly crystalline and/or porous structure exhibit excellent ion transport properties and enable rapid electrolyte diffusion; so, the electrochemical process proceeds with high efficiency due to accelerated molecular adsorption [162]. Most earlier reported studies have proven that TiO_2 can significantly improve the performance of membrane separators, which is beneficial for building safer and high-performance secondary batteries such as LIBs and NIBs [35].

2.4.2.1.5. Other ceramic particles

Designing and preparing unique composite separators that combine features beyond the state of the art is a major challenge, requiring unique strategies and multifunctional and thermally stable materials. Most of the prepared composite separators display high thermal stability without any dimensional shrinkage at high temperatures, mainly due to the thermal stability of ceramic nanofillers acting as robust supporting layers for PE-based membrane separators. Notably, numerous reports have proven that coating a hybrid inorganic ceramic layer (no matter what ceramic particles are used) onto polymeric separators is an effective way to enhance the performance of batteries because the inorganic material bestows both the wettability and rigidity of the separator simultaneously [163]. Although silica, alumina, zirconia, and titania are regarded as

the most adaptable and wieldy ceramic materials employed to function as composite membrane separators for batteries. Other ceramic particles such as AlOOH, MgO, CeO_2, NiO, magnesium hydroxide $Mg(OH)_2$, calcium phosphate ($Ca_3(PO_4)_2$) and borate-based particles have shown promising functionality when well-designed to serve as composite battery separators with excellent comprehensive properties.

2.4.2.2. Inorganic nanoparticle-grafted composite separators

As mentioned formerly, one of the main drawbacks is that the commercial PE separator has hydrophobic surface properties and poor surface energy, resulting in low wettability to liquid electrolytes [15]. Also, PE separators with a glass transition and melting point of (T_g = -68 °C, T_m = ~135 °C) have low thermal stability when operated at elevated temperatures. They undergo sizeable thermal shrinkage as temperature increases, which may lead to a short circuit of batteries and cause thermal runaway [164]. A typical tactic to overcome these issues is constructing composite membranes consisting of inorganic or/and organic materials coating/grafting on the surface of commercial PE-based separators [48]. Ceramic-coated PE separators have been widely studied to ensure safety and enhance the electrochemical performance of various secondary batteries (such as LIBs and NIBs). Ceramic-coated separators have quite enough mechanical strength and thermal stability to prevent an internal short circuit. Unfortunately, their increased thickness and obstructed porous structure would reduce the battery's energy and power density. Moreover, the uneven distribution of ceramic particles, along with the weak binding of polymeric binders, would result in particle detachment from the separators during cell construction and operation [165]. Accordingly, surface grafting under appropriate low irradiation is a potential modification method to fabricate thermostable separators without causing significant impairment of the polymer matrix [32]. Irradiation-treated PE separators such as gamma ray, plasma, ultraviolet, and electron beam technologies are valuable and advanced procedures to amend the structure, wettability, and electrochemical performance [166].

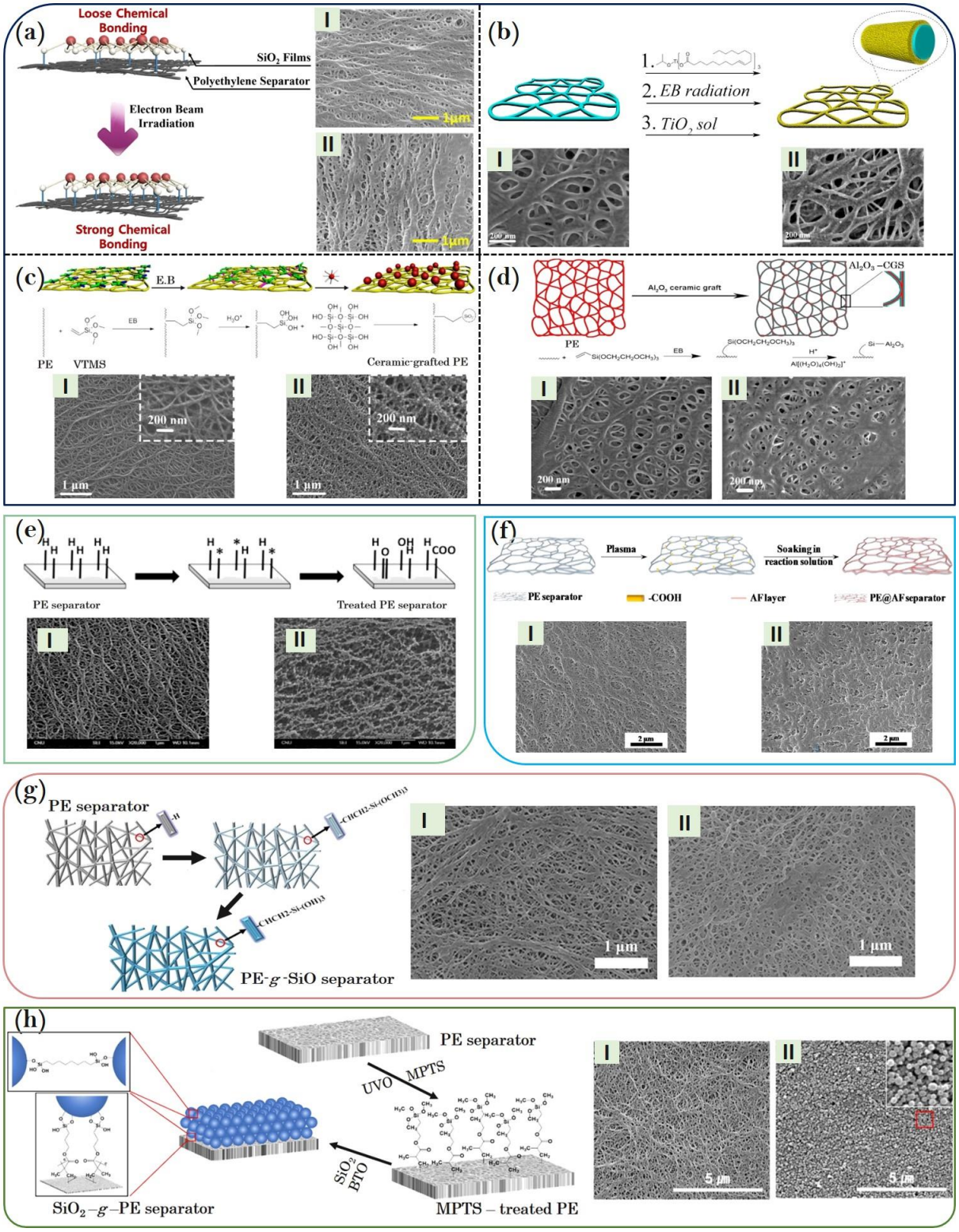

Figure 2-9: Inorganic ceramic-grafted onto composite PE separators: (a-d) E.B - induced grafting; SEM micrographs of (I) PE separator and (II) Inorganic ceramic-grafted PE separators using

various inorganic ceramic materials (a) SiO_2 [167]. (b) TiO_2 [35]. (c) SiO_2 [32]. (d) Al_2O_3 [165]. (e-f) plasma treated PE separator: (e) Surface activations of PE separators via oxygen plasma treatments; SEM images of (I) untreated and (II) plasma-treated PE separators [168]. (f) Plasma assisted fabrication of PE@AF composite separator via an in-situ immersion reaction; surface SEM micrographs of (I) pure PE and (II) composite PE@AF separators [169]. (g) γ-ray irradiated PE separator: VTMS grafted onto the PE separator by γ-irradiation; surface SEM micrographs of (I) pure PE and (II) composite PE-g-SiO separator [170]. (h) Silica-grafted PE separator via UVO treatment; SEM micrographs of (I) bare PE and (II) SiO_2-grafted PE separator [171].

The high-energy irradiation can generate free radicals that trigger the crosslinking reaction of polymer chains, considerably improving the physiochemical properties of the separator [11]. As a primary superiority, irradiated composite separators have stronger chemical bonding without any change in thickness [167].

2.4.2.2.1. Ultraviolet irradiation-induced polymerization

Ultraviolet (UV) treatment technology has been broadly used in coatings manufacturing to construct optical [172], flame-retardant [173], and super-hydrophilic [174] thin film coatings. Supposing films made up of photoreactive monomers and photoinitiator molecules. The photoinitiator molecules absorb UV light upon exposure, producing radicals that react with the monomers and cause chain reactions to produce polymers [175]. It has been emphasized that the UV-developed coatings are potentially appropriate and applicable for producing thin-film layers on polymeric membranes for battery separators (**Figure 2-10h**).

2.4.2.2.2. Electron beam-induced grafting

The high-energy electron beam (E.B) irradiation causes C–C and C–H bonds to cleavage and generates free radicals to initiate the cross-linking reaction of polymer chains, thereby significantly influencing the surface and physicochemical properties of the polymeric membrane separator [176]. The irradiated polymeric separators exhibited improved thermal stability and electrochemical performance with no change in thickness. However, excessive radiation doses can cause severe polymer chain damage. Therefore, controlling chain cross-linking while avoiding polymer backbone scission is very tricky [32]. The resulting alkyl radicals are unstable and enter a complex reaction system, leading to chain scission formation of C=C double bonds, oxidation,

cross-linking, and conversion to more stable allyl and peroxy radicals [177]. It is implicit that the formation of the C=C bond will not have a significant effect, but all other reactions will unfavourably affect wear and mechanical properties. Oxidation of VHMWPE in the presence of oxygen during E.B irradiation will lead to immediate oxidative degradation and is always associated with chain scission. Chain scission results in low molecular weight polyethylene, which has poorer abrasion resistance and mechanical properties than unirradiated VHMWPE. Immediate oxidative degradation can be diminished by irradiating in an inert condition [178]. The induced grafting polymerization of organic (monomers) and inorganic (ceramic) materials onto polymeric separators surfaces through E.B radiation is one of the convenient and practical techniques for the modification of structure and properties of polymer materials, as E.B can uniformly form active sites, initiate grafting through the membrane surface at a relatively fast rate, and react moderately [179]. Numerous researchers have attempted to modify the surface of polyethylene separators by high-energy E.B irradiation **Figure 2-9 (a-d).**

2.4.2.2.3. Plasma-assisted grafting

The plasma treatment is a dry, contamination-free, and energy-efficient technique used to modify the surface properties of various substrates by increasing surface energy, wettability, and chemical compatibility with joining materials [180]. The plasma process is a favored and convenient method when considering large-scale manufacture and commercialization of membranes due to its several benefits over other competitive procedures, such as environmental safety, uniformity, reproducibility, and selective modification without a severe loss of volumetric properties [168; 181]. The activation of the substrates in by the oxygen plasma treatment might produce a large abundance of hydrophilic oxygen-containing functional groups (such as C=O, C–OH, COOH) on the surfaces of polymer substrates. For instance, Ahn and co-workers, [168] applied oxygen plasma treatments to amend the surface of commercial PE separators with multifunctional groups **Figure 2-9 (e-f)**). The oxidation reaction improves the hydrophilicity and wettability of PE separators. In contrast, it has negatively affected and induced a chain scission of the PE surface, resulting in surface etching and eventually lowering the mechanical properties of treated separators. Cells with plasma-treated PE separators demonstrated enhanced charge-discharge capability, decreased interfacial resistance, and stable cycling performance. There are two types of plasma-assisted graft polymerization: the traditional process and the new innovative grafting process. The traditional

approach is a multi-step process, where the reaction between the substrate and monomers occurs after the plasma activates the substrate. Alternatively, the newly discovered revolutionary plasma-induced graft polymerization is extremely simple and easy to execute since the surface is transformed in a single step, allowing interactions between the substrate, plasma, and monomers to occur simultaneously. The former strategy has been used to alter the surface of polyolefin-based separators [182]. Surface grafting under plasma treatment is widely employed to prepare separators with functional groups, which exhibits unique advantages, including an environmentally friendly process, low production cost, and easy commercialization.

2.4.2.2.4. Gamma irradiation-assisted polymerization

Gamma-ray irradiation is an effective and convenient process for activating the inactive surfaces of polymers and adding polar groups to their surfaces [183]. Under high-energy irradiation conditions, γ-ray irradiation on polymeric (such as polyethylene) membranes acts as electron beam irradiation, causing major changes induced by C-H bond cleavage, culminating in hydrogen release and, chain scission and cross-linking eventually [190]. The carbonization of the polymer is caused by the emission of hydrogen. In addition to the hydrogen released upon irradiation, oxidation is another substantial consequence of this irradiation treatment. Irradiation of the material in the air can cause it to oxidize, thereby significantly changing the physicochemical properties of materials. The reaction of oxygen with allyl radicals produces oxidation products, forming hydrophilic polar groups on the polymer surface [184]. Gamma-ray radiation has been utilized to amend the molecular structure, physicochemical properties, and surface structure of PE separators for batteries, as in **Figure 2-9 g**.

2.4.2.3.Inorganic nanoparticle-filled composite separators

PE-based composite separators are physically coated with a composite layer that includes a polymer binder and ceramic nanoparticles (NPs), such as SiO_2, ZrO_2, and Al_2O_3, to enhance their thermal and mechanical properties [171]. Furthermore, the ceramic NPs were chemically grafted and attached to PE separators through different processes such as plasma treatments, irradiation and synthesis to improve their physiochemical properties and electrochemical performance [131; 179]. Physical coating and chemical grafting of ceramic particles on PE membrane separators

generally improve mechanical strength, thermal stability, and wettability, thereby enhancing electrochemical performance. In addition to coating and grafting microporous PE membranes with inorganic particles, incorporating inorganic NPs directly into the PE matrix is an effective and straightforward method for producing composite membranes. Properly ascribing the role of certain features is beneficial to achieving an optimal balance between various functions, from introducing inorganic fillers to considering trade-offs between essential parameters for ideal membrane separators intended for developing high-performance LIBs and NIBs batteries [142]. Adding inorganic nanofillers into PE matrixes can reduce their crystallinity and promote rapid migration of lithium and sodium ions [13]. Regardless of separator characteristics and types, the purpose of inorganic nanoparticle-filled composite separators can be classified into five categories based on their key parameters in batteries: (i) enhancing Li/Na-ions diffusion, (ii) improving mechanical performance, (iii) increasing thermal stability, (iv) decreasing interfacial resistance, and (v) suppressing Li/Na dendrite formation [142]. Incorporating inorganic NPs into PE matrices is anticipated to provide a better way out and mitigate the restrictions of inorganic NPs-coated composite separators for batteries. Furthermore, it can combine the fabrication of the PE matrix and the modification of inorganic ceramic NPs in one step, reducing the cost and time of preparation and post-processing, which could be an industrially scalable process [83]. Our group [83] successfully manufactured very high molecular weight polyethylene VHMWPE/SiO_2 nanocomposite membrane separators through the scalable biaxial stretching technique without additional post-modifications (**Figure 2-10a**). SiO_2 NPs did not block the pores of the obtained nanocomposite separator, which was of great significance for improving permeability, porosity, electrolyte uptake, and ionic conductivity to be more remarkable than those of pure UHMEPE membrane. The cells with the VHMWPE/SiO_2 separator have a higher C-rate capability of 164.6 mAh g^{-1} at 0.1 C-rate and exceptional cycling performance over 100 cycles with a coulombic efficiency of 99.93% and no capacity fading. In another study [166], we developed an advanced nanocomposite separator with significant commercialization possibilities using VHMWPE and SiO_2 NPs by combining a scalable biaxial stretching process with an E.B cross-linking procedure (**Figure 2-10b**).

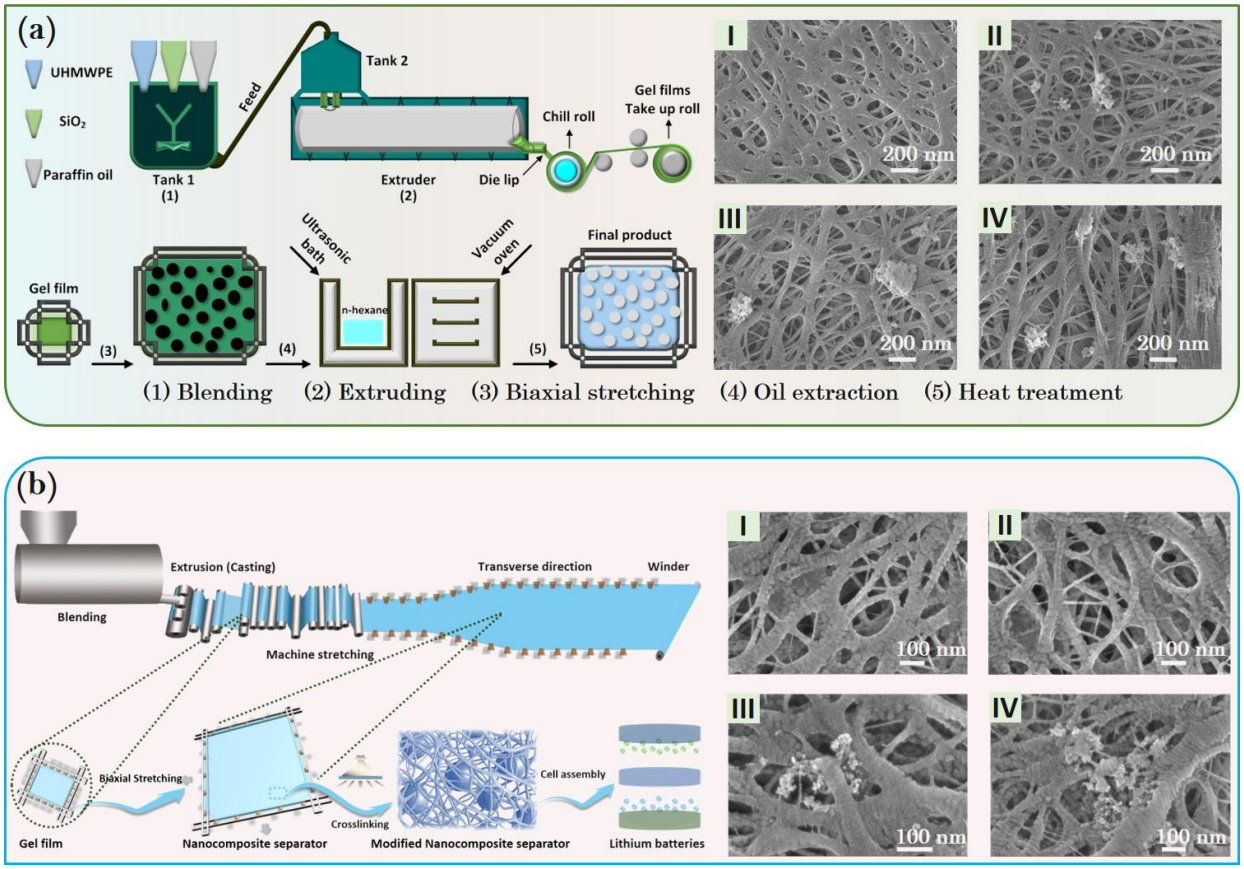

Figure 2-10: Incorporating inorganic nanofillers into PE matrixes via the scalable biaxial stretching method: (a) Schematic illustration for the fabrication process of hybrid VHMWPE/SiO_2 nanocomposites separators; (I-IV) SEM photographs of nanocomposite VHMWPE/SiO_2 with different ratios of SiO_2 (I) pure VHMWPE separator (0 wt% SiO_2); (II) VHMWPE/SiO_2 "5 wt% SiO_2"; (III) 10 wt% SiO_2; and (IV) 20 wt% SiO_2 separators [83]. (b) Schematic representation of manufacturing of PE nanocomposite separators followed by electron beam irradiation crosslinking; (I-IV) SEM snapshots for nanocomposite VHMWPE separators before and after crosslinking; (I) untreated VHMWPE membrane; (II) VHMWPE- 150 kGy; (III) untreated VHMWPE-SiO_2; and (IV) nanocomposite VHMWPE-SiO_2 -150 kGy separators [166].

2.4.3. Novel processes for advanced polyethylene separators

2.4.3.1. Self-assembly

Layer-by-layer (LbL) self-assembly is regarded as the simplest, versatile, and most promising approach for preparing multilayers on the surface of polymer substrates and allows the combination of various functional structures for particular applications [158]. Unlike other techniques, LbL can adjust the composition, surface properties, and coating thickness of constructed multilayers at the molecular level with tunable structures and properties [185],[186]. This modification approach is shown to improve the wettability and electrochemical performance of the PE membrane separator without compromising its microporous structure [187]. Hence, numerous studies focused on enhancing PE separators with organic-inorganic hybrid multilayers via LbL self-assembly, driven by their perceived advantages. For instance, Zhu and co-authors [188] LbL assembled the oppositely charged polyethyleneimine (PEI) and SiO_2 NPs to manufacture an ultrathin layer on the surface of the PE separator for LIBs (**Figure 2-11**).

Figure 2-11: Schematic illustrations of the cross-sectional map of PE separator before and after self-assembly and the intermolecular interactions during the self-assembly process [188].

The PEI/SiO_2-modified PE separator showed improved hydrophilic nature, which greatly increased its electrolyte uptake (398%) compared to that of the pure PE separator (153%). On continuous storage, the PE-PEI/SiO_2 separator demonstrated significantly improved interfacial

compatibility with the Li^+ electrode. As a result, the PE-PEI/SiO_2 separator improved ionic conductivity, Li^+ transference number, and battery cell with exceptional capacity retention at high C-rates and better cycle performance.

2.4.3.2.Atomic layer deposition

Atomic Layer Deposition (ALD) is a thin film deposition process that uses a vapour phase and features self-limiting and saturated surface reactions, which has received increased attention as an ideal technique for surface chemistry and engineering in energy-related devices, including supercapacitors, solar cells, fuel cells, and rechargeable batteries due to its excellent advantageous [189; 190]. ALD is a thin-film coating deposition technology that typically involves alternately feeding two precursors into a vacuum deposition chamber. The vacuum chamber normally carries the substrate to be covered and is preheated to speed up the chemical processes that enable the film to emerge [191]. In the ALD process, gas-phase precursors are sequentially exposed to the substrate, resulting in self-limited and saturated surface reactions. Previously, several review reports have illustrated the unique growth mechanism of ALD using some dual compounds, with two-cycle self-terminating half-reaction via ligand exchange [191-193]. The general mode of ALD growth mechanism in **Figure 2-12a**, assuming that water serves as an oxygen precursor for metal oxide (MO) and that ML_2 (M = metal and L = ligand) serves as a metal precursor [194]. The overall reaction is as described in Eq. (2-8):

$$\mathbf{ML_2(g) + H_2O(g) \rightarrow MO + 2HL(g)} \qquad \mathbf{(2\text{-}8)}$$

This reaction mechanism confers several advantages to ALD-deposited inorganic thin films, including precise thickness control at the Angstrom level, excellent uniformity and consistency, adjustable composition and relatively low deposition temperature [190; 195]. These thin films have been employed as surface coating layers on the cathode and anode of LIBs to address structural and interfacial problems and obtain a homogeneous distribution of nanofillers onto the separator. In addition, nanoparticles can be deposited on substrates via ALD by controlling nucleation sites on the substrate surface through pre-implanted functional groups. This is because nucleation sites, such as hydroxyl groups, defect sites, and heteroatom doping sites, are prerequisites for ALD surface reactions to occur [189; 190]. Over the past few decades, ALD has been intensively investigated and made remarkable progress in energy storage and conversion

applications. ALD can significantly enhance batteries' performance through material-nanostructuring, crystallization optimization, size control at the Angstrom level, and the search for new materials, which contribute to developing high-performance LIBs, NIBs, and other battery systems. For example, Chao et al. developed a Roll-to-roll ALD process to coat the TiO_2 layer uniformly on the PE separator for LIBs **(Figure 2-12b)** [196]. In detail, the R2R ALD technique using titanium isopropoxide and water as precursors allows precise control over the growth of TiO_2 nanolayer on PE separators. The resultant ALD cycles consist of two half self-limiting reactions that can be conducted within four stages: (step I) TTIP pulse, (step II) N_2 purge, (step III) H_2O pulse, and (step IV) N_2 purge. (I) The first self-limiting reaction involves the adsorption of TTIP molecules onto the oxygenated surface and (II) includes the removal of the byproducts, (III) The resulting reaction composes the surface reaction of water molecules, and (IV) the byproduct removal. Due to the self-limiting nature of the reaction, the thickness of the TiO_2 layer entering the PE separator increases with the number of ALD cycles. It is worth noting that precise control of the sample moving rate (or linear speed) is a key role in engineering and designing the TiO_2 gravimetric loading within the PE separator. For instance, at high line speed (e.g., 40 mm s^{-1}), the TTIP cannot diffuse adequately on PE surfaces, generating low TTIP-adsorbed, accordingly resulting in low TiO_2 loading. At low line speed (e.g., 5 mm s^{-1}), TTIP and H_2O molecules are given sufficient time to diffuse through the PE separators and construct a high coverage of TiO_2 nuclei over the PE surface. Depositing TiO_2 ceramic nanolayers on PE separators significantly improves thermal and dimensional stability due to the formation of a stable and robust framework within the PE matrix. The titania-coated PE film preserved a highly porous structure and improved electrolyte wettability throughout the cycling at a high temperature. Therefore, TiO_2 nanolayers play a crucial role in enhancing ionic conductivity and improving performance resulting in high safety and significant cycling performance during high-temperature operation. Park's group also suggested an ALD-based hybrid organic/inorganic coating approach that improves the thermal and dimensional stability of the PE battery separator without increasing its thickness [197]. In detail, an innovative method to improve PE separators' thermal stability and performance by first subjecting PE separators to a plasma treatment. The ALD approach uses plasma-treated PE separators that are uniformly coated with a few-nanometer-thick inorganic Al_2O_3 NPs coating layer. Afterwards, the PE/Al_2O_3 separators were again followed by PDA coated layer through the dip-coating process (**Figure 2-12c**). The PE separator with the hybrid Al_2O_3@PDA double coating layers showed

better thermal stability. Furthermore, the improved separator wettability leads to increased electrolyte uptake, resulting in an excellent electrochemical performance of LIBs.

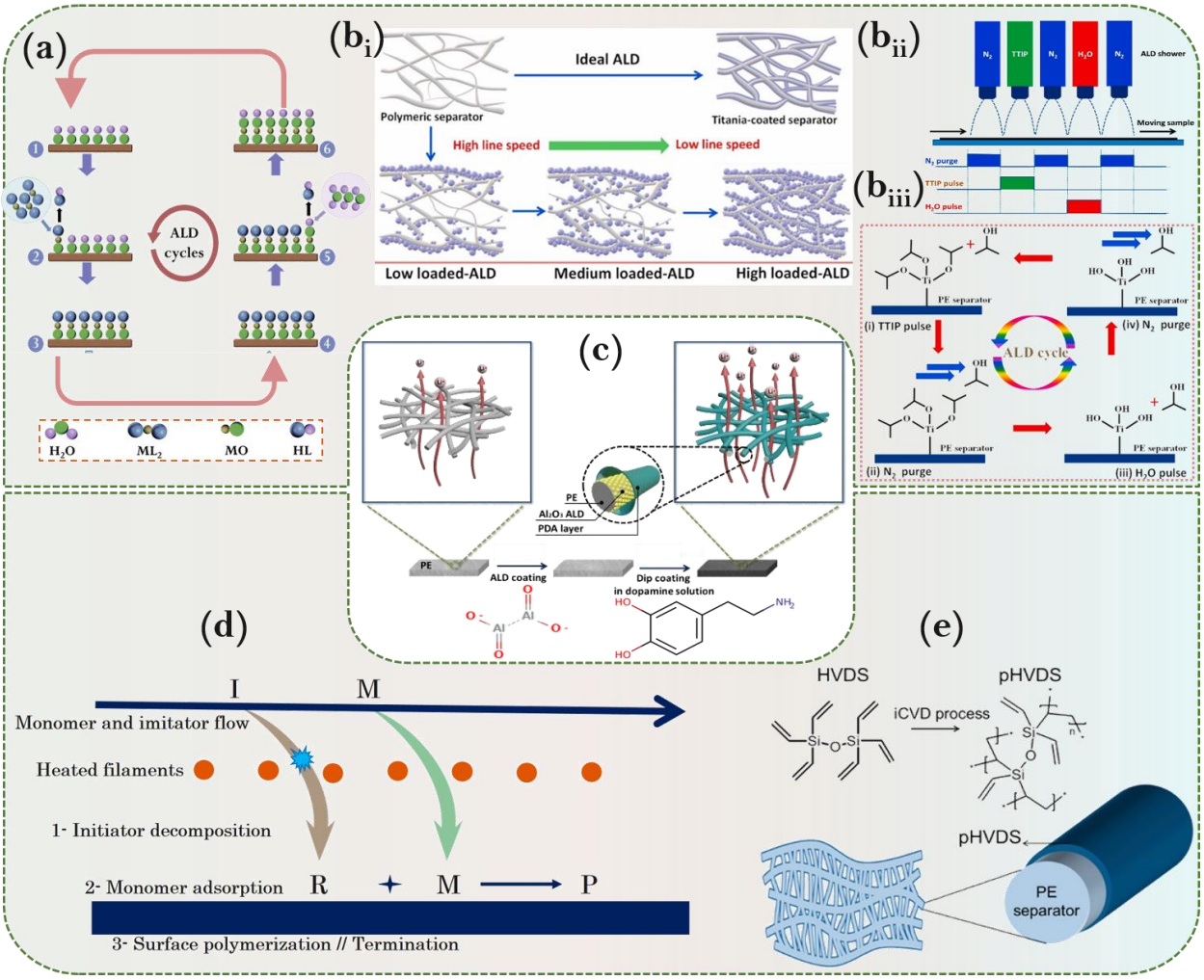

Figure 2-12: (a) A typical ALD procedure of MO employing ML_2 (M = metal and L = ligand) and water as precursors. (b) The scheme of R2R ALD process coating on PE separators for LIBs; (i) The schematic illustration of cross-sectional sights of TiO_2-loaded separators, involving ideal ALD, low, medium, and high ALD loading of TiO_2 coating into PE separators, (ii) R2R ALD shower for one ALD cycle "consisted of three nitrogen purges, one TTIP pulse, and one water vapor pulse"; (iii) the reaction map and surface intermediates for the ALD pathway of TiO_2 layer growth using TTIP and H_2O as precursors [196]. (c) A schematic illustration of the preparation of the PE/Al_2O_3/PDA separator via ALD [197]. (d) The suggested reaction mechanism during iCVD polymerization. Initiator (I) is thermally degraded by heated filaments in a vapour stage. From the vapour phase to the surface, primary radicals (R) and monomers (M) are absorbed. Polymerization

occurs at the substrate surface by radical addition through initiation, propagation, and termination procedures to form the polymer (P) coating. (e) Schematic illustration of pHVDS-coated PE separator by the iCVD process to deposit pHVDS on the PE separator conformally [198].

2.4.3.3.Chemical vapour deposition

Chemical vapor deposition (CVD) is a powerful technology for surface engineering. Chemical vapor deposition technologies such as plasma polymerization, molecular layer deposition, oxidative chemical vapor deposition (oCVD), and initiated chemical vapor deposition (iCVD) allow for conformal polymer coatings in micro- and/or nano-scale topography that are not achievable through solution processing because of de-wetting, liquid thinning, and surface tension effects [199]. In the iCVD process, the polymerization mechanism consists of three stages: (I) introduction and mixing of vaporized monomers and initiator molecules; (II) initiator decomposition to generate free radicals and transfer reactive free radical species and monomers to the substrate surface, and (III) polymerize and form a solid thin film on the cooled substrate [200]. The *i*CVD technology performs radical polymerization in the vapour phase by using a vaporized monomer and an initiator. Once vaporized initiator molecules come into contact with a hot filament, they are thermally fragmented and generate radicals. The radicals ignite the vaporized monomer to initiate the chain reaction. As an outcome, polymer films are deposited on the chamber substrate, which is held at a moderate temperature (15-40 °C). This process is a one-step, solvent-free procedure for depositing polymer films conformally onto multiple complex surface configurations of substrates [201]. The reaction mechanism consists of three steps (**Figure 2-12d**): (Stage 1) initiation, it boosts the number of free radicals; (Stage 2) propagation, that raises the molecular weight of the expanding chain while maintaining the number of free radicals; and (Step 3) termination, which reduces the total quantity of free radicals [202]. Rather than being produced directly from monomers, free radicals are typically created through the degradation of initiators. The free radicals then hit reaction sites, most commonly the vinyl functionality of monomers, and initiate polymer chain formation. Chain reactions are terminated by radical-radical recombination or by transfer of reactive radicals [203]. CVD polymerization converts gas phase monomers directly to thin solid macromolecular films that may be applied to practically any substrate. Indeed, for particular polymers and substrates, CVD polymerization may be the only manufacturing choice.

Because of the low surface temperatures, CVD polymers may be formed directly on delicate things like tissue paper and porous polymeric membranes. Yoo et al. [198] established the iCVD technique for altering PE separators in an attempt to increase the thermal stability of battery separators while also improving their poor wettability and affinity toward liquid electrolytes. The iCVD process was applied to conformally coat a highly cross-linked polyhexavinyldisiloxane (pHVDS) onto a PE separator while maintaining the microporosity and preserving the lowest growth in separator thickness (**Figure 2-12e**). The pHVDS-coated PE exhibited significantly enhanced thermal stability, after incubation for 30 min at 140 °C, the pHVDS-coated PE displayed a thermal shrinkage of (12%) versus high shrinkage for the unmodified PE separator of (90%). The thickness of the coating is precisely controlled by the deposition time to a level where the pore size is reduced to less than 7% compared to the original dimension of the unmodified PE separator. The electrolyte wettability of the PE–HVDS separator was enhanced due to the polar Si–O–Si groups in the HVDS, which facilitated fast ionic transport and increased the ionic conductivity from 0.66 to 0.84 mS cm^{-1}. Due to adequate electrolyte wettability and increased ionic conductivity, the HVDS modified – PE separator showed improved rate performance compared to the pure PE separator.

Table 2.6: Summary of some composite membranes based on PE matrix using ceramic particles materials for modification, their preparation processes, and electrochemical performance as separators for rechargeable batteries.

No	Inorganic modifier	Modification process	Electrode/ Electrolyte	Wettability/ uptake (%)	Conductivity (mS cm^{-1})	Capacity (mAh g^{-1})	Ref.
Coating, casting and grafting of inorganic ceramic particles on PE matrixes to construct composite separators							
1	ZrO_2	Dip-coating	Hard carbon/1M $NaClO_4$ (EC:PC)	Better wet	0.7	Retained~ 96% (50c)	[37]
2	SiO_2	Dip-coating	$LiCoO_2$/1M $LiPF_6$ (EC:DEC:EMC)	310	0.32	125 (0.5C)	[61]
3	SiO_2	Dip-coating	$LiCoO_2$/1M $LiPF_6$ (EC:DMC:EMC)	~870	~0.65	~142 (0.5C)	[147]
4	SiO_2	Dip-coating	Li_2MnO_4/1M $LiPF_6$ (EC:DEC:DMC)	80	0.98	106 (0.5C)	[148]
5	SiO_2	Dip-coating	$Li[NiCoMn]_{1/3}O_2$/1M $LiPF_6$ (EC:DEC)	~ 500	1.85	170.91 (0.1C)	[204]
6	SiO_2	Bioinspired dipping	$LiMn_2O_4$/1M $LiPF_6$ (EC:DEC)	121 ± 3.4 /	0.35	120 (1.0C)	[205]
7	ePOSS@Al_2O_3	Dip-coating	$LiCoO_2$/1.15M $LiPF_6$ (EC/EMC)	Better wet	0.855	144 (0.5C)	[206]
8	POSS	Dip-coating	$LiCoO_2$/1M $LiPF_6$ (EC:DMC:EMC)	301	0.45	~142 (0.5C)	[207]
9	Z-SiO_2	Dip-coating	NCM523/ 1M $LiPF_6$ (EC:DEC)	280	1.03	169 (0.5C)	[208]
10	Silane based	Dip-coating	$LiCoO_2$/1M $LiPF_6$ (EC:DEC)	185	5.79	143.1 (0.1C)	[209]
11	SiO_2	Dip-coating	$LiCoO_2$/1M $LiPF_6$ (EC:DEC:EMC)	277.3	0.624	~ 155 (0.2C)	[210]
12	SiO_2	Dip-coating	$LiCoO_2$/1M $LiPF_6$ (EC:DMC:EMC)	269	0.45	Retained~92% (100c)	[211]
13	Amino-SiO_2	Hydrolysis/dip-coating	$LiNi_{0.5}Mn_{1.5}O_4$/1M LiPF6 (EC:EMC)	Better wet	0.79	131.6 (0.5C)	[212]

14	BS-Al_2O_3	Dip-coating	$LiCoO_2$/1M $LiPF_6$ (EC:PC:DEC)	268.7	0.683	~150 (0.5C)	[151]
15	BS-Al_2O_3	Dip-coating	NCM/1M $LiPF_6$ (EC:PC:DEC)	268.7	0.683	142.1 (0.5C)	[151]
16	γ-Al_2O_3	Dip-coating	$LiCoO_4$/1 M $LiClO_4$ (EC:DEC)	157	1.3	Retained ~99%(0.5C)	[213]
17	AlOOH	Dip-coating	$LiFePO_4$/1M$LiPF_6$ (EC:DEC:DMC)	173.1	1.08	157.1 (0.2C)	[214]
18	NiO	Dip-coating	NMC/1M $LiPF_6$ (EC:DEC)	Better wet	2.12	145.7 (0.2C)	[215]
19	ZrO_2	Dip-coating	$LiCoO_2$/1M $LiPF_6$ (EC:EMC)	~120	0.61	150 (1C)	[36]
20	$Ca_3(PO_4)_2$	Dip-coating	$LiCoO_2$/1 M $LiPF_6$ (EC:DEC)	312	0.52	130.9 (1C)	[216]
21	$Mg(OH)_2$	Dip-coating	$LiCoO_2$/1.15M $LiPF_6$ (EC:EMC)	115	0.808	140 (0.5C)	[217]
22	HMDSO	Reactive pressure plasma	$LiFePO_4$/1M $LiPF_6$ (EC:DEC:DMC)	103.1	0.361	143.2 (1C)	[218]
23	PEDOT-*co*-PEG/AlF_3	Copolymer coating	$LiNi_{1/3}Co_{1/3}Mn_{1/3}O_2$/1.15M $LiPF_6$ (EC:EMC:DEC) having FEC (5 wt%)	Good affinity	3.2	182.2 (0.5C)	[219]
24	LSO-SiO_2	Blade coating	$LiCoO_2$/1M $LiPF_6$ (EC:DMC:EMC)	333	0.41	Retained ~86% (0.2C)	[220]
25	Zeolite@SiO_2	Hybrid coating	$LiCoO_2$/1M $LiPF_6$ (EC:DMC:EMC)	430.9	0.54	Retained ~94% (0.2C)	[221]
26	Amino-Al_2O_3	Blade coating	$LiCoO_2$/1m $LiPF_6$ (EC:DEC:FEC)	Superior wet	0.39	125 (1C)	[222]
27	Al_2O_3	Doctor blade coating	$LiMn_2O_4$/1.15M $LiPF_6$ (EC:EMC)	119.5	0.758	Retained ~99% (0.5C)	[223]
28	Al_2O_3	Bar coating process	$LiMn_2O_4$/1.15M $LiPF_6$ (EC:EMC)	100	0.846	113.5 (0.5C)	[34]
29	SiO_2	Core–shell coating	$LiNMnO_2$/1.15M $LiPF_6$ (EC:DEC)	231.7	0.79	173.5 (0.5C)	[224]
30	SiO_2	Core–shell coating	Li_2MnO_4/1M $LiPF_6$ (EC:DEC:DMC)	89.5	1.08	~108 (0.5C)	[30]
31	AlOOH	Spreader coating	NCM-111/1M $LiPF_6$ (EC:DEC:DMC)	187	1.00	147.1 (0.2C)	[225]
32	Al_2O_3	Auto scraper coating	$LiFePO_4$/1M $LiPF_6$ (EC:DMC:EMC)	88.5	0.55	147 (0.2C)	[226]

33	SiO_2	Blade coating	NCM/1.15m $LiPF_6$ (EC:EMC)	195.4	0.81	176.3 (0.1C)	[227]
34	Al_2O_3	Doctor blade coating	LMnO/1.5M $LiPF_6$ (EC:DEC:EMC)	192.3	0.56	165.8 (0.5C)	[149]
35	CeO_2	Doctor blade casting	LiMnO/1M $LiPF_6$ (EMC:EC:DEC)	81 g m^{-2}	2.5	125 (0.2C)	[228]
36	Al_2O_3	Doctor-blade coating	$LiCoO_2$/1M $LiPF_6$ (EC:DMC:EMC)	277	0.40	Retained~ 92.3 (100c)	[229]
37	AlOOH	Roller coated both sides	$Li_4Ti_5O_{12}$/1M $LiPF_6$ (EC:DEC)	Better wet	6.56	150 (1C)	[230]
38	SiO_2	Spray coating	NMC811/1M $LiPF_6$ (EC:DMC:EMC)	Better wet	N/A	149.1 (5C)	[231]
39	Al_2O_3	Plasma-assisted coating	$LiMn_2O_4$/1.16M $LiPF_6$ (EC:EMC)	85	1.182	109.9 (0.2C)	[232]
40	γ-AlOOH	Blade casting machine	NCA/1M $LiPF_6$ (EC:DEC)	136.8	0.3162	Retained ~81% (200c)	[152]
41	Silica tube	Film coating machine	$LiMn_2O_4$/1M $LiPF_6$ (EC:DEC:DMC)	105	~0.82	~107 (0.2C)	[233]
42	Al_2O_3	Film coating machine	$LiCoO_2$ / N/A	77	0.70	~107 (0.5C)	[234]
43	Al_2O_3	Film coating machine	NMC811/1M$LiPF_6$(EC:EMC)	N/A	N/A	Retained ~94% (150c)	[235]
44	Al_2O_3	Film coating machine	$LiCoO_2$ / N/A	70	1.13	~100 (0.5C)	[33]
45	TiO_2	Blade coating layer	$LiFePO_4$/1M $LiPF_6$ (EC:DEC)	135	0.53	143 (0.5C)	[236]
46	SiO_2	Surface grafting	$LiFePO_4$/1M $LiPF_6$ (EC:DEC:DMC)	N/A	0.45	125 (0.5C)	[32]
47	Al_2O_3	Surface grafting	$LiFePO_4$/1M$LiPF_6$ (EC:DEC:EMC)	N/A	0.53	~120 (0.5C)	[165]
48	SiO_2	Surface grafting	$LiFePO_4$/1M $LiPF_6$ (EC:DEC)	Better wet	0.84	156 (0.1C)	[171]
49	TiO_2	Surface grafting	$LiFePO_4$/1M $LiPF_6$ (EC:DEC:DMC)	Better wet	0.50	133 (0.2C)	[35]
50	VTMS	Surface grafting	$LiCoO_2$/ 1M $LiPF_6$ (EC:DEC)	139.3	t_{Li}^{+} (0.38)	125 (1C)	[170]
51	SiO_2-PZS	One-pot noncovalent	$LiCoO_2$/1M $LiPF_6$ (EC:DEC:DMC)	~170	0.104	~150 (0.5C)	[237]
52	TiO_2	Multistep synthesis	NVP/1 M $NaClO_4$ (EC:PC:FEC)	186.5	0.342	Retained~98% (200c)	[238]

Inorganic nanoparticle-filled composite PE membranes, sandwich trilayer and phase inversion based on the PE matrix							
53	Al_2O_3	Blend/extrusion/stretching	NMC811/1M $LiPF_6$ (EC:EMC:DMC)	Better wet	0.37	Retained 92% (100c)	[239]
54	5wt% SiO_2	Biaxial stretching	$LiFePO_4$/ Commercial (SS-HFGX046)	318	1.64	150.5 (0.5C)	[83]
55	10wt% SiO_2	Biaxial stretching	$LiFePO_4$/ Commercial (SS-HFGX046)	431	2.2	153.9 (0.5C)	[83]
56	20wt% SiO_2	Biaxial stretching	$LiFePO_4$/ Commercial (SS-HFGX046)	472	3.38	152.5 (0.5C)	[83]
57	SiO_2	Biaxial stretching + E.B	$LiFePO_4$/ Commercial (SS-HFGX046)	484	1.6	153.9 (0.5C)	[166]
58	SiO_2@PI	Sandwich trilayer	$LiCoO_2$/1M $LiPF_6$ (EC:DEC)	575	0.941	162.4 (0.2C)	[64]
59	PBI	Phase inversion	$LiFePO_4$/1M $LiPF_6$ (EC:DMC:EMC)	225	0.596	Retained~ 98 (100c)	[85]
Some of advanced procedures for preparation composite PE separators							
60	SiO_2	CVD	Hard carbon/1M $NaClO_4$ (EC:DMC)	Fully wet	1.0	333 (0.2C)	[240]
61	PEI/SiO_2	Self-assembly	$LiCoO_2$/1M LiPF6 (EC:DEC:EMC)	398	0.49	140 (0.5C)	[188]
62	SiO_2	Self-assembly	Hard carbon/1M $NaPF_6$ (EC:PC)	143.9	0.134	Retained~91.4 (0.5C)	[29]
63	PAA/ZrO_2	LbL self-assembly	$LiCoO_2$ /1M $LiPF_6$ (EC:EMC:DMC)	325	0.51	~140 (0.5C)	[158]
64	ZrO_2/POSS	LbL self-assembly	$LiCoO_2$/1M $LiPF_6$ (EC:DEC:EMC)	340	0.46	~140 (0.5C)	[157]
65	ZrO_2/POSS-GPE	LbL self-assembly	$LiCoO_2$/1.1M$LiPF_6$(EC:EMC:DEC:PC)	N/A	0.39	Retained~ 60% (0.5C)	[241]
66	TiO_2	Atomic layer deposition	NCM/1M $LiPF_6$ (PC:DEC:EMC)	Better wet	0.108	Retained ~92% (100c)	[196]
67	Al_2O_3	Atomic layer deposition	$LiCoO_2$/1M $LiPF_6$ (EC:DE)	~450	~0.65	Retained 79% (200c)	[197]
68	pHVDS	iCVD	$LiFePO_4$/1M $LiPF_6$ (EC:EMC)	106.43	8.4	126 (1C)	[198]
69	Al_2O_3	EB-PVD	NMC111/1M $LiPF_6$ (EC:DMC:EMC)	57.6	N/A	~133 (0.5C)	[242]

2.5. Summary

This chapter summarized the current progress of polyethylene-based composite membrane separators for lithium-ion (Li-ion) and sodium-ion (Na-ion) batteries applications. The chapter briefly exemplified the developments and categories for battery separators and concisely illustrated the characteristics and challenges of various classifications of battery separators. It provided a comprehensive discussion on the fundamental requirements and properties (e.g., structural properties, physical/chemical properties, functional properties and other outstanding required properties) of ideal porous separators for high-performance LIBs and NIBs. The recent progress in several categories of battery separators, such as microporous separators, non-woven separators, modified microporous membranes, composite separators, and electrolyte membranes and their structural construction prepared from various materials through different fabrication processes were briefly deliberated. In order to address the concerns raised by the shortcomings of microporous polyethylene membranes and for superior battery performance, microporous PE membrane separators can still be enhanced in terms of thermal stability, wettability, conductivity, and sustainability. For the purpose of constructing composite separators based on PE matrixes with enhanced properties and performance, microporous PE membranes have been modified with inorganic ceramic particles using a variety of techniques, including deep coating, blade coating, physical process with the help of binders, chemical grafting processes under irradiation, and some other advanced modifications strategies. Numerous studies were conducted to fabricate composite PE separators to overcome restrictions and improve and meet the needs of battery separators. As summarised, the features of composite PE separators, such as thermal stability, mechanical strength, electrolyte wettability, ionic conductivity, and overall electrochemical performance, were improved compared to pure and unmodified PE membrane separators.

CHAPTER 3. Hybrid VHMWPE/SiO_2 Separators via the Biaxial Stretching Process for LIBs

3.1. Introduction

The lithium-ion batteries (LIBs) have become the dominant energy storage device for modern society, and it's widely used in various new-energy devices ranging from portable electronic devices, including digital cameras, mobile phones, and notebook computers [243; 244] to electric vehicles and emerging smart grids [13]. Continuous efforts have been attempted to increase the macroscopic performance of LIBs. Despite investigations related to the anode and cathode, the optimization of separator has proven to be an efficient strategy to improve the properties of LIBs, i.e., safety, cycle life, power density and energy density [13]. The separator's fundamental purpose is to avoid physical contact between the electrodes while facilitating ion migration during the charge-discharge process [245]. The conventionally LIBs separators used on a large scale are polyolefin separators, which are polyethylene (PE) and polypropylene (PP) or their multilayer formations [51; 246]. Very high molecular weight polyethylene (VHMWPE) membrane, as a polyolefin membrane, is widely used as a lithium-ion battery due to its good chemical stability, excellent corrosion resistance, high tensile strength and economic advantages [51; 148; 243]. Unfortunately, most of the polyolefin separators, including the VHMWPE separator, exhibit a high thermal shrinkage on the dimensions and low affinity for liquid electrolytes due to the electrolytephobic behavior and poor ability to retain electrolytes during cycling, which limit their uses in high-temperature, high capacity and high power LIBs [51; 148].

To mitigate these limitations, uncountable researchers reported their work in reducing the restrictions of PE separators, i.e., for example, grafting of hydrophilic monomers to membrane surfaces [40], coating of PE separators with hydrophilic organic materials [157], and combining membranes with multifunctional groups and inorganic particles [13; 247]. Among these modification approaches, the polymeric nanocomposite membrane is well-known as an efficient strategy [243; 248; 249]. Nanocomposite membranes have been confirmed as promising solutions for LIBs, thanks to the unique properties of inorganic nanoparticles such as superior thermal stability and excellent affinity to the liquid electrolyte [250; 251]. Polymeric nanocomposite membranes are categorized into

two main parts: (a) thin-film nanocomposite membranes and (b) blended nanocomposite membranes. In the thin-film composite membrane, the nanoparticles are self-assembled on the film's surface by dip coating and spin coating technology to form a thin-film or deposited on the prepared membrane surface. For the blending nanocomposite membrane, nanoparticles are dispersed with the polymer's casting solution [252-255]. The most used inorganic nanoparticles for the development of PE membranes/separators are SiO_2, Al_2O_3, and TiO_2 [243; 256]. These can enhance the mechanical strength and thermal stability of the membranes/separators [220; 252]. They can also promote the absorption of the liquid electrolyte to achieve a good electrolyte uptake during the charging-discharging process, which will lead to the enhancement of the battery's performance [257]. For instance, W. Na et al. grafted silica nanoparticles onto a polyethylene separator's surface to enhance thermal stability and cell performance [171]. D.W. Lee et al. reported the coating of the PE surface with aluminum oxide (Al_2O_3) nanoparticles. The separators exhibit a high level of porosity and good electrolyte uptake [258]. T. Lee et al. developed a PDA/Al_2O_3-coated surface PE separator, which shown great thermal stability and electrochemical performance [259]. Nevertheless, when these inorganic nanoparticles are introduced into the PE separator, there will still be some adverse effects. For example, dense particles will inevitably lead to a decrease in porosity, leading to higher internal resistance and lower ionic conductivity, and poorer power density [151; 220; 260]. Apart from this, the used methods may lead to other severe problems, i.e., time-consuming preparation process, difficulty in quality control, and a significant increase in thickness [261]. Besides, most of these methods involve expensive equipment and complicated procedures, which are not appropriate for large-scale commercial applications of LIBs.

Herein, motivated by the unique properties of SiO_2 nanoparticles, including excellent wettability due to its affinity to liquid electrolytes and significant-high thermal stability, we propose a novel idea of preparing a nanocomposite separator consisting of VHMWPE and SiO_2 that can effectively reduce the limitations of PE membranes/separators and extend the life of the LIBs. There are innumerable reports on composite membranes based on organic (VHMWPE)/inorganic (SiO_2) composite membranes prepared through different techniques such as coating and modification methods. However, a few reports of VHMWPE/SiO_2 nanocomposite membranes via the biaxial stretching process for lithium-ion batteries separators. Therefore, we first described our efforts to prepare and industrialize VHMWPE/SiO_2 nanocomposite membranes through a biaxial stretching process with no additional post-modifications. Different

characterizations, i.e., SEM, EDS, ATR-FTIR, WAXS and TGA, were used to check the incorporation of SiO_2 into the VHMWPE matrix and its spatial distribution. The performances of the current hybrid membrane as a battery separator was supreme compared with reported results in literature on both commercially available separators and other experimentally investigated PE composites. This technique is expected to deliver a better battery separator solution because it is well-known as an industrially scalable process. More importantly, it combines the manufacture of VHMWPE nanofibrous separators and the modification of SiO_2 in a single step and reduces the preparation and post-treatments' cost and time. Further, the presence of SiO_2 nanoparticles into the VHMWPE structure can improve the electrolyte's absorption and wettability, enhance thermal stability, maintain mechanical performance, ensure electrochemical stability, and battery performance.

3.2. Experimental Method

3.2.1. Raw materials

A powder of VHMWPE (very high molecular weight polyethylene) with an average (molecular weight "Mw") of 600000 g mol^{-1} was supplied by China Lucky Group Corporation (Hebei, China). Inorganic nanofillers (silicon dioxide "SiO_2") with a particle size of 20 nm were brought from Nanjing Paukert Advanced Material Co., Ltd (Nanjing, China). Paraffin oil was purchased from Zhejiang CHXIN Oil Technology Co., LTD (Zhejiang, China). N-hexane was procured from Nanjing Oriental Pearl Chemical Co., Ltd (Nanjing, China). BASF Antioxidant was attained from BASF Gao-Qiao Performance Chemicals Shanghai Co., Ltd (Shanghai, China). Liquid electrolyte for lithium-ion battery (SS-HFGX046) was gotten from Dongguan Shanshan Battery Material Co. LTD (Anhui, China). N-butanol was acquired from Sinopharm Group Chemical Reagent Co., Ltd, (China). The commercial lithium sheet (Li) anode was acquired from China Energy Lithium Co., Ltd and the commercial lithium iron phosphate ($LiFePO_4$) cathode was gotten from Hefei Gotion High-tech Power Energy Co., Ltd. All materials were used directly as received without any further modifications.

3.2.2. Membrane preparation

The process for producing a commercial nanocomposite VHMWPE/SiO_2 nanofibrous membrane comprises several steps [42], as illustrated in **Figure 3-1**. Firstly, VHMWPE powder, SiO_2 powder, paraffin oil, and antioxidants were blended in Tank 1 at room temperature to prepare composite solutions. After that, composite solutions were conveyed to a specially designed stirring-tank (Tank 2) at 100 °C to form homogeneous nanocomposite gels that contain 25 wt % powder (different percentages between VHMWPE and SiO_2) and 75 wt % paraffin oil, as summarized in **Table 3.1**. Secondly, to form a stretchable composite gel-like sheet, as-prepared composite gels were extruded directly on a top of the chill roll by a twin-screw extruder. The casting machine with a sheet-forming die lip at a die temperature of 220°C and chill roll temperature of approximately 30°C to obtain uniform VHMWPE and VHMWPE/SiO_2 gel-like membranes (composite casting membranes). The thickness of the gel films was about 0.5 mm. Thirdly, the resultant composite gel-like sheets were stretched by the biaxial stretching process. VHMWPE and VHMWPE/SiO_2 gel membranes were cut and prepared into a square shape with 100 × 100 mm for the biaxial stretching step. The stretching process of the gel-like film is carried out sequentially along the machine direction (MD) and then the transverse direction (TD). The membranes were first heat in the stretching oven 3 minutes before stretching. Afterward, start the stretching. The constant stretching rate was 10 mm/s in both MD and TD directions. After successfully stretched, films were placed in a stretching oven at 120°C for 2 minutes for heat setting, and then cool to room temperature. Fourthly, the membrane-forming solvent (paraffin oil) extraction was done by washing the biaxially stretched membrane in n-hexane with sonication three times, each time for 30 minutes, then drying the achieved nanocomposite nanofibrous membranes using a vacuum oven for 30 minutes at 40 °C. Finally, nanocomposite membranes were again fixed onto the biaxial stretching machine for heat treatment along with TD at 140 °C. This procedure proposes to increase the thermal and mechanical properties of final products.

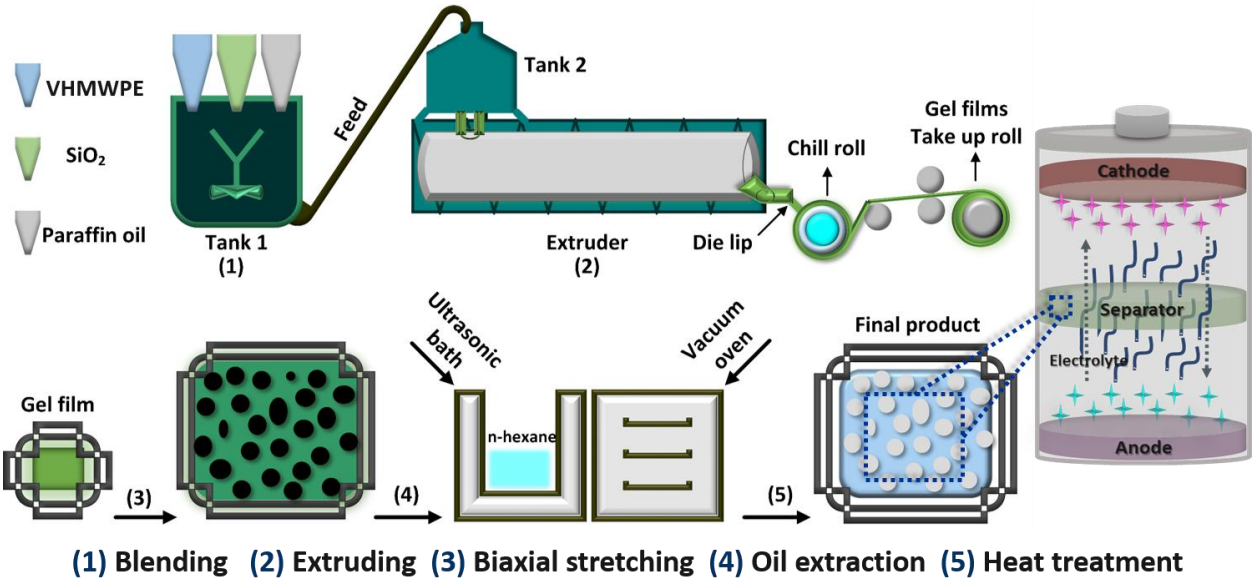

Figure 3-1: Schematic illustration of the preparation and fabrication of nanofibrous membranes.

Table 3.1: Composite solutions with different ratios of VHMWPE and SiO_2 for extrusion.

Membrane ID	VHMWPE (Kg)	SiO_2(Kg)	Oil (Kg)	Anti-oxidant (Kg)
S1	1	0	3	0.02
S2	0.95	0.05	3	0.02
S3	0.9	0.1	3	0.02
S4	0.8	0.2	3	0.02

S1 (100/0); S2 (95/5); S3 (90/10); S4 (80/20) wt% (VHMWPE/SiO_2).

3.2.3. Characterization

3.2.3.1. Crystallinity and crystal size

Wide-Angle X-ray Scattering (WAXS) was employed to obtain the information of crystallinity and crystal size of VHMWPE and VHMWPE/SiO_2 membranes. WAXS measurement

was done using an in-house micro-beam X-ray source with Cu Kα radiation (λ=0.154 nm), which has been described in detail previously [262]. The crystallinity (*Xc*) of the membranes was evaluated using peak-fitting of the 1D integrated profiles and calculated using Turner-Jone's method as following [42; 263]:

$$\boldsymbol{Crystallinity\ (Xc)(\%) = \frac{\sum A_c}{\sum A_c + \sum A_c} * 100\%} \qquad \textbf{(3-1)}$$

Where A_c and A_a represent the fitted areas of 1D integrated WAXS curves for crystalline and amorphous phases, respectively. The crystal size L_{hkl} in the direction perpendicular to (hkl) plane was evaluated by the Scherrer equation [42; 264]:

$$\boldsymbol{Crystal\ size\ (L_{hkl})(nm) = \frac{K\lambda}{FWHM * COS\ \theta}} \qquad \textbf{(3-2)}$$

Where *K* represents the crystal shape factor, which is taken as 0.9 in this experiment, λ is the wavelength of X-ray (0.154 nm), and the full width at half maximum "*FWHM*" of the diffraction peak (*hkl*) of 1D WAXS curve, and 2θ is the peak position.

3.2.3.2. Morphological and structure characterization

Scanning electron microscopy (SEM) and Energy Dispersive Spectrometer (EDS) (SEM and EDS, Zeiss Libra, Germany) were used to investigate the surface morphology, cross-sections and elemental compositions of cast films, VHMWPE nanofibrous membrane before and after composite with SiO_2 nanoparticles as well. The air permeability of the membrane was measured using Gurley precision instruments (Gurley 4110N), Troy, N. Y, USA. The air permeability was estimated by 100 cc airflow to go through a part area of the membranes. Attenuated Total Reflection, Fourier Transform Infrared (ATR-FTIR) spectra of VHMWPE membranes with/without SiO_2 nanoparticles, were collected from an ATR-FTIR mode (Bruker Tensor 27, Germany). Identification of the elemental composition and chemical states of elements was carried out by X-ray photoelectron spectroscopy (XPS, ESCALAB 250, Thermo Scientific, USA). The membrane average pore size was measured using the bubble point technique via a capillary flow porometer (CFP-1500-AE, Porous Materials, Inc. USA).

3.2.3.3. Mechanical properties

The mechanical tests of VHMWPE nanofibers membranes and VHMWPE/SiO_2 nanocomposite membranes both in MD and TD directions were carried out on the HD-B604-S micro-control electronic universal testing machine (Dongguan, China). The puncture test of VHMWPE nanofibers and VHMWPE/SiO_2 nanocomposite membranes was carried out by the Chinese national standard GB-T-36363-2018 on a universal tensile testing machine (CMT6202). The impact velocity was 100 mm/min, membranes size was 100 mm×100 mm, the puncture angle was 0˚. Each membrane was tested three-time and the given puncture strength is the average.

3.2.3.4. Thermal properties

The thermo-gravimetric analysis (TGA) was carried out with a TGA Q5000IR under the air atmosphere. The thermal stability of VHMWPE and VHMWPE/SiO_2 membranes was estimated by calculating the dimensional change of the film after treatment at a temperature of 120°C for 60 minutes. The thermal shrinkage of the membranes in both MD and TD was calculated using the following equation [265]:

$$\textbf{Thermal shrinkage}\ (\%) = \frac{A_0 - A_1}{A_0} * 100\% \qquad \textbf{(3-3)}$$

Where A_0 and A_1 are the length of the membrane in MD, the width of the membrane in TD before and after being treated with 120 °C for 1 h, respectively.

3.2.3.5. Electrolyte uptake and wettability

The liquid electrolyte contact angle of membranes was measured on an automatic contact angle machine (SDC-350, Shengding, China) under the ambient environment. The liquid electrolyte drops (2 μL) were dropped carefully on the surface of membranes. Each sample's reported contact angle was an average of 5 measurements taken from different positions on the same membrane. To measure the membrane electrolyte uptake, membranes were soaked in a liquid electrolyte at an ambient atmosphere for 60 minutes and then gently absorbed with tissue paper. Subsequently, the liquid electrolyte uptake was calculated using the following formula [266]:

$$\textbf{Uptake amount}\ (\%) = \frac{M_2 - M_1}{M_1} * 100\% \qquad \textbf{(3-4)}$$

Where *M1* and *M2* symbolize the membrane's weight before and after being immersed into electrolytes, respectively.

3.2.4. Electrochemical analysis

3.2.4.1. The ionic conductivity

The ionic conductivity of the membranes considers a key influence to estimate the conduction of ionic carriers. The ionic conductivity was assessed by electrochemical impedance spectroscopy (EIS) using a coin cell with a sandwiched (stainless steel (SS) /separator/ SS). The ionic conductivity was measured by AC impedance spectroscopic with a temperature: 23.0±2℃, humidity: 50±10%, as per the following equation [245]:

$$\textbf{Ionic conductivity}\ (K) = \frac{d}{RA} \qquad \textbf{(3-5)}$$

Where *K* represents the ionic conductivity, *d* = the separator's thickness, *R* = the bulk resistance obtained from the impedance, and *A* = the contact area between the stainless steel and the separator.

3.2.4.2. Rate capability and cyclic performance

The charging/discharging capacities, discharge C-rate capabilities, and cycling performance of membranes were estimated with coin-cells on a NEWARE battery cycle system. The charging/discharging cyclic performance was measured at a current density of 1/1 C for 100 cycles, and C-rate capability was conducted from 0.1 C to 5 C, respectively. Separators are assembled into a coin-cell with commercial lithium iron phosphate ($LiFePO_4$)/lithium sheet (Li) to test LIBs performance. The cycle performance of the cells was evaluated under the constant current mode over the range of 2.0-4.2 V at ambient conditions. The electrochemical impedance of the coin-cells was concluded by an electrochemical workstation (NEWARE，CT—4008—5V10mA—164).

3.3. Results and discussion

3.3.1. Fabrication, morphological and structural characterization

The overall manufacturing technology of the membrane is shown in **Figure 3-1**. The final blended uniform gels were entered into the extruder to obtain uniform gel films. The surface morphology and chemical compositions of gel films with and without SiO_2 were investigated using SEM-EDS. **Figure 3-2** displays perfect surface morphology and elemental composition snapshots.

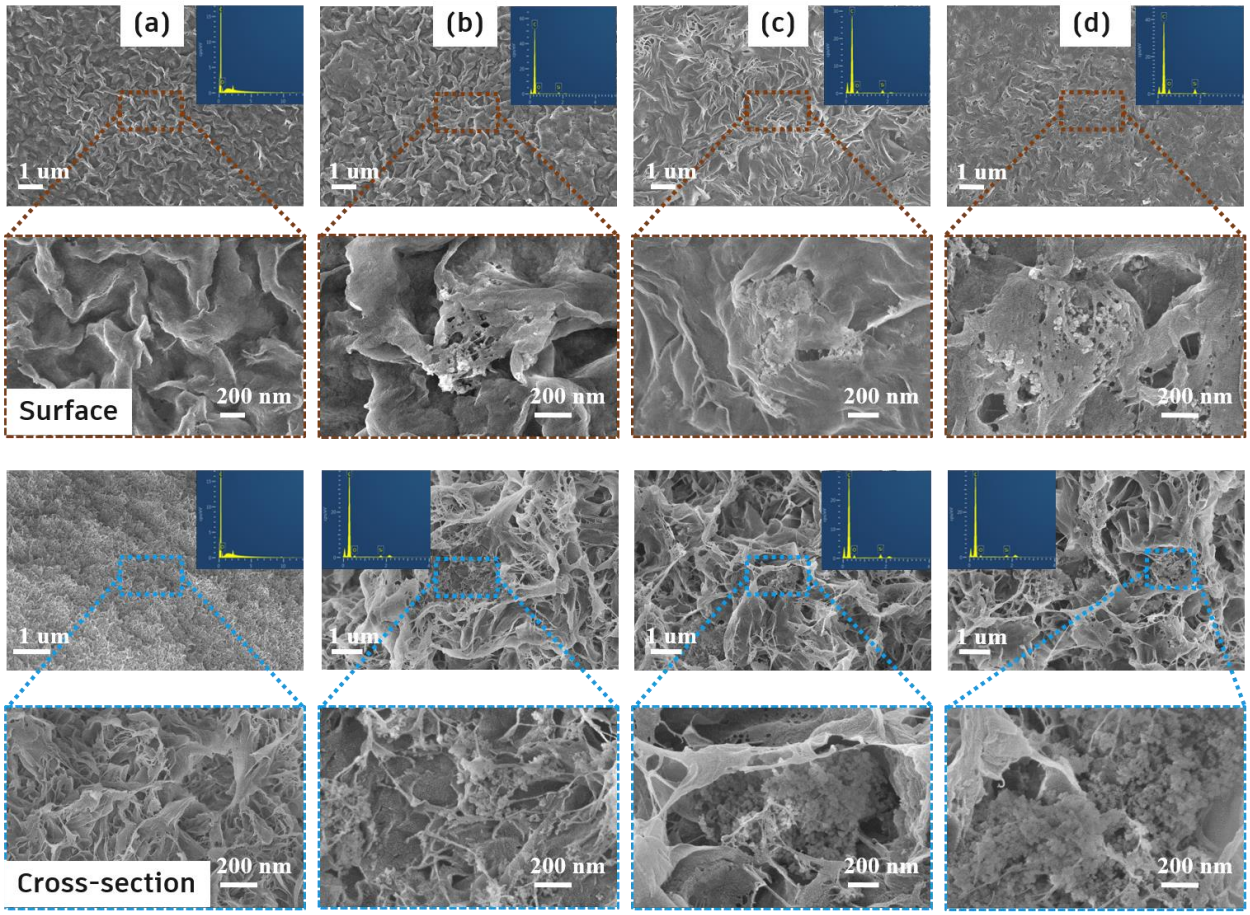

Figure 3-2: SEM snapshots of the surface and cross-section of gel membranes: (a) pure PE, and different ratios of VHMWPE-SiO_2 nanocomposite membranes (VHMWPE-SiO_2/ 95-5, 90-10, and 80-20) corresponding to (b), (c), and (d), respectively. (insert are EDS elementals maps).

It was clear that the pure VHMWPE casting film showed no particle on it, while SiO_2 particles appeared after blended VHMWPE with SiO_2, and the quantity of the SiO_2 was showed

increased when added more content of SiO_2 in the blend solutions. Further, the cross-section of casting membranes was also explored using SEM and EDS to see the presence of SiO_2 inside the casting gel membranes (**Figure 3-2**). Subsequently, the cast gel films were cut and biaxially stretched by a home-made biaxial stretching machine [5]. Lastly, the biaxially stretched membranes after oil extraction and heat treatment were named and labeled as following: (S1) for Pure VHMWPE membranes, (S2, S3, and S4) for different ratios of VHMWPE/SiO_2 nanocomposite membranes 95-5, 90-10, and 80-20 wt%, respectively.

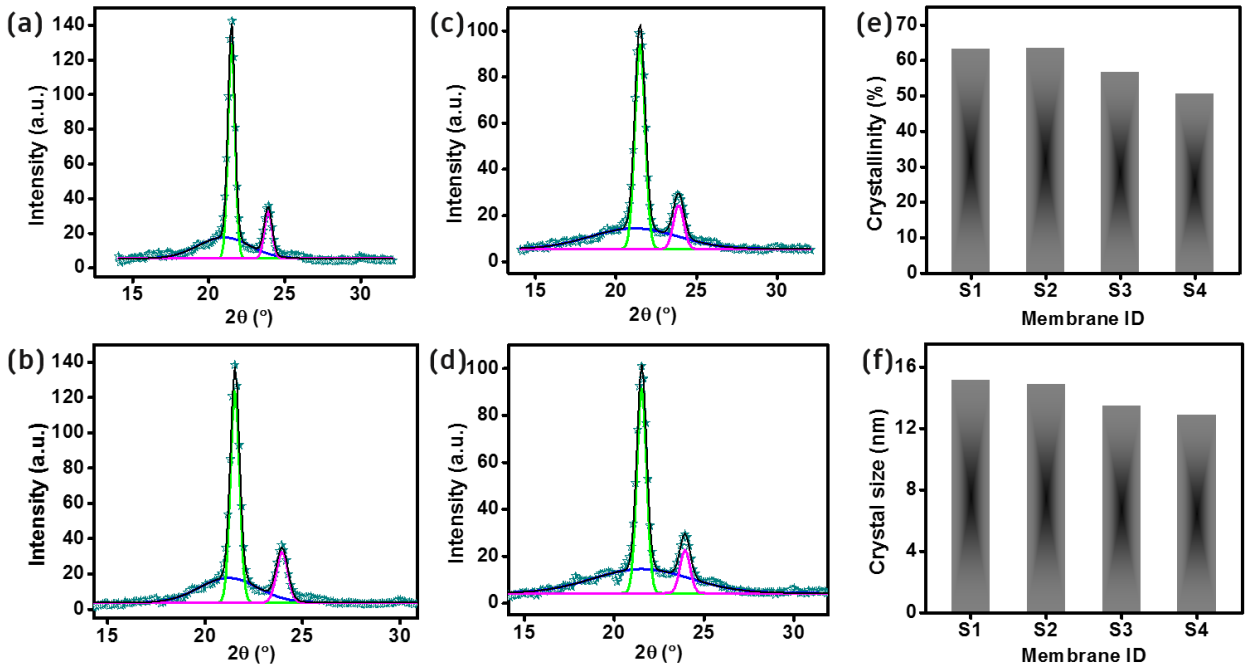

Figure 3-3: Multiple peaks fitted of the1D integrated WAXS curves for (**a**) pure nanofibrous VHMWPE membrane "S1", **(b, c, and d)** different concentrations of nanocomposite VHMWPE/SiO_2 membranes (b) 95-5 wt%, (c) 90-10 wt%, and (d) 80-20 wt%". (**e**) The crystallinity, and (**f**) the crystal size of S1, S2, S3, and S4, corresponding to a, b, c, and d, respectively.

The crystal structures of the VHMWPE nanofibrous membrane and VHMWPE/SiO_2 nanocomposite membranes are characterized by 2D WAXS measurement at room temperature. **Figure 3-3** shows a diagram depiction of Gaussian fitted-peaks of the amorphous and crystalline region to calculate the crystallinity and the crystal size of S1, S2, S3, and S4. The crystallinity almost remains constant for S1 and S2 (**Figure 3-3**e). Nevertheless, it slightly decreased when added more SiO_2 to the membranes. The crystal size was reduced by adding more SiO_2

nanoparticles, as presented in **Figure 3-3**f. The slight reduction in crystallinity and crystal size was mainly due to the existence of SiO_2 nanoparticles in the structures of membranes. The reason is that the molecules of the nanoparticles do not melt in the crystalline region of the polymer [267], which will result in a higher amorphous – to – crystalline proportion in the nanocomposite structures of membranes. SEM-EDS, ATR-FTIR, and TGA further characterize the existence of SiO_2 nanoparticles.

Figure 3-4 displays SEM photographs, EDS maps and cross-section micrographs of pure VHMWPE and different proportions of nanocomposite VHMWPE/SiO_2 membranes. According to the results, nanofibrous membranes with and without SiO_2 exhibited a uniform cross-linked fibril morphology, with nanopores distributed in the network. The dispersion of inorganic SiO_2 nanoparticles in hybrid VHMWPE/SiO_2 nanocomposite separators may change with increasing SiO_2 content, depending on the specific experimental conditions and the properties of SiO_2 nanoparticles and PE matrix. When SiO_2 nanoparticles are added to the VHMWPE matrix, they form agglomerates or clusters due to van der Waals forces and electrostatic interactions. These agglomerates affect the dispersion of SiO_2 nanoparticles in the VHMWPE matrix and the physical and mechanical properties of the resulting hybrid membrane separator. The dispersed morphology of the inorganic SiO_2 nanoparticles can have a considerable impact on the electrochemical performance of the hybrid nanocomposite separator. For example, when SiO_2 nanoparticles are uniformly distributed all over the VHMWPE matrix, they can build an interconnected pore network that facilitates the transport of electrolyte ions, thereby improving electrochemical performance. As can be seen from **Figure 3-4**a, the pure VHMWPE nanofibrous membrane shows a relatively small average pore size of 47.1 nm on its network. Combining the pore size information shown in **Table 3.2**, the membrane morphology in **Figure 3-4**, has demonstrated a significantly enhanced VHMWPE/SiO_2 nanocomposite membranes average pores sizes of S2 ~ 48.8 nm, S3 ~ 57.4 nm, and S4 ~ 63.5 nm. Additionally, the present amount and agglomeration degree of SiO_2 nanoparticles are increasing when adding more SiO_2 to membranes as depicted in SEM cross-section snapshots for pure VHMWPE nanofibrous (S1) and different ratios of VHMWPE/SiO_2 nanocomposite membranes (S2, S3, and S4). The presence of SiO_2 nanoparticles was further confirmed by analyzing C, Si, O elements in weight percentage EDS and XPS analysis. Correspondingly, EDS results in weight percentage shown in **Figure 3-5**a, indicates that the Si element increased due to the different contents of SiO_2 in the network of nanofibrous membranes.

Table 3.2: Summary of the pore size distribution and average diameters of membranes

Membrane ID	Diameter at MAX. Pore Size Distribution (nm)	Mean Pore Diameter (nm)	STDEV of AVG. Pore Diameter (%)
S1	48.40	47.10	0.88
S2	52.60	48.80	1.42
S3	59.10	57.40	2.05
S4	62.80	63.50	2.55

MAX (Maximum); STDEV of AVG (Standard deviation of average).

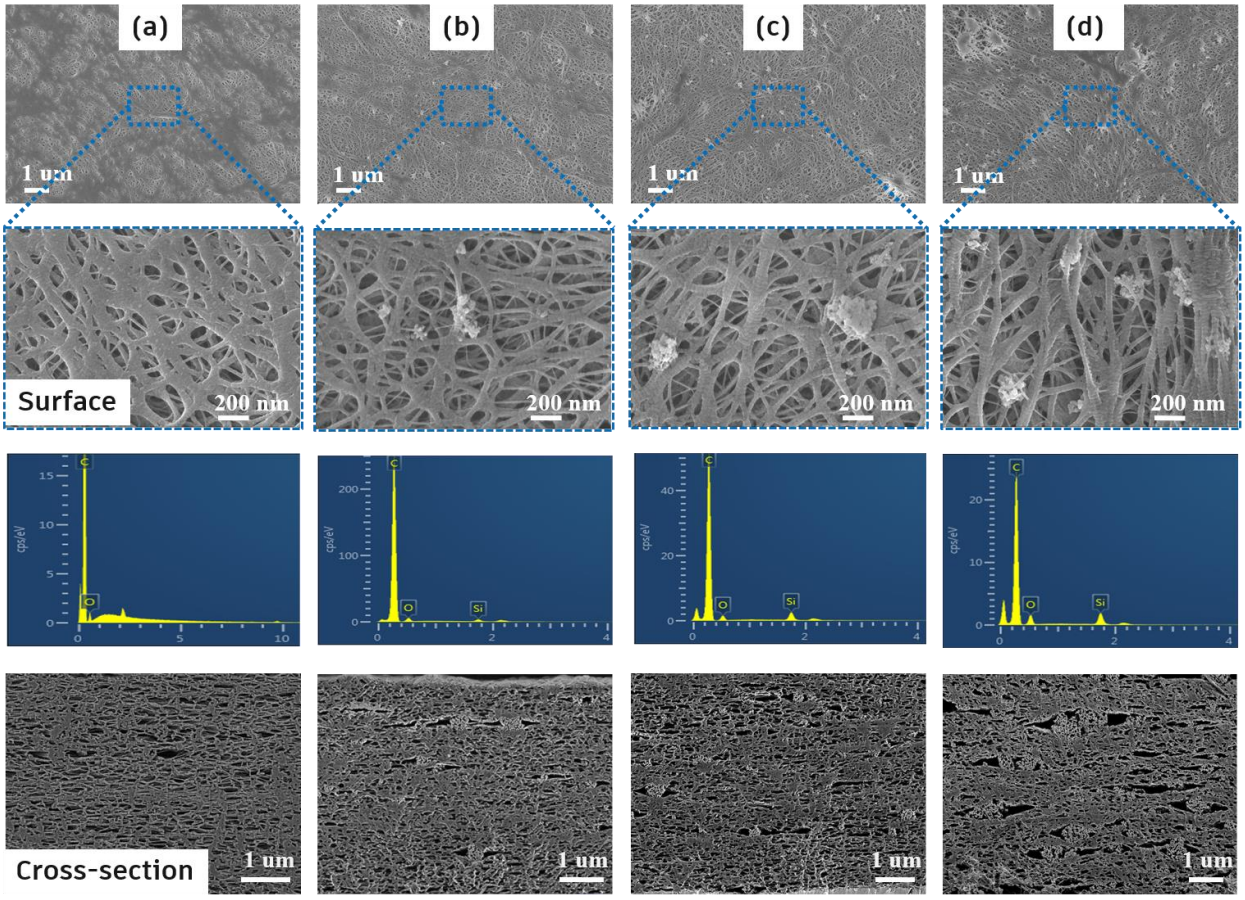

Figure 3-4: SEM photographs, EDS maps and cross-section snapshots of (**a**) pure nanofibrous VHMWPE membrane "**S1**", and (**b**, **c**, and **d**) different ratios of VHMWPE/SiO_2 nanocomposite membranes corresponding to (VHMWPE/SiO_2 - 95/5 "**S2**", 90/10 "**S3**", and 80/20 "**S4**") respectively.

In addition, XPS spectra of pure VHMWPE membrane and different ratios of VHMWPE/SiO_2 nanocomposite membranes were presented in **Figure 3-5**b. On comparing XPS spectra of Si2p scan for all membranes, it can be seen that the intensities peaks of Si2p at 102.9 eV increased when the quantities SiO_2 increased, which is attributed to more contents of SiO_2 in the network of nanofibrous membranes.

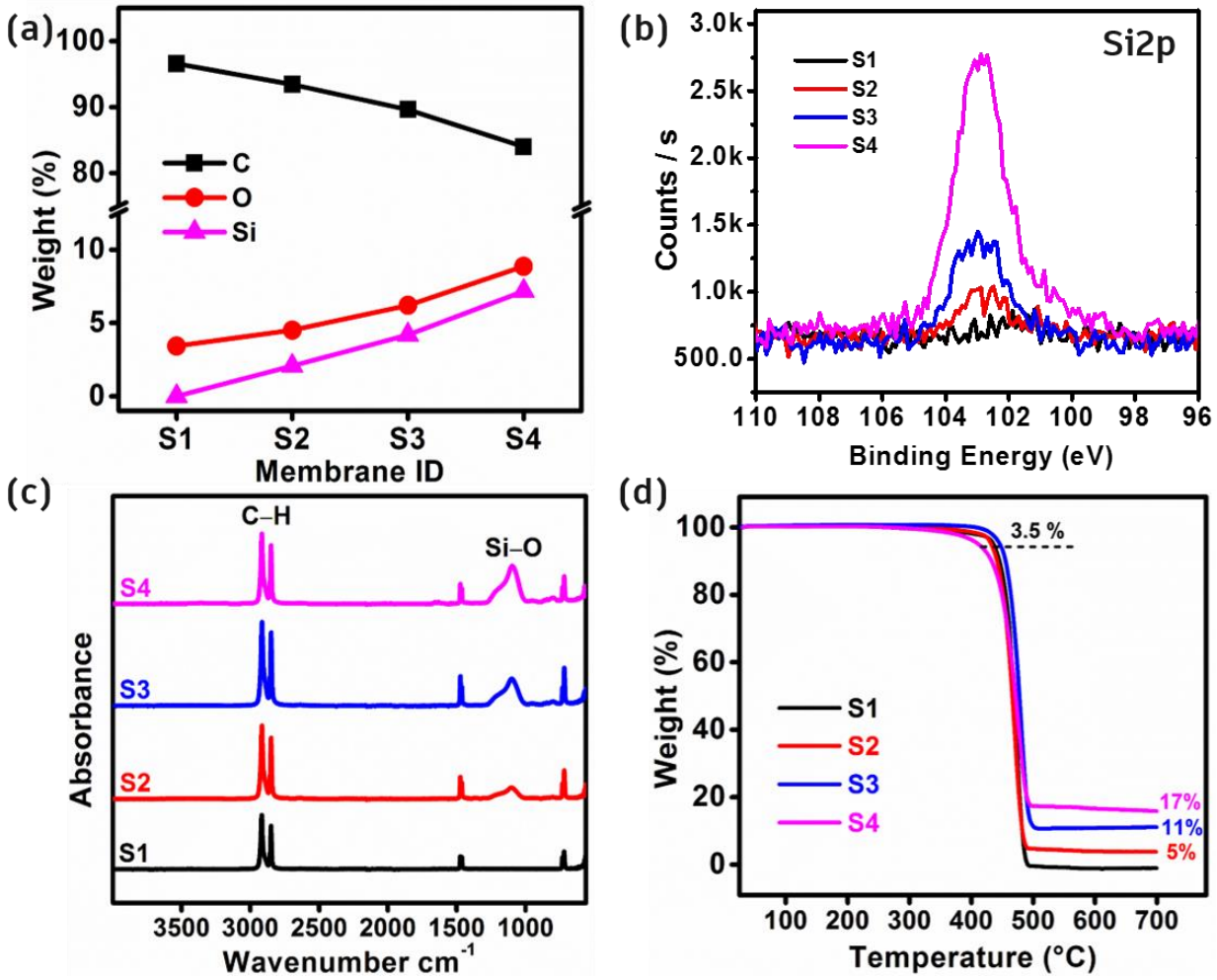

Figure 3-5: Elementals compositions of VHMWPE membranes with/without SiO_2: (a) EDS results, (b) XPS spectra of Si2p scan, (c) ATR Spectra, (d) TGA curves for pure VHMWPE "S1" and different ratios between VHMWPE/SiO_2 nanocomposite "S2, S3, S4" membranes.

ATR-FTIR measurement was conducted to confirm the chemical composition of the pure VHMWPE membrane and VHMWPE/SiO_2 nanocomposite membranes. As presented in **Figure 3-5**c, ATR spectra of the pure VHMWPE separator shows two absorption peaks at 2915 cm^{-1} and 2848 cm^{-1}, corresponding to the symmetric/asymmetric stretching of CH_2. Two more absorption

peaks at 1472 cm^{-1} and 719 cm^{-1} stand for the bending and rocking deformations of CH_2, respectively [268; 269]. Compared with the pure VHMWPE separator, a new absorption at 1100 cm^{-1} appears in the VHMWPE/SiO_2 nanocomposite separator (S2), which is ascribed to the stretching vibration of the Si–O bond [188; 269]. The increased intensity of the Si–O peak at 1100 cm^{-1} in "S3 and S4" is undoubtedly ascribed to the increased amounts of SiO_2 nanoparticles in the network of membranes.

TGA was used to confirm the VHMWPE/SiO_2 nanocomposite membrane's fabrication and investigate the VHMWPE membrane's thermal stability before and after combined with SiO_2 nanoparticles. The results are briefly summarized in **Figure 3-5**d. TGA curve reveals the weight loss of VHMWPE and VHMWPE/SiO_2 membranes as a function of temperature between 25°C and 700°C in an air atmosphere. It can be observed that the pure VHMWPE separator (S1) shows no residual in the temperature range of 500-700°C, which is attributed to the complete decomposition of the VHMWPE separator. However, for VHMWPE/SiO_2 separators, approximately 5% residues are observed in S2 compared to S1 separator, which is due to the existence of inorganic SiO_2 nanoparticles in the membrane network. Compared to the S1 membrane, a weight loss of nearly 3.5 % is observed between 350-450 °C for S3 and S4, which can be attributed to the increased quantity of SiO_2 in nanocomposite membranes, that led to the increasing instability of membranes. This resulted in nanocomposite membranes containing higher SiO_2 content being decomposed earlier. Unsurprisingly, the total amount of the remaining weight increased with increasing the content of inorganic SiO_2, for the reason that SiO_2 nanoparticles did not decompose along with the VHMWPE when heated to 700 °C, which is also a strong proof for the successful fabrication of nanocomposite membranes. Compared with S1, S2 and S3 films, nearly 3.5% weight loss was observed for S4 films between 350-450 °C, which can be attributed to the decomposition of C-O-Si groups and the oxidation of nanocomposite membrane. There are more SiO_2 nanoparticles in the S4 membrane than S2 and S3, resulting in a higher oxygen content in the membrane network, which causes the nanocomposite membrane containing a higher SiO_2 content to be decomposed earlier.

3.3.2. Mechanical properties and thermal stability

The good mechanical properties of separators are considered one of the principal requirements for an ideal separator. It must be sufficiently durable to resist the winding operation's tension during the battery cell's assembly [13; 51]. The stress-strain curves of VHMWPE nanofibrous and VHMWPE/SiO_2 nanocomposite membranes were determined at room temperature. Membranes were cut into a rectangular shape for both MD and TD with typical dimensions (length 100 mm X width 15 mm X thickness 0.0110-0.0183 mm). The stress-strain curves of VHMWPE nanofibrous and VHMWPE/SiO_2 nanocomposite membranes are shown in **Figure 3-6**.

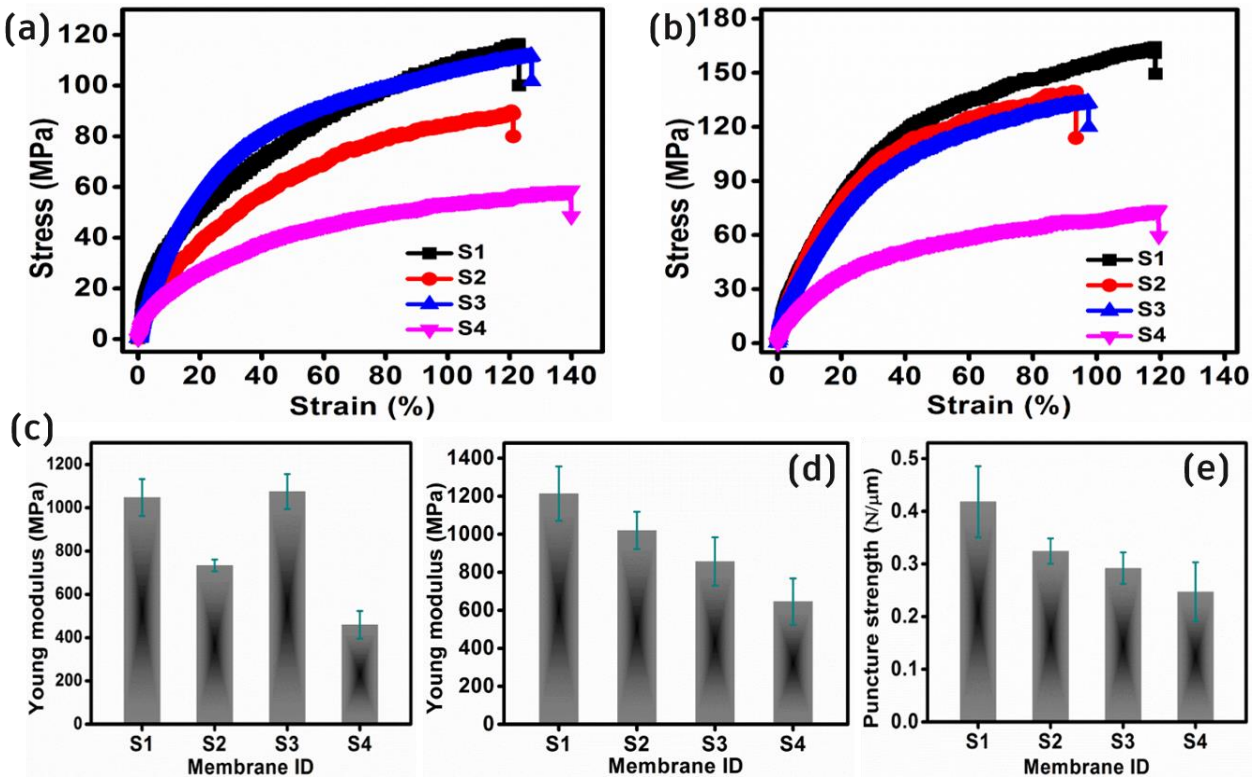

Figure 3-6: The stress-strain curves of the pure VHMWPE "S1", and different percentages of VHMWPE/SiO_2 nanocomposite "S2, S3, S4" membranes for (a) machine direction "MD", (b) transverse direction "TD", (c) and (d) corresponding Young modulus for (a) and (b) respectively. And (e) the puncture strength of pure VHMWPE and VHMWPE/SiO_2 nanocomposite membranes.

As displayed in **Figure 3-6**a, the MD tensile strength of nanocomposite membranes shows slightly decreased for S2 (92 ± 12 MPa) and S3 (111 ± 11 MPa), whereas for S4, the tensile strength dropped to 59.5 ± 5.9 MPa compared to the pure VHMWPE membrane S1 (120.5 ± 5 MPa). This

is possibly caused by the presence of SiO_2 nanoparticles in the VHMWPE membrane network, which reduced the crystallinity and crystal size with somehow fewer fibrils sizes, as showed in WAXS results and SEM photographs. Likewise, the stress-strain curves of nanocomposite membranes in TD are given in **Figure 3-6**b. Furthermore, the Young modulus of all membranes along both MD and TD directions were calculated and summarized in **Figure 3-6**c-d, respectively. The Young modulus shows a decreasing trend in both MD and TD directions. The young modulus of membranes in MD decreased from (S1~ 1048 ± 85 MPa) to (S2~ 734 ± 27 MPa) and displays high increased (S3~ 1075 ± 80 MPa) then again reducing to (S4~ 460 ± 63 MPa). As for TD direction, it can be seen that the Young modulus of all membranes decreased from (S1~ 1214 ± 143 MPa) to (S2~ 1020 ± 98 MPa) to (S3~ 857 ± 127 MPa) to (S4~ 646 ± 122 MPa). Young's modulus and tensile strength were higher in the transverse direction (TD) than in the machine direction (MD). This is caused by the orientation of the polymer chains during the second stretching step in the manufacturing process, also known as the heat setting step in TD. Moreover, the puncture strength of pure VHMWPE membranes and VHMWPE/SiO_2 nanocomposite membranes was presented in **Figure 3-6**e. The puncture strength of S1 is the highest, and that of S4 is the lowest. The puncture strength reduced from (S1 ~ 0.418 ± 0.067 N/μm) to (S2 ~ 0.325 ± 0.024 N/μm) to (S3 ~ 0.292 ± 0.031 N/μm) to (S4 ~ 0.247 ± 0.056 N/μm). It is worth mentioning that the overall trend of mechanical properties was decreased when added more SiO_2, yet these membranes have presented robust mechanical stability, especially S1, S2, and S3.

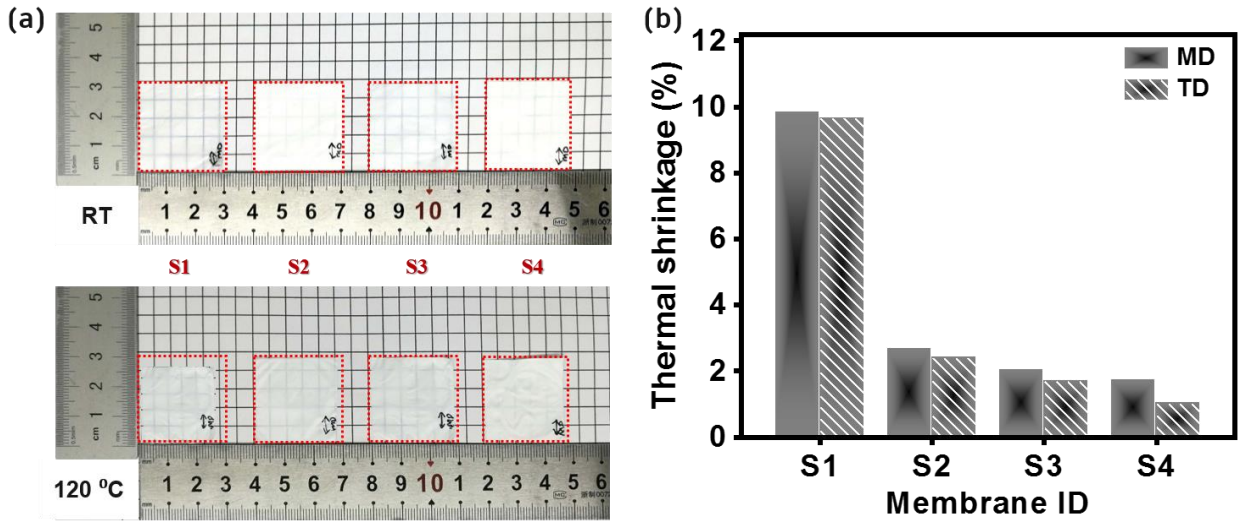

Figure 3-7: (a) Photographs of the pure VHMWPE "S1" and different percentages of VHMWPE/SiO_2 nanocomposite "S2, S3, S4" membranes at room temperature "top" and after

being annealed for 1 h at 120 °C "bottom", (b) the corresponding thermal shrinkage of both MD and TD directions.

The separator's thermal stability is a crucial aspect of guaranteeing battery safety [226]. Commonly, the thermal stability of the separator is determined by the dimensional stability after annealing. Thermal shrinkage requirements of separators are generally less than 5% after annealing at 90 °C for 60 minutes [13; 270]. Here in this work, the thermal stability test was carried out at a temperature of 120 °C for 60 minutes. **Figure 3-7**a displays snapshots of S1, S2, S3, S4 membranes at room temperature (top photograph) and after being annealed to 120 °C for 60 minutes (bottom photograph). The thermal shrinkage percentages of the pure VHMWPE and VHMWPE/SiO_2 separators were shown in **Figure 3-7**b. Form the given **Figure 3-7**, it can be seen that the pure VHMWPE membrane (S1) shrinks sharply in both MD (9.8%) and TD (9.6%) at 120°C. In comparison, VHMWPE/SiO_2 separators possess excellent thermal stability (2.6, 2, and 1.7%) for MD, (2.4, 1.7, and 1%) for TD, correspond to (S2, S3, and S4), respectively. The improvement of the separators' thermal stability may be attributed to the high thermal resistance of SiO_2 nanoparticles in the network of the membrane.

3.3.3. Permeability, electrolyte uptake, and wettability

The Gurley value is frequently employed to symbolize the separator's air permeability. If the Gurley value is low, then the porosity of the separator is high [13]. Characterization of the air permeability via Gurley identifies that the value is declined from 133 ± 5 sec. 100 cc^{-1} (S1) to 124 ± 11 sec. 100 cc^{-1} (S2) to 116 ± 8 sec. 100 cc^{-1} (S3) to 89 ± 5 sec. 100 cc^{-1} (S4). The air permeability result in **Figure 3-8**a is consistent with SEM photographs presented in **Figure 3-4**, and average pore size in **Table 3.2**. It was anticipated that the presence of SiO_2 nanoparticles in the separators would increase the wettability of the separator, as presented in **Figure 3-8**b that the liquid electrolyte contact angle (LECA) of nanocomposites separators (S2-4) is improved compared to the pure VHMWPE separator (S1), as well as the value of the contact angle has decreased continuously over time, which results in an enhancement in the electrolyte uptake. The liquid electrolyte uptake of separators is improved from 175 ± 2% (S1) to 318 ± 14% (S2) to 431 ± 21% (S3) to 473 ± 12% (S4) as in **Figure 3-8**c. In addition, the ionic conductivity in **Figure 3-8**d revealed an increased from 1.5 ± 0.1 × 10^{-3} S cm^{-1} (S1) to 1.7 ± 0.2 × 10^{-3} S cm^{-1} (S2) 2.2 ±

0.05×10^{-3} S cm^{-1} (S3) to $3.4 \pm 0.6 \times 10^{-3}$ S cm^{-1} (S4). The improvement in the ionic conductivity is probable attributed to the superior electrolyte uptake and wettability, caused by the enhancements of electrolyte affinity by SiO_2 nanoparticles. The enriched liquid uptake and ion conductivity increase are thoroughly associated with increased power performance during the battery process.

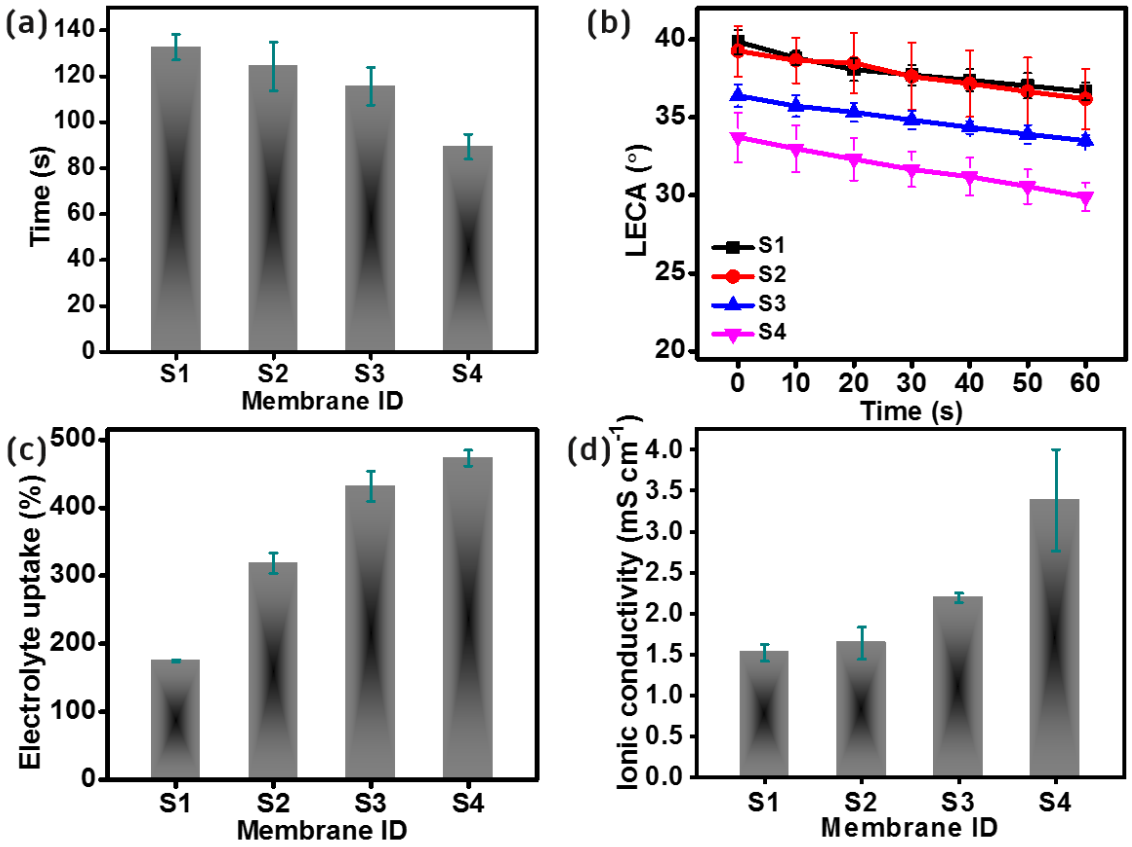

Figure 3-8: (a) The air permeability, (b) liquid electrolyte contact angle "LECA", (c) electrolyte uptake, and (d) ionic conductivity for pure VHMWPE (S1), different percentages of VHMWPE/SiO_2 nanocomposite membranes (S2), (S3), and (4).

3.3.4. Electrochemical performance

The electrochemical measurements of LIBs cells prepared with the VHMWPE and VHMWPE/SiO_2 separators were recorded in **Figure 3-9**. Coin cells were assembled using ($LiFePO_4$)/ (S1-4)/ (Li), and charged by a voltage range from 2.0 V to 4.2 V at a constant charging current density of 1 C and discharging at several current densities from 0.1 C to 5.0 C. **Figure 3-9**a represents the discharge C-rate capacity of the cells at various current densities using S1, S2, S3, and S4. **Figure 3-9**b displays the charge-discharge profiles of S4 at different C-rates. **Figure 3-9**c-d discloses the cyclic performance and coulombic efficiencies at charge/discharge current density of 1/1 C for 100 cycles, respectively. For all separators, the discharging capacities of cells gradually decrease as the discharging current density increases. As the C-rate increases, nanocomposite separators "especially S3 and S4", show enhanced discharge capacities and coulombic efficiencies compared to the discharge capacity and coulombic efficiency of S1. For instance, at 5 C-rate, S4 maintained an excellent coulombic efficiency of 99.2 % with a significantly high discharging capacity of 123 mAh g^{-1}. A coulombic efficiency of 98.6 % with a high discharge capacity of 122 mAh g^{-1} for S3, whereas S1 and S2 kept fewer discharging capacities of 109 mAh g^{-1}, and 118 mAh g^{-1}, with coulombic efficiencies of 97.9 % and 97.8 %, for S1 and S2, respectively. According to these results, S3 and S4 separators achieved high capacities than S1 and S2 separators, especially at a higher C-rate of 5 C. The enhancement in capability at the high C-rate ascribed to the existence of SiO_2 nanoparticles in the separator's network, which causes an excellent electrolyte affinity and high ionic conductivity. **Figure 3-9**b displays the charging-discharging profiles of the cells with the S4 using different current densities. The cell with S4 showed a slight decrease in the capacity profiles when the C-rate increased. However, in comparison with S1 and S2 separators at high and lower current densities, S1 from (0.1C ~ 165 mAh g^{-1}) to (5C ~ 109 mAh g^{-1}) and S2 from (0.1C ~ 162.2 mAh g^{-1}) to (5C ~ 118 mAh g^{-1}). S3 and S4 separators show higher discharge capacities with less drop when the C-rate increases as for S3 from (0.1C ~ 164.1 mAh g^{-1}) to (5C ~ 122 mAh g^{-1}), and from (0.1C ~ 164.6 mAh g^{-1}) to (5C ~ 123 mAh g^{-1}) for S4. Additionally, the cycling performance of the cells assembled with different separators applying a voltage range of 2.0−4.2 V at a constant charging-discharging (1C / 1C) for 100 cycles was investigated. The discharge capacities of all separators have shown obvious increases in the first few cycles for all cells, followed by gradual minor

decreases that might have been attributed to the reason that the cells are fresh and thus need a certain duration of time for a solid electrolyte interface to form on the electrode [271]. As presented in **Figure 3-9**c, all separators show higher discharge capacities of (S1 ~ 144 mAh g^{-1}), (S2 ~ 146.6 mAh g^{-1}), (S3 ~ 145.7 mAh g^{-1}), and (S4 ~ 146.2 mAh $g^{-1\ 1}$) over 100 cycles. Moreover, the coulombic efficiencies (**Figure 3-9**d) of the cell assembled with all separators at 1 C during the cycling process were as follows: 99.88 %, 99.97 %, 99.89 %, 99.93% corresponding to S1, S2, S3, S4, respectively.

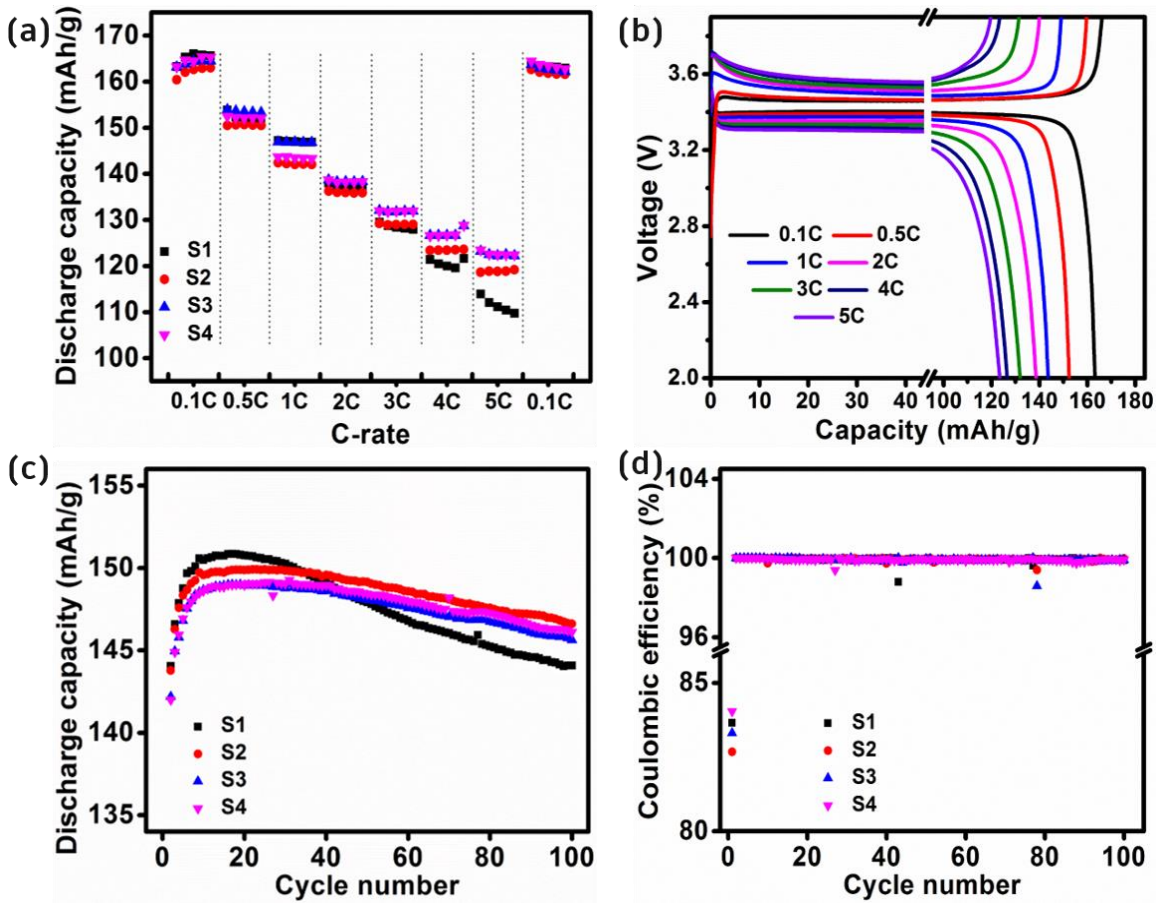

Figure 3-9: Electrochemical performance of LIBs with $LiFePO_4$/Li and different separators; (a) discharge capacities of the cells at various current densities using S1, S2, S3, and S4, (b) Charge-discharge curves of S4 at different C-rates, (c) cycling performance and (d) coulombic efficiency at charging/discharging current density of 1C / 1C for 100 cycles with S1, S2, S3, and S4.

On comparing the main factors between our work and some others' previous work-related separators used in LIBs (**Table 3.3**), our nanocomposite separators have shown comparable

thermal properties, but considerably higher ionic conductivity enhanced porous structure, an excellent electrolyte uptake, and a greater discharge capacity.

Table 3.3: The comparison of key parameters between our work and other previous reports.

Separator	Thermal stability	Gurley value (s 100 cc^{-1})	Ionic conductivity (mS cm^{-1})	Electrolyte uptake (%)	Discharge Capacity (mAh g^{-1})	Ref
PDA/SiO_2-PE	[i]220 °C 0.5 h	-	0.98	80	[ii]106 (0.5C)	[148]
Silica-PE	[i]140 °C 1 h	-	0.35	121 ± 3.4	115 (1C)	[205]
PEI/SiO_2-PE	[i]120 °C 0.5 h	280	0.49	398	140 (0.5C)	[188]
Commercial PE,	[iii]130 °C 0.5 h	-	0.55,	126,	147.5 (0.2C),	[225]
AlOOH-coated PE	[i]150 °C 0.5 h		1.00	187	147.1 (0.2C)	
SiO_2-grafted PE	[i]150 °C 0.5 h	-	0.45	-	125 (0.5C)	[32]
Celgard separator	[iii]100 °C 0.5 h		0.19	80.30	150.5 (0.2C)	[69]
Celgard 2500	[i]130 °C 1 h		0.77	207.4	144 (0.2C)	[272]
PE@AF composite	[i]145 °C 0.5 h	559.0	0.362	225.0	119 (0.4C)	[169]
Nanocomposite PE-SiO_2	[i]120 °C 1 h	89.4 ± 5.4	3.38 ± 0.62	472 ± 11.5	152 (0.5C)	Our work

[i] after treated for 0.5 h at 120 °C, the separator shows good thermal stability (shrinkage< 10%). [ii] at 0.5 C-rate, the discharge capacity is 140 mAh g^{-1}. [iii] after being treated for 0.5 h at 130 °C, the separator exhibits lower thermal stability (shrinkage>10%).

3.3.5. Summary

VHMWPE/SiO_2 nanocomposite membranes were successfully constructed via the sequential biaxial stretching method without any subsequent post-modifications. The structure and properties of pure VHMWPE and nanocomposite VHMWPE/SiO_2 nanocomposite separators were systematically investigated by various characterization techniques, e.g., WAXS, SEM-EDS, FT-IR, XPS, TGA, contact angle measurement, permeability, tensile strength test, thermal stability, and electrochemical performances. The pure VHMWPE separator exhibits a high thermal shrinkage of MD (9.8%) and TD (9.6%). In contrast, the nanocomposite VHMWPE/SiO_2 nanofibrous separators show superior thermal stability, e.g., S3 containing 10 wt% SiO_2 shows enhanced thermal shrinkage of MD (2%) and TD (1.7%). The porosity, air permeability, and electrolyte uptake of obtained nanocomposite membranes are greater than those of pure VHMEPE membrane. Correspondingly, the ion conductivity increased from S1 ~ 1.5 mS cm^{-1} to S2 ~ 1.7 mS cm^{-1} to S3 ~ 2.2 mS cm^{-1} to S4 ~ 3.4 mS cm^{-1}. Besides, VHMWPE/SiO_2 nanocomposite separators show good electrolyte retention capability and excellent mechanical properties. Ascribed to the advantages mentioned above, the obtained LIBs cells with VHMWPE/SiO_2 separator achieve excellent cycle capacity with high Coulombic efficiency of 99.93 % over 100 cycles and C-rate capability 146.2 mAh g^{-1} at a current rate of 1 C. This work provides a facile, cost-effective, and efficient process for designing and manufacturing high-efficient nanocomposite membranes for improving electrochemical performance. Therefore, this effort has broad prospects in promoting the practical application of lithium-ion batteries in the future.

CHAPTER 4. E. Beam Cross-linked VHMWPE/SiO_2 Nanocomposite Separators for LIBs

4.1. Introduction

Rechargeable lithium-ion batteries (LIBs) are a promising next-generation energy storage system due to their high power density, high energy, ultra-fast charging, and no memory effect [273; 274]. Owing to their high specific capacity, long cycle life, and environmental friendliness, rechargeable LIBs have been used in electric vehicles, robots, and various electronic devices such as mobile phones, cameras, and power tools [44; 274-276]. As a vital section of the LIBs, the separator is used to electrically insulate electrodes (anode and cathode) while guaranteeing ions migration between them [276]. Fundamentally, lithium battery separators must have excellent chemical and electrochemical stability to electrolyte and electrode materials. Furthermore, they must possess robust mechanical properties to endure tension during battery assembly. Structurally, the separator porosity should be sufficient architecturally to absorb the liquid electrolyte and provide optimum ionic conductivity [60]. In addition to the basic requirements, the unique structural features given to the separator are now gaining widespread attention as they provide a vital alternative to battery development, including performance and safety [277].

Very high molecular weight polyethylene (VHMWPE) is considered one of the commercially available polyolefin separators widely applied in LIBs owing to its outstanding mechanical properties, excellent chemistry and comparatively cheaper [271]. Nevertheless, it suffers from low thermal stability, which causes the inevitable dimensional thermal shrinkage at high temperatures. Also, polyethylene's inherent hydrophobic behavior permits poor wettability and retention with current commercial electrolytes [278]. Extensive research has been conducted to enhance the thermal stability of commercial separators and increase their affinities toward liquid electrolytes, including grafting polymerization [179; 279], surface coatings and modifications [280; 281]. However, most approaches can result in other severe difficulties and drawbacks, including high-cost equipment, time-consuming preparation processes, increase in thickness and difficulty in control [232; 261]. Lately, ceramic-coated separators have shown significantly enhanced dimensional thermostability, outstanding electrolyte uptake, and wettability owing to ceramic materials'

excellent thermal stability and hydrophilic nature [32]. Nevertheless, properly incorporating these inorganic nanoparticles into separators without damaging their porosity and thickness remains a considerable challenge [220; 261; 282]. In view of that, the modification of commercial separators with unique properties such as high thermal stability, preferred electrolyte wettability, and sufficient permeability without change in microporous structure is greatly desired.

In **chapter 3**, nanocomposite VHMWPE-SiO_2 microporous separators were prepared through the sequential biaxial stretching technique without any crosslinking [83]. The reported nanocomposite separators revealed great electrolyte uptake, adequate ionic conductivity, and superb electrochemical performances. One of the new research directions is to apply advanced techniques to modify nanocomposite separators for enhancing separators' requirements to be endowed with excellent ionic conductivity and extraordinary electrochemical performances. Irradiation is recognized as a valuable and advanced procedure to amend the wettability, structure, and properties of polyethylene (PE) [283]. Irradiation-treated PE membranes by high energy irradiations for instance plasma [284; 285], gamma irradiation [286; 287], and electron beam (E.B) technologies [167; 176; 283]. Among them, E.B has been extensively applied [35; 288]. The high-energy E.B irradiation causes cleavage in C-C and C-H bonds, which lead to the formation of free radicals, chain scission, and the release of hydrogen, leading to crosslinking of the polymer chains [289-291]. The construction of free radicals and chain scission on the polymer structure is anticipated to change the crystallinity of polymers into an amorphous state [292]. Numerous available reports in the literature have studied the effect of E.B irradiation crosslinking on the properties and the structure of PE films with no additional post-modifications or/and grafting. However, few reports help understand the experimental results of E. beam crosslinking PE composite membranes as lithium-ion battery separators. To the best of the author's knowledge, there is no comprehensive work on preparing nanocomposite VHMWPE-SiO_2 microporous membranes using the biaxial stretching technology followed by E. Beam crosslinking for any LIBs separators.

In this study, we aim to prepare commercial VHMWPE-SiO_2 nanocomposite separators, subsequently applying the high-energy E.B irradiation for crosslinking without post-treatments toward overcoming the limitations of commercial separators and improving the electrochemical performance. The impacts of the E.B irradiation on the structure, properties, and electrochemical performances of nanocomposite VHMWPE-SiO_2 separators were intensely studied. Furthermore,

the requirements of separators were systematically studied and compared. The combination of the two proposed processes promotes electrolyte absorption/wettability, improves thermal stability, guarantees safety, and enhances the electrochemical performance of commercial separators without sacrificing their microporous structures and increasing their thicknesses.

4.2. Experimental section

4.2.1. Materials and Methods

Chapter 3 comprehensively describes the nanocomposite separator's raw materials and manufacturing processes. The composite solutions were prepared using 0.9 Kg of VHMWPE powder and 0.1 Kg of SiO_2 nanofillers, which were taken to a specially designed stirring-tank at 100 °C to form homogeneous composite gels of (25 wt% VHMWPE and SiO_2) as powders, 75 wt% paraffin oil as a solvent, and 0.02 Kg Anti-oxidant. Briefly, the manufacturing process involves numerous steps, including blending (composite solutions), solidification (extrusion), stretching (biaxial stretching process), paraffin oil extraction, and finally, heat treatment. Subsequently, separators were further cross-linked by the high-energy electron beam irradiation without post-treatments. Identical steps were repeated using pure VHMWPE without SiO_2 inorganic nanofillers for better comparison and supplementary studies. The schematic illustrations of the preparation and fabrication steps of the VHMWPE-SiO_2 nanocomposite separator (M2) are given in **Figure 4-1**.

4.2.2. Electron beam irradiation crosslinking

Initially, separators were vacuum-sealed in polyethylene plastic bags, then filled with N_2 gas (3-4) times. The remaining air and gas were removed using an electric vacuum packing system (multi-functional vacuum QH-05; made in China). Subsequently, the as-prepared VHMWPE (M1) and VHMWPE-SiO_2 (M2) separators without any pretreatments were directly exposed to the electron beam (E.B) irradiation using an electron accelerator at Anhui Times Innovation Technology Investment Development Co. Ltd., (Hefei, China) at room temperature with irradiation doses of 20 kGy, 50 kGy, and 150 kGy. Finally, M1 and M2 separators after being

irradiated with different E.B doses were coded and given as follows: untreated pure VHMWPE, VHMWPE-20 kGy E.B cross-linked, VHMWPE-50 kGy E.B cross-linked and VHMWPE-150 kGy E.B cross-linked were named as M1-0, M1-20, M1-50 and M1-150, respectively. And the same applies for VHMWPE-SiO_2, which they were coded as M2-0, M2-20, M2-50 and M2-150 corresponding to untreated VHMWPE-SiO_2, VHMWPE-SiO_2 (20 kGy E.B), VHMWPE-SiO_2 (50 kGy E.B) and VHMWPE-SiO_2 (150 kGy E.B), respectively.

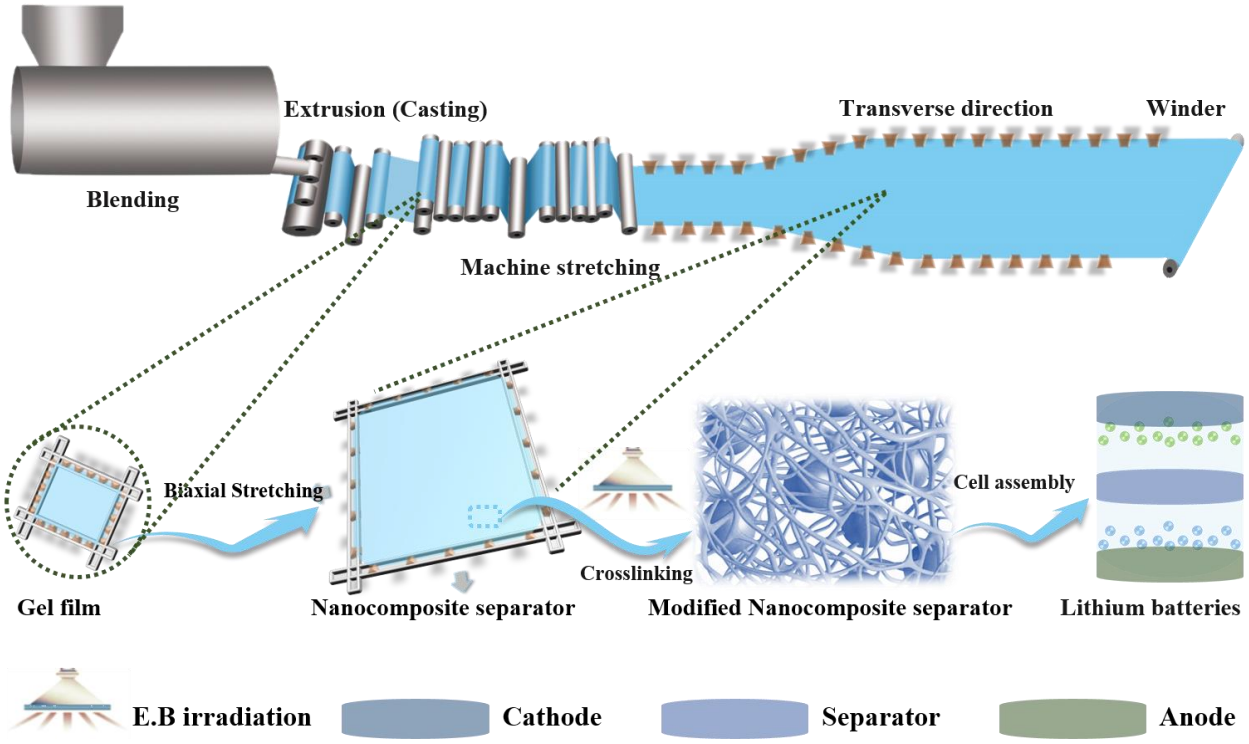

Figure 4-1: Schematic representation of manufacturing and crosslinking of nanocomposite separators.

4.3. Characterization

4.3.1. Morphological and structural characterization

Chapter 3 provides detailed information on characterization instruments including SEM, ATR-FTIR, and Gurley precision instruments which were used to explore the surface morphologies and microstructure of nanofibrous VHMWPE (M1) and nanocomposite VHMWPE-

SiO2 (M2), as well as M1 and M2 membranes before and after E.B crosslinking under different circumstances (N2 and O2 atmosphere).

4.3.2. Differential scanning calorimetry

The differential scanning calorimetry (DCS) tests were performed on a TA Instruments (Q2000 DSC, USA) with samples of approximately 5 mg sealed in aluminum (Al) pans in N_2 atmosphere in the heat range of 40-220 °C using a heating rate of 5 °C /min. DSC experiments were carried out on M1 and M2 to determine the effect of SiO_2 nanofillers on the VHMWPE thermal properties and to evaluate the influence of the electron beam irradiation on the crystallinity of both M1 and M2 membranes. The melting temperature (T_m) and heat of fusion (ΔH), were recorded, and the degree of crystallinity (X_C) was calculated Eq. (4-1):

$$\textbf{Degree of crystallinity } (\boldsymbol{X_C}) = (\boldsymbol{\Delta H})/(\boldsymbol{\Delta H_0} * \boldsymbol{w_{PE}}) * \mathbf{100} \qquad \textbf{(4-1)}$$

where $\boldsymbol{\Delta H}$ is the heat of fusion for the composite, $\boldsymbol{\Delta H_0}$ is the heat of fusion of totally crystallized VHMWPE (289.9 J/g), $\boldsymbol{w}$ is the weight fraction of the polymer matrix.

4.3.3. Mechanical properties and thermal stability tests

The separators must be sufficiently strong to survive the tension of the winding procedure during the assembly of the cell. The mechanical and thermal properties characterization of separators reported in this Chapter were carried out by the same approaches used in **Chapter 3**. The thickness of pure VHMWPE (M1) separators is approximately 10 ± 0.5 um and nanocomposite VHMWPE-SiO_2 (M2) separators in the range of 13 - 18 um (the thickness change is due to the presence of inorganic nanofillers inside the structure of M2 membranes, which is difficult to control).

4.3.4. Electrolyte wettability/uptake and porosity of separators

The electrolyte wettability and uptake of separators presented in this Chapter were determined using the same methods as in **Chapter 3**.

In additional, the N-butanol soaking method estimated the porosity of pure M1 and nanocomposite M2 separators before and after E.B irradiation for 60 mins in ambient atmosphere. The porosity was determined according to the Eq. (4-2):

$$\textbf{Porosity}\ (\%) = (\boldsymbol{W_w} - \boldsymbol{W_d})/\ (\boldsymbol{\rho_L} * \boldsymbol{V_m}) * \mathbf{100}\% \qquad \textbf{(4-2)}$$

where $\boldsymbol{W_d}$ is the weight of the dry separator, $\boldsymbol{W_w}$ is the weight of the wet separator after being immersed in N-butanol for 60 minus, $\boldsymbol{\rho_L}$ is the density of the liquid (N-butanol), $\boldsymbol{V_m}$ is the volume of the dry separator.

4.3.5. Electrochemical measurements

4.3.5.1. Electrochemical stability and conductivity

The ionic conductivity was determined using the same method provided in **Chapter 3**.

The electrochemical stability of pure M1 and nanocomposite M2 separators before and after E.B irradiation was measured by the linear sweep voltammetry (LSV) of (Li "China Energy Lithium Co., Ltd" /separator / stainless steel sheet) cells using a voltage range from 2.5 to 6 (V versus Li/Li^+).

4.3.5.2. Rate capability and cyclic performance

The electrochemical performance, including charging-discharging at various C-rates, C-rate capacities, and cycling performance of LIBs, was performed in coin cells. To measure the output of LIBs, different separators using lithium iron phosphate ($LiFePO_4$) as a cathode and lithium sheet (Li) as an anode are used to assemble into a coin cell. The charge/discharge cycling was calculated at a constant current density of 1C/1C for 100 cycles, while the C-rate capabilities were evaluated in the range of 0.1 C to 8 C. At ambient temperatures, the performance of cells was evaluated in a voltage range of 2.0-3.6 V. The electrochemical performance of the cells was determined with (NEWARE, CT-4008-5V10mA-164) electrochemical workstation.

4.4. Results and discussion

4.4.1. The morphology and microstructure of separators

The nanocomposite of VHMWPE and SiO_2 is fabricated via the biaxial stretching technique using a fixed combination, which was chosen as a suitable model among three other composites from our previous report [83]. The selected nanocomposite M2 and pure M1 were extruded to obtain casting films. SEM surface and cross-section photographs of casting films before the biaxial stretching for M1 and M2 membranes were given in **Figure 4-2**A-D. The high-energy E.B irradiation was applied for crosslinking without any further modification to amend the properties of separators. In order to clearly understand the structure, properties and the performance of the VHMWPE-SiO_2 separator after E.B crosslinking, a pure VHMWPE separator was prepared and E.B cross-linked identically for better comparison.

To explore the surface morphologies of both nanofibrous VHMWPE (M1) and nanocomposite VHMWPE-SiO_2 (M2) separators cross-linked using different E.B irradiation, the SEM photographs test was performed. **Figure 4-2** displayed SEM pictures of M1 and M2 separators cross-linked using different irradiation doses. As seen in **Figure 4-2**a and **Figure 4-2**e, both microporous separators M1 and M2 before E.B treatment show continuous cross-linked micro-fibrils morphologies with distinct pore size, pore orientation and nanopores distributed in the network of membranes. Further, the M2-0 separator in **Figure 4-2**e shows some nanoparticles scattered in the surface of the membrane, suggesting that SiO_2 nanofillers were compactly encapsulated in the VHMWPE matrix. The existence of inorganic nanoparticles has a considerable impact on the microstructure properties of VHMWPE-SiO_2 membranes. Additionally, cross-section SEM images were performed to observe the presence of inorganic nanofillers in the cross-section structure of the nanocomposite M2 separator. As it can be seen **Figure 4-2**j demonstrates some nanofillers in the cross-section image of the M2 separator while M1 in **Figure 4-2**i shows no nanoparticles in its cross-section structure. In addition, when both M1 and M2 separators were E.B irradiated, noticeable changes in the microstructures of membranes with and without nanofillers were witnessed. It is observed that the smallest size micro-fibrils have begun to break, and this breakage increased with the dosage of E.B irradiation. It's well-known that the high

irradiation splits the molecular chain and produces defects in the crystal regions, thus reducing the lamella thickness [293]. Accordingly, the high E.B dosage, specifically 150 kGy in **Figure 4-2**d and **Figure 4-2**h, results in smaller micro-fibrils and more open pores than un-irradiated samples (different magnifications of SEM snapshots in the supporting information **Figure 4-3**). Further characterizations, including DSC, FTIR-ATR, permeability, electrolyte uptake, porosity, etc., were conducted to study the changes in crystallinity, microporous structure, physicochemical and electrochemical properties.

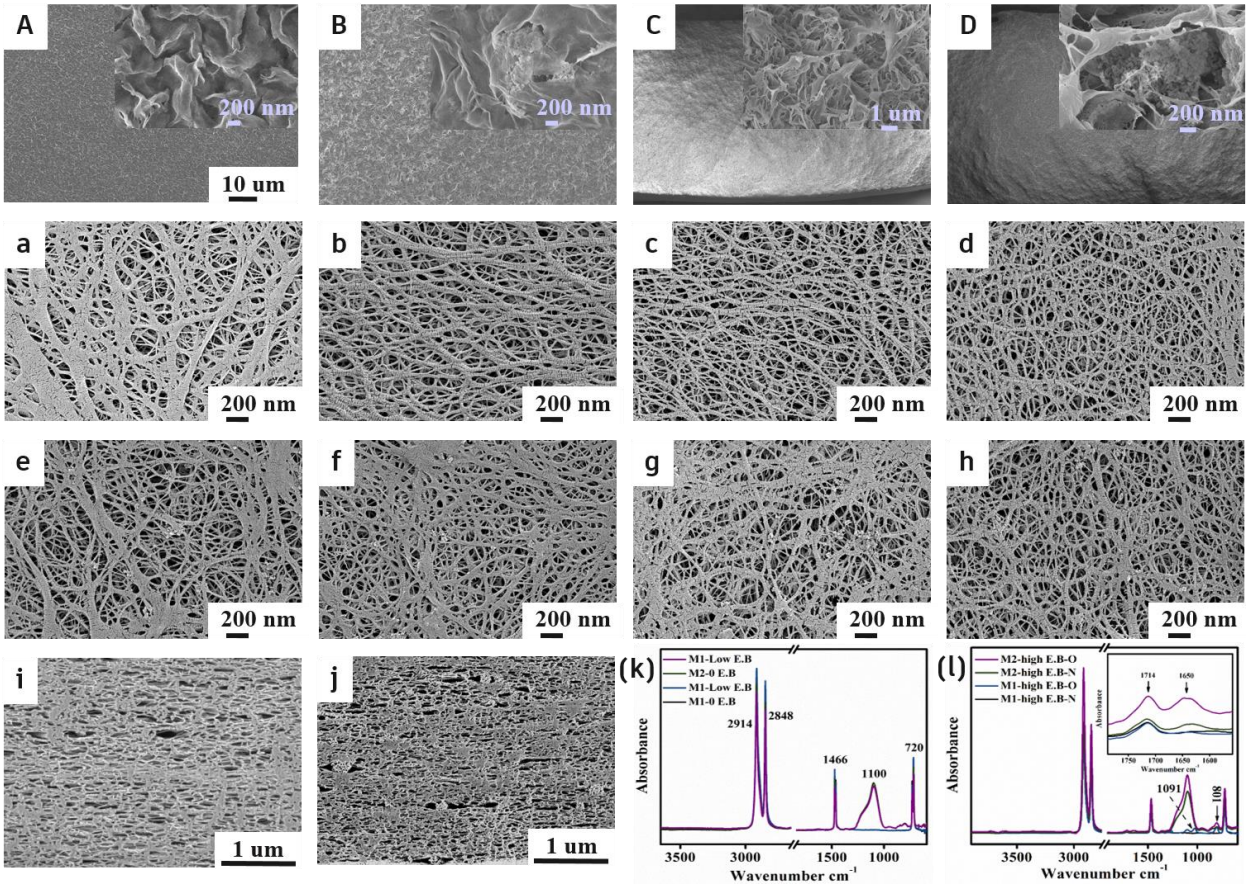

Figure 4-2: (**A** and **B**) Surface morphology and (**C** and **D**) Cross-section SEM photographs of casting films before the biaxial stretching for pure M1 and nanocomposite M2 membranes, respectively. (**a, b, c** and **d**) SEM photographs of (M1-0, M1-20, M1-50 and M1-150kGy), and (**e, f, g** and **h**) SEM pictures of (M2-0, M2-20, M2-50 and M2-150kGy), respectively. (**i**) and (**j**) The corresponding cross-section SEM snapshots for M1-0 and M2-0 separators. (**k**) ATR-FT-IR

spectra of M1 and M2 before and after E.B cross-linked with a low irradiation dose, and (**l**) Cross-linked with high irradiation doses under nitrogen and oxygen atmospheres.

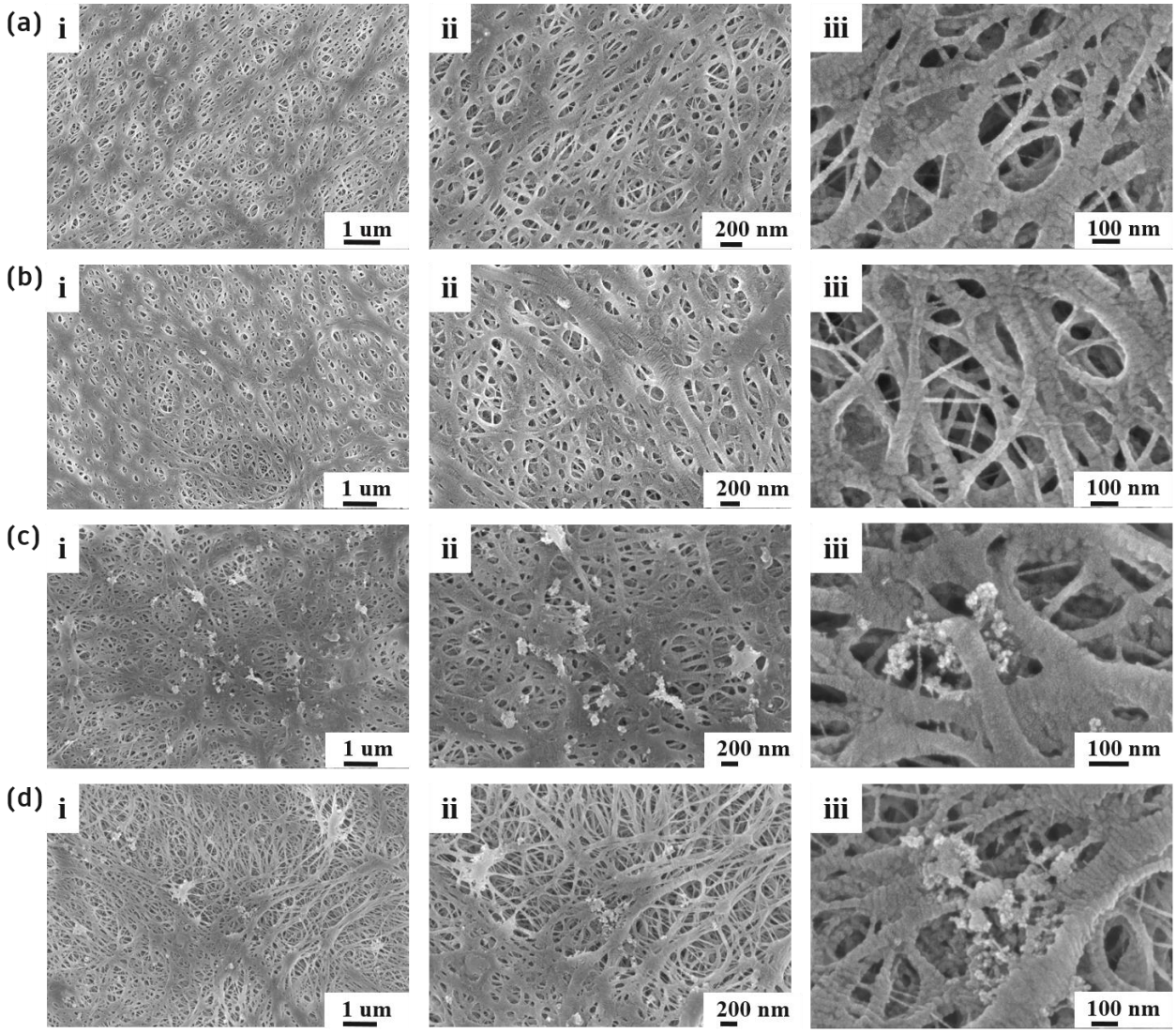

Figure 4-3: (i, ii, and iii) different magnifications of SEM snapshots for (a) M1-0, (b) M1-150, (c) M2-0, and (d) M2-150 separators.

Figure 4-2k-l revealed FTIR-ATR spectrum of M1 and M2 separators before E.B crosslinking, E.B cross-linked with a low and high irradiation dose under N_2 atmosphere and E.B cross-linked with a high irradiation dose under O_2 atmosphere. All M1 and M2 microporous membranes with/without inorganic fillers and E.B irradiation revealed peaks at 2914 cm^{-1} and 2848 cm^{-1} which correspond to CH_2 stretching, 1466 cm^{-1} ascribed to CH_2 bending, and 720 cm^{-1}

attributed to CH_2 rocking [284]. All M2 nanocomposite membranes presented a new absorption peak at 1100 cm^{-1}, which attributed to the Si–O stretching vibration band in SiO_2 [185]. No new peaks were witnessed for the low E.B irradiation under N_2 condition in **Figure 4-2**k, because the low E.B dose did not influence the absorbance of C=C and C=O groups. The high E.B irradiation dose of both M1 and M2 separators under nitrogen and oxygen conditions in **Figure 4-2**l results in new low-intensity peaks appearing nearby 1714 cm^{-1} correspond to carbonyl C=O bonds, attributable to the reaction of polyethylene with oxygen in the atmosphere during the E.B irradiation [176; 294]. The generation of carbonyl bonds caused by the high-energy E.B irradiation crosslinking promotes fast Li^+ migration and increases the polar solvent affinity of both M1-150 and M2-150 separators, resulting in superior ionic conductivities and enhanced rate capabilities [176]. Moreover, M1-150 and M2-150 separators displayed a new peak at 801 cm^{-1}, corresponding to the trans-vinylene absorption group [295]. And nanocomposite M2 separators displays C=C stretch peaks in the range of 1620–1680 cm^{-1} [296]. A new absorption bands at 1091 cm^{-1} is attributed to the C–O stretching vibration caused by the oxidation of M1-150 after being irradiated with high E.B under the oxygen atmosphere [297]. Such results suggest that both M1 and M2 separators have been successfully cross-linked by E.B irradiation.

DSC experiments were carried out in a heat range of 40–210 °C to investigate the impact of high energy E.B irradiation on the thermal and structural properties of VHMWPE (M1) and VHMWPE-SiO_2 (M2) separators, including melting temperature (T_m), the heat of fusion (ΔH) and the degree of crystallinity (X_C). DSC first heating scans, DSC cooling scans and DSC second heating curves are recorded in **Figure 4-4**, respectively**.** The first heating cycle (T_m, ΔH and X_C) were reported in **Table 4.1**. The first heating scan curves in **Figure 4-4**a-d were used for studying the E.B irradiation-induced crystallinity changes in M1 and M2, respectively. It can be seen that the addition of the inorganic SiO_2 has a slight impact on the melting temperature and crystallinity of M2. Before the irradiation, the nanocomposites separator M2 has a T_m of 140 °C compared to 138.7 °C for pure nanofibrous M1. And the crystallinity slightly decreased from 79.1 % for M1 to 75.5 % for M2 (**Table 4.1**). The slight increase in T_m and the decrease in X_C indicate that the inorganic nanofillers have amended the VHMWPE melting temperature and reduce the crystallinity of the VHMWPE matrix. However, T_m and X_C slightly decreased in M1 and M2 membranes after E.B irradiation, as revealed **Figure 4-4** and **Table 4.1**. The slight increase in T_m

indicates that the inorganic nanofillers have amended the VHMWPE melting temperature due to the high thermal stability of the inorganic SiO_2 nanofillers.

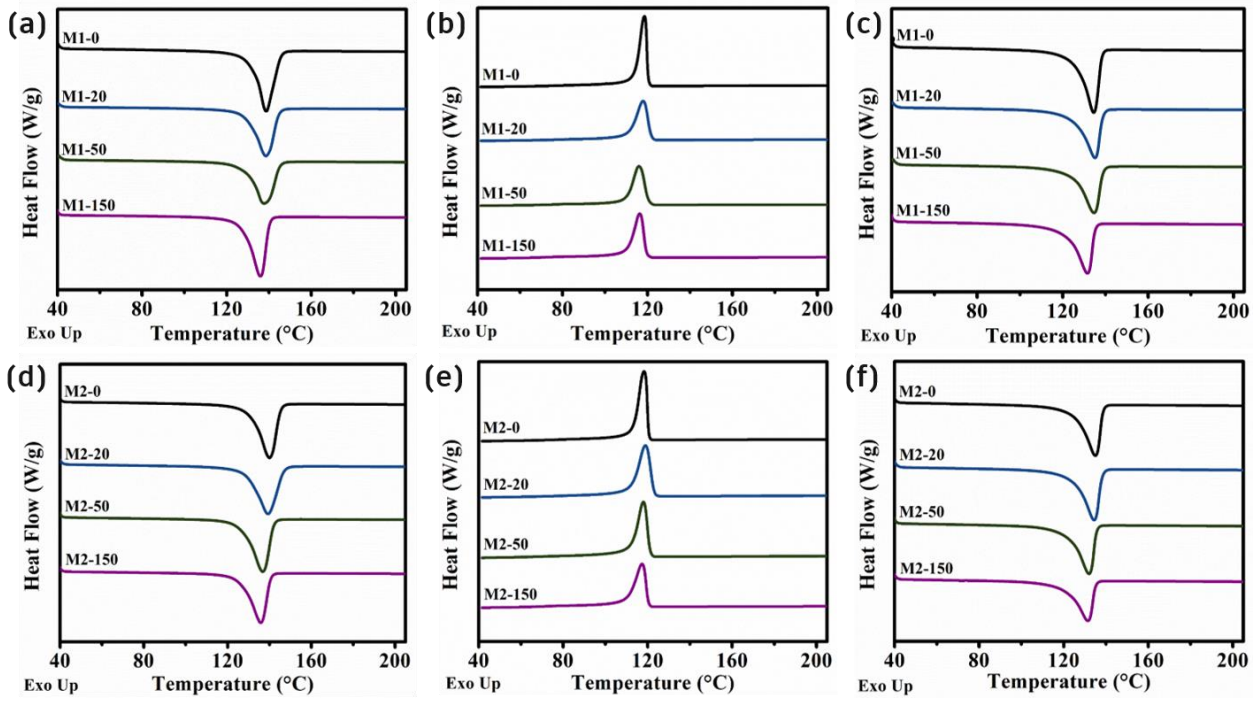

Figure 4-4: (a) The first heating cycle (b) Cooling curve and (c) Second heating curves of DSC curves for pure VHMWPE "M1" cross-linked with different irradiation doses. (d) The first heating cycle (e) Cooling curve and (f) Second heating curves of DSC curves for nanocomposites VHMWPE-SiO_2 separators "M2" cross-linked with different irradiation doses.

Furthermore, incorporating SiO_2 nanofillers reduced the VHMWPE matrix's crystallinity because the molecules of SiO_2 nanoparticles do not melt in the crystalline area VHMWPE, which will result in a higher amorphous-to-crystalline region in the structures of nanocomposite M2 separator [83]. T_m and X_C slightly decreased in M1 and M2 membranes after E.B irradiation, as revealed in **Figure 4-4** and **Table 4.1**. The T_m and X_C of E.B irradiated samples decreased as E.B irradiation doses increased from 20-150 kGy. The slight decrease in T_m with increasing E.B irradiation dosages might be explained by the fact that radicals are formed in the crystalline region, where they are frozen, owing to the hindered movement of polymer chains to prevent crosslinking in crystalline areas [294]. Moreover, the cooling scans of M1 and M2 separators were presented in **Figure 4-4**b-e, respectively. It was found that all membranes were influenced by the E.B

irradiation crosslinking, and the T_m and the corresponding heat of fusion (ΔH) decreased when the E.B irradiation dose increased. Ordinarily, increasing the E.B irradiation dose increases the degree of cross-linking, which dampens the polymer chain mobility, and gradually reduces crystallization parameters [298]. **Figure 4-4**c-f displayed the corresponding DSC second heating cycles for the E.B cross-linked M1 and M2. It can be seen that the E.B irradiation-induced crosslinking changes in crystalline structure for both M1 and M2 and all crystallization parameters peaks including T_m and ΔH shifted to lower temperatures as the E.B irradiation dose increased. The obtained results indicate that the decreases in crystallinity of both pure M1 and nanocomposite M2 are associated with the increase in E.B irradiation doses causing differences in the physicochemical properties. These changes in physicochemical properties greatly affect other properties including mechanical properties and electrochemical performance. As it is well known that mechanical properties are associated with various factors, for instance, crystallinity and microstructure of separators. The high E.B irradiation doses increase chain scission, which causes a decrease in crystallinity, as presented in **Figure 4-4** and **Table 4.*1*** This will also influence the electrochemical performances, including the ionic conductivity, rate capabilities, charging-discharging, and cycle performances, as reported by numerous scientists.

Table 4.1: Effect of E.B doses on the crystallization parameters of M1 and M2 separators.

E.B dose (kGy)	M1			M2		
	T_m (°C)	ΔH (J g^{-1})	X_C (%)	T_m (°C)	ΔH (J/g)	X_C (%)
0	138.7	228.7	79.1	140.0	196.5	75.5
20	138.5	215.1	74.4	139.3	189.7	72.9
50	137.7	207.1	71.7	136.7	179.5	69.1
150	135.9	201.2	69.6	135.9	169.7	65.2

E.B: Electron beam, T_m: Melting temperature, ΔH: Heat of fusion, X_C: Degree of crystallinity.

4.4.2. The mechanical properties

The mechanical characteristics of separators significantly influence the ionic conductivity, which will lead to a considerable impact on LIBs electrochemical performances including charge-

discharge and cycle performances [51]. As displayed in **Figure 4-5**, pure M1 separators showed the highest mechanical properties compared to nanocomposite M2 separators and this is probably caused by the existence of inorganic SiO_2 nanofillers in the VHMWPE matrix. As well, it can be noticed that the mechanical properties of both M1 and M2 separators demonstrated improvements in TD compared to MD, which is due to the heat-setting stage of TD direction during the fabrication procedures. Moreover, **Figure 4-5a-d** exhibit typical stress-strain curves for M1 and M2 separators under different E.B irradiation doses in MD and TD directions. From the summarized and recorded data in **Figure 4-5i-j**, the average tensile strength in both MD and TD of M1 decreases at E.B dose of 20 kGy, increases at E.B dose of 50 kGy, and then decreases with an increase in the E.B irradiation dose of 150 kGy. Also, the mechanical behaviours of M2 at different irradiation doses were recorded and given in **Figure 4-5k-l.**

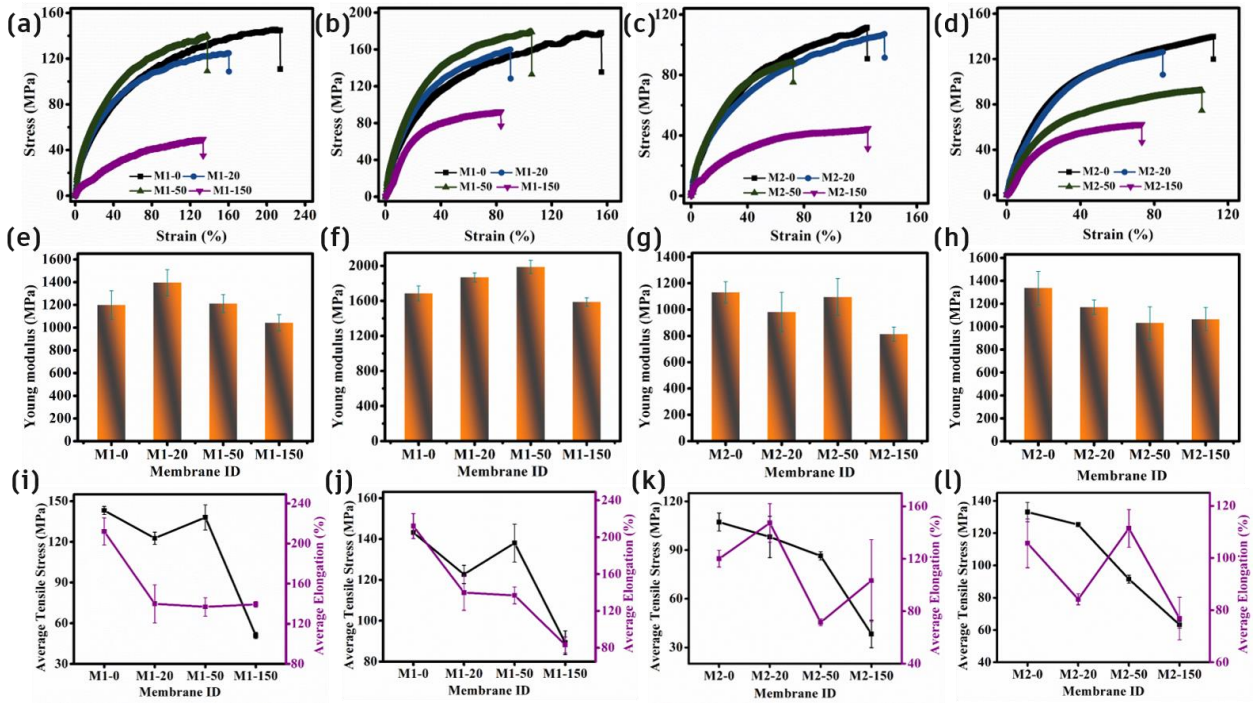

Figure 4-5: Mechanical properties of M1 and M2 separators at different irradiation doses: (a-d) Stress-strain curves, (e-h) Young modulus, and (i-l) Summary of tensile strength and elongation at break; (a, e, and i) M1 in MD, (b, f, and j) M1 in TD, (c, g, k) M2 in MD, and (d, h, l) M2 in TD directions.

Tensile strengths of M2 in MD and TD decreased as the E.B irradiation doses increased, while the elongation in MD increased at E.B dosage of 20 kGy, decreased at E.B dose of 50 kGy and then increased at E.B dose of 150 kGy. The tensile strength and elongation results disclosed that the mechanical properties of both M1 and M2 are noticeably influenced by E.B irradiation crosslinking. Moreover, Young's modulus of M1 and M2 separators in MD and TD cross-linked with various E.B irradiation doses were determined and reported in **Figure 4-5e-h**. As presented, Young's modulus of M1 and M2 before E.B irradiation was the highest. On the other hand, Young's modulus decreases when the E.B cross-linking was applied and it is visibly reduced when E.B doses increase. Furthermore, puncture strengths of M1 and M2 separators before and after E.B irradiation were recorded in **Table 4.2**. The puncture strength of both M1 and M2 separators before irradiations showed higher puncture strength of M1 and M2 after irradiations. The decreasing trend of mechanical properties, including tensile strength, elongation, Young's modulus, and puncture strength correlates with the decrease in crystallinity caused by increasing doses of E.B irradiation and the increases of the chain scission.

Table 4.2: The puncture strength of M1 and M2 separators before and after E.B irradiation

Membrane ID	M1		M2	
	Before irradiation	After irradiation	Before irradiation	After irradiation
Puncture strength (g)	429.7	223.7	367.3	238.0

4.4.3. The thermal stability

The thermal stability “shrinkage” is directly correlated with battery safety. The standard requirement for the thermal shrinkage of separators is less than 5% when annealing at 90 °C for 1h. This study carried the thermal shrinkage test in MD and TD after placing a membrane of approximate size (3×3 cm) at 120 °C for 1h. **Figure 4-6a** shows M1 and M2 separators photographs with/without E.B irritation at RT and **Figure 4-6b** after being annealed for 1h at 120 °C. The corresponding thermal shrinkage rates in MD and TD directions are displayed in **Figure 4-6c**. Remarkably, the M2 separator demonstrates excellent thermal stability (less thermal shrinkage) of (MD ~2.1%) and (TD ~2.3%), whereas the M1 shrunk sharply (MD ~ 9.8%) and

(TD ~9.6%). This finding shows that the M2 separator's thermal shrinkage is significantly modified compared to the pure M1 separator due to the existence of inorganic SiO_2 nanofillers. In addition, after M1 and M2 were E.B. irradiated, both separators showed enhanced thermal stability (less shrinkage in MD and TD), because E.B irradiation-induced crosslinking radically impedes the polymer chain mobility, which hinders the thermal shrinkage of separators [299]. Therefore, E.B irradiation crosslinking significantly reduces the thermal shrinkage rate of M1 and M2 separators, especially at high E.B irradiation doses. For example, the overall thermal shrinkage rate of the M1-150 separator is (MD ~1.7%) and (TD ~0.7%) respectively. Similarly, M2-150 exhibits unique thermal stability of (MD ~1%) and (TD ~0%). The outstanding amendment on the thermal stability of M2-150 is due to the simultaneous presence of SiO_2 nanofillers and E.B irradiation crosslinking.

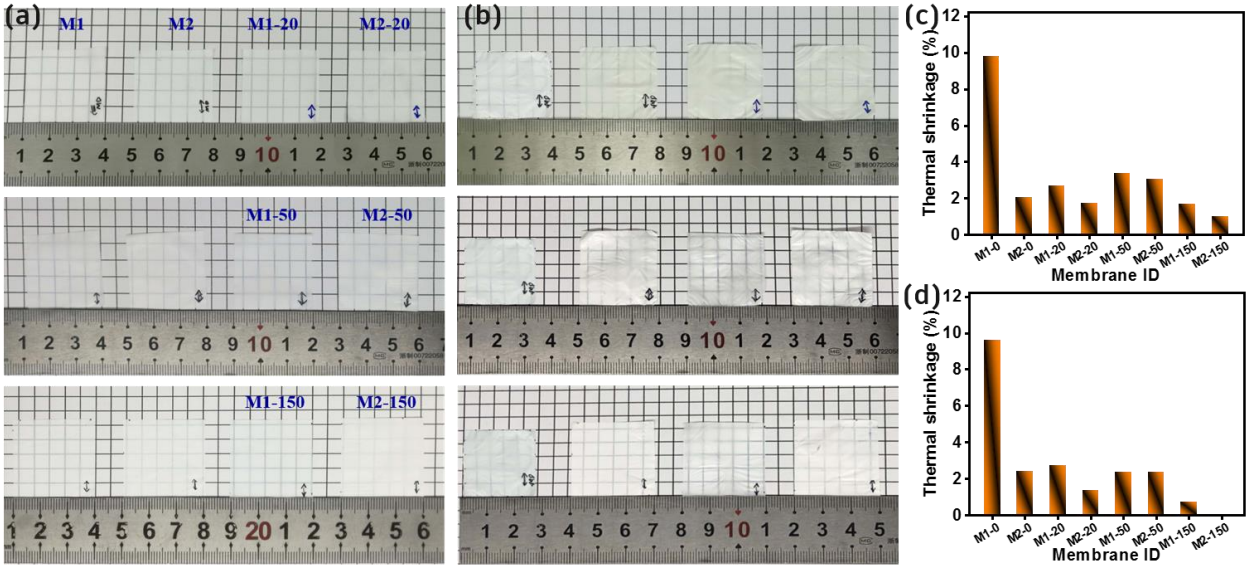

Figure 4-6: (a) Photographs of M1 and M2 separators before and after E.B irritation at RT, (b) After being annealed for 1 h at 120°C, (c) and (d) The corresponding thermal shrinkage in MD and TD directions, respectively.

4.4.4. Electrolyte uptake, wettability, permeability and porosity.

The electrolyte wettability is a key performance of LIBs separators, because electrolyte uptake is critical for ionic passage. A separator with high electrolyte uptake and sufficient porosity tends to increase ionic conductivities and improve discharge capacities [169]. **Figure 4-7**a&b show

the liquid electrolyte contact angle (LECA) for M1 and M2 at different E.B irradiation. The M1-0 exhibited the highest LECA value. In contrast, M2-0 showed better wettability than M1-0, attributable to the presence of SiO_2 nanofillers. After E.B cross-linked, both M1 and M2 presented better wettability by presenting less LECA value, which led to superior electrolyte uptake. The air permeability of the separator can be defined through the MacMullin number, which is often symbolized by the Gurley value [13]. Typically, M1-0 shows a highest curly value and lowest porosity in **Figure 4-7**c&d, respectively.

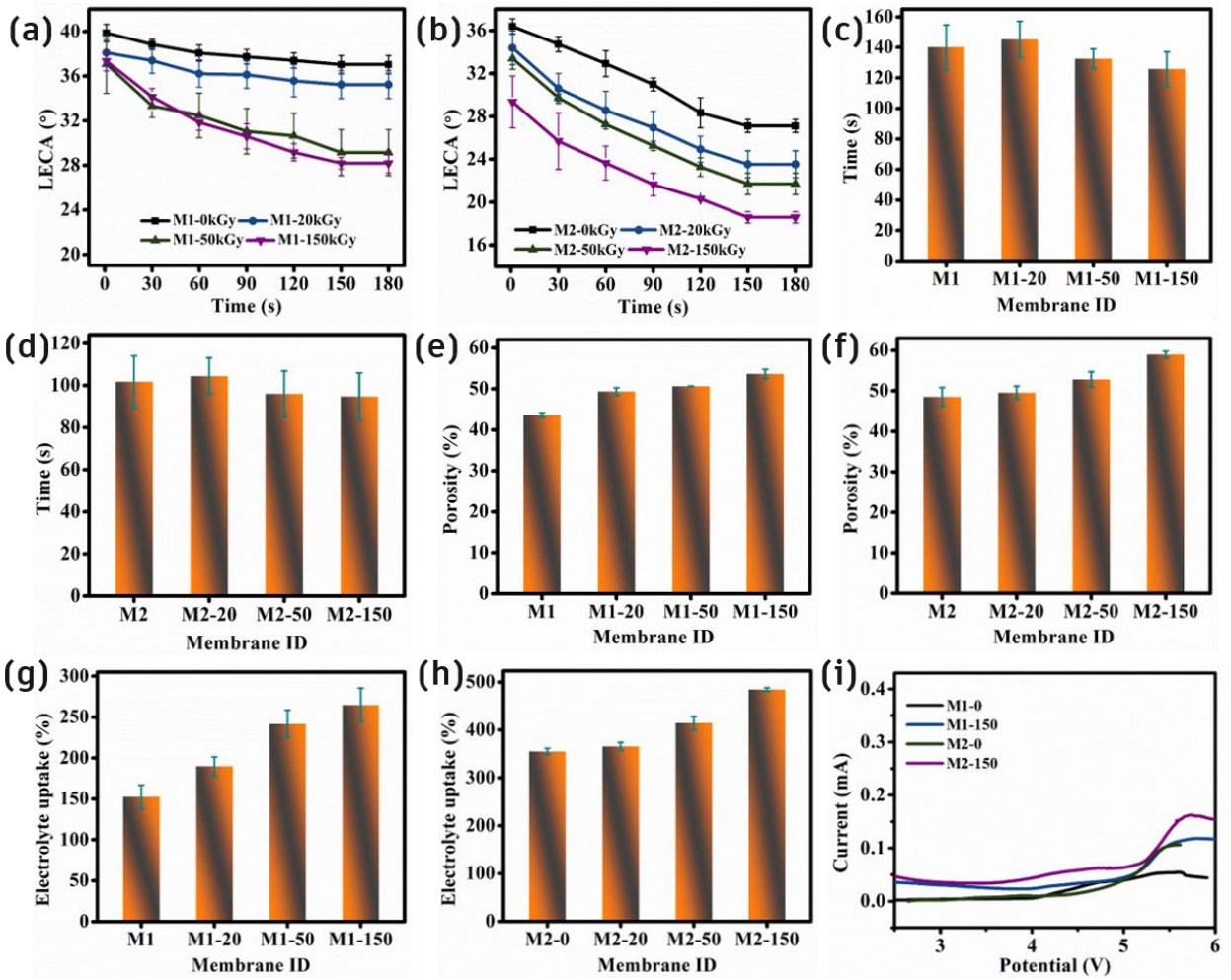

Figure 4-7: (a and b) Recorded liquid electrolyte contact angle "LECA", (c and d) Air permeability values, (e and f) Porosities, and (g and h) Electrolyte uptakes of pure M1 and nanocomposite M2 separators at different radiation doses, respectively. (i) Linear sweep voltammetry (LSV) curves

of (Li sheet/ electrolyte-soaked separator/ SS sheet) cells assembled employing pure M1 and nanocomposite M2 separators before and after E.B irradiations.

When the E.B irradiation dose increased, the permeability to some extent increased, and the porosity enhanced. The nanocomposite M2-0 presented better permeability and porosity than M1-0. Likewise, for E.B irradiation cross-linked M2 membrane separators, permeability and porosity considerably increased as E.B dose increased, as revealed in **Figure 4-7**e-f. The M2-150 displayed the greatest porosity due to its microporous structure resulting from the combination of SiO_2 nanofillers and the E.B irradiation crosslinking. The electrolyte uptakes of M1 and M2 are revealed in **Figure 4-7**g-h. As it can be seen that electrolyte uptakes of both M1 and M2 are significantly improved after E.B irradiation crosslinking. The excellent electrolyte uptake/wettability of separators will accelerate a high-efficiency transmission of ions and achieve superior ionic conductivity [76; 286]. E.B irradiation crosslinking increased the wettability of the nanocomposite separators with polar liquid electrolyte, thus resulting in enhanced C-rate performance and more stable cycling.

4.4.5. Electrochemical performance

4.4.5.1.The electrochemical stability and ionic conductivity

The electrochemical stability of the nanocomposite separator is an essential factor for its practical application in LIBs. The electrochemical oxidation limits of electrolyte-soaked different separators can be determined by the fast increase in the current, which indicates the starting point of the decomposition. The linear sweep voltammetry (LSV) test was conducted to compare the electrochemical stability windows of pure M1 and nanocomposite M2 separators before and after E.B crosslinking. According to the results presented in **Figure 4-7**i, the electrolytic-soaked M1-0 separator displays a stability of about 4.5 V, while that of the M2-0 separator is improved to ~ 4.8 V. This result means that the M2-0 separator can withstand the operating voltage of the cell more stable than the M1 separator. Further, no noticeable electrochemical decomposition of any components occurs at less than 4.5 V for irradiated M1 and M2 separators, indicating that both M1-150 and M2-150 are more stable than non-irradiated M1-0 and M2-0 separators. The great stability enhancements in the nanocomposite M2 separator might have been ascribed to the better

interfacial compatibility of the nanocomposite separator by accumulating the two steps of SiO_2 nanofillers and E.B irradiation crosslinking. The E.B irradiation crosslinking of M1 and M2 separators is valuable for increasing the ionic passage since it improves the electrolyte wettability and uptake of M1 and M2 separators [176]. The Nyquist curves of the liquid electrolyte-soaked pure M1 and nanocomposite M2 separators with different irradiation doses are presented in **Figure 4-8**a-b, respectively. The ionic conductivity of M1 was calculated from the bulk resistance and recorded in **Figure 4-8**c-d. As it can be seen in **Figure 4-8**, ionic conductivities of both M1 and M2 separators were noticeably improved when E.B irradiation doses increased.

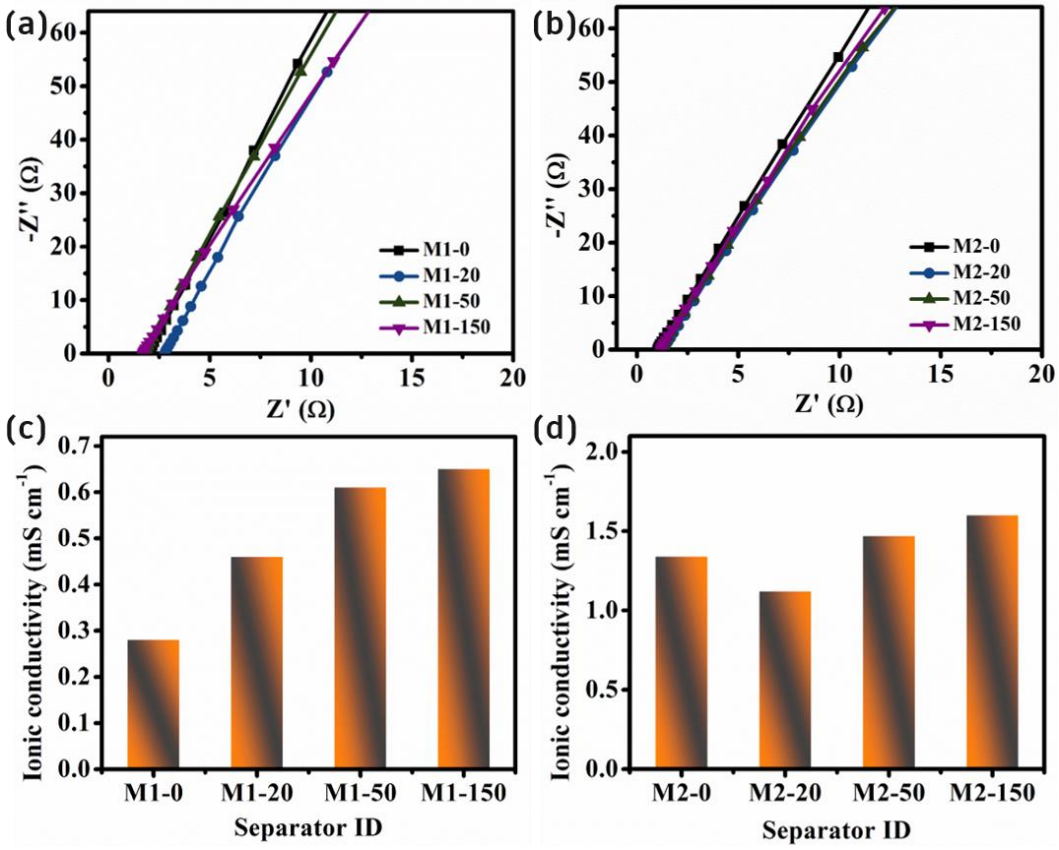

Figure 4-8: Nyquist plots of (SS/liquid electrolyte-soaked separators/SS) cells for (a) M1 and (b) M2 separators at different irradiation doses. (c-d) The corresponding ionic conductivity of (a-b).

The initial characteristics of the membrane separator and the E.B dosages used for crosslinking are a few instances of various factors that may have an effect on how the E.B irradiation crosslinking influences the thickness and ion conductivity of the nanocomposite M2

separator. Similar to this, a variety of variables, including changes in crosslinking density, differences in morphology, and irradiation-induced degradation, can contribute to the complicated behavior of ionic conductivity as a function of E.B dose in M2 membranes. The thickness of PE-SiO_2 nanocomposite (M2) separators, as described in the characterization section, ranges from 13-18 um; the slight variation in thickness is caused by the presence of difficult-to-control inorganic SiO_2 nanofillers inside the M2 separator structure. The fact that M2-20 has a comparatively higher thickness than other separators may be the cause of the small drop in ionic conductivity that was observed in M2-20. Incorporating inorganic nanoparticles reduces the crystallinity of the polymer and increases its amorphous status, which is considered a common way of enhancing ionic conductivity [300]. Since amorphous structures exhibit higher ionic conductivity [301], it is obvious that the M2-150 separator exhibits significantly superior ionic conductivity, owing to the combination of inorganic nanofillers and E.B irradiation crosslinking. The increase in ionic conductivities of E.B modified nanocomposite membranes is mainly due to the special morphological structure and the decreased crystallinity produced by the high-energy E.B irradiation crosslinking. Also, SiO_2 nanoparticles are polar and hydrophilic inorganic materials that will help improve the liquid electrolyte uptakes, increasing the ionic transmission between electrodes. The excellent electrolyte uptake/wettability of separators will accelerate a high-efficiency transmission of ions and achieve superior ionic conductivity. Therefore, by accumulating the two steps of inorganic nanofillers and E.B irradiation, more amorphous regions appear in the membrane structure, strengthening the membranes' electrolyte wettability behavior and promoting the rapid transmission of ions between electrodes, thereby increasing ion conductivities and enhancing the electrochemical performance.

4.4.5.2. Rate capability

The rate capabilities of Li │ $LiFePO_4$ cells assembled with M1-0, M2-0, M1-150 and M2-150 separators were studied at constant current charge-discharge rates from 0.1C to 8C. As presented in **Figure 4-9**, the discharge capacities of all cells slowly decreased with the rise of discharge current densities. All separators demonstrated a slight difference in initial discharge capacities at low C-rates (0.1C), whereas, at higher C-rates (8C), the cell exhibits a significant change in discharge capacities of all separators in **Figure 4-9**a**.** The corresponding coulombic

efficiencies for cells using different separators at various C-rates were displayed in **Figure 4-9**b. In detail, CE at low 0.1 C-rates, the cell with M1-0, M2-0, M1-150 and M2-150 separators obtained discharge capacities of 158.6, 159.2, 161.8 and 161.5 mAh g^{-1} with corresponding efficiencies of 99.91, 99.14, 99.34 and 99.85 %, respectively. At higher 8 C-rates, the cell with M1-150 and M2-150 achieved significantly high discharging capacities of 109.1 mAh g^{-1} and 116.7 mAh g^{-1} with outstanding coulombic efficiencies of 99.06 % and 99.57 %. However, M1-0 and M2-0 displayed rare discharge capacities of 98.2 mAh g^{-1}, and 105.1 mAh g^{-1}, with excellent efficiencies of 98.74% and 99.16 %, for M1-0 and M2-0, respectively. As a result, M1-150 and M2-150 separators performed better than M1-0 and M2-0 separators, specifically at higher current densities of 3C, 4C, 5C and 8C.

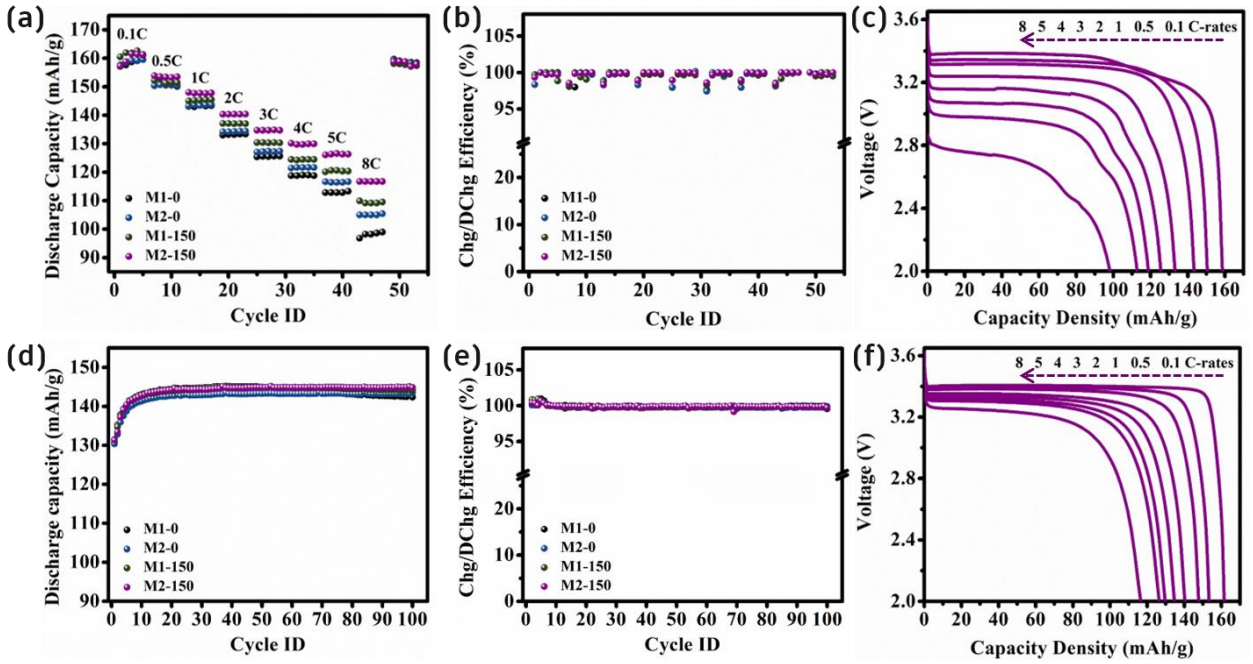

Figure 4-9: Electrochemical performance of Li/Separator/$LiFePO_4$ cells (a) Comparison of discharge C-rate capability of cells at different C-rates having different separators, and (b) The corresponding coulombic efficiency of cells. (c) Discharge profiles of cells at different C-rates using the M1-0 separator. The cyclic performance of cells using different separators: (d) Discharge capacities of cells and (e) Corresponding coulombic efficiencies. (f) Discharge profiles of cells at different C-rates using the M2-150 separator.

The improvement in rate capabilities of the cell using M1-150 and M2-150 separators at high C-rates is attributed to the E.B irradiation crosslinking. Moreover, discharge profiles of Li │ $LiFePO_4$ cells at different C-rates using various separators in the voltage range of 2.0–3.6 V are presented in **Figure 4-9**c-f. The discharge capacity values at different C-rates of 0.1, 0.5, 1, 2, 3, 4, 5 and 8C are (158.6, 150.6, 143.4, 133.2, 125.5, 118.9, 112.8 and 98.2 mAh g^{-1}) for M1-0, whereas the M2-0 separator displays (159.2, 150.8, 143.4, 134.3, 127.4, 121.6, 116.4 and 105.1 mAh g^{-1}). The M1-150 separator exhibits discharge capacities of 161.8, 151.2, 145.3, 137.1, 130.3, 124.4, 120.6 and 109.1 mAh g^{-1}, while M2-150 separator reveals 161.5, 153.4, 147.7, 140.3, 134.7, 129.8, 126.5 and 116.7 mAh g^{-1}, respectively. From such data, E.B crosslinking improved the discharge capacities of both M1 and M2 separators. The highest discharge capacities of M2-150 separators at high C-rate (8C) can be attributed to the massive electrolyte uptake and increased ionic conductivity resultant from the combination of inorganic nanofillers and subsequent E.B irradiation crosslinking.

4.4.5.3. Cycling performance

The cycling performance of Li │ $LiFePO_4$ cells using M1-0, M2-0, M1-150 and M2-150 separators was further tested at a constant charging/discharging rate of 1C/1C for 100 cycles. As presented in **Figure 4-9**d, cells assembled with all modified separators exhibit outstanding cyclic stability and no capacity fading, confirming that our amended separators play a key role in improving electrochemical performance. In comparison, the specific discharge capacity of the cell assembling with M1-0 separator displayed high discharge capacity. However, there was an obvious gradual decrease in discharging capacities as the number of cycles increased which reached (142.37 mAh g^{-1}) after100 cycles. The cell utilizing the M2-0 separator showed quite low discharge capacity than all separators and demonstrated no significant decrease of (143.48 mAh g^{-1}) after 100 cycles. After E.B crosslinking, the cell using M1-150 separator revealed the highest discharge capacity. However, after numerous cycles, the discharge capacity slightly decreased to (144.16 mAh g^{-1}) after 100 cycles. As shown in **Figure 4-9**e, CE of cells assembled with M1-0, M2-0, M1-150 and M2-150 separators after 100 cycles were 99.57 %, 99.90 %, 99.74 %, 99.73 %. The cell using the M2-150 separator exhibited the largest discharge capacity even after 100 cycles of 144.88 mAh g^{-1}, which is greater than that of M1-0, M2-0 and M1-150 separators, owing to its

unique microstructure. Comparing the cycle life of the battery cell assembled with non-irradiated and irradiated separators, the cell made with irradiated separators, especially the nanocomposite M2 separator displayed higher discharge capacity, which indicates that E.B irradiation crosslinking has no negative effect on the cycle performance LIBs.

4.5. Summary

A fresh and straightforward commercial process was demonstrated to prepare an advanced nanocomposite separator between VHMWPE and inorganic SiO_2, followed by E.B crosslinking without post-treatments. The microstructural characteristics of the two separators were reasonably examined before and after E.B crosslinking, and they were carefully compared using various characterization methods. The effects of inorganic nanofillers and high energy E.B irradiation on the microstructure and surface morphologies of hybrid nanocomposite VHMWPE-SiO_2 (M2) separators cross-linked by different E.B irradiation doses of 0, 20, 50, and 150 kGy were investigated and compared to that of pure VHMWPE (M1) using SEM, DSC and ATR spectra. The ATR-FTIR spectrum revealed the difference between M1 and M2 before E.B irradiation, as well as the formation of transvinylene (C=C) and carbonyl (C=O) bonds after E.B irradiation. Nanocomposite separators cross-linked by E.B irradiation were more thermally stable than those without E.B crosslinking. Moreover, E.B irradiated separators had higher electrolyte wettability, air permeability, and porosity than those without E.B irradiation. Owing to the greater porosity and enhanced wettability by a liquid electrolyte, both amended separators have achieved excellent ionic conductivities of approximately 0.65 mS cm^{-1} for M1-150 and nearly 1.60 mS cm^{-1} for M2-150. As a result, LIBs cells assembled with M1-150 and M2-150 displayed the highest rate capabilities of 161.8 mAh g^{-1} and 161.5 mAh g^{-1} at low C-rate 0.1C, respectively. In contrast, cells made with M1-150 and M2-150 demonstrated superior rate capacities of 109.1 mAh g^{-1} and 116.7 mAh g^{-1} at a high C-rate 8C. Furthermore, cells made with M1-150 and M2-150 separators exhibit outstanding cyclic stability, no capacity fading even after 100 cycles. These results verify that our modified separators are vital and play a key role in improving electrochemical performances. Thus, this study shows that high-energy E.B irradiation-induced crosslinking of biaxially stretched nanocomposite membranes can be used as an alternative strategy to improve the requirements of separators for lithium-ion batteries.

CHAPTER 5. Polyethylene-Based Hybrid Separators for Lithium-/Sodium Batteries

5.1. Introduction

Microporous membrane separators are the heart of rechargeable lithium-/ sodium-metal batteries (LMBs and NMBs) because they play a dominant role in battery safety and determining the electrochemical performance by serving as a channel for the transport of ions during charge-discharge processes [48; 83; 302-304]. The separator, also called the third electrode, separates the anode ("negative") and cathode ("positive") electrodes, thereby playing a key role in protecting the LMBs/NMBs from thermal runaway and potentially high risk of an explosion [56; 83; 305]. Glass fiber (GF) separators are often used in NMBs due to their high porosity and ionic conductivity [306]. However, GF separators are difficult to use in practical applications due to their fragility, massive electrolyte leakage, and environmental hazards, and their large thickness reduces the gravimetric energy density [37; 307]. As the battery assembling process necessitates rolling/stacking the separator and electrodes, the membrane separator must be robust, thin and flexible, rendering GF separators improper for large-scale battery fabrications [29; 308]. Conventional polyolefin-based membrane separators (e.g., poly (propylene) (PP) and poly(ethylene) (PE)) are commonly used in rechargeable batteries due to their high mechanical strength, chemical stability, and relatively low cost [309; 310]. Nevertheless, they shrink easily at high temperatures, increasing the possibility of internal short circuits, eventually leading to fire or even explosion [28; 311; 312]. Then again, polyolefins are non-polar and have a low affinity towards polar electrolytes, interfering with their electrochemical performance [131; 313]. The separator's poor wettability and porosity can significantly impact the conductivity of Li^+/Na^+ ions, affecting the performance of batteries [314].

Innumerable techniques based on blending modification, surface engineering, composite modification, and other modification techniques using various inorganic ceramics, such as silicon dioxide (SiO_2) [29; 31; 32], aluminium oxide (Al_2O_3) [33; 34], titanium dioxide (TiO_2) [35], and zirconium dioxide (ZrO_2) [37] were developed to overcome these constraints. Among these procedures, surface engineering/modification of the biaxially stretched poly(ethylene) (PE)-membrane is well-known as an effective approach for improving safety and electrochemical performances. Applying

ceramic materials to the PE separator surface is critical to enhancing electrochemical performance and ensuring the battery's safety [315]. Nevertheless, ceramic-coated polyolefin separators face quite a lot of problems. For example, (i) the adhesion and linkage of an inorganic ceramic coating to the polyolefin-based membrane is insufficient, and the ceramic particle layer is easy to fall off, which leads to short-life batteries; (ii) adding a binder to boost bonding strength reduces the permeability and porosity of the separator and increases the battery's internal resistance; (iii) modifications by conventional methods using ceramic particles inevitably thicken the resultant separator and easily cover its pores, thus lowering battery performance; and (iv) ceramic particles usually have a bulky mass, resulting in a heavyweight [32; 41; 158]. Therefore, it is highly demanded to construct hybrid nanocomposite separators to endow them with great wettability, extraordinary Li^+/Na^+ ions conductivity, and superior thermostability without scarifying their microstructural properties [11].

Dopamine (DA) is widely used for developing polymeric surfaces due to its simplicity, versatility and ability to adjust surfaces with desired properties [197; 316; 317]. Polydopamine (PDA) is generally composed of dihydroxyindole, indoledione, and dopamine units, which have been covalently bonded [318]. The oxidation of DA produces PDA is mostly opportune for modifying various polymeric surfaces without damaging their structure; as a result, it is widely utilized in amending polyolefin separators for batteries [319; 320]. Owing to its excellent properties, such as inexpensive, lightweight, and great thermal stability, boehmite (BH) has attracted substantial interest in surface engineering [214]. BH is widely used as a ceramic filler to improve the thermal stability of the separator and increase ionic conductivity by lowering the interfacial resistance between the separator and the electrode and providing excellent compatibility with liquid electrolytes, thereby improving the overall performance and safety of batteries [321]. Though various strategies for constructing inorganic-modified polyolefin separators have been reported, improving the stability of inorganically coated films on polyolefin matrices without annihilating their structure and microporosity remains a great challenge. Despite no ideal separator can still provide optimal electrochemical performance, and safety under all operating conditions, most efforts to find alternatives to PE separators have failed because it is still preferable to other separators when all criteria are evaluated [131]. Lately, a few academics have focused on using BH as a softer ceramic coating for battery separators due to its better dispersion in aqueous slurries than other ceramics (e.g., Al_2O_3) [214; 225; 230; 322]. However, they do not often involve comprehensive research on surface bonding, stabilizing microporous structure, and electrochemical stability

factors. On the other hand, the impact of boehmite hybrid separators on the electrochemical performance and their potential usage as ceramic composites based on PE separators for NMBs have yet to be broadly studied. Typically, the commercially adopted composite polyolefin separator has a 3 μm or thicker Al_2O_3 coat on each side, accounting for approximately 25% of the overall separator thickness [230]. Besides, BH is cheaper than Al_2O_3, which is also important for large-scale commercial applications [225]. Subsequently, there is space for supplementary advancement in boosting higher energy density and lowering battery expenditures by reducing separator coating thickness while preserving its microstructure and high thermostability. The most practical approach for acquiring this purpose is reinforcing the interconnection between the hybrid layer and polyolefin membranes.

Inspired by the features mentioned above, we present a straightforward approach to design an advanced hybrid nanocomposite separator based on PE separators for increasing the safety and overall performance of LMBs/NMBs without compromising their microstructure. The hybrid nanocomposite layer between high thermal stability BH and multi-polarity self-polymerized DA demonstrated a promising microstructure, making it a proper thin-film to decorate polyolefin-based membrane separators for high-performance LMBs and NMBs. The current project takes these characteristic features into consideration and introduces an innovative and cost-effective polyolefin-based hybrid separator that uses lightweight and inexpensive BH and DA bonded onto its internal pores and surface interface without applying polymeric binders via a scalable in-situ wet process as a promising candidate for commercial LMB/NMB separators. The hybrid DA@BH (DH) thin layer maintained the PE separator thickness while improving carbonate-based electrolyte wettability, resulting in faster electrolyte permeability and rapid ionic conductivity, preserving high energy density, and extending battery life. As a result, assembled LMBs and NMBs cells employing the hybrid nanocomposite separator exhibit optimal performance and greatly enhanced cycling stability. The current hybrid separators demonstrated a supreme performance for lithium- and sodium-metal batteries compared to the commercial PP Celgard membrane results and the reported literature on experimentally modified PE membrane separators.

5.2. Experimental part

5.2.1. Materials

The commercial Celgard (3501) separator was acquired from Shenzhen Sentai Technology Co., LTD. The biaxially stretched polyethylene (PE) microporous membrane (W12-600, ~12 μm thick) was obtained from W-Scope Korea Co., Ltd. (Korea). Aluminum oxide hydroxide (Boehmite, BH powder) with a particle size of 15 nm was purchased from Shanghai Buwei Applied Materials Technology Co., Ltd. Dopamine hydrochloride "DA" ($C_8H_{11}NO_2$–HCl), Tris–Hydrochloride Buffer (Tris–HCl) (1M, pH 8.5), and Lithium iron phosphate ($LiFePO_4$) powder were purchased from Shanghai Aladdin Biochemical Technology Co., Ltd. N-butanol and Ethanol were brought from Sinopharm Group Chemical Reagent Co., Ltd. N-methyl-2-pyrrolidone (NMP) and Conductive carbon (Carbon black Super-P ~ TIMCAL) were acquired from Sinopharm Chemical Reagent Co. LTD. Polyvinylidene fluoride (PVDF) was gotten from Suzhou Dodo Chemical Technology Co., LTD. Commercial lithium sheet (Li) anode was brought from Tianjin Zhongneng Lithium Co. LTD. Liquid electrolyte (SS–HFGX046) was brought from Dongguan Shanshan Battery Material Co., Ltd. The liquid electrolyte used for LMBs consisted of 1.0 M $LiPF_6$ in ethyl carbonate (EC) and dimethyl carbonate (DMC) (1:1 by volume), was purchased from Zhangjiagang GuotaiHuarong New Chemical Material Co., Ltd. Commercial hard carbon anode, sodium metal, and the electrolyte used for NIBs consisted of 1M $NaPF_6$ in EC/DMC (1:1 by volume), purchased from Kuraray Co., Ltd. (Japan). All materials were used as received.

5.2.2. Preparations and manufacturing procedures

In summary, first, the PE membrane was treated via corona discharge treatment (CDT) to create multifunctional polar groups (–OH, C–O, C=O) because the activation of corona discharge/plasma in the air atmosphere will bring uniform reactive sites onto the surface of the separator [169]. Second, a pre-treatment process was performed on the separator just after CDT since wetting pre-treatment by ethanol is advantageous for uniformly constructing the hybrid layer on both surfaces and inside the separator's slits, as well as increasing the bond formation strength between the separator and the DA-based hybrid layer during the optimization process [323]. Finally,

treated the BSPE membrane followed by a hybrid nanocomposite decoration layer of organic (DA) and inorganic (BH) nanoparticles via an in-situ solvent procedure (**Figure 5-1** and **Figure 5-2**).

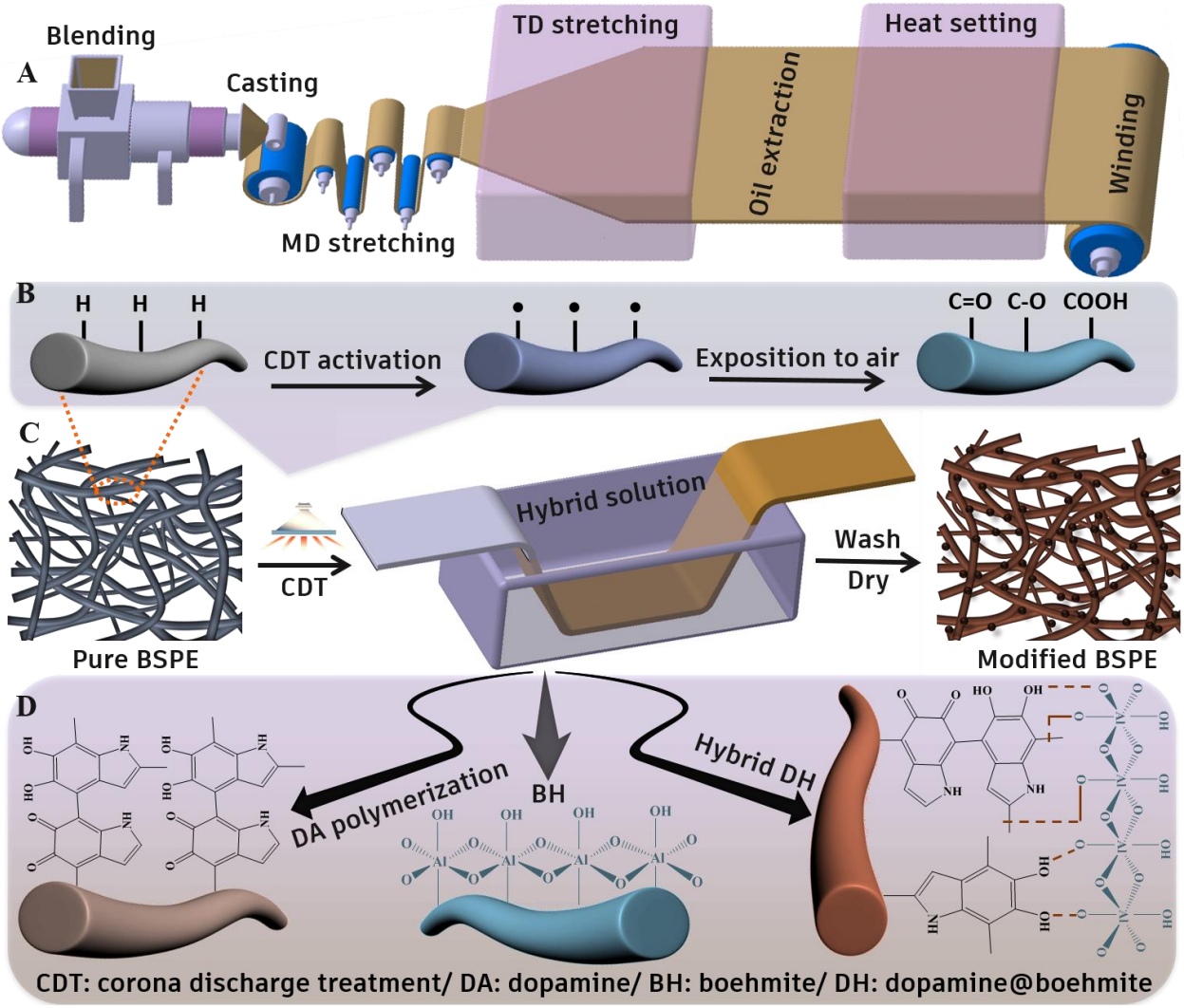

Figure 5-1: Schematic representation of manufacturing and decoration processes of the PE separator; (A) biaxial stretching procedure of PE, (**B**) the activation of PE by CDT, (**C**) the hybrid film decoration step after CDT, (**D**) the possible mechanism for PE separators.

5.2.2.1. Corona discharge treatment (CDT)

To activate the surface, generate polar groups, and create reactive sites on the BSPE separator for enhancing the interaction between the membrane and additives, the BSPE separator was treated with a corona discharge machine. Treatments were performed on a corona machine in

our laboratory (Ruian Zhi Lin Technology Co., Ltd., "China") using different power energies at a fixed speed of nearly 2 m/min.

5.2.2.2. Preparation of the hybrid PEDH separator

Dopamine (2 g) was added to tris–hydrochloride buffer (Tris–HCl), pH ~ 8.5 (100 mL), stirred at room temperature overnight, then dopamine (DA) was self-polymerized into polydopamine (PDA), and the solutions changed to a dark-brown color (PDA solution obtained). The boehmite (2 g) was dissolved in deionized (DI) water (100 mL) and stirred overnight at room temperature to form a cloudy solution (BH solution was obtained). The hybrid combination of DA@BH (DH) was created by first preparing the DA solution, and then an equal amount of BH powder was added without adding water. The hybrid (DH) solution was stirred overnight at room temperature to obtain a homogeneous hybrid solution whose color changed to dark brown. CTD activated-BSPE membranes were cut into a fixed shape and immersed in ethanol to be washed and cleaned. Subsequently, wet membranes were immersed in the above-prepared solutions in the surrounding atmosphere for (1–8 h). Then the membranes were taken out and rinsed with a mix of ethanol and water (50:50 by volume) and washed with DI water three times to remove the residual and unattached macromolecules from the surface of the separator. Afterward, modified separators were dried in an oven at 60 ºC for 4 h, and as-prepared separators were denoted as BSPE (untreated), PE-CDT (corona discharge treated BSPE), and PE–DA (dopamine modified BSPE), PE–BH (boehmite modified BSPE), and PE-DH (hybrid nanocomposite dopamine@ boehmite modified BSPE). **Figure 5-1** and **Figure 5-2** show the decoration process of the BSPE separator.

5.2.3. Characterizations

5.2.3.1. Characterization of the separator

Detailed descriptions about the separator characterizations and electrochemical measurements including air permeability, SEM, EDS, XPS, ATR-FTIR, TGA, DSC mechanical properties, porosity, contact angle and uptake of electrolyte, ionic conductivity and electrochemical stability were provided in **CHAPTER 3&4**. Some supplementary measurements and characterizations were carried out with different approaches.

The thermal shrinkage of PE separators before and after decorations is examined by calculating the change of separators' dimensions after annealing at different temperatures for 60 minutes. The shrinkage rate can be calculated by Eq. (5-1):

$$\textbf{Thermal shrinkage}\ (\%) = (A_{before} - A_{after})/A_{before} * 100\% \qquad \textbf{(5-1)}$$

where A_{before} and A_{after} point to the areas of the separator before and after being treated in the oven at 90 °C, 120 °C, and 140 °C for 60 minutes.

5.2.3.2. Electrochemical characterizations

Linear sweep voltammetry (LSV) was used to evaluate the electrochemical stability and decomposition of separators. Lithium metal (Li) and stainless steel (SS) sheets were used as electrodes and countered electrodes and the electrolyte 1M Lithium bis(fluorosulfonyl)imide (LiFSI) in fluoroethylene carbonate (FEC) and difluoroethylene carbonate (DFEC) (1M LiFSI in FEC:DFEC) with a scan rate of 1 mV s^{-1} at 25 °C using a voltage range from 2.5 to 6.

5.2.3.3. Cells assembly and electrochemical measurement testing

For LMBs, the $LiFePO_4$ cathode was initially obtained by making a slurry of $LiFePO_4$ powder, conductive carbon, and PVDF binder in NMP solvent with weight ratios of 7:2:1. Then, the slurry was uniformly coated on aluminum (Al) foil and transferred to a vacuum oven for 12 h at 50 °C to evaporate the NMP solvent. Next, a coin-type test cell (2032), which is composed of an as-prepared $LiFePO_4$ (LFP) cathode/separator/Li anode, was assembled and filled with electrolyte (1M $LiPF_6$ in EC/DMC (1:1)) for electrochemical measurements. The cycling performance was measured at a constant current density of 1C/1C for 365 cycles for LMBs. Similarly, sodium-metal batteries (NMBs) cells were assembled using a sodium (Na) metal cathode/separator/hard carbon anode filled with electrolyte (1M $NaPF_6$ EC: DMC/ 1: 1) for electrochemical measurements. The charge-discharge, rate capabilities, and cycling life of NMBs were tested. The rate performance was evaluated at current densities of 0.1, 0.3, 0.5, and 1 A g^{-1}, and they were measured for more than five cycles. Alike, the cycle life was measured at a constant current density of 0.3 A g^{-1} for 365 cycles.

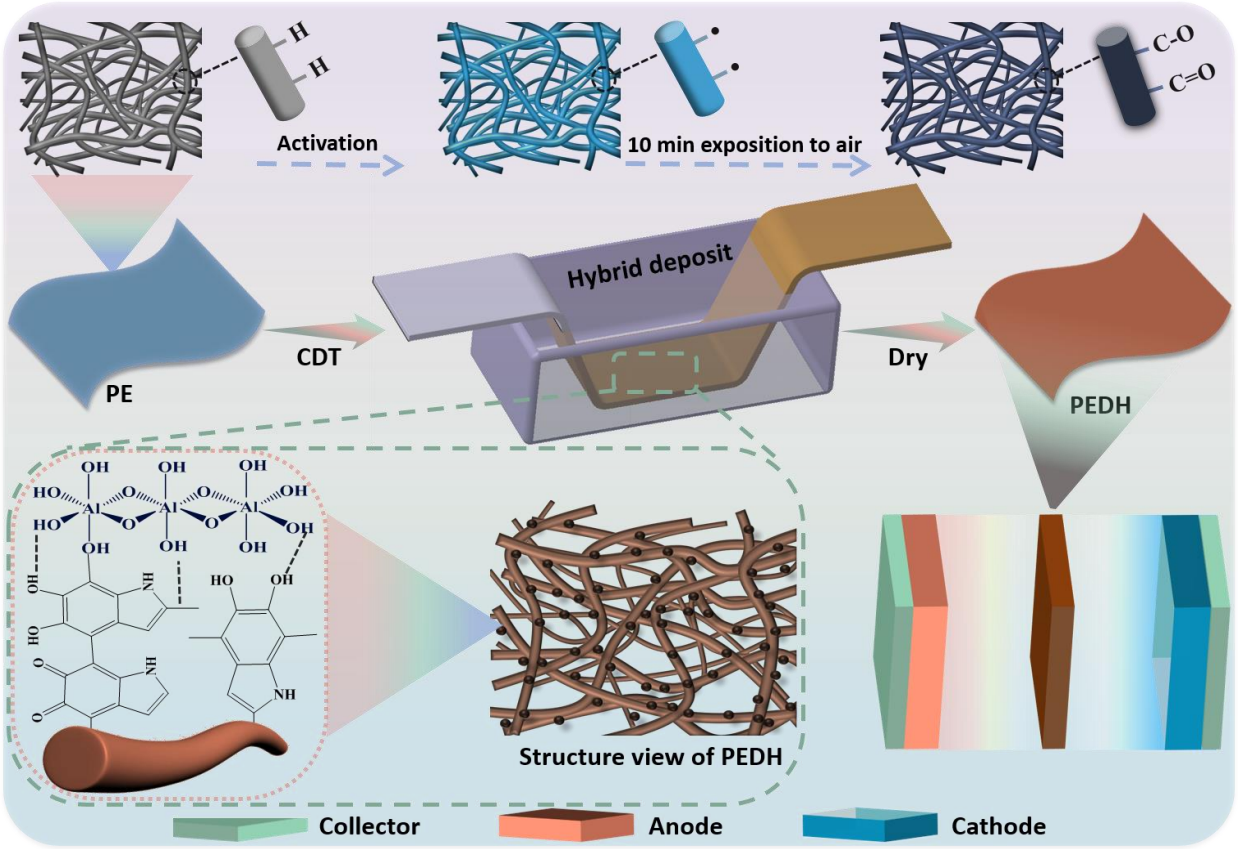

Figure 5-2: Schematic illustration of the preparation of the PEDH hybrid separator.

5.3. Results and discussion

5.3.1. Microstructural and morphological characterization

The surface and cross-section morphologies of PE before and after corona discharge treatments (CDT) and PEDH separators are typically characterized by SEM photographs in **Figure 5-3** and **Figure 5-4**. Pure PE separators were activated thru corona discharge treated (CDT) using different corona powers to determine the influence of CDT on the surface and macrostructure of the separator and then fix a proper power as a model for activating the separator surface. As can be noticed, after the PE surface being treated by CDT, the macrostructure and morphology were altered affectedly together with mechanical properties, but air permeability improved (**Figure 5-5**), and wettability (**Figure 5-6**) enhanced caused by the attached multi-polar groups (e.g., C=O, C=O, and –OH) as revealed in ATR (**Figure 5-7**). As shown in **Figure 5-3A**, the surface

macrostructure and morphology of the naked PE separator is relatively smooth and has comparatively large pore diameters, with no DA layer or ceramic BH nanoparticles observed on its surface. The pure ceramic inorganic BH–decorated PE separator exhibited nanoscale particles distributed rarely on the nanofiber structure of the PE separator and the pure organic DA–decorated PE separator displayed a smooth surface with a densely painted thin layer in **Figure 5-3B-C**.

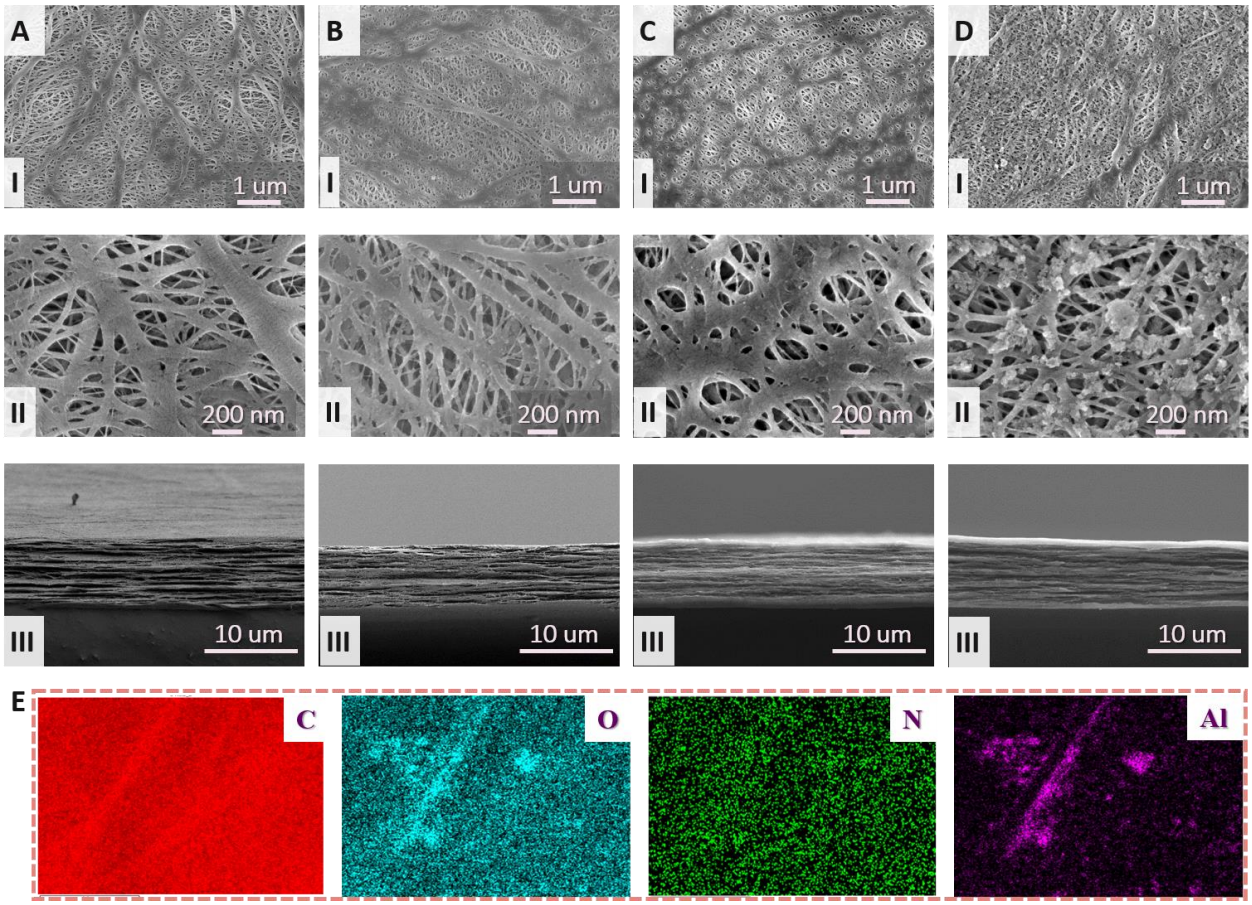

Figure 5-3: (I-II) SEM photographs and (**III**) corresponding cross-sectional snapshots of PE separators before and after decoration (**A**) Bare PE, (**B**) BH – decorated PE (PE–BH), (**C**) DA – decorated PE "PE–DA", (**D**) DH – decorated PE "PEDH" separators, and (E) EDS map elements of C, O, N, and Al for the PEDH separator.

The hybrid combination between DA@BH– decorated PE separator (PEDH) showed rough surfaces and nanoscale particles distributed uniformly on the surface and accumulated with increasing time of the decoration process. EDS elemental mapping images are shown in **Figure 5-3E**, which indicate that O, Al, and N, from BH and DA, are distributed on the surface and inside

the matrix slits of the PEDH separator, which define the presence and uniformity of the resulting hybrid decoration layer onto PE separators.

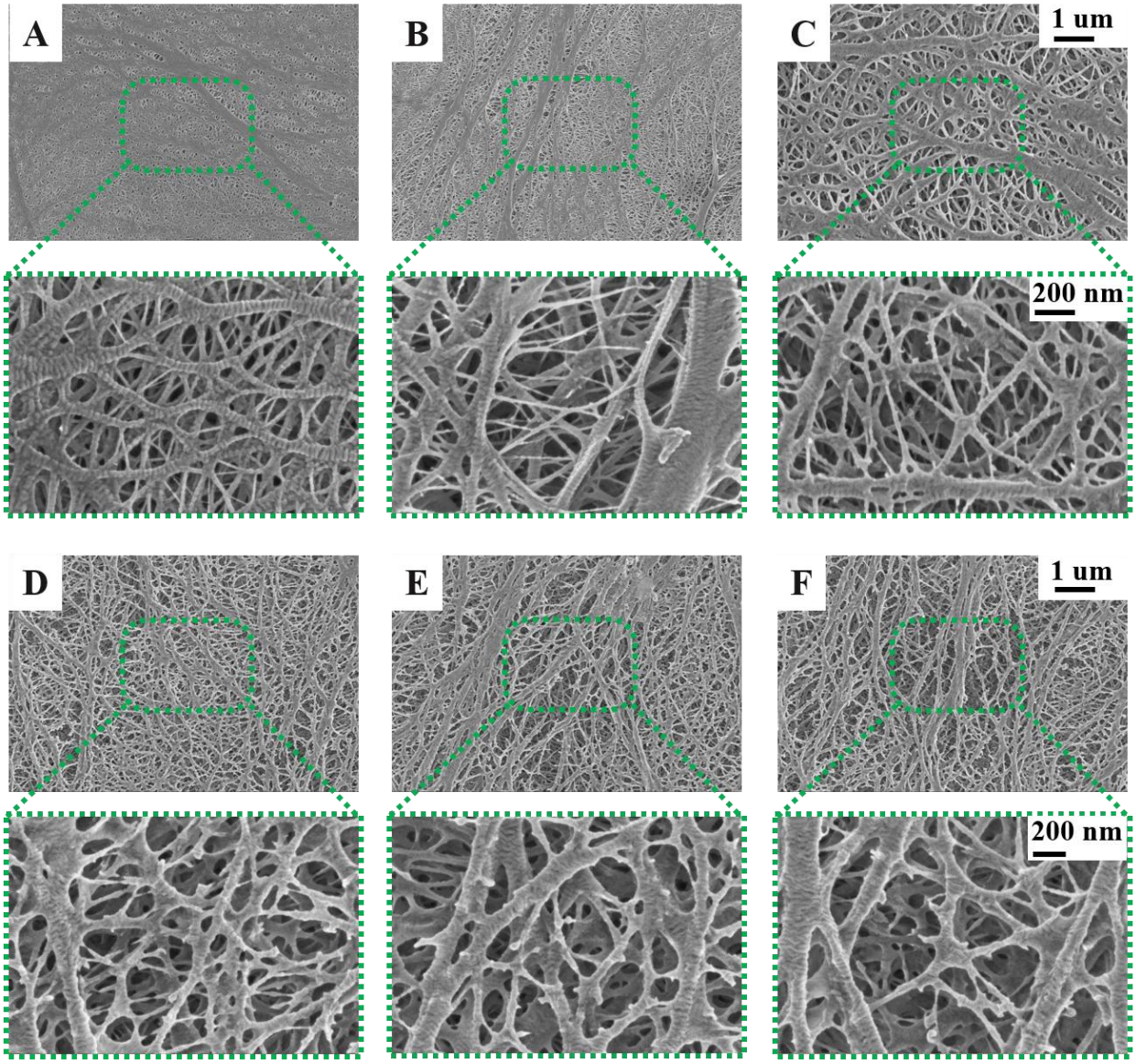

Figure 5-4: SEM photographs of **(A)** bare PE membranes and (**B-F**) various power energies of PE treated on one side to choose the idea power: **(B)** PE-300W, **(C)** PE-400W, **(D)** PE-500W, **(E)** PE-600W, **(F)** PE-700W separators.

The Gurley value of the separator (air permeability) is usually used to define its porosity. Low value means high porosity for the separator [166]. The Gurley value indicates that the pure PE separator value (~139 sec) after corona treatment is reduced to (~123 sec). The surface microstructure seems to be damaged as the activation power of the corona discharge treatment

increases (**Figure 5-4)**, resulting in the decreasing value of the permeability (**Figure 5-5)**.

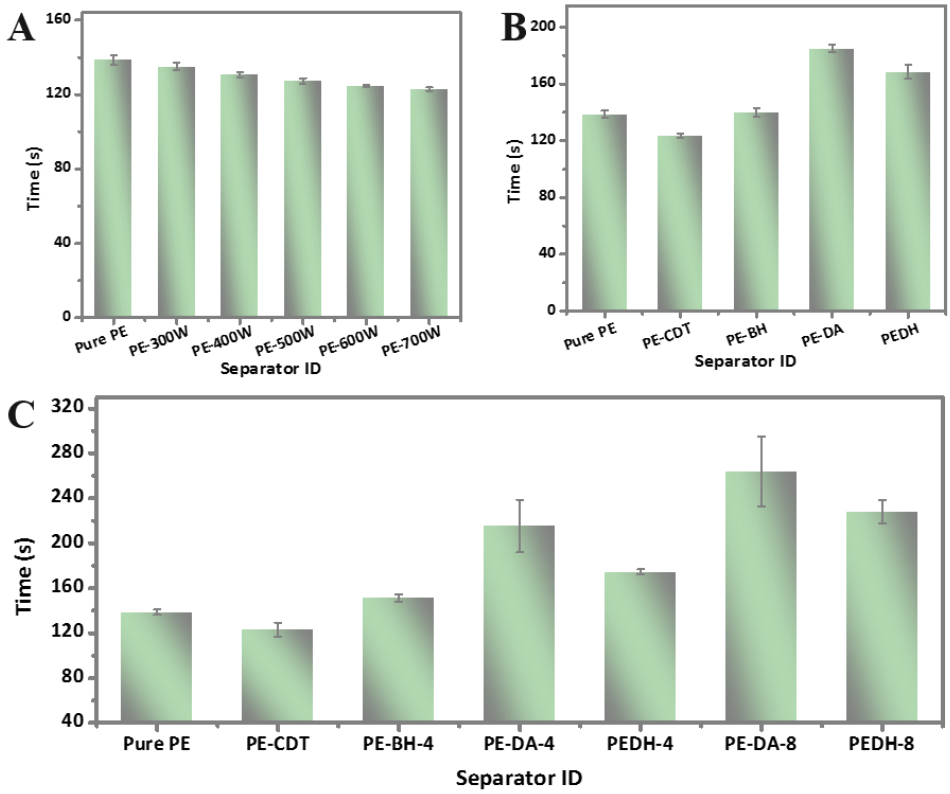

Figure 5-5: Air permeability of **(A)** PE membranes treated with different power energies on one sides "PE- CDT 300-700 W", **(B)** bare PE membrane, CDT-400W treated PE separators on both sides, BH, DA, DH – decorated PE separators (1h). **(C)** BH, DA, DH – decorated PE separators (4h) and DH – decorated PE separators (8h).

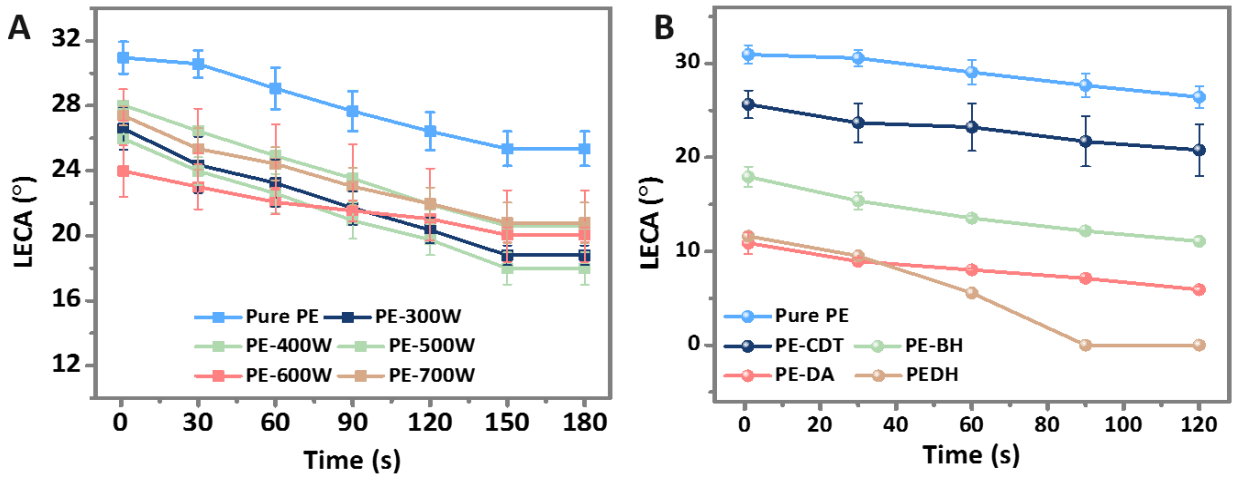

Figure 5-6: (**A**) Recorded liquid electrolytes contact angle "LECA" within 180s for pure

"untreated" and different power dosages of corona discharge -treated PE separators, and (**B**) LECA for PE and modified PE separators with inorganic BH, organic DA, and DH hybrid.

After the PE membrane has been splattered with DA, BH, and DA@BH (DH), the Gurley value of all modified separators increased because of the hybrid layers that apparently covered some separator pores, for example, PE-BH (~151), PE-DA (~215 sec), and PEDH (~175 sec). It's worth noting that as the deposition time increases, the Gurley value rises.

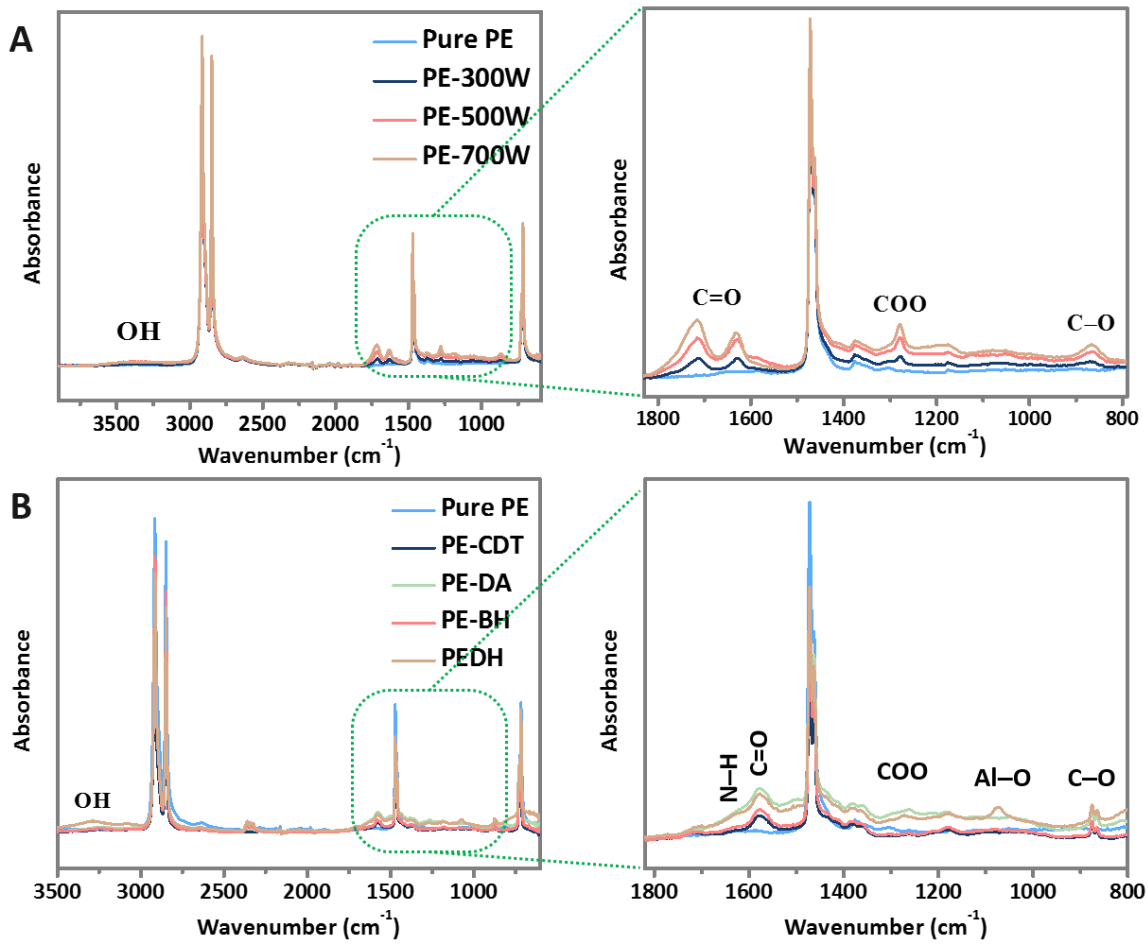

Figure 5-7: ATR-FTIR spectra of (A) the pure PE separator before and after activated with varied power dosages of corona discharge treatment and (B) the pure PE, and modified PE separators with inorganic BH, organic DA, and hybrid DA@BH (DH) layer.

ATR-FTIR and XPS are performed to investigate the change in chemical structures of the PE and hybrid PEDH separators. ATR spectra of the pure PE separator in **Figure 5-7** revealed absorption peaks at 2918, 2848, and 1471 cm^{-1}, which resulted from C–H stretching vibration or

C–H bending deformation. For the PE–CDT membrane, multiple absorption peaks appeared at 3294, 1714, 1578, and 1380 cm^{-1}, corresponding to (–OH, C=O, and COO^{-}), resulting from the corona treatment. The intensity of peaks increased when the power applied for the treatment increased (**Figure 5-7A**). The PE–BH separator showed a new absorption band at 1070 cm^{-1} related to the Al–O bond of boehmite. The PE–DA showed an increase in the hydroxyl (–OH) band and exhibited two new absorption peaks around 1626 cm^{-1} and 1550 cm^{-1}, corresponding to the resonance vibrations of C=C in the benzene and N–H of dopamine [324], respectively. For the hybrid combination DH-modified PE separator, all the peaks mentioned above were observed (**Figure 5-7B**), indicating the existence of boehmite and dopamine on the PE separator structure.

To further confirm that, the XPS test was conducted and presented **Figure 5-8**. As it can be seen in the XPS survey (**Figure 5-8A**) the PE separator revealed only a C1s peak, while the PE–CTD exhibited C1s and O1s peaks, confirming the CDT activation. The PE–DA showed an increase in O1s peak and demonstrated a new N1s peak. As for PE–BH, a new Al 2p peak appeared, and the content of the O1s peak increased, whereas C1s decreased.

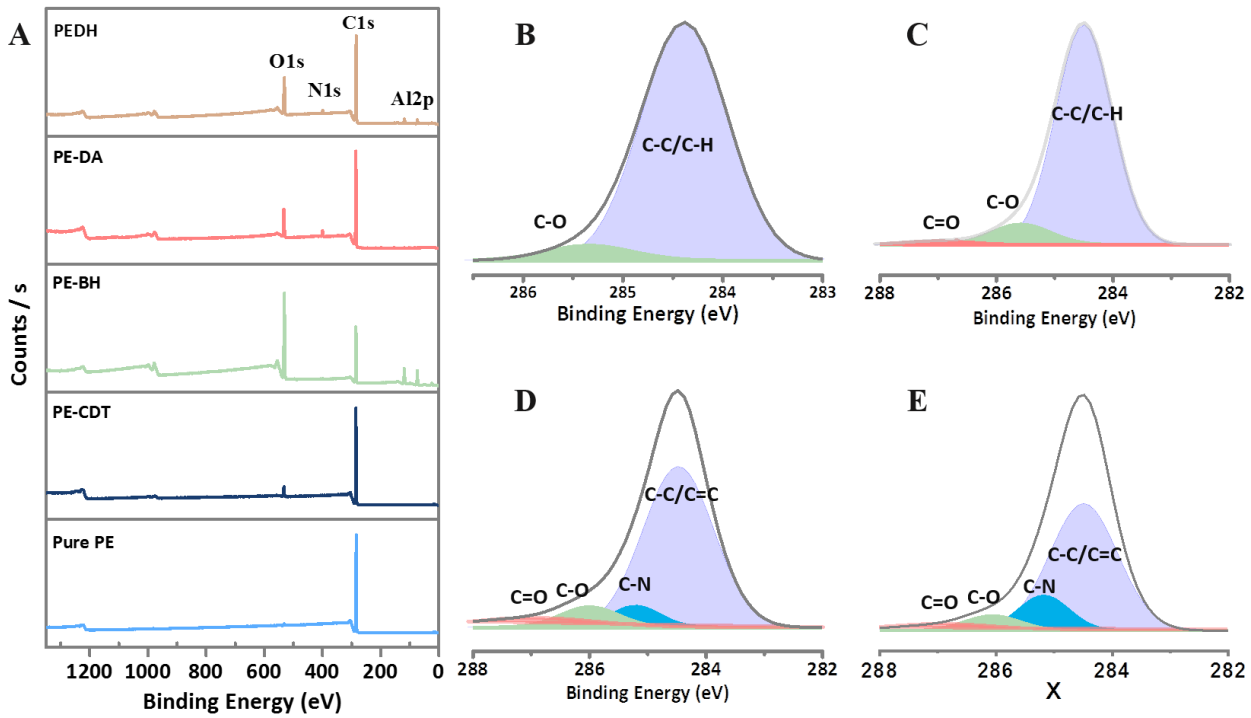

Figure 5-8: (**A**) XPS survey of PE separators before and after decorations. XPS High-resolution spectra of (**B**) pure PE (**C**) PE–BH, (**D**) PE–DA and (**E**) hybrid PEDH separators.

For the hybrid PEDH separator, C1s, O1s, Al2p, and N1s peaks are remarkably observed,

which confirming it consistency with the ATR spectra. Furthermore, C1s high-resolution XPS spectra of PE separators before and after decoration were analyzed and detailed in **Figure 5-8B-E** indicating the existence of some new functional groups related to dopamine and boehmite, which provide strong evidence of the formation of a hybrid DH nanocomposite thin layer on the PE separator.

5.3.2. Mechanical and thermal properties

The separator's mechanical strength must be high enough to handle cylindrical battery winding and withstand tension during the assembly process, making it a crucial component for battery safety [56]. The typical stress-strain curves of the one-side activated PE separator with different corona power are illustrated in **Figure 5-9**.

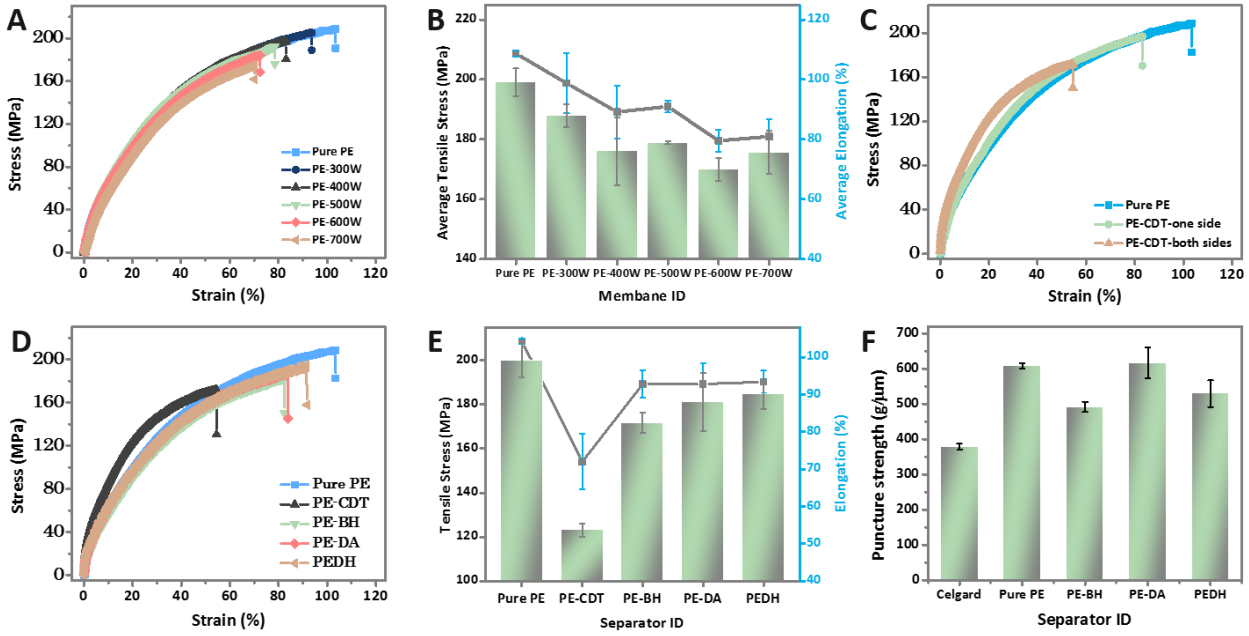

Figure 5-9: (A and **B)** The typical stress-strain curves of one-side activated PE separator with different corona powers, and the corresponding summary for tensile strength and elongation strain, **(C)** stress-strain curves pure PE, one-side, and both-sides activated PE separators, (**D**) stress-strain curves, (**E**) average of tensile strength and elongation strain for unmodified and modified PE separators, and (**F**) the puncture strength of pure and decorated PE separators compared to Celgard.

The tensile strength and elongation strain of the separator are affected by the treatment power; as seen in **Figure 5-9A-B**, the mechanical properties are reduced with increasing the

activation power The PE separator treated on both sides using a power value of 400 W (the selected model for the modification) shows the lowest mechanical properties (**Figure 5-9C**). Subsequently, mechanical properties have shown significant enhancement after the modification with the hybrid DH layer in **Figure 5-9D-E**. The puncture strength of the PE and hybrid separators are also presented in **Figure 5-9F**. The puncture strength of the non-modified PE separator displayed a puncture strength value of (607 ± 8 g μm^{-1}), which was the highest strength value. The value is then reduced after modifications for PE-BH (491 ± 14 g μm^{-1}) because the irradiation of corona decreased mechanical properties. The puncture strength exhibits an increasing trend after the hybrid layer is assembled on the PE separator, especially when using dopamine and the hybrid combination of DA@BH; e.g., puncture strength of PE–DA (616 ± 43 g μm^{-1}), and PEDH (529 ± 38 g μm^{-1}). These results also showed an improved trend of PEDH puncture strength compared to the Celgard separator (378 ± 8 g μm^{-1}), which is advantageous for LMBs/NMBs practical applications.

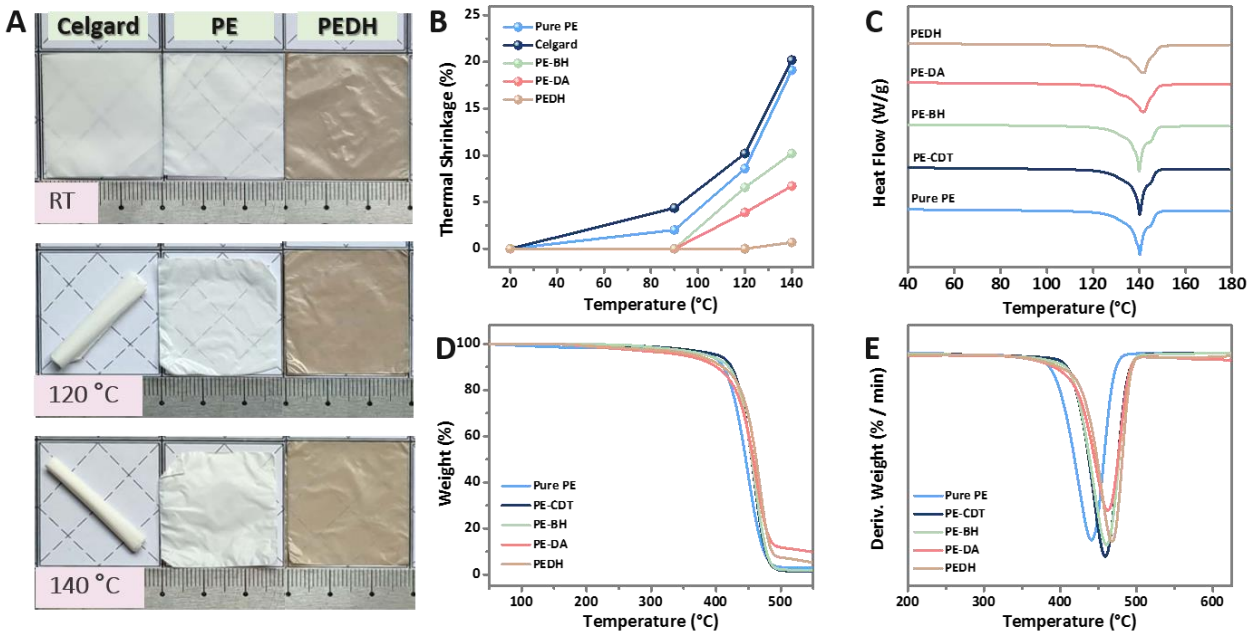

Figure 5-10: (**A**) Photographs at room temperature and after being treated for 60 minutes at different temperatures, (**B**) the thermal shrinkage, (**C**) DSC curves, (**D**) TGA curves, and (**E**) DTG curves of PE separators before and after optimizations.

The thermal characteristics of the PE, PE–BH, PE–DA, and PEDH separators are investigated by dimensional thermostability, DSC, and TGA tests, as presented in **Figure 5-10**. In

the dimensional thermostability test, separators were kept at 90~140 °C for 60 minutes. As displayed in **Figure 5-10A-B**, both Celgard and bare PE separators started to shrink at 90 °C, and the shrinkage dramatically grew at 120 and 140 °C. The PE–BH and PE–DA separators began to shrink at 120 °C (**Figure 5-10B**). In contrast, the PEDH separator exhibited excellent thermal stability and maintained its dimensionality even after 140 °C owing to the hybrid combination of thermally stable boehmite nanoparticles and dopamine. The DSC curves of the pure PE, PE–BH, PE–DA, and PEDH separators are shown in **Figure 5-10C**. The non-modified PE separator showed a melting temperature (T_m) of approximately 139 °C, whereas the T_m the PE–CDT separator was reduced to 138 °C due to corona discharge irradiation. Thanks to the existence of BH nanoparticles and dopamine, the T_m of PE–BH, PE–DA, and PEDH separators slightly increased to 139, 140, and 141 °C, respectively. Moreover, TGA and the corresponding DTG curves for pristine PE and hybrid nanocomposite PEDH separators are presented in **Figure 5-10D-E**. From the given TGA data, it can be seen that the thermal stability of the pristine PE separator was around 511 °C after hybrid nanocomposite layer decoration, PEDH was progressively enhanced to 561 °C.

5.3.3. The porosity, wettability, and electrolyte uptake

Since the electrolyte uptake (EU) is crucial for the passage of ions, LMBs/NMBs separators must have excellent electrolyte wettability. The liquid electrolyte contact angle (LECA) can be obtained by dropping the electrolyte on the separator and measuring the droplet's shape over time. If the LECA exceeds 90°, it indicates poor wetting behaviour. Contrariwise, the lower the LECA of the separator, the greater the affinity. As recorded in **Figure 5-11A**, the pure PE separator showed the highest value of LECA. In contrast, the PEDH separator exhibited superior wettability and became (~ 0 after 90 s), attributable to the decoration layer constructed between dopamine and boehmite. Moreover, snapshots of wetting behaviour and LECA of the PE before and after optimization over 120 s are depicted in **Figure 5-11B**. As it can be observed, the electrolyte drop that was placed on the surface of the PE separator did not wet sufficiently because of the hydrophobic surface. In contrast, modified PE–BH, PE–DA, and PEDH separators were quickly wet by electrolyte droplets (**Figure 5-11B**). The electrolyte spread over a wide area of the hybrid PEDH separator attributable to the multipolar hydrophilic groups. Moreover, liquid electrolyte

uptake (EU) and porosity were tested and calculated before and after modifications, which were displayed in **Figure 5-11C-D**. As shown, the bare PE separator has a high porosity and less EU than all other modified separators.

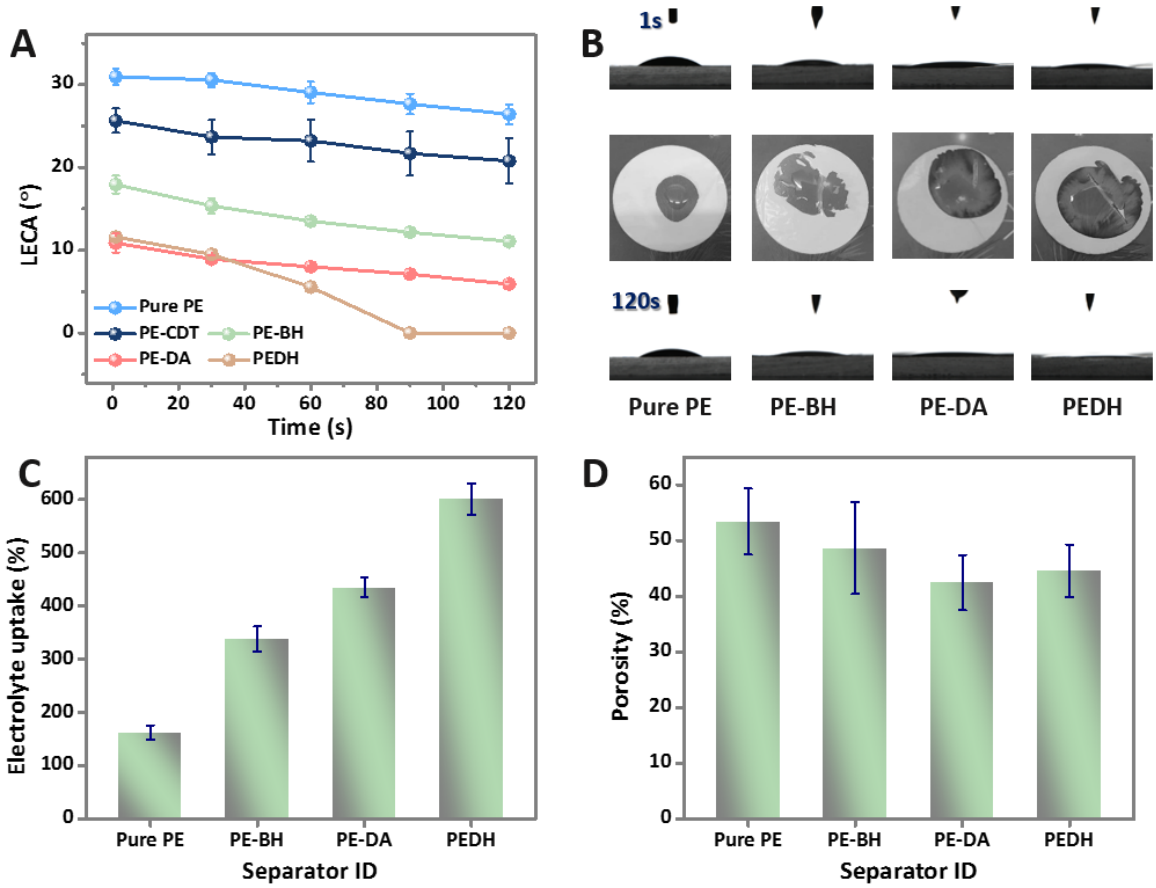

Figure 5-11: (**A**) The recorded contact angle of liquid electrolyte "LECA", (**B**) contact angle and wetting property pictures within 120 s (*colours transformed to white-black for better observation*), (**C**) electrolyte uptake, and (**D**) porosity of the PE separator before and after optimizations.

Hybrid separators showed a relatively slight decrease in porosity because some of the porous structures on their surfaces were partially covered.Whereas the hybrid PEDH separator reached a liquid electrolyte uptake of (~530 %), which was greater than that of the bare PE separator after soaking in liquid electrolytes for 60 minutes. Furthermore, all modified separators demonstrated higher electrolyte uptakes due to their high affinity. The hybrid PEDH separator has a higher EU value and sufficient porosity than other separators. Therefore it tends to accelerate the passage of ions, increasing ionic conductivity and enhancing electrochemical performance.

5.3.4. Electrochemical measurements

5.3.4.1. Electrochemical stability

The electrochemical stability of the separator is an essential feature for its application in LMBs and NMBs systems. The current ***vs.*** voltage curve of the separator was measured by a linear sweep voltammetry (LSV) test. The onset voltage of the sudden rise in the current was regarded as the electrochemical stability window; the large stability window is an essential feature for high battery performance. From **Figure 5-12A**, we can observe that all separators' curves were stable in voltages below 4.3 V, showing no noticeable decomposition of any components below 4.3 V. Moreover, the decomposition potentials for the Celgard, pure PE, and PEDH separators were 4.66, 4.95, and 5.20 V, respectively, which verifies that the hybrid PEDH separator has excellent electrochemical stability in a typical voltage range of high-performance LMBs and NMBs batteries.

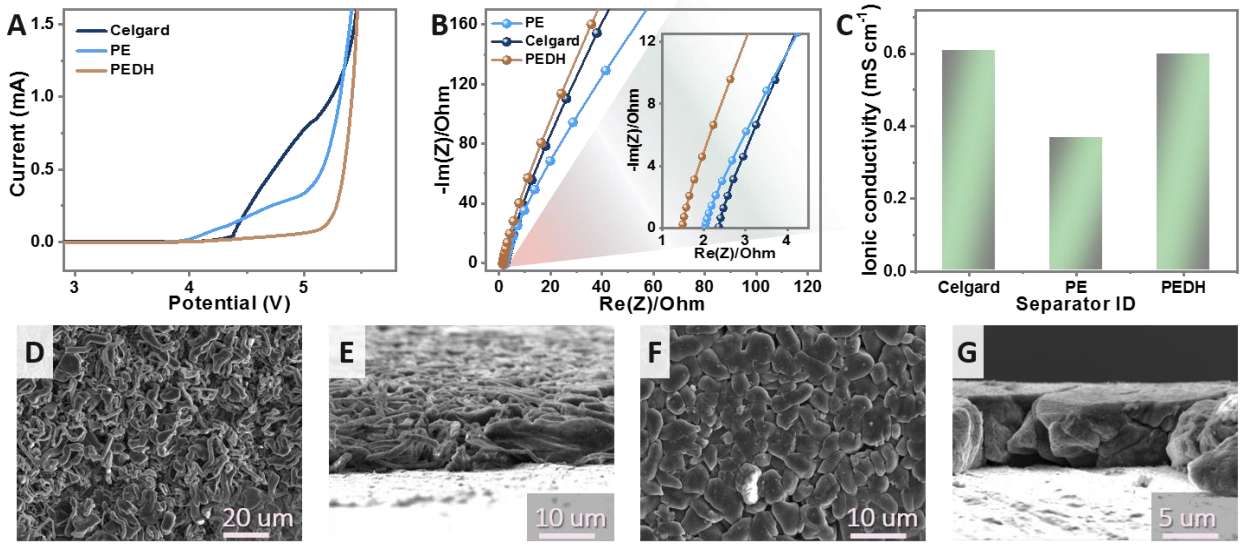

Figure 5-12: (**A**) Linear sweep voltammetry (LSV) of Li/separator/SS cells, (**B**) Nyquist plot of cells SS/separator/SS, and (**C**) the corresponding ionic conductivity for Celgard, PE, and PEDH separators. (**D–G) Characterization studies of lithium deposition morphology**: SEM surface and cross-section photographs of Li morphologies using (**D** and **E**) the bare PE separators and (**F** and **G**) the hybrid PEDH separator, respectively.

5.3.4.2. Ionic conductivity and Li Metal Deposition Morphology

AC impedance spectroscopy (**Figure 5-12B**) was used to measure interface and bulk impedance. The ionic conductivity of the separator before and after optimization was investigated by measuring the bulk resistance ($\mathbf{R_b}$) of all separators, which was determined by the intercept of the Nyquist curve on the real (Z') axis. The conductivities of the Celgard, pure PE, and hybrid PEDH separators were calculated to be 0.61, 0.37, and 0.60 mS cm^{-1}, respectively (**Figure 5-12C**). The higher conductivity of PEDH is attributed to its excellent wettability and uptake of electrolytes, and unique hybrid groups into its surface and structure, which would therefore contribute to better performance. The Li deposition morphology of bare PE and hybrid PEDH separators in carbonate-based electrolytes was evaluated by using coin-type Li || Cu cells. **Figure 5-12D-G** show the Li deposition morphology with 1 mAh cm^{-2} deposited on the copper surface at current density of 0.5 mA cm^{-2}. The morphology of Li in the pure PE separator exhibited severe dendritic growth. In contrast, the Li deposition morphology of the hybrid PEDH separator exhibited a smooth large particle morphology, which greatly inhibited the growth of lithium dendrites [325]. Based on the results of the Li deposition morphology, the modified groups and structural changes in the hybrid separator can simultaneously promote ion transport and uniform Li-ion flow, which leads to uniform Li deposition [326]. Therefore, enhancing the cycle stability performance of Li metal batteries.

5.3.4.3. Electrochemical performance of LMBs

Battery performance is an accurate way to assess the electrochemical performance and long-term cycle stability of the separator. **Figure 5-13A** illustrates the discharge C-rate capabilities of cells assembled with the modified/unmodified PE separators. The cells were charged at a constant charge current density of 0.2C and discharged at various current densities ranging from 0.2, 0.5, 1, 3, to 5 C. The discharge capacity of all cells gradually declines as the discharge current density increases, indicating the capacity losses incurred by the increasing ohmic polarization influence and severe overpotential at high current density levels [327]. The cell assembled using the hybrid PEDH separator showed a higher discharge capacity at a higher discharge current density of 5C. Because high current density affects the ionic passage, the difference in discharge capacities between modified hybrid PEDH separators and pure PE separators will come to be more noticeable

at higher current densities [210]. Li/Li symmetric cells using PE and hybrid PEDHH separators were further tested and reported in **Figure 5-13B.** After 100 h, the Li/Li symmetric cell with pure PE separator could not be operated any further owing to an internal short circuit. In contrast, Li/Li cells using the hybrid PEDH separators operated stably without a short circuit for more than 300 h.

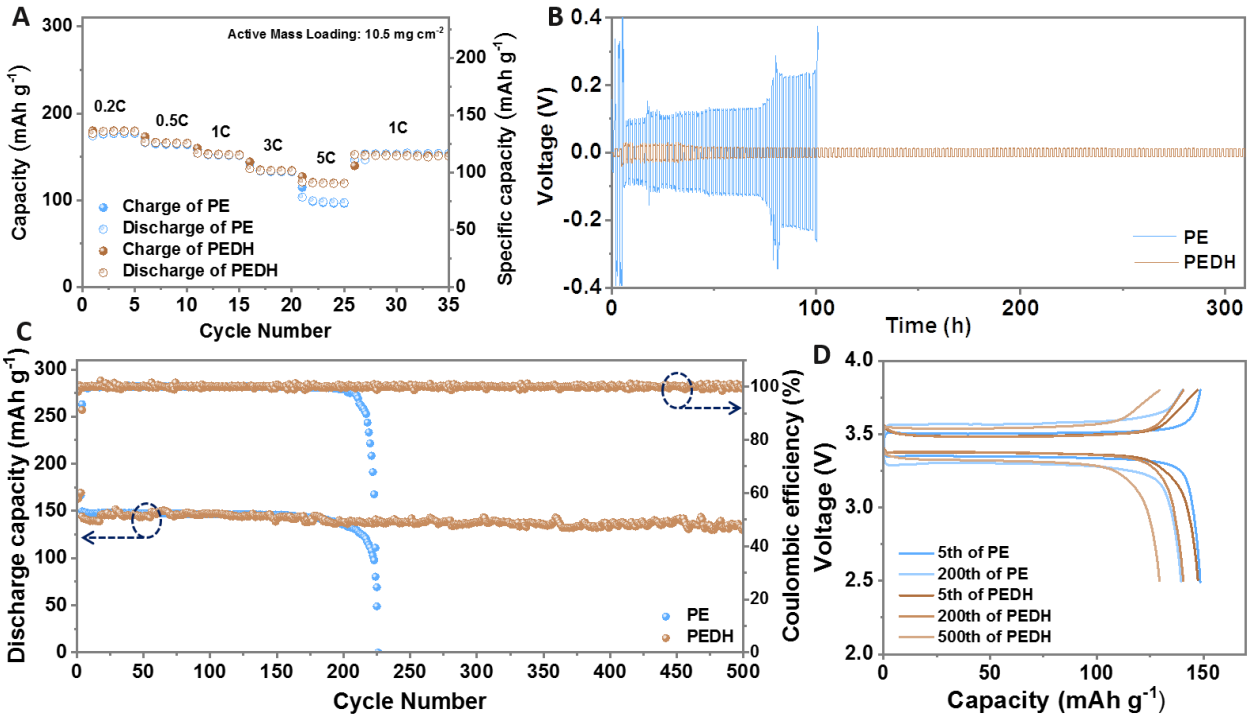

Figure 5-13: Electrochemical performance of LFP/Li cells: (A) Rate performance, **(B)** Galvanostatic cycling profiles of Li/Li symmetric cells at 0.1 mA cm^{-2}, (**C**) and (**D**) The cyclic performance and corresponding charge-discharge curves LMBs cells with the bare PE, and hybrid PEDH separator.

The cycle life of LFP/Li cells assembled using the unmodified PE and modified PEDH separators was studied at the current density of 0.1/0.1 C and 1/1 C (**Figure 5-13C**). The initial discharge capacities of cells employing PE and PEDH separators were 148.5, and 147.4 mAh g^{-1}, respectively. For the initial few cycles, a gradual increase in the discharge capacity of the cell was observed, because the separator was completely immersed and the complete formation of the channels activated the Cathode. After long-term cycling, the discharge capacity of the cell using the unmodified PE separator decreases drastically, demonstrating only 148.5 and 139.5 mAh g^{-1} at the 5^{th} and 200^{th} cycles, respectively. In contrast, the LMBs cells using the PEDH separator

exhibited discharge capacities of 147.4, 140.6, and 129.4 mAh g^{-1} at the 5th, 200th, and 500th cycles at current density of 1C, respectively (**Figure 5-13D**). In addition, the average Coulombic efficiencies at the 500th cycle of cells utilizing the PE and PEDH separators were 99.5% and 99.9%, respectively. As can be seen that the cell assembled with the PEDH separator showed excellent and stable specific capacity and Coulombic efficiency, and excellent cyclic life after 500 cycles. These results indicate that introducing DA@BH (DH) into the PE membrane enables a strong affinity for electrolytes and facilitates the formation of the continuous channels for ions transport, resulting in superior ionic conductivity, which leads to the separator becoming feasible for achieving high cell performance.

5.3.4.4.Electrochemical performance of NMBs

The electrochemical performance of the bare PE and PEDH separators was further investigated in NMB cells by employing the commercial hard carbon anode and sodium (Na) metal cathode, as presented in **Figure 5-14**.

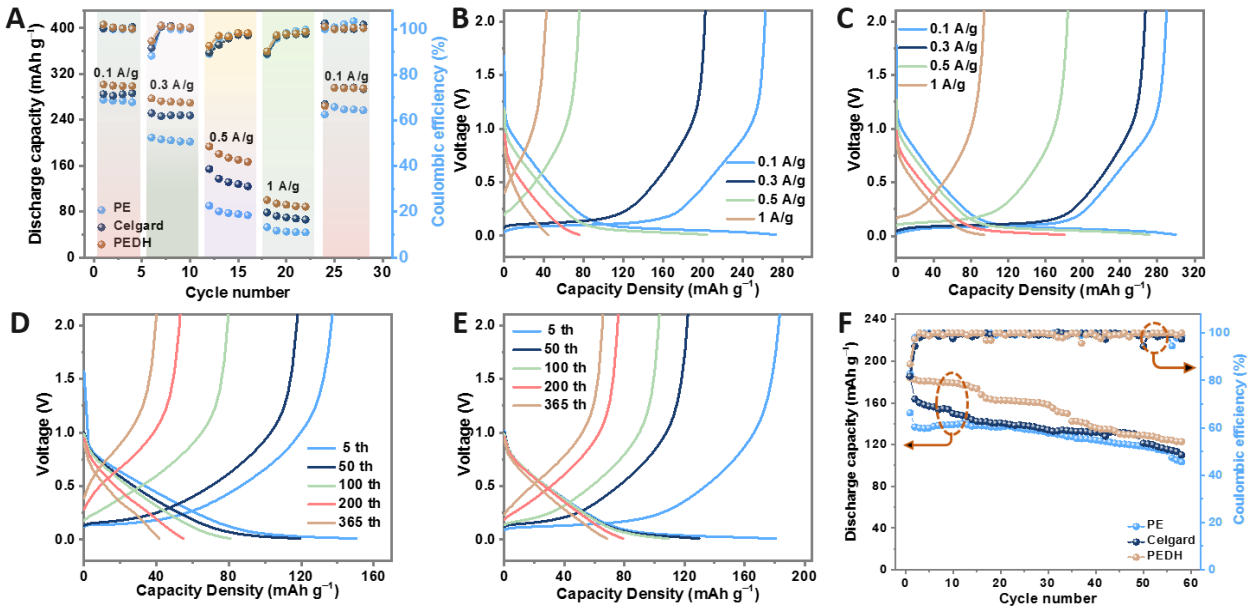

Figure 5-14: Electrochemical performance of Na/hard carbon cells: (**A**) C–rate performance of discharge capacities and corresponding efficiencies of the cells employing Celgard, pure PE, and hybrid PEDH separators. (**B** and **C**) Charge–discharge curves of NIB cells at a current density of 0.1, 0.3, 0.5, and 1 A g^{-1}, (**D** and **E**) Charge-discharge curves of NIBs cells using base PE and

hybrid PEDH separators at 5th, 50th, 100th, 200th, and 365th cycles, respectively. (**F**) The cycling performance of NMB cells using the bare PE, Celgard and hybrid PEDH separator at a current density of 0.3 A g^{-1}.

The rate capability and charge–discharge performance of cells using bare and modified PE separators at different C-rates from 0.1 C to 1 A g^{-1}. **Figure 5-14A-C** displayed the discharge capacities and corresponding efficiencies of NMBs cells containing the bare PE, and hybrid PEDH separators at a current density of 0.1 A g^{-1}, 0.3 A g^{-1}, 0.5 A g^{-1}, and 1 A g^{-1}. The cyclic stability of NMBs using PE and PEDH separators was investigated and the charge-discharge curves of the cell using PE and hybrid PEDH separators at 0.3 A g^{-1} in a voltage window of 0.01–2.2 V (vs. Na/Na^+) were displayed in **Figure 5-14D-F**, respectively. To compare the cycling life of NMBs using the pure PE and PEDH separators, the NMB cell cycle performance using Celgard under the same conditions was tested and recorded. As shown in **Figure 5-14D-F**, the battery that used PEDH separator exhibited better cycle stability with a discharge capacity of 66.6 mA h g^{-1} after 365 cycles at 0.3 A g^{-1}**,** which is higher than that of the cell with the unmodified PE separator (41.5 mA h g^{-1}), with coulombic efficiencies of about 97～100 % all the time for all samples. As it can be observed that with the increase in the number of cycles, the discharge capacity decreased rapidly between the 25th and 80th cycles, especially for the pure PE separator. However, the hybrid PEDH separator showed stable capacities at each state after the 100th cycle, indicating excellent recovery and reversible cycle life performance. Although the initial specific discharge capacities of cells using both Celgard and pure PE separators are slightly lower than those of the PEDH separator, the cell using the hybrid PEDH separator exhibits a slower decay after the 80th cycle, and nearly a stable specific discharge capacity as the cycle number increases between 200th to 365th cycles.

Therefore, such electrochemical stability of the PEDH separator are associated with enriched electrolyte wettability and high ionic conductivity, which may originate from multifunctional groups of PDA with high thermostable BH nanoparticles and the in-situ engineering strategy for optimizing the separator. Notably, the hybrid combination is suitable for practical application in highly safe separators at high temperatures, indicating that the introduction of the DH is an effective way to increase affinity with electrolyte and faster ion diffusion, thereby improving the electrochemical performance of the cell. In comparing primary characteristics of previous work–related PE-based battery separators and our work when used in both LMBs and

NMBs (**Table 5.1**), our hybrid PEDH separators have exhibited fairly higher ionic conductivity, excellent discharge capacity for LMBs, considerable extended life span cyclability in batteries for more than 500 cycles.

Table 5.1: A comparison of critical parameters between our work and some literature reports that used ceramic nanoparticles to develop PE separators for batteries

No	*Ceramic coating*	*Electrodes*	*Electrolyte*	*Electrolyte uptake (%)*	*Conductivity (mS cm^{-1})*	*Battery performance*	*Ref*
1	Al_2O_3	$LiMn_2O_4$	1.16 M $LiPF_6$ in (EC:EMC)	85	1.182	109.9 (0.2C)	[232]
2	SiO_2	$LiCoO_2$	1 M $LiPF_6$ in (EC:DMC:EMC)	269	0.45	Retained~92% (100 cycles)	[211]
3	Al_2O_3	$LiCoO_2$	1 M $LiPF_6$ in (EC:DMC:EMC)	277	0.40	Retained~92% (100 cycles)	[229]
4	SiO_2	$LiCoO_2$	1 M $LiPF_6$ in (EC:DMC:EMC)	333	0.41	Retained ~86% (0.2C)	[220]
5	γ-AlOOH	NCA	1 M $LiPF_6$ in (EC:DEC)	~137	0.3162	Retained~81% (200 cycles)	[152]
6	Al_2O_3	$LiCoO_2$	1 M $LiPF_6$ in (EC:DE)	450	0.65	Retained~79% (200 cycles)	[197]
7	ZrO_2	Hard carbon	1 M $NaClO_4$ in (EC:PC)	–	0.7	Retained ~ 96% (50 cycles)	[37]
8	SiO_2	Hard carbon	1 M $NaPF_6$ in (EC:PC)	~144	0.134	Retained~91% (0.5C)	[29]
9	Boehmite	$LiFePO_4$	1 M $LiPF_6$ in (EC:DMC)	537	0.6	Retained~81% (365 cycles)	This work

5.4. Summary

To summarize, a novel, cost-effective polyolefin-based hybrid separator is presented via a scalable in-situ wet process for commercial high performance and a long life span of LMBs and NMBs batteries. Self-polymerized multi-polars dopamine (DA) and high thermostable boehmite (BH) are successfully bonded and engineered into the PE separator internal pores and surface interface via corona discharge activation and pre-treatment processes, without applying polymeric binders. The uniform hybrid nanocomposite layer on the surface and inside a network of the PE separator makes the PE separator thickness well-maintained while significantly improving the wettability and affinity of the composite separator toward liquid electrolytes and obtained superior thermal stability at an elevated temperature of 140 °C. The as-prepared hybrid separator exhibits enhanced mechanical puncture strength of (529 ± 38 g μm^{-1}) compared to the Celgard separator (378 ± 8 g μm^{-1}). The Li || LFP cell assembled with the PEDH separator shows an outstanding cycling life span stability with excellent capacity retention of ~ 88% after 500 cycles at higher charge/discharge cureent density (1 C) with an average Coulombic efficiency at the 500^{th} cycle of the cell (99.9%). Li || Li symmetric cells demonstrated that after 100 h, the cell with a pure PE separator could no longer be operated due to an internal short circuit. In comparison, the cell with the hybrid PEDH separator can run continuously for more than 300 h without a short circuit. In comparing some previous work related to PE based battery diaphragms with our work in LMB and NMB, both have shown excellent overall performance and extended life cycleability.It is expected that the PEDH separator will serve to broaden the application area of commercial battery separators by developing hybrid separators based on biaxial stretched membranes for safe and high-performance lithium/sodium-meal batteries.

CHAPTER 6. Conclusion and Prospects

6.1. Conclusion

This dissertation has covered research work completed on developing hybrid nanocomposite separators based on polyethylene membranes via various manufacturing methods for energy storage systems. In order to provide a complete understanding of this project, this thesis overviews a general background and summarizes the existing characteristics of different membrane separators for high-performance batteries. **In chapter 1**, the thesis gives a general introduction and background on porous polymeric membranes, their categories, fabrication techniques, and applications. Membrane separators for secondary batteries, such as lithium-ion batteries (LIBs) and sodium-ion batteries (NIBs), are also introduced. The typical architecture of rechargeable LIBs and NIBs, components of the cell, electrode manufacturing steps, and cell preparations are briefly studied. Owing to its excellent chemical/mechanical properties, interconnect ed microporous networks, and good electrochemical stability polyethylene (PE) membrane is regarded as the most commercialized polyolefin separator for LIBs and NIBs. A detailed description of this work's main goals and objectives and its aim of contributing to the search for solutions to overcome the limitations of conventional PE membrane separators are also given. As previously stated, no single separator can meet the requirements of every battery application. To address concerns raised by the shortcomings of microporous PE separators, PE membranes can be optimized in terms of thermal stability, wettability, conductivity, and electrochemical performance. Inorganic nanoparticles (INPs) have been shown to have great potential for improving the thermal stability, physicochemical properties, and electrochemical performance of polyolefin-based membrane separators because of their superior thermal stability, wettability, and mechanical properties. The most frequently used way to enhance the properties of PE separators for rechargeable batteries is to build composite PE separators by incorporating these inorganic ceramic particles into PE membranes.

In **chapter 2**, a comprehensive discussion on polyethylene-based composite separators for batteries applications are summarized. The chapter overviewes the current progress and developments for battery separators and concisely illustrated the characteristics and challenges of various classifications of battery separators. The major state-of-the-art requirements of membrane

separators for high-performance batteries are discussed. It provides a comprehensive discussion on the fundamental requirements and properties (e.g., structural properties, physical/chemical properties, functional properties and other outstanding required properties) of ideal porous separators for high-performance LIBs and NIBs. The recent progress in several categories of battery separators, such as microporous separators, non-woven separators, modified microporous membranes, composite separators, and electrolyte membranes and their structural construction prepared from various materials through different fabrication processes are briefly deliberated. Current progresses in developments of adavenced hybrid PE separators are also summarized.

In an effort to develop battery separators with enhanced electrochemical performances and thermal stability. Aiming at manufacturing commercialized nanocomposite separators for high-performance batteries, hybrid nanocomposite membrane separators consisting of VHMWPE and inorganic SiO_2 nanoparticles for LIBs were processed by the scalable biaxial stretching technique and results are presented in **chapter 3**. The structure and properties of pure nanofibrous VHMWPE membrane "S1", and different concentrations of VHMWPE/SiO_2 nanocomposite (VHMWPE/SiO_2 - 95/5 "S2", 90/10 "S3", and 80/20 "S4") separators were systematically investigated thru various characterization techniques. Blending SiO_2 nanoparticles into the VHMWPE matrix exhibited great porosity and permeability, improved electrolyte uptake, and excellent electrochemical stability. The pure microporous VHMWPE separator exhibits a high thermal shrinkage of MD (9.8%) and TD (9.6%). In contrast, the nanocomposite VHMWPE/SiO_2 nanofibrous separators show superior thermal stability, e.g., S3 containing 10 wt% SiO_2 shows enhanced thermal shrinkage of MD (2%) and TD (1.7%). The porosity, air permeability, and electrolyte uptake of obtained nanocomposite membranes are greater than those of pure VHMEPE membranes. Correspondingly, The liquid electrolyte uptake of separators is improved from 175 ± 2% (S1) to 318 ± 14% (S2) to 431 ± 21% (S3) to 473 ± 12% (S4). In addition, the ion conductivity increased from S1 ~ 1.5 mS cm^{-1} to S2 ~ 1.7 mS cm^{-1} to S3 ~ 2.2 mS cm^{-1} to S4 ~ 3.4 mS cm^{-1}. Besides, VHMWPE/SiO_2 nanocomposite separators show good electrolyte retention capability and excellent mechanical properties. Ascribed to the abovementioned advantages, the obtained LIBs cells with VHMWPE/SiO_2 separator achieve excellent cycle capacity with high Coulombic efficiency of 99.93 % over 100 cycles and C-rate capability 146.2 mAh g^{-1} at a current rate of 1 C. To conclude this part, we present a facile, cost-effective, and efficient process for designing and manufacturing high-performance nanocomposite membranes for improving electrochemical

performance. The same study also inspires the expansion for designing future hybrid inorganic-organic nanocomposite separators for next-generation batteries.

Chapter 4 studied the influence of inorganic nanoparticles combined with high-energy electron beam (E.B) irradiation on physicochemical properties, and electrochemical measurements of nanocomposite VHMWPE/SiO_2 separators. The effect of inorganic nanofillers and high energy E.B irradiation on the microstructure and surface morphologies of nanocomposite VHMWPE-SiO_2 (M2) separators cross-linked by different E.B irradiation doses of 0, 20, 50, and 150 kGy were investigated and compared to that of pure VHMWPE (M1). The effect of E.B crosslinking on the crystallization parameters of M1 and M2 separators was investigated using DSC, and it was revealed that crystallinity decreased as the E.B irradiation dose increased. The ATR-FTIR spectrum revealed the difference between M1 and M2 before E.B irradiation, as well as the formation of transvinylene (C=C) and carbonyl (C=O) bonds after E.B irradiation. Mechanical properties of M1 and M2 E.B cross-linked by different E.B irradiation doses, such as tensile strengths, Young's modulus and elongation at break were reduced with the increase in E.B irradiation dose. The hybrid VHMWPE/SiO_2 nanocomposite separators cross-linked by E.B irradiation were more thermally stable than those without E.B crosslinking. E.B cross-linked nanocomposite VHMWPE/SiO_2 separators showed great electrolyte wettability and uptake and increased ionic conductivity. As a result of the greater porosity and enhanced wettability by a liquid electrolyte, both modified separators have achieved excellent ionic conductivity of about 0.65 mS cm^{-1} for M1-150 and 1.60 mS cm^{-1} for M2-150. LIBs cells assembled with M1-150 and M2-150 displayed the highest rate capabilities of 161.8 and 161.5 mAh g^{-1} at low C-rate 0.1C, respectively, whereas cells made with M1-150 and M2-150 demonstrated superior rate capacities of 109.1 and 116.7 mAh g^{-1} at high C-rate 8C. Additionally, cells using M1-150 and M2-150 separators exhibit outstanding cyclic stability, and no capacity fading even after 100 cycles, which confirms that our modified separators play a key role in improving electrochemical performances. Hence, this study suggests that high-energy E.B irradiation-induced crosslinking of biaxially stretched nanocomposite separators can be used as an alternative strategy to improve the requirements of rechargeable battery separators.

A novel hybrid composite separator made of organic dopamie (DA) and boehmite (BH) modified biaxially stretched polyethylene (PE) for high-performance and a long life span for

lithium-/ sodium-metal batteries (LMBs/NMBs) is successfully fabricated via a facile and in-situ solvent method and the results are presented in **chapter 5**. High thermostable BH and self-polymerized (DA) with multifunctional polar groups "–OH and $–NH_2$" can minimize thermal shrinkage and improve the separator's affinity towards electrolytes, enhancing the batteries' performance and safety. The uniform hybrid decoration layer on both surfaces and inside network of the PE separator significantly improves the affinity of the composite separator towred organic liquid electrolytes, as exhibited by the contact angle of liquid electrolyte (~ 0 after 90 s) and excellent electrolyte wettability (~537%). The presence of the AlOOH of BH and benzene ring of PDA on the BSPE matrix also improves the thermal stability of the BSPE separator at an elevated temperature of 140 °C. The as-prepared composite separator exhibits enhanced mechanical puncture strength of (529 ± 38 g μm^{-1}) compared to the Celgard separator (378 ± 8 g μm^{-1}). The LFP/Li cell assembled with the PEDH separator shows an outstanding cycling life span stability with excellent capacity retention of 80.6% after 365 cycles at higher charge/discharge cureent density (1/1C) compared to pure PE (36.8%) and of commercial PP Celgard (55.7%). In comparing the primary features of some previous work-related PE-based battery separators and our work when used in both LMBs and NMBs, our hybrid separator has presented outstanding overall performance and extended life span cyclability in both LMBs and NMBs for more than 500 cycles. It is expected that the PEDH separator will serve to broaden the application area of commercial battery separators by developing hybrid separators based on biaxial stretched membranes for safe and high-performance lithium/sodium-meal batteries.

6.2. Prospects

Though the research work reported in this thesis has achieved some accomplishments in preparing composite separators for battery applications, it has also raised more demands. Due to the lack of time, several adaptations, measurements, and experiments have been left for the future. To overwhelmed the restrictions accompanying composite PE separators, particularly wettability, thermal stability, and safety, which will enable the commercialization of composite separators for secondary batteries such as LIBs and NIBs, some additional prospects and research endeavors could be undertaken to fulfill the demand for advanced composite separators (structure, properties, and performance) which are categorized and summarized below:

The research in composite PE separators typically made of a combination of PE matrix and inorganic ceramic materials could be promising for next-generation secondary batteries. Incorporating inorganic ceramic particles into PE membranes is an attractive technique for obtaining high-performance battery separators with unique physical properties and electrochemical performance. Nevertheless, merging inorganic particles with organic PE matrix continues to remain challenging. The innovative composite PE membrane separators should be attempted for effective development by first studying the link between organic PE matrixes and various inorganic ceramic materials. Additionally, optimizing different features of battery separators to obtain high battery performance while preserving safety and low cost without abandoning their microstructure and keeping the lowest separator thickness increments.

Several studies have concentrated on using inorganic ceramic nanoparticles (such as SiO_2 and Al_2O_3) to modify PE membranes because of their superior thermal stability and great affinity with liquid electrolytes. Inorganic ceramic materials can offer strength to PE separators by increasing mechanical properties and minimizing the formation and growth of dendritic, enhancing the wettability of PE separators resulting in increased ionic conductivity and high electrochemical stability. In addition, PE separators with all-inorganic components could provide excellent stabilities for long-lasting batteries. However, when coating these ceramic nanoparticles onto the surface of PE membranes, they exhibit a high increase in the separator's thickness and block their porous, leading to poor electrochemical performance owing to the low conduction at the interface between the separator and electrodes. Therefore, finding innovative hybrid materials or a combination of different materials through advanced scalable fabrication methods for commercial composite separators could be used to overcome the limitations of the simple coating.

Presently and in the future, the demand for advanced battery separators with unique properties, including primary and cutting-edge requirements, will continue to rise in advanced next-generation batteries. Unique techniques such as atomic layer deposition and chemical vapor depositions have been proven to obtain advanced battery separators with excellent features, properties, and performance. However, few studies have been reported on these processes for preparing advanced composite separators for batteries (LIBs and NIBs). Accordingly, further research for developing unique composite separators through these unique techniques is needed to fulfill desired battery separators structures and requirements and achieve advanced and reliable

batteries with tremendous performance. Additionally, applying advanced surface engineerings processes such as atomic layer deposition and chemical vapor deposition to produce a conformal hybrid layer on PE separators can be involved to mitigate the restrictions of conventional surface coating and engineering.

Lately, much work has been put into characterization technologies to study the separator performance and electrolyte interactions. The development of new sophisticated computational simulation and in-situ characterization testing is of great help for observing and understanding the interaction between separators, electrolytes, and electrodes. Similarly, establishing computational approaches and merging with experimental processes for investigating new advanced materials can bring a deeper understanding of electrochemical performance and stability to achieve batteries with unique features now and much more later. Accordingly, an investigation on microstructure evolution, trace components, and multiscale characterization using advanced computational simulations and in-situ characterization techniques (e.g. Density Functional Theory (DFT), Computed Tomography (CT), and synchrotron-based characterizations including in-situ SAXS/WAXS and X-Ray Absorption Spectroscopy (XAFS)) for different battery components (separators, hybrid inorganic-organic, electrodes, additives, interface, etc.) is waiting for us.

Furthermore, apart from stability and electrochemical performance, high density, long life, and safer batteries are urgently needed. Many efforts are needed to address the issues. This can be done considering the performance of different parts (cathode, anode, separators, and electrolyte) and interactions among all of them in batteries. Although this thesis focuses on polyethene-based composite separators, it should be noted that other types of membrane separators, solid electrolyte membranes, and battery components must certainly not be ignored. Since the overall battery performance results from these different components, the advances in other materials in addition to separators and solid electrolytes which considers promising alternatives to polymer-based membrane separators will also be a focus of our future work. Solving battery problems requires a holistic approach, which calls for scientific and engineering research efforts to power our future with clean and safe energy.

REFERENCES

[1]Wu D, Xu F, Sun B, et al. Design and preparation of porous polymers[J]. Chem Rev, 2012, 112(7): 3959-4015.

[2]Jiang J-X, Trewin A, Su F, et al. Microporous poly (tri (4-ethynylphenyl) amine) networks: synthesis, properties, and atomistic simulation[J]. Macromolecules, 2009, 42(7): 2658-2666.

[3] Tan X, Rodrigue D. A review on porous polymeric membrane preparation. Part ii: Production techniques with polyethylene, polydimethylsiloxane, polypropylene, polyimide, and polytetrafluoroethylene[J]. Polymers, 2019, 11(8): 1310.

[4]Gohil J M, Choudhury R R: Introduction to Nanostructured and Nano-enhanced Polymeric Membranes: Preparation, Function, and Application for Water Purification, Nanoscale Materials in Water Purification: Elsevier, 2019: 25-57.

[5]Meng L-P, Lin Y-F, Xu J-L, et al. A Universal equipment for biaxial stretching of polymer films[J]. Chin J Polym Sci, 2015, 33(5): 754-762.

[6]Takita K, Kikuchi S, Yamada K, et al. Microporous polyethylene membrane, its production method, and battery separator. Google Patents, 2014.

[7]Demeuse M: Academic investigations of biaxially stretched films, Biaxial Stretching of Film: Elsevier, 2011: 117-124.

[8]Cheng Q, He W, Zhang X, et al. Recent advances in composite membranes modified with inorganic nanoparticles for high-performance lithium ion batteries[J]. RSC Advances, 2016, 6(13): 10250-10265.

[9]Zhao H, Deng N, Kang W, et al. Designing of multilevel-nanofibers-based organic–inorganic hybrid gel electrolyte enabling an innovative lithium-ion battery with superior ionic transport capability and advanced security[J]. Chemical Engineering Journal, 2020, 390: 124571.

[10]Asghar M R, Anwar M T, Naveed A. A Review on Inorganic Nanoparticles Modified Composite Membranes for Lithium-Ion Batteries: Recent Progress and Prospects[J]. Membranes, 2019, 9(7): 78.

[11]Yuan B, Wen K, Chen D, et al. Composite Separators for Robust High Rate Lithium Ion Batteries[J]. Advanced Functional Materials, 2021, 31(32): 2101420.

[12]Liu Z, Jiang Y, Hu Q, et al. Safer Lithium-Ion Batteries from the Separator Aspect: Development and Future Perspectives[J]. ENERGY & ENVIRONMENTAL MATERIALS, 2021, 4(3): 336-362.

[13]Lee H, Yanilmaz M, Toprakci O, et al. A review of recent developments in membrane separators for rechargeable lithium-ion batteries[J]. Energy & Environmental Science, 2014, 7(12): 3857-3886.

[14] Li J, Zhang Y, Shang R, et al. Recent advances in lithium-ion battery separators with reversible/irreversible thermal shutdown capability[J]. Energy Storage Materials, 2021, 43: 143-157.

[15]Heidari A A, Mahdavi H. Recent Development of Polyolefin-Based Microporous Separators for Li−Ion Batteries: A Review[J]. The Chemical Record, 2020, 20(6): 570-595.

[16]Ojanguren A, Mittal N, Lizundia E, et al. Stable Na Electrodeposition Enabled by Agarose-Based Water-Soluble Sodium Ion Battery Separators[J]. ACS Applied Materials & Interfaces, 2021, 13(18): 21250-21260.

[17]Ortiz-Vitoriano N, Drewett N E, Gonzalo E, et al. High performance manganese-based layered oxide cathodes: overcoming the challenges of sodium ion batteries[J]. Energy & Environmental Science, 2017, 10(5): 1051-1074.

[18]Yang B, Wang L, Zhang M, et al. Advanced separators based on aramid nanofiber (ANF) membranes for lithium-ion batteries: a review of recent progress[J]. Journal of Materials Chemistry A, 2021, 9(22): 12923-12946.

[19]Li J, Fleetwood J, Hawley W B, et al. From Materials to Cell: State-of-the-Art and Prospective Technologies for Lithium-Ion Battery Electrode Processing[J]. Chemical Reviews, 2022, 122(1): 903-956.

[20]Costa C M, Lizundia E, Lanceros-Méndez S. Polymers for advanced lithium-ion batteries: State of the art and future needs on polymers for the different battery components[J]. Progress in Energy and Combustion Science, 2020, 79: 100846.

[21]Fichtner M, Edström K, Ayerbe E, et al. Rechargeable Batteries of the Future—The State of the Art from a BATTERY 2030+ Perspective[J]. Advanced Energy Materials, 2022, 12(17): 2102904.

[22] Nunes-Pereira J, Costa C M, Lanceros-Méndez S. Polymer composites and blends for battery separators: State of the art, challenges and future trends[J]. J Power Sources, 2015, 281: 378-398.

[23]Hwang J-Y, Myung S-T, Sun Y-K. Sodium-ion batteries: present and future[J]. Chemical Society Reviews, 2017, 46(12): 3529-3614.

[24]Costa C M, Lanceros-Mendez S. Recent advances on battery separators based on poly(vinylidene fluoride) and its copolymers for lithium-ion battery applications[J]. Current Opinion in Electrochemistry, 2021, 29: 100752.

[25]Niu X, Li J, Song J, et al. Interconnected Porous Poly(ether imide) Separator for Thermally Stable Sodium Ion Battery[J]. ACS Applied Energy Materials, 2021, 4(10): 11080-11089.

[26]Coustan L, Tarascon J-M, Laberty-Robert C. Thin Fiber-Based Separators for High-Rate Sodium Ion Batteries[J]. ACS Applied Energy Materials, 2019, 2(12): 8369-8375.

[27]Chen C-Y, Matsumoto K, Nohira T, et al. Na2MnSiO4 as a positive electrode material for sodium secondary batteries using an ionic liquid electrolyte[J]. Electrochemistry Communications, 2014, 45: 63-66.

[28]Zhang T-W, Shen B, Yao H-B, et al. Prawn Shell Derived Chitin Nanofiber Membranes as Advanced Sustainable Separators for Li/Na-Ion Batteries[J]. Nano Letters, 2017, 17(8): 4894-4901.

[29]Mun J, Yim T, Gap Kwon Y, et al. Self-assembled nano-silica-embedded polyethylene separator with outstanding physicochemical and thermal properties for advanced sodium ion batteries[J]. Chemical Engineering Journal, 2021, 405: 125844.

[30]Yang P, Zhang P, Shi C, et al. The functional separator coated with core–shell structured silica–poly(methyl methacrylate) sub-microspheres for lithium-ion batteries[J]. Journal of Membrane Science, 2015, 474: 148-155.

[31]Park J-H, Cho J-H, Park W, et al. Close-packed SiO2/poly(methyl methacrylate) binary nanoparticles-coated polyethylene separators for lithium-ion batteries[J]. Journal of Power Sources, 2010, 195(24): 8306-8310.

[32]Zhu X, Jiang X, Ai X, et al. A Highly Thermostable Ceramic-Grafted Microporous Polyethylene Separator for Safer Lithium-Ion Batteries[J]. ACS Applied Materials & Interfaces, 2015, 7(43): 24119-24126.

[33]Shi C, Zhang P, Chen L, et al. Effect of a thin ceramic-coating layer on thermal and electrochemical properties of polyethylene separator for lithium-ion batteries[J]. Journal of Power Sources, 2014, 270: 547-553.

[34]Jeon H, Yeon D, Lee T, et al. A water-based Al2O3 ceramic coating for polyethylene-based microporous separators for lithium-ion batteries[J]. Journal of Power Sources, 2016, 315: 161-168.

[35] Zhu X, Jiang X, Ai X, et al. TiO2 ceramic-grafted polyethylene separators for enhanced thermostability and electrochemical performance of lithium-ion batteries[J]. Journal of Membrane Science, 2016, 504: 97-103.

[36]Kim K J, Kwon H K, Park M-S, et al. Ceramic composite separators coated with moisturized ZrO2 nanoparticles for improving the electrochemical performance and thermal stability of lithium ion batteries[J]. Physical Chemistry Chemical Physics, 2014, 16(20): 9337-9343.

[37]Suharto Y, Lee Y, Yu J-S, et al. Microporous ceramic coated separators with superior wettability for enhancing the electrochemical performance of sodium-ion batteries[J]. Journal of Power Sources, 2018, 376: 184-190.

[38]Ma Z-Y, Xue Y-R, Yang H-C, et al. Surface and Interface Engineering of Polymer Membranes: Where We Are and Where to Go[J]. Macromolecules, 2022, 55(9): 3363-3383.

[39]Lu Y, Liu W, Liu J, et al. A review on 2D porous organic polymers for membrane-based separations: Processing and engineering of transport channels[J]. Advanced Membranes, 2021, 1: 100014.

[40]Lu W, Yuan Z, Zhao Y, et al. Porous membranes in secondary battery technologies[J]. Chemical Society Reviews, 2017, 46(8): 2199-2236.

[41]Arora P, Zhang Z. Battery Separators[J]. Chemical Reviews, 2004, 104(10): 4419-4462.

[42]Wan C, Chen X, Lv F, et al. Biaxial stretch-induced structural evolution of polyethylene gel films: Crystal melting recrystallization and tilting[J]. Polymer, 2019, 164: 59-66.

[43]Demeuse M T: Chapter 5 - Wet process for battery separator production, Demeuse M T, editor, Polymer-Based Separators for Lithium-Ion Batteries: Elsevier, 2021: 71-91.

[44]Luo W, Cheng S, Wu M, et al. A review of advanced separators for rechargeable batteries[J]. Journal of Power Sources, 2021, 509: 230372.

[45]Demeuse M T: Chapter 4 - Dry process for battery separator production, Demeuse M T, editor, Polymer-Based Separators for Lithium-Ion Batteries: Elsevier, 2021: 55-70.

[46]Yoneda H, Nishimura Y, Doi Y, et al. Development of microporous PE films to improve lithium ion batteries[J]. Polym J, 2010, 42(6): 425-437.

[47]Lagadec M F, Zahn R, Wood V. Characterization and performance evaluation of lithium-ion battery separators[J]. Nature Energy, 2019, 4(1): 16-25.

[48]Zhang L, Li X, Yang M, et al. High-safety separators for lithium-ion batteries and sodium-ion batteries: advances and perspective[J]. Energy Storage Materials, 2021, 41: 522-545.

[49] Zhong S, Yuan B, Guang Z, et al. Recent progress in thin separators for upgraded lithium ion batteries[J]. Energy Storage Materials, 2021, 41: 805-841.

[50] Santhanagopalan S, Zhang Z: Rechargeable Batteriesrechargeable battery, Separators for, Meyers R A, editor, Encyclopedia of Sustainability Science and Technology, New York, NY: Springer New York, 2012: 8715-8757.

[51] Waqas M, Ali S, Feng C, et al. Recent Development in Separators for High-Temperature Lithium-Ion Batteries[J]. Small, 2019, 15(33): 1901689.

[52] Demeuse M T: Chapter 2 - Background and design of battery separators, Demeuse M T, editor, Polymer-Based Separators for Lithium-Ion Batteries: Elsevier, 2021: 21-34.

[53] Wang J, Liu Y, Cai Q, et al. Hierarchically Porous Silica Membrane as Separator for High-Performance Lithium-Ion Batteries[J]. Advanced Materials, 2022, 34(3): 2107957.

[54] Palacín M R. Recent advances in rechargeable battery materials: a chemist's perspective[J]. Chemical Society Reviews, 2009, 38(9): 2565-2575.

[55] Gu Q-Q, Fu C-L, Sun Z-Y. Resin-silica composite nanoparticle grafted polyethylene membranes for lithium ion batteries[J]. Journal of Applied Polymer Science, 2021, 138(30): 50713.

[56] Francis C F J, Kyratzis I L, Best A S. Lithium-Ion Battery Separators for Ionic-Liquid Electrolytes: A Review[J]. Advanced Materials, 2020, 32(18): 1904205.

[57] Jung B, Lee B, Jeong Y-C, et al. Thermally stable non-aqueous ceramic-coated separators with enhanced nail penetration performance[J]. Journal of Power Sources, 2019, 427: 271-282.

[58] Sheidaei A, Xiao X, Huang X, et al. Mechanical behavior of a battery separator in electrolyte solutions[J]. Journal of Power Sources, 2011, 196(20): 8728-8734.

[59] Demeuse M T: Chapter 3 - Characterization techniques for battery separators, Demeuse M T, editor, Polymer-Based Separators for Lithium-Ion Batteries: Elsevier, 2021: 35-53.

[60] Zhang S S. A review on the separators of liquid electrolyte Li-ion batteries[J]. Journal of Power Sources, 2007, 164(1): 351-364.

[61] Chen W, Shi L, Zhou H, et al. Water-Based Organic–Inorganic Hybrid Coating for a High-Performance Separator[J]. ACS Sustainable Chemistry & Engineering, 2016, 4(7): 3794-3802.

[62] Zhang Z, Yuan W, Li L. Enhanced wettability and thermal stability of nano-SiO2/poly(vinyl alcohol)-coated polypropylene composite separators for lithium-ion batteries[J]. Particuology, 2018, 37: 91-98.

[63]Peng L, Kong X, Li H, et al. A Rational Design for a High-Safety Lithium-Ion Battery Assembled with a Heatproof–Fireproof Bifunctional Separator[J]. Advanced Functional Materials, 2021, 31(10): 2008537.

[64]Liu J, Liu Y, Yang W, et al. Lithium ion battery separator with high performance and high safety enabled by tri-layered SiO2@PI/m-PE/SiO2@PI nanofiber composite membrane[J]. Journal of Power Sources, 2018, 396: 265-275.

[65]Jeon D H. Wettability in electrodes and its impact on the performance of lithium-ion batteries[J]. Energy Storage Materials, 2019, 18: 139-147.

[66]Pramanik S, Das P: Chapter 3 - Metal-Based Nanomaterials and Their Polymer Nanocomposites, Karak N, editor, Nanomaterials and Polymer Nanocomposites: Elsevier, 2019: 91-121.

[67]Dong D, Zhang H, Zhou B, et al. Porous covalent organic frameworks for high transference number polymer-based electrolytes[J]. Chemical Communications, 2019, 55(10): 1458-1461.

[68]Liang Y, Liu Y, Chen D, et al. Hydroxyapatite functionalization of solid polymer electrolytes for high-conductivity solid-state lithium-ion batteries[J]. Materials Today Energy, 2021, 20: 100694.

[69]Liao C, Wang W, Han L, et al. A flame retardant sandwiched separator coated with ammonium polyphosphate wrapped by SiO2 on commercial polyolefin for high performance safety lithium metal batteries[J]. Applied Materials Today, 2020, 21: 100793.

[70]Aslam M K, Niu Y, Hussain T, et al. How to avoid dendrite formation in metal batteries: Innovative strategies for dendrite suppression[J]. Nano Energy, 2021, 86: 106142.

[71]Patrike A, Yadav P, Shelke V, et al. Research Progress and Perspective on Lithium/Sodium Metal Anodes for Next-Generation Rechargeable Batteries[J]. ChemSusChem, n/a(n/a): e202200504.

[72]Ren W, Zheng Y, Cui Z, et al. Recent progress of functional separators in dendrite inhibition for lithium metal batteries[J]. Energy Storage Materials, 2021, 35: 157-168.

[73]Li Y, Yu L, Hu W, et al. Thermotolerant separators for safe lithium-ion batteries under extreme conditions[J]. Journal of Materials Chemistry A, 2020, 8(39): 20294-20317.

[74]Liao C, Mu X, Han L, et al. A flame-retardant, high ionic-conductivity and eco-friendly separator prepared by papermaking method for high-performance and superior safety lithium-ion batteries[J]. Energy Storage Materials, 2022, 48: 123-132.

[75]Chou L-Y, Ye Y, Lee H K, et al. Electrolyte-Resistant Dual Materials for the Synergistic Safety Enhancement of Lithium-Ion Batteries[J]. Nano Letters, 2021, 21(5): 2074-2080.

[76]Zhai P, Liu K, Wang Z, et al. Multifunctional separators for high-performance lithium ion batteries[J]. Journal of Power Sources, 2021, 499: 229973.

[77]Lv F, Wang Z, Shi L, et al. Challenges and development of composite solid-state electrolytes for high-performance lithium ion batteries[J]. Journal of Power Sources, 2019, 441: 227175.

[78]Zhou B, He D, Hu J, et al. A flexible, self-healing and highly stretchable polymer electrolyte via quadruple hydrogen bonding for lithium-ion batteries[J]. Journal of Materials Chemistry A, 2018, 6(25): 11725-11733.

[79]Liu R, Yuan B, Zhong S, et al. Poly(vinylidene fluoride) separators for next-generation lithium based batteries[J]. Nano Select, 2021, 2(12): 2308-2345.

[80]Yuan S, Li X, Zhu J, et al. Covalent organic frameworks for membrane separation[J]. Chemical Society Reviews, 2019, 48(10): 2665-2681.

[81]Huang X, Hitt J. Lithium ion battery separators: Development and performance characterization of a composite membrane[J]. Journal of Membrane Science, 2013, 425-426: 163-168.

[82]Yang J, Zhang H, Zhou Q, et al. Safety-Enhanced Polymer Electrolytes for Sodium Batteries: Recent Progress and Perspectives[J]. ACS Applied Materials & Interfaces, 2019, 11(19): 17109-17127.

[83]Babiker D M D, Wan C, Mansoor B, et al. Superior lithium battery separator with extraordinary electrochemical performance and thermal stability based on hybrid UHMWPE/SiO2 nanocomposites via the scalable biaxial stretching process[J]. Composites Part B: Engineering, 2021, 211: 108658.

[84]Leng X, Yang M, Li C, et al. High-performance separator for lithium-ion battery based on dual-hybridizing of materials and processes[J]. Chemical Engineering Journal, 2022, 433: 133773.

[85]Li D, Shi D, Yuan Z, et al. A low cost shutdown sandwich-like composite membrane with superior thermo-stability for lithium-ion battery[J]. Journal of Membrane Science, 2017, 542: 1-7.

[86]Li S, Zhang S-Q, Shen L, et al. Progress and Perspective of Ceramic/Polymer Composite Solid Electrolytes for Lithium Batteries[J]. Advanced Science, 2020, 7(5): 1903088.

[87]Huang X, He R, Li M, et al. Functionalized separator for next-generation batteries[J]. Materials Today, 2020, 41: 143-155.

[88]Yang Y, Wang W, Meng G, et al. Function-directed design of battery separators based on microporous polyolefin membranes[J]. Journal of Materials Chemistry A, 2022, 10(27): 14137-14170.

[89]Weber C J, Roth M: Separators, Korthauer R, editor, Lithium-Ion Batteries: Basics and Applications, Berlin, Heidelberg: Springer Berlin Heidelberg, 2018: 75-88.

[90]Wang J, Wang Z, Ni J, et al. Electrospinning for flexible sodium-ion batteries[J]. Energy Storage Materials, 2022, 45: 704-719.

[91]Ding Y, Hou H, Zhao Y, et al. Electrospun polyimide nanofibers and their applications[J]. Progress in Polymer Science, 2016, 61: 67-103.

[92]Ma X, Kolla P, Yang R, et al. Electrospun polyacrylonitrile nanofibrous membranes with varied fiber diameters and different membrane porosities as lithium-ion battery separators[J]. Electrochimica Acta, 2017, 236: 417-423.

[93] Hao J, Lei G, Li Z, et al. A novel polyethylene terephthalate nonwoven separator based on electrospinning technique for lithium ion battery[J]. Journal of Membrane Science, 2013, 428: 11-16.

[94]Chen Y, Qiu L, Ma X, et al. Electrospun PMIA and PVDF-HFP composite nanofibrous membranes with two different structures for improved lithium-ion battery separators[J]. Solid State Ionics, 2020, 347: 115253.

[95]Kong L, Wang Y, Yu H, et al. In Situ Armoring: A Robust, High-Wettability, and Fire-Resistant Hybrid Separator for Advanced and Safe Batteries[J]. ACS Applied Materials & Interfaces, 2019, 11(3): 2978-2988.

[96]Kim J R, Choi S W, Jo S M, et al. Electrospun PVdF-based fibrous polymer electrolytes for lithium ion polymer batteries[J]. Electrochimica Acta, 2004, 50(1): 69-75.

[97]Liu Z, Hu Q, Guo S, et al. Thermoregulating Separators Based on Phase-Change Materials for Safe Lithium-Ion Batteries[J]. Advanced Materials, 2021, 33(15): 2008088.

[98]Li Y, Li Q, Tan Z. A review of electrospun nanofiber-based separators for rechargeable lithium-ion batteries[J]. Journal of Power Sources, 2019, 443: 227262.

[99] Kong L, Yan Y, Qiu Z, et al. Robust fluorinated polyimide nanofibers membrane for high-performance lithium-ion batteries[J]. Journal of Membrane Science, 2018, 549: 321-331.

[100]Evans T, Lee J-H, Bhat V, et al. Electrospun polyacrylonitrile microfiber separators for ionic liquid electrolytes in Li-ion batteries[J]. Journal of Power Sources, 2015, 292: 1-6.

[101]Wu D, Shi C, Huang S, et al. Electrospun Nanofibers for Sandwiched Polyimide/Poly (vinylidene fluoride)/Polyimide Separators with the Thermal Shutdown Function[J]. Electrochimica Acta, 2015, 176: 727-734.

[102]Zhang L, Feng G, Li X, et al. Synergism of surface group transfer and in-situ growth of silica-aerogel induced high-performance modified polyacrylonitrile separator for lithium/sodium-ion batteries[J]. Journal of Membrane Science, 2019, 577: 137-144.

[103]Yanilmaz M, Lu Y, Zhu J, et al. Silica/polyacrylonitrile hybrid nanofiber membrane separators via sol-gel and electrospinning techniques for lithium-ion batteries[J]. Journal of Power Sources, 2016, 313: 205-212.

[104]Park S, Son C W, Lee S, et al. Multicore-shell nanofiber architecture of polyimide/polyvinylidene fluoride blend for thermal and long-term stability of lithium ion battery separator[J]. Scientific Reports, 2016, 6(1): 36977.

[105]Shubha N, Prasanth R, Hng H H, et al. Study on effect of poly (ethylene oxide) addition and in-situ porosity generation on poly (vinylidene fluoride)-glass ceramic composite membranes for lithium polymer batteries[J]. Journal of Power Sources, 2014, 267: 48-57.

[106] Angulakshmi N, Stephan A M. Electrospun Trilayer Polymeric Membranes as Separator for Lithium–ion Batteries[J]. Electrochimica Acta, 2014, 127: 167-172.

[107]Lee H, Alcoutlabi M, Toprakci O, et al. Preparation and characterization of electrospun nanofiber-coated membrane separators for lithium-ion batteries[J]. Journal of Solid State Electrochemistry, 2014, 18(9): 2451-2458.

[108] Janakiraman S, Khalifa M, Biswal R, et al. High performance electrospun nanofiber coated polypropylene membrane as a separator for sodium ion batteries[J]. Journal of Power Sources, 2020, 460: 228060.

[109]Chen W, Liu Y, Ma Y, et al. Improved performance of PVdF-HFP/PI nanofiber membrane for lithium ion battery separator prepared by a bicomponent cross-electrospinning method[J]. Materials Letters, 2014, 133: 67-70.

[110]Huang F, Xu Y, Peng B, et al. Coaxial Electrospun Cellulose-Core Fluoropolymer-Shell Fibrous Membrane from Recycled Cigarette Filter as Separator for High Performance Lithium-Ion Battery[J]. ACS Sustainable Chemistry & Engineering, 2015, 3(5): 932-940.

[111]Xiao K, Zhai Y, Yu J, et al. Nanonet-structured poly(m-phenylene isophthalamide)–polyurethane membranes with enhanced thermostability and wettability for high power lithium ion batteries[J]. RSC Advances, 2015, 5(68): 55478-55485.

[112]Saito Y, Kataoka H, Quartarone E, et al. Carrier Migration Mechanism of Physically Cross-Linked Polymer Gel Electrolytes Based on PVDF Membranes[J]. The Journal of Physical Chemistry B, 2002, 106(29): 7200-7204.

[113]Wang H, Wang T, Yang S, et al. Preparation of thermal stable porous polyimide membranes by phase inversion process for lithium-ion battery[J]. Polymer, 2013, 54(23): 6339-6348.

[114]Li D, Shi D, Feng K, et al. Poly (ether ether ketone) (PEEK) porous membranes with super high thermal stability and high rate capability for lithium-ion batteries[J]. Journal of Membrane Science, 2017, 530: 125-131.

[115]De Moraes A C M, Hyun W J, Luu N S, et al. Phase-Inversion Polymer Composite Separators Based on Hexagonal Boron Nitride Nanosheets for High-Temperature Lithium-Ion Batteries[J]. ACS Applied Materials & Interfaces, 2020, 12(7): 8107-8114.

[116]Ribeiro C, Costa C M, Correia D M, et al. Electroactive poly(vinylidene fluoride)-based structures for advanced applications[J]. Nature Protocols, 2018, 13(4): 681-704.

[117]Barbosa J C, Gonçalves R, Valverde A, et al. Metal organic framework modified poly(vinylidene fluoride-co-hexafluoropropylene) separator membranes to improve lithium-ion battery capacity fading[J]. Chemical Engineering Journal, 2022, 443: 136329.

[118]Casas X, Niederberger M, Lizundia E. A Sodium-Ion Battery Separator with Reversible Voltage Response Based on Water-Soluble Cellulose Derivatives[J]. ACS Applied Materials & Interfaces, 2020, 12(26): 29264-29274.

[119]Kassenova N, Kalybekkyzy S, Kahraman M V, et al. Photo and thermal crosslinked poly(vinyl alcohol)-based nanofiber membrane for flexible gel polymer electrolyte[J]. Journal of Power Sources, 2022, 520: 230896.

[120]Zhai Y, Liu H, Li L, et al.: Chapter 22 - Electrospun Nanofibers for Lithium-Ion Batteries, Ding B, Wang X, Yu J, editor, Electrospinning: Nanofabrication and Applications: William Andrew Publishing, 2019: 671-694.

[121]Sanchez L M, Espinosa E, Mendoza Zélis P, et al. Cellulose nanofibers/PVA blend polymeric beads containing in-situ prepared magnetic nanorods as dye pollutants adsorbents[J]. International Journal of Biological Macromolecules, 2022, 209: 1211-1221.

[122]Weng B, Xu F, Alcoutlabi M, et al. Fibrous cellulose membrane mass produced via forcespinning® for lithium-ion battery separators[J]. Cellulose, 2015, 22(2): 1311-1320.

[123]Lizundia E, Costa C M, Alves R, et al. Cellulose and its derivatives for lithium ion battery separators: A review on the processing methods and properties[J]. Carbohydrate Polymer Technologies and Applications, 2020, 1: 100001.

[124]Asghar M R, Zhang Y, Wu A, et al. Preparation of microporous Cellulose/Poly(vinylidene fluoride-hexafluoropropylene) membrane for lithium ion batteries by phase inversion method[J]. Journal of Power Sources, 2018, 379: 197-205.

[125]Asghar M R, Anwar M T, Xia G, et al. Cellulose/Poly(vinylidene fluoride hexafluoropropylene) composite membrane with titania nanoparticles for lithium-ion batteries[J]. Materials Chemistry and Physics, 2020, 252: 123122.

[126]Xiao W, Zhao L, Gong Y, et al. Preparation and performance of poly(vinyl alcohol) porous separator for lithium-ion batteries[J]. Journal of Membrane Science, 2015, 487: 221-228.

[127]Lian F, Wen Y, Ren Y, et al. A novel PVB based polymer membrane and its application in gel polymer electrolytes for lithium-ion batteries[J]. Journal of Membrane Science, 2014, 456: 42-48.

[128]Song S, Dong Z, Fernandez C, et al. Nanoporous ceramic-poly(ethylene oxide) composite electrolyte for sodium metal battery[J]. Materials Letters, 2019, 236: 13-15.

[129] Krishna Jyothi N, Vijaya Kumar K, Sunita Sundari G, et al. Ionic conductivity and battery characteristic studies of a new PAN-based Na+ ion conducting gel polymer electrolyte system[J]. Indian Journal of Physics, 2016, 90(3): 289-296.

[130]Miao Y-E, Zhu G-N, Hou H, et al. Electrospun polyimide nanofiber-based nonwoven separators for lithium-ion batteries[J]. Journal of Power Sources, 2013, 226: 82-86.

[131] Ryou M-H, Lee Y M, Park J-K, et al. Mussel-Inspired Polydopamine-Treated Polyethylene Separators for High-Power Li-Ion Batteries[J]. Advanced Materials, 2011, 23(27): 3066-3070.

[132]Vijayakumar V, Anothumakkool B, Kurungot S, et al. In situ polymerization process: an essential design tool for lithium polymer batteries[J]. Energy & Environmental Science, 2021, 14(5): 2708-2788.

[133]Wang H, Song J, Zhang K, et al. A strongly complexed solid polymer electrolyte enables a stable solid state high-voltage lithium metal battery[J]. Energy & Environmental Science, 2022.

[134]Pawlicka A, Donoso J P: 3 - Polymer electrolytes based on natural polymers, Sequeira C, Santos D, editor, Polymer Electrolytes: Woodhead Publishing, 2010: 95-128.

[135]Liang S, Yan W, Li M, et al.: Polymer Electrolytes for Lithium Ion Batteries and Challenges: Part I, Polymer Electrolytes, 2020: 187-199.

[136]Sequeira C a C, Santos D M F: 1 - Introduction to polymer electrolyte materials, Sequeira C, Santos D, editor, Polymer Electrolytes: Woodhead Publishing, 2010: 3-61.

[137]Liang J, Luo J, Sun Q, et al. Recent progress on solid-state hybrid electrolytes for solid-state lithium batteries[J]. Energy Storage Materials, 2019, 21: 308-334.

[138]Ren Z, Li J, Gong Y, et al. Insight into the integration way of ceramic solid-state electrolyte fillers in the composite electrolyte for high performance solid-state lithium metal battery[J]. Energy Storage Materials, 2022, 51: 130-138.

[139]Chen A, Qu C, Shi Y, et al. Manufacturing Strategies for Solid Electrolyte in Batteries[J]. Frontiers in Energy Research, 2020, 8.

[140] Han L, Lehmann M L, Zhu J, et al. Recent Developments and Challenges in Hybrid Solid Electrolytes for Lithium-Ion Batteries[J]. Frontiers in Energy Research, 2020, 8.

[141]Dinoto V, Negro E, Lavina S, et al.: 6 - Hybrid inorganic–organic polymer electrolytes, Sequeira C, Santos D, editor, Polymer Electrolytes: Woodhead Publishing, 2010: 219-277.

[142]Mong A L, Shi Q X, Jeon H, et al. Tough and Flexible, Super Ion-Conductive Electrolyte Membranes for Lithium-Based Secondary Battery Applications[J]. Advanced Functional Materials, 2021, 31(12): 2008586.

[143]Yu X, Manthiram A. A review of composite polymer-ceramic electrolytes for lithium batteries[J]. Energy Storage Materials, 2021, 34: 282-300.

[144] Gandi S, Chidambara Swamy Vaddadi V S, Sripada Panda S S, et al. Recent progress in the development of glass and glass-ceramic cathode/solid electrolyte materials for next-generation high capacity all-solid-state sodium-ion batteries: A review[J]. Journal of Power Sources, 2022, 521: 230930.

[145]Xu R, Sheng L, Gong H, et al. High-Performance Al2O3/PAALi Composite Separator Prepared by Water-Based Slurry for High-Power Density Lithium-Based Battery[J]. Advanced Engineering Materials, 2021, 23(3): 2001009.

[146]Chen K, Li Y, Zhan H. Advanced separators for lithium-ion batteries[J]. IOP Conference Series: Earth and Environmental Science, 2022, 1011(1): 012009.

[147]Kim Y B, Tran-Phu T, Kim M, et al. Facilitated Ion Diffusion in Multiscale Porous Particles: Application in Battery Separators[J]. ACS Applied Materials & Interfaces, 2015, 7(8): 4511-4517.

[148]Dai J, Shi C, Li C, et al. A rational design of separator with substantially enhanced thermal features for lithium-ion batteries by the polydopamine–ceramic composite modification of polyolefin membranes[J]. Energy & Environmental Science, 2016, 9(10): 3252-3261.

[149]Ahn J H, Kim H-M, Lee Y-J, et al. Nanostructured reactive alumina particles coated with water-soluble binder on the polyethylene separator for highly safe lithium-ion batteries[J]. Journal of Power Sources, 2021, 506: 230119.

[150]Ahn J H, You T-S, Lee S-M, et al. Hybrid separator containing reactive, nanostructured alumina promoting in-situ gel electrolyte formation for lithium-ion batteries with good cycling stability and enhanced safety[J]. Journal of Power Sources, 2020, 472: 228519.

[151]Qiu Z, Yuan S, Wang Z, et al. Construction of silica-oxygen-borate hybrid networks on Al2O3-coated polyethylene separators realizing multifunction for high-performance lithium ion batteries[J]. Journal of Power Sources, 2020, 472: 228445.

[152]Xiao Y, Fu A, Zou Y, et al. High safety lithium-ion battery enabled by a thermal-induced shutdown separator[J]. Chemical Engineering Journal, 2022, 438: 135550.

[153]Eray S: 6 - Application of metal oxides in composites, Al-Douri Y, editor, Metal Oxide Powder Technologies: Elsevier, 2020: 101-119.

[154]Cai H, Yang G, Meng Z, et al. Water-Dispersed Poly(p-Phenylene Terephthamide) Boosting Nano-Al2O3-Coated Polyethylene Separator with Enhanced Thermal Stability and Ion Diffusion for Lithium-Ion Batteries[J]. Polymers, 2019, 11(8): 1362.

[155]Jing P, Liu M, Wang P, et al. Flexible nonwoven ZrO2 ceramic membrane as an electrochemically stable and flame-resistant separator for high-power rechargeable batteries[J]. Chemical Engineering Journal, 2020, 388: 124259.

[156]Xiao W, Gong Y, Wang H, et al. Preparation and electrochemical performance of ZrO2 nanoparticle-embedded nonwoven composite separator for lithium-ion batteries[J]. Ceramics International, 2015, 41(10, Part B): 14223-14229.

[157]Chi M, Shi L, Wang Z, et al. Excellent rate capability and cycle life of Li metal batteries with ZrO2/POSS multilayer-assembled PE separators[J]. Nano Energy, 2016, 28: 1-11.

[158]Xu W, Wang Z, Shi L, et al. Layer-by-Layer Deposition of Organic–Inorganic Hybrid Multilayer on Microporous Polyethylene Separator to Enhance the Electrochemical Performance of Lithium-Ion Battery[J]. ACS Applied Materials & Interfaces, 2015, 7(37): 20678-20686.

[159]Mao L, Zhao X, Cheng Q, et al. Recent advances and perspectives of two-dimensional Ti-based electrodes for electrochemical energy storage[J]. Sustainable Energy & Fuels, 2021, 5(20): 5061-5113.

[160]Ge M, Cao C, Huang J, et al. A review of one-dimensional TiO2 nanostructured materials for environmental and energy applications[J]. Journal of Materials Chemistry A, 2016, 4(18): 6772-6801.

[161]Zhang R-X, Braeken L, Luis P, et al. Novel binding procedure of TiO2 nanoparticles to thin film composite membranes via self-polymerized polydopamine[J]. Journal of Membrane Science, 2013, 437: 179-188.

[162]Weng Z, Guo H, Liu X, et al. Nanostructured TiO2 for energy conversion and storage[J]. RSC Advances, 2013, 3(47): 24758-24775.

[163]Pi J-K, Wu G-P, Yang H-C, et al. Separators with Biomineralized Zirconia Coatings for Enhanced Thermo- and Electro-Performance of Lithium-Ion Batteries[J]. ACS Applied Materials & Interfaces, 2017, 9(26): 21971-21978.

[164]Zhang X, Sun Q, Zhen C, et al. Recent progress in flame-retardant separators for safe lithium-ion batteries[J]. Energy Storage Materials, 2021, 37: 628-647.

[165]Jiang X, Zhu X, Ai X, et al. Novel Ceramic-Grafted Separator with Highly Thermal Stability for Safe Lithium-Ion Batteries[J]. ACS Applied Materials & Interfaces, 2017, 9(31): 25970-25975.

[166]Babiker D M D, Yu R, Usha Z R, et al. High performance ultra-high molecular weight polyethylene nanocomposite separators with excellent rate capabilities designed for next-generation lithium-ion batteries[J]. Materials Today Physics, 2022, 23: 100626.

[167]Choi Y, Kim J I, Moon J, et al. Electron beam induced strong organic/inorganic grafting for thermally stable lithium-ion battery separators[J]. Applied Surface Science, 2018, 444: 339-344.

[168]Jin S Y, Manuel J, Zhao X, et al. Surface-modified polyethylene separator via oxygen plasma treatment for lithium ion battery[J]. Journal of Industrial and Engineering Chemistry, 2017, 45: 15-21.

[169]Gu Q-Q, Xue H-J, Li Z-W, et al. High-performance polyethylene separators for lithium-ion batteries modified by phenolic resin[J]. Journal of Power Sources, 2021, 483: 229155.

[170]Sheng L, Xie X, Sun Z, et al. Role of Separator Surface Polarity in Boosting the Lithium-Ion Transport Property for a Lithium-Based Battery[J]. ACS Applied Energy Materials, 2021, 4(5): 5212-5221.

[171] Na W, Koh K H, Lee A S, et al. Binder-less chemical grafting of SiO2 nanoparticles onto polyethylene separators for lithium-ion batteries[J]. Journal of Membrane Science, 2019, 573: 621-627.

[172] Kourtakis K, Bekiarian P, Blackman G, et al. Novel thermal and photo curable anti-reflective coatings using fluoroelastomer nanocomposites and self-assembly of nanoparticles[J]. Journal of Coatings Technology and Research, 2016, 13(5): 753-762.

[173] Gu Z, Nan Y, Zhang Y, et al. Synthesis and properties of phosphorus-containing cardanol-based acrylates for flame-retardant UV/EB-cured coatings[J]. Journal of Coatings Technology and Research, 2021, 18(5): 1353-1364.

[174] Liang T, Li H, Lai X, et al. A facile approach to UV-curable super-hydrophilic polyacrylate coating film grafted on glass substrate[J]. Journal of Coatings Technology and Research, 2016, 13(6): 1115-1121.

[175] Yamamura M. Reaction-driven solvent transport in UV-curable phase-separating coatings[J]. Journal of Coatings Technology and Research, 2022.

[176] Kim K J, Park M-S, Yim T, et al. Electron-beam-irradiated polyethylene membrane with improved electrochemical and thermal properties for lithium-ion batteries[J]. Journal of Applied Electrochemistry, 2014, 44(3): 345-352.

[177] Costa L, Bracco P: Chapter 11 - Mechanisms of Crosslinking and Oxidative Degradation of UHMWPE, Kurtz S M, editor, The UHMWPE Handbook, San Diego: Academic Press, 2004: 245-261.

[178] Slouf M, Synkova H, Baldrian J, et al. Structural changes of UHMWPE after e-beam irradiation and thermal treatment[J]. Journal of Biomedical Materials Research Part B: Applied Biomaterials, 2008, 85B(1): 240-251.

[179] Lee J Y, Lee Y M, Bhattacharya B, et al. Separator grafted with siloxane by electron beam irradiation for lithium secondary batteries[J]. Electrochimica Acta, 2009, 54(18): 4312-4315.

[180] Sabetzadeh N, Falamaki C, Riahifar R, et al. Plasma treatment of polypropylene membranes coated with zeolite/organic binder layers: Assessment of separator performance in lithium-ion batteries[J]. Solid State Ionics, 2021, 363: 115589.

[181] Kim J Y, Lee Y, Lim D Y. Plasma-modified polyethylene membrane as a separator for lithium-ion polymer battery[J]. Electrochimica Acta, 2009, 54(14): 3714-3719.

[182]Han M, Kim D-W, Kim Y-C. Charged Polymer-Coated Separators by Atmospheric Plasma-Induced Grafting for Lithium-Ion Batteries[J]. ACS Applied Materials & Interfaces, 2016, 8(39): 26073-26081.

[183]Sheng L, Zhang Y, Xie X, et al. Polyethylene separator activated by γ-ray irradiation for improving lithium-based battery performance[J]. Journal of Materials Science, 2021, 56(36): 20026-20036.

[184]Abdul-Kader A M, Turos A, Radwan R M, et al. Surface free energy of ultra-high molecular weight polyethylene modified by electron and gamma irradiation[J]. Applied Surface Science, 2009, 255(17): 7786-7790.

[185]Babiker D M D, Zhu L, Yagoub H, et al. The change from hydrophilicity to hydrophobicity of HEC/PAA complex membrane for water-in-oil emulsion separation: Thermal versus chemical treatment[J]. Carbohydrate Polymers, 2020, 241: 116343.

[186]Borges J, Mano J F. Molecular Interactions Driving the Layer-by-Layer Assembly of Multilayers[J]. Chemical Reviews, 2014, 114(18): 8883-8942.

[187]Jin R, Fu L, Zhou H, et al. High Li+ Ionic Flux Separator Enhancing Cycling Stability of Lithium Metal Anode[J]. ACS Sustainable Chemistry & Engineering, 2018, 6(3): 2961-2968.

[188]Wang Z, Guo F, Chen C, et al. Self-Assembly of PEI/SiO2 on Polyethylene Separators for Li-Ion Batteries with Enhanced Rate Capability[J]. ACS Applied Materials & Interfaces, 2015, 7(5): 3314-3322.

[189]George S M. Atomic Layer Deposition: An Overview[J]. Chemical Reviews, 2010, 110(1): 111-131.

[190] Zhao Y, Zhang L, Liu J, et al. Atomic/molecular layer deposition for energy storage and conversion[J]. Chemical Society Reviews, 2021, 50(6): 3889-3956.

[191] Meng X, Wang X, Geng D, et al. Atomic layer deposition for nanomaterial synthesis and functionalization in energy technology[J]. Materials Horizons, 2017, 4(2): 133-154.

[192] Puurunen R L. Surface chemistry of atomic layer deposition: A case study for the trimethylaluminum/water process[J]. Journal of Applied Physics, 2005, 97(12): 121301.

[193]Dasgupta N P, Meng X, Elam J W, et al. Atomic Layer Deposition of Metal Sulfide Materials[J]. Accounts of Chemical Research, 2015, 48(2): 341-348.

[194]Meng X. Atomic-scale surface modifications and novel electrode designs for high-performance sodium-ion batteries via atomic layer deposition[J]. Journal of Materials Chemistry A, 2017, 5(21): 10127-10149.

[195]Johnson R W, Hultqvist A, Bent S F. A brief review of atomic layer deposition: from fundamentals to applications[J]. Materials Today, 2014, 17(5): 236-246.

[196]Chao C-H, Hsieh C-T, Ke W-J, et al. Roll-to-roll atomic layer deposition of titania coating on polymeric separators for lithium ion batteries[J]. Journal of Power Sources, 2021, 482: 228896.

[197]Moon J, Jeong J Y, Kim J I, et al. An ultrathin inorganic-organic hybrid layer on commercial polymer separators for advanced lithium-ion batteries[J]. Journal of Power Sources, 2019, 416: 89-94.

[198]Yoo Y, Kim B G, Pak K, et al. Initiated Chemical Vapor Deposition (iCVD) of Highly Cross-Linked Polymer Films for Advanced Lithium-Ion Battery Separators[J]. ACS Applied Materials & Interfaces, 2015, 7(33): 18849-18855.

[199]Baxamusa S: Conformal Polymer CVD, CVD Polymers, 2015: 87-109.

[200]Alf M E, Asatekin A, Barr M C, et al. Chemical Vapor Deposition of Conformal, Functional, and Responsive Polymer Films[J]. Advanced Materials, 2010, 22(18): 1993-2027.

[201]Yoo Y, You J B, Choi W, et al. A stacked polymer film for robust superhydrophobic fabrics[J]. Polymer Chemistry, 2013, 4(5): 1664-1671.

[202]Lau K K S, Gleason K K. Initiated Chemical Vapor Deposition (iCVD) of Poly(alkyl acrylates): An Experimental Study[J]. Macromolecules, 2006, 39(10): 3688-3694.

[203]Im S G, Gleason K K. Solvent-free modification of surfaces with polymers: The case for initiated and oxidative chemical vapor deposition (CVD)[J]. AIChE Journal, 2011, 57(2): 276-285.

[204]Prasanna K, Kim C-S, Lee C W. Effect of SiO2 coating on polyethylene separator with different stretching ratios for application in lithium ion batteries[J]. Materials Chemistry and Physics, 2014, 146(3): 545-550.

[205]Kang S M, Ryou M-H, Choi J W, et al. Mussel- and Diatom-Inspired Silica Coating on Separators Yields Improved Power and Safety in Li-Ion Batteries[J]. Chemistry of Materials, 2012, 24(17): 3481-3485.

[206] Jeon H, Roh Y, Jin D, et al. Crosslinkable polyhedral silsesquioxane-based ceramic-coated separators for Li-ion batteries[J]. Journal of Industrial and Engineering Chemistry, 2019, 71: 277-283.

[207]Wang Y, Shi L, Zhou H, et al. Polyethylene separators modified by ultrathin hybrid films enhancing lithium ion transport performance and Li-metal anode stability[J]. Electrochimica Acta, 2018, 259: 386-394.

[208]Wu J, Zuo X, Chen Q, et al. Functional composite polymer electrolytes with imidazole modified SiO2 nanoparticles for high-voltage cathode lithium ion batteries[J]. Electrochimica Acta, 2019, 320: 134567.

[209]Shin S C, Kim J, Modigunta J K R, et al. Bio-mimicking organic-inorganic hybrid ladder-like polysilsesquioxanes as a surface modifier for polyethylene separator in lithium-ion batteries[J]. Journal of Membrane Science, 2021, 620: 118886.

[210]Chen W, Shi L, Wang Z, et al. Porous cellulose diacetate-SiO2 composite coating on polyethylene separator for high-performance lithium-ion battery[J]. Carbohydrate Polymers, 2016, 147: 517-524.

[211] Zhi Y, Sun X, Li N, et al. UV curable organic-inorganic hybrid coatings on microporous polyethylene separator for enhancing mechanical and electrochemical performance[J]. Journal of Alloys and Compounds, 2018, 743: 756-762.

[212]Zuo X, Wu J, Ma X, et al. A poly(vinylidene fluoride)/ethyl cellulose and amino-functionalized nano-SiO2 composite coated separator for 5 V high-voltage lithium-ion batteries with enhanced performance[J]. Journal of Power Sources, 2018, 407: 44-52.

[213]Nho Y-C, Sohn J-Y, Shin J, et al. Preparation of nanocomposite γ-Al2O3/polyethylene separator crosslinked by electron beam irradiation for lithium secondary battery[J]. Radiation Physics and Chemistry, 2017, 132: 65-70.

[214]Wang Y, Wang Q, Wei X, et al. A novel three-dimensional boehmite nanowhiskers network-coated polyethylene separator for lithium-ion batteries[J]. Ceramics International, 2021, 47(7, Part A): 10153-10162.

[215]Prasanna K, Subburaj T, Lee W J, et al. Polyethylene separator: stretched and coated with porous nickel oxide nanoparticles for enhancement of its efficiency in Li-ion batteries[J]. Electrochimica Acta, 2014, 137: 273-279.

[216]Xie X, Sheng L, Xu R, et al. In situ mineralized Ca3(PO4)2 inorganic coating modified polyethylene separator for high-performance lithium-ion batteries[J]. Journal of Electroanalytical Chemistry, 2022, 920: 116570.

[217]Yeon D, Lee Y, Ryou M-H, et al. New flame-retardant composite separators based on metal hydroxides for lithium-ion batteries[J]. Electrochimica Acta, 2015, 157: 282-289.

[218]Qin S, Wang M, Wang C, et al. Binder-Free Nanoparticulate Coating of a Polyethylene Separator via a Reactive Atmospheric Pressure Plasma for Lithium-Ion Batteries with Improved Performances[J]. Advanced Materials Interfaces, 2018, 5(19): 1800579.

[219]Shin W-K, Yoo J-H, Kim D-W. Surface-modified separators prepared with conductive polymer and aluminum fluoride for lithium-ion batteries[J]. Journal of Power Sources, 2015, 279: 737-744.

[220] Zheng H, Wang Z, Shi L, et al. Enhanced thermal stability and lithium ion conductivity of polyethylene separator by coating colloidal SiO2 nanoparticles with porous shell[J]. Journal of Colloid and Interface Science, 2019, 554: 29-38.

[221]Mao X, Shi L, Zhang H, et al. Polyethylene separator activated by hybrid coating improving Li+ ion transference number and ionic conductivity for Li-metal battery[J]. Journal of Power Sources, 2017, 342: 816-824.

[222]Zhang H, Sheng L, Bai Y, et al. Amino-Functionalized Al2O3 Particles Coating Separator with Excellent Lithium-Ion Transport Properties for High-Power Density Lithium-Ion Batteries[J]. Advanced Engineering Materials, 2020, 22(11): 1901545.

[223]Lee H, Jeon H, Gong S, et al. A facile method to enhance the uniformity and adhesion properties of water-based ceramic coating layers on hydrophobic polyethylene separators[J]. Applied Surface Science, 2018, 427: 139-146.

[224] Shin W-K, Kim D-W. High performance ceramic-coated separators prepared with lithium ion-containing SiO2 particles for lithium-ion batteries[J]. Journal of Power Sources, 2013, 226: 54-60.

[225]Wang Y, Wang Q, Lan Y, et al. Aqueous aluminide ceramic coating polyethylene separators for lithium-ion batteries[J]. Solid State Ionics, 2020, 345: 115188.

[226]Li D, Qin D, Nie F, et al. Enhancement of electrochemical performance of lithium-ion battery by single-ion conducting polymer addition in ceramic-coated separator[J]. Journal of Materials Science, 2018, 53(15): 11038-11049.

[227]Cho J, Jung Y-C, Lee Y S, et al. High performance separator coated with amino-functionalized SiO2 particles for safety enhanced lithium-ion batteries[J]. Journal of Membrane Science, 2017, 535: 151-157.

[228]Luo X, Liao Y, Zhu Y, et al. Investigation of nano-CeO2 contents on the properties of polymer ceramic separator for high voltage lithium ion batteries[J]. Journal of Power Sources, 2017, 348: 229-238.

[229] Wang Q, Yang J, Wang Z, et al. Dual-Scale Al2O3 Particles Coating for High-Performance Separator and Lithium Metal Anode[J]. Energy Technology, 2020, 8(5): 1901429.

[230] Yang C, Tong H, Luo C, et al. Boehmite particle coating modified microporous polyethylene membrane: A promising separator for lithium ion batteries[J]. Journal of Power Sources, 2017, 348: 80-86.

[231] Tan L, Sun Y, Wei C, et al. Design of Robust, Lithiophilic, and Flexible Inorganic-Polymer Protective Layer by Separator Engineering Enables Dendrite-Free Lithium Metal Batteries with LiNi0.8Mn0.1Co0.1O2 Cathode[J]. Small, 2021, 17(13): 2007717.

[232] Jeon H, Jin S Y, Park W H, et al. Plasma-assisted water-based Al2O3 ceramic coating for polyethylene-based microporous separators for lithium metal secondary batteries[J]. Electrochimica Acta, 2016, 212: 649-656.

[233] Zhang P, Chen L, Shi C, et al. Development and characterization of silica tube-coated separator for lithium ion batteries[J]. Journal of Power Sources, 2015, 284: 10-15.

[234] Shi C, Dai J, Shen X, et al. A high-temperature stable ceramic-coated separator prepared with polyimide binder/Al2O3 particles for lithium-ion batteries[J]. Journal of Membrane Science, 2016, 517: 91-99.

[235] Chen X, Chen S, Lin Y, et al. Multi-functional ceramic-coated separator for lithium-ion batteries safety tolerance improvement[J]. Ceramics International, 2020, 46(15): 24689-24697.

[236] Wang X, Hua H, Peng L, et al. Functional separator for promoting lithium ion migration and its mechanism study[J]. Applied Surface Science, 2021, 542: 148661.

[237] Fu W, Xu R, Zhang X, et al. Enhanced wettability and electrochemical performance of separators for lithium-ion batteries by coating core-shell structured silica-poly(cyclotriphosphazene-co-4,4′-sulfonyldiphenol) particles[J]. Journal of Power Sources, 2019, 436: 226839.

[238] Zhu T, Zuo X, Lin X, et al. High-Wettability Composite Separator Embedded with in Situ Grown TiO2 Nanoparticles for Advanced Sodium-Ion Batteries[J]. Energy Technology, n/a(n/a): 2200409.

[239] Lee C-H, Huang Y-C, Kinzlinger U, et al. A Novel Cavity-Enhanced Polyethylene/Nanostructured-Alumina Separator with Long Cycle Life and High Rate Capability for Advanced Lithium-Ion Batteries[J]. ACS Sustainable Chemistry & Engineering, 2021, 9(4): 1590-1598.

[240] Kim J I, Heo J, Park J H. Tailored Metal Oxide Thin Film on Polyethylene Separators for Sodium-Ion Batteries[J]. Journal of The Electrochemical Society, 2017, 164(9): A1965-A1969.

[241]Qiu Z, Shi L, Wang Z, et al. Surface activated polyethylene separator promoting Li+ ion transport in gel polymer electrolytes and cycling stability of Li-metal anode[J]. Chemical Engineering Journal, 2019, 368: 321-330.

[242]Gogia A, Wang Y, Rai A K, et al. Binder-Free, Thin-Film Ceramic-Coated Separators for Improved Safety of Lithium-Ion Batteries[J]. ACS Omega, 2021, 6(6): 4204-4211.

[243]Costa C M, Lee Y-H, Kim J-H, et al. Recent advances on separator membranes for lithium-ion battery applications: From porous membranes to solid electrolytes[J]. Energy Storage Materials, 2019, 22: 346-375.

[244]Zhu Y, Yin M, Liu H, et al. Modification and characterization of electrospun poly (vinylidene fluoride)/poly (acrylonitrile) blend separator membranes[J]. Composites Part B: Engineering, 2017, 112: 31-37.

[245]Liu M, Turcheniuk K, Fu W, et al. Scalable, safe, high-rate supercapacitor separators based on the Al2O3 nanowire Polyvinyl butyral nonwoven membranes[J]. Nano Energy, 2020, 71: 104627.

[246]Lyu P, Liu X, Qu J, et al. Recent advances of thermal safety of lithium ion battery for energy storage[J]. Energy Storage Materials, 2020, 31: 195-220.

[247]Deng N, Liu Y, Li Q, et al. Functional mechanism analysis and customized structure design of interlayers for high performance Li-S battery[J]. Energy Storage Materials, 2019, 23: 314-349.

[248]Xia L, Vemuri B, Saptoka S, et al.: Antifouling membranes for bioelectrochemistry applications, Microbial Electrochemical Technology: Elsevier, 2019: 195-224.

[249] Zahid M, Rashid A, Akram S, et al. A comprehensive review on polymeric nano-composite membranes for water treatment[J]. J. Membr. Sci. Technol, 2018, 8(2).

[250]Kim J-K, Cheruvally G, Li X, et al. Preparation and electrochemical characterization of electrospun, microporous membrane-based composite polymer electrolytes for lithium batteries[J]. Journal of Power Sources, 2008, 178(2): 815-820.

[251]Kim K M, Park N-G, Ryu K S, et al. Characteristics of PVdF-HFP/TiO2 composite membrane electrolytes prepared by phase inversion and conventional casting methods[J]. Electrochimica Acta, 2006, 51(26): 5636-5644.

[252] Song Q, Li A, Shi L, et al. Thermally stable, nano-porous and eco-friendly sodium alginate/attapulgite separator for lithium-ion batteries[J]. Energy Storage Materials, 2019, 22: 48-56.

[253] Vatanpour V, Madaeni S S, Khataee A R, et al. TiO2 embedded mixed matrix PES nanocomposite membranes: Influence of different sizes and types of nanoparticles on antifouling and performance[J]. Desalination, 2012, 292: 19-29.

[254] Upadhyaya L, Oliveira B, Pereira V J, et al. Nanocomposite membranes from nano-particles prepared by polymerization induced self-assembly and their biocidal activity[J]. Separation and Purification Technology, 2020, 251: 117375.

[255] Deng W, Li Y. Novel superhydrophilic antifouling PVDF-BiOCl nanocomposite membranes fabricated via a modified blending-phase inversion method[J]. Separation and Purification Technology, 2021, 254: 117656.

[256] Rahman M M, Mateti S, Cai Q, et al. High temperature and high rate lithium-ion batteries with boron nitride nanotubes coated polypropylene separators[J]. Energy Storage Materials, 2019, 19: 352-359.

[257] Jung Y S, Cavanagh A S, Gedvilas L, et al. Improved functionality of lithium‐ion batteries enabled by atomic layer deposition on the porous microstructure of polymer separators and coating electrodes[J]. Advanced Energy Materials, 2012, 2(8): 1022-1027.

[258] Lee D-W, Lee S-H, Kim Y-N, et al. Preparation of a high-purity ultrafine α-Al2O3 powder and characterization of an Al2O3-coated PE separator for lithium-ion batteries[J]. Powder Technology, 2017, 320: 125-132.

[259] Lee T, Lee Y, Ryou M-H, et al. A facile approach to prepare biomimetic composite separators toward safety-enhanced lithium secondary batteries[J]. RSC Advances, 2015, 5(49): 39392-39398.

[260] Jeong H-S, Lee S-Y. Closely packed SiO2 nanoparticles/poly (vinylidene fluoride-hexafluoropropylene) layers-coated polyethylene separators for lithium-ion batteries[J]. Journal of power sources, 2011, 196(16): 6716-6722.

[261] Zhao H, Yan J, Deng N, et al. A versatile nano-TiO2 decorated gel separator with derived multi-scale nanofibers towards dendrite-blocking and polysulfide-inhibiting lithium-metal batteries[J]. Journal of Energy Chemistry, 2021, 55: 190-201.

[262] Zhou W, Meng L, Lu J, et al. Inducing uniform single-crystal like orientation in natural rubber with constrained uniaxial stretch[J]. Soft Matter, 2015, 11(25): 5044-5052.

[263] Jones A T, Aizlewood J M, Beckett D. Crystalline forms of isotactic polypropylene[J]. Die Makromolekulare Chemie: Macromolecular Chemistry and Physics, 1964, 75(1): 134-158.

[264]Li X, Lin Y, Ji Y, et al. Strain and temperature dependence of deformation mechanism of lamellar stacks in HDPE and its guidance on microporous membrane preparation[J]. Polymer, 2016, 105: 264-275.

[265]Xue C, Jin D, Nan H, et al. A novel polymer-modified separator for high-performance lithium-ion batteries[J]. Journal of Power Sources, 2020, 449: 227548.

[266]Kang S M, Ryou M, Choi J W, et al. Mussel- and Diatom-Inspired Silica Coating on Separators Yields Improved Power and Safety in Li-Ion Batteries[J]. Chemistry of Materials, 2012, 24(17): 3481-3485.

[267]Kononova S V, Gubanova G N, Korytkova E N, et al. Polymer Nanocomposite Membranes[J]. Applied Sciences, 2018, 8(7): 1181.

[268]Li J, Zhang C, Chen T, et al. Preparation of a Thermally Insulating Nanocomposite by Blending Ultra-High-Molecular-Weight Polyethylene with Gas-Phase Silica[J]. Industrial & Engineering Chemistry Research, 2015, 54(23): 6093-6099.

[269]Shi G, Cao Z, Yan X, et al. In-situ fabrication of a UHMWPE nanocomposite reinforced by SiO2 nanospheres and its tribological performance[J]. Materials Chemistry and Physics, 2019, 236: 121778.

[270]Yang M, Hou J. Membranes in Lithium Ion Batteries[J]. Membranes, 2012, 2(3): 367-383.

[271]Habumugisha J C, Usha Z R, Yu R, et al. Thermally stable and high electrochemical performance ultra-high molecular weight polyethylene/poly(4-methyl-1-pentene) blend film used as Li-ion battery separator[J]. Applied Materials Today, 2021, 24: 101136.

[272]Dong T, Arifeen W U, Choi J, et al. Surface-modified electrospun polyacrylonitrile nano-membrane for a lithium-ion battery separator based on phase separation mechanism[J]. Chemical Engineering Journal, 2020, 398: 125646.

[273]Lin L, Ning H, Song S, et al. Flexible electrochemical energy storage: The role of composite materials[J]. Composites Science and Technology, 2020, 192: 108102.

[274] Zhu Q, Yu L, Song S, et al. Ultrafast charge in Zn-based batteries through high-potential deposition[J]. Materials Today Physics, 2021, 19: 100425.

[275]Nunes-Pereira J, Kundu M, Gören A, et al. Optimization of filler type within poly(vinylidene fluoride-co-trifluoroethylene) composite separator membranes for improved lithium-ion battery performance[J]. Composites Part B: Engineering, 2016, 96: 94-102.

[276]Cheng N, Ren L, Xu X, et al. Application of organic-inorganic hybrids in lithium batteries[J]. Materials Today Physics, 2020, 15: 100289.

[277]Pan Y, Chou S, Liu H K, et al. Functional membrane separators for next-generation high-energy rechargeable batteries[J]. National Science Review, 2017, 4(6): 917-933.

[278]Waqas M, Ali S, Chen D, et al. A robust bi-layer separator with Lewis acid-base interaction for high-rate capacity lithium-ion batteries[J]. Composites Part B: Engineering, 2019, 177: 107448.

[279]Nasef M M, Gürsel S A, Karabelli D, et al. Radiation-grafted materials for energy conversion and energy storage applications[J]. Progress in Polymer Science, 2016, 63: 1-41.

[280]Lei Q-K, Zhang Q, Wu X-Y, et al. Towards ultra-stable lithium metal batteries: Interfacial ionic flux regulated through LiAl LDH-modified polypropylene separator[J]. Chemical Engineering Journal, 2020, 395: 125187.

[281]Zhao P, Yang J, Shang Y, et al. Surface modification of polyolefin separators for lithium ion batteries to reduce thermal shrinkage without thickness increase[J]. Journal of Energy Chemistry, 2015, 24(2): 138-144.

[282]Zheng W, Zhu Y, Na B, et al. Hybrid silica membranes with a polymer nanofiber skeleton and their application as lithium-ion battery separators[J]. Composites Science and Technology, 2017, 144: 178-184.

[283]Khonakdar H A, Jafari S H, Wagenknecht U, et al. Effect of electron-irradiation on cross-link density and crystalline structure of low- and high-density polyethylene[J]. Radiation Physics and Chemistry, 2006, 75(1): 78-86.

[284]Ren Y, Ding Z, Wang C, et al. Influence of DBD plasma pretreatment on the deposition of chitosan onto UHMWPE fiber surfaces for improvement of adhesion and dyeing properties[J]. Applied Surface Science, 2017, 396: 1571-1579.

[285]Teodoru S, Kusano Y, Rozlosnik N, et al. Continuous Plasma Treatment of Ultra-High-Molecular-Weight Polyethylene (UHMWPE) Fibres for Adhesion Improvement[J]. Plasma Processes and Polymers, 2009, 6(S1): S375-S381.

[286]Kim K J, Kim Y H, Song J H, et al. Effect of gamma ray irradiation on thermal and electrochemical properties of polyethylene separator for Li ion batteries[J]. Journal of Power Sources, 2010, 195(18): 6075-6080.

[287]Elnahas H H, Abdou S M, El-Zahed H, et al. Structural, morphological and mechanical properties of gamma irradiated low density polyethylene/paraffin wax blends[J]. Radiation Physics and Chemistry, 2018, 151: 217-224.

[288]Sohn J-Y, Im J S, Gwon S-J, et al. Preparation and characterization of a PVDF-HFP/PEGDMA-coated PE separator for lithium-ion polymer battery by electron beam irradiation[J]. Radiation Physics and Chemistry, 2009, 78(7): 505-508.

[289]Wang H, Xu L, Hu J, et al. Radiation-induced oxidation of ultra-high molecular weight polyethylene (UHMWPE) powder by gamma rays and electron beams: A clear dependence of dose rate[J]. Radiation Physics and Chemistry, 2015, 115: 88-96.

[290] Melk L, Emami N. Mechanical and thermal performances of UHMWPE blended vitamin E reinforced carbon nanoparticle composites[J]. Composites Part B: Engineering, 2018, 146: 20-27.

[291]Hikmet R a M, Thomassen R. Electron-Beam-Induced Crosslinking of Electroluminescent Polymers for the Production of Multi-Color Patterned Devices[J]. Advanced Materials, 2003, 15(2): 115-117.

[292]Sheng H, Zheng H, Jia S, et al. Atomistic manipulation of reversible oxidation and reduction in Ag with an electron beam[J]. Nanoscale, 2019, 11(22): 10756-10762.

[293]Tan Z, Wang X, Fu C, et al. Effect of electron beam irradiation on structural and thermal properties of gamma poly (vinylidene fluoride) (γ-PVDF) films[J]. Radiation Physics and Chemistry, 2018, 144: 48-55.

[294]Murray K A, Kennedy J E, Mcevoy B, et al. The effects of high energy electron beam irradiation on the thermal and structural properties of low density polyethylene[J]. Radiation Physics and Chemistry, 2012, 81(8): 962-966.

[295] Pokharel P, Jian W, Choi S. Evaluation of fatigue crack behavior in electron beam irradiated polyethylene pipes[J]. Radiation Physics and Chemistry, 2016, 126: 103-110.

[296]Shen C, Oyadiji S O. The processing and analysis of graphene and the strength enhancement effect of graphene-based filler materials: A review[J]. Materials Today Physics, 2020, 15: 100257.

[297]Rocha M, Mansur A, Mansur H. Characterization and Accelerated Ageing of UHMWPE Used in Orthopedic Prosthesis by Peroxide[J]. Materials, 2009, 2(2): 562-576.

[298]Qian J, Fu C, Wang X, et al. The formation of cross‐linking networks in a fluorinated polymer composite system by electron beam irradiation[J]. Advances in Polymer Technology, 2018, 37(8): 3159-3170.

[299]Lee J H, Jeong H Y, Lee S Y, et al. Effects of Electron Beam Irradiation on Mechanical and Thermal Shrinkage Properties of Boehmite/HDPE Nanocomposite Film[J]. Nanomaterials, 2021, 11(3): 777.

[300]Wu Y, Lei D, Wang C. The formation of LiAl5O8 nanowires from bulk Li-Al alloy enables dendrite-free Li metal batteries[J]. Materials Today Physics, 2021, 18: 100395.

[301]Acauan L H, Zhou Y, Kalfon-Cohen E, et al. Multifunctional nanocomposite structural separators for energy storage[J]. Nanoscale, 2019, 11(45): 21964-21973.

[302]Tian X, Yi Y, Fang B, et al. Design Strategies of Safe Electrolytes for Preventing Thermal Runaway in Lithium Ion Batteries[J]. Chemistry of Materials, 2020, 32(23): 9821-9848.

[303]Liu Y, Lin D, Jin Y, et al. Transforming from planar to three-dimensional lithium with flowable interphase for solid lithium metal batteries[J]. Science Advances, 2017, 3(10): eaao0713.

[304]Liao C, Wang W, Wang J, et al. Magnetron sputtering deposition of silicon nitride on polyimide separator for high-temperature lithium-ion batteries[J]. Journal of Energy Chemistry, 2021, 56: 1-10.

[305]Yim T, Park M-S, Woo S-G, et al. Self-Extinguishing Lithium Ion Batteries Based on Internally Embedded Fire-Extinguishing Microcapsules with Temperature-Responsiveness[J]. Nano Letters, 2015, 15(8): 5059-5067.

[306]R A, Vijaya Kumar Saroja A P, Sundara R. Barium Titanate-Based Porous Ceramic Flexible Membrane as a Separator for Room-Temperature Sodium-Ion Battery[J]. ACS Applied Materials & Interfaces, 2019, 11(4): 3889-3896.

[307]Vijaya Kumar Saroja A P, R A K, Moharana B C, et al. Design of porous calcium phosphate based gel polymer electrolyte for Quasi-solid state sodium ion battery[J]. Journal of Electroanalytical Chemistry, 2020, 859: 113864.

[308]Liu K, Liu W, Qiu Y, et al. Electrospun core-shell microfiber separator with thermal-triggered flame-retardant properties for lithium-ion batteries[J]. Science Advances, 2017, 3(1): e1601978.

[309]Yang H, Shi X, Chu S, et al. Design of Block-Copolymer Nanoporous Membranes for Robust and Safer Lithium-Ion Battery Separators[J]. Advanced Science, 2021, 8(7): 2003096.

[310]Yuan B, He N, Liang Y, et al. A surfactant-modified composite separator for high safe lithium ion battery[J]. Journal of Energy Chemistry, 2023, 76: 398-403.

[311]Song Y, Liu X, Ren D, et al. Simultaneously Blocking Chemical Crosstalk and Internal Short Circuit via Gel-Stretching Derived Nanoporous Non-Shrinkage Separator for Safe Lithium-Ion Batteries[J]. Advanced Materials, 2022, 34(2): 2106335.

[312]Yuan M, Liu K. Rational design on separators and liquid electrolytes for safer lithium-ion batteries[J]. Journal of Energy Chemistry, 2020, 43: 58-70.

[313]Das M, Das P S, Basu R N, et al. Cellulose-ceramic composite flexible paper separator with improved wettability and flame retardant properties for lithium-ion batteries[J]. Cellulose, 2022, 29(18): 9899-9917.

[314]Yu J, Dong N, Liu B, et al. A newly-developed heat-resistance polyimide microsphere coating to enhance the thermal stability of commercial polyolefin separators for advanced lithium-ion battery[J]. Chemical Engineering Journal, 2022, 442: 136314.

[315]Liu K, Liu Y, Lin D, et al. Materials for lithium-ion battery safety[J]. Science Advances, 2018, 4(6): eaas9820.

[316]Zhao Z, Li Y, Jin D, et al. Modification of an anion exchange membrane based on rapid mussel-inspired deposition for improved antifouling performance[J]. Colloids and Surfaces A: Physicochemical and Engineering Aspects, 2021, 615: 126267.

[317] Liu F, Liu X, Chen F, et al. Mussel-inspired chemistry: A promising strategy for natural polysaccharides in biomedical applications[J]. Progress in Polymer Science, 2021, 123: 101472.

[318]Liebscher J, Mrówczyński R, Scheidt H A, et al. Structure of Polydopamine: A Never-Ending Story?[J]. Langmuir, 2013, 29(33): 10539-10548.

[319]Jung Y S, Cavanagh A S, Gedvilas L, et al. Improved Functionality of Lithium-Ion Batteries Enabled by Atomic Layer Deposition on the Porous Microstructure of Polymer Separators and Coating Electrodes[J]. Advanced Energy Materials, 2012, 2(8): 1022-1027.

[320] Wang H, Wu J, Cai C, et al. Mussel Inspired Modification of Polypropylene Separators by Catechol/Polyamine for Li-Ion Batteries[J]. ACS Applied Materials & Interfaces, 2014, 6(8): 5602-5608.

[321]Li X, Chen S, Xia Z, et al. High performance of boehmite/polyacrylonitrile composite nanofiber membrane for polymer lithium-ion battery[J]. RSC Advances, 2020, 10(46): 27492-27501.

[322]Xu R, Lin X, Huang X, et al. Boehmite-coated microporous membrane for enhanced electrochemical performance and dimensional stability of lithium-ion batteries[J]. Journal of Solid State Electrochemistry, 2018, 22(3): 739-747.

[323]Liu L, Wang Y, Gao C, et al. Ultrathin ZrO2-coated separators based on surface sol-gel process for advanced lithium ion batteries[J]. Journal of Membrane Science, 2019, 592: 117368.

[324]Ko S, Baek M-J, Wi T-U, et al. Understanding the Role of a Water-Soluble Catechol-Functionalized Binder for Silicon Anodes by Diverse In Situ Analyses[J]. ACS Materials Letters, 2022, 4(5): 831-839.

[325]Li T, Li Y, Sun Y, et al. New Insights on the Good Compatibility of Ether-Based Localized High-Concentration Electrolyte with Lithium Metal[J]. ACS Materials Letters, 2021, 3(6): 838-844.

[326]Mu J, Yu M, Jiang H, et al. Fe2O3 Nanoparticle Interfacial Reaction Redistributing Li-Ion Flux in Flexible Hierarchically Porous Membrane Electrodes for Dendrite-Free Lithium Metal Batteries[J]. ACS Materials Letters, 2022: 133-143.

[327]Zhang S, Luo J, Du M, et al. Highly porous zeolitic imidazolate framework-8@bacterial cellulose composite separator with enhanced electrolyte absorption capability for lithium-ion batteries[J]. Cellulose, 2022, 29(9): 5163-5176.

LIST OF PUBLICATIONS

1) **Dafaalla M.D. Babiker**, et al., Recent progress of composite polyethylene separators for lithium/sodium batteries, ***Journal of Power Sources*** 564 (2023) 232853.

2) **Dafaalla M.D. Babiker**, et al., High performance ultra-high molecular weight polyethylene nanocomposite separators with excellent rate capabilities designed for next-generation lithium-ion batteries, *Materials Today Physics* 23 (2022) 100626.

3) **Dafaalla M.D. Babiker**, et al., Superior lithium battery separator with extraordinary electrochemical performance and thermal stability based on hybrid UHMWPE/SiO_2 nanocomposites via the scalable biaxial stretching process, *Composites Part B: Engineering* 211 (2021) 108658.

4) **Dafaalla M.D. Babiker**, et al., A polyolefin-based hybrid separator for safe, durable and long-life lithium/sodium metal batteries (2023) (submitted).

5) Z.R. Usha, **Dafaalla M.D. Babiker**, et al., Super hydrophilic modified biaxially oriented polypropylene microporous membrane for excellent gravity-driven oil/water emulsion separation, *Journal of Membrane Science* 660 (2022) 120840.

6) Z. R. Usha, **Dafaalla M.D. Babiker**, et al., Robust super-wetting biaxial polypropylene membrane with multi-scale roughness structures for highly efficient oil/water emulsion separation, *Journal of Environmental Chemical Engineering* 11 (2023) 109670.

7) Z. R. Usha, **Dafaalla M.D. Babiker**, et al., Advanced super-wetting biaxial polypropylene membrane with hierarchical rough surface for multipollutant removal from oily wastewater, *Journal of Environmental Chemical Engineering* (under review).

8) J.C. Habumugisha, Z.R. Usha, R. Yu, **Dafaalla M.D. Babiker**, et al., Thermally stable and high electrochemical performance ultra-high molecular weight polyethylene/poly(4-methyl-1-pentene) blend film used as Li-ion battery separator, *Applied Materials Today* 24 (2021) 101136.